IJL, Issue 1, Vol. 23, 2024
https://doi.org/10.31900/ijl.v23i1.393

Research Article

IRAQI JOURNAL OF LASER

Efficacy of low-level laser therapy on postoperative sequelae following extraction of impacted mandibular third molars

Osama A. Ali[1,*], Zainab F. Mahdi[1], Balsam S. Abdulhameed[2],

[1]*Institute of Laser for Postgraduate Studies, University of Baghdad, Baghdad, Iraq*
[2]*Al-Imamen Al-Kadmen Medical City, Ministry of Health, Baghdad, Iraq*
* *Email address of the Corresponding Author: Usama.abdulkadim1202a@ilps.uobaghdad.edu.iq*

Article history: Received 10 Jun. 2023; Revised 31 Aug. 2023; Accepted 17 Sept. 2023; Published online 15 Jun. 2024

Abstract

Background: In dentistry, extraction of the impacted mandibular third molar is a routine treatment. The most frequent consequences following this procedure are pain, trismus, and edema. To address these issues, systemic drugs have been employed; however, due to their side effects, non-medication therapies have evolved, such as cryotherapy, ice packs, low-level laser therapy, and ozone, which treat these consequences without side effects. Low-level laser therapy induces biostimulation, speeds up tissue regeneration, enhances wound healing, and reduces pain and swelling through an anti-inflammatory effect. This might be due to the effect of a low-energy laser that increases phagocytic activity and the number and diameter of lymphatic vessels, decreases the permeability of blood vessels, and restores microcapillary function.
Aim: Its purpose was to assess the effects of low-level laser therapy on sequelae following impacted third molar surgery.
Patients and methods: Thirty patients were enrolled in the current study and were randomly divided into two equal groups. Preoperative clinical examination included measurement of maximum mouth opening and facial swelling measurements. The position and configuration of the impacted lower third molar, the surrounding bone, the mandibular canal, and the neighboring tooth were all assessed radiographically using a panoramic radiograph. Low-level laser therapy was applied extra and intra-orally immediately after surgery. On the second and seventh days after surgery, the maximum mouth opening and facial swelling dimensions were again assessed in addition to the measurement of pain by a numerating rating scale. Statistics were used to asses each reading.
Conclusion: A therapeutic option utilizing a low-energy laser following the extraction of impacted mandibular third molars has clinically beneficial effects on reducing pain, edema, and trismus.

Keywords: Impacted third molar, improved postoperative sequelae, low-level laser therapy, pain, trismus, swelling.

1. Introduction

One of the most frequent surgical operations in oral surgery is the removal of third molar teeth (wisdom teeth) [Grossi et al., 2007]. Pain, trismus, and edema are the most frequent complications after surgical removal of impacted lower wisdom teeth [Barone et al., 2010]. Pain reaches maximum intensity between

three to five hours after local anesthesia has worn off, continues for two to three days, and gradually reduces until the seventh day [Markovic and Todorovic, 2006; Lago et al., 2007]. Swelling reaches peak intensity in 12–48 h, resolving between the fifth and seventh day [Ra'ed Mohammed et al., 2013; Ferrante et al., 2013]. Trismus subsides when pain and edema decrease [López-Ramírez et al., 2012].
Nonsteroidal anti-inflammatory Drugs (NSAIDs) and local or systemic corticosteroids are frequently advised. However, the majority of these may cause harmful effects, including susceptibility to systemic bleeding, gastrointestinal problems, and allergic reactions. [Thaer Abdul Lateef et al., 2010, Ferrante et al., 2013]. These findings support efforts to develop a novel strategy for postoperative pain management that does not result in adverse effects like the use of surgical closure techniques with or without incorporation of drains, ice packs, herbals, platelet-rich plasma, platelet-rich fibrin, and cryotherapy have been suggested [Gelesko et al, 2011, Ali S. Abdul-Kareem, 2019]. Ozone therapy and low-level laser therapy (LLLT) have been introduced as alternatives over the past 20 years.

Light Amplification by Stimulated Emission of Radiation, or LASER, is the abbreviation. The energy output determines the laser into a "hard" and "soft" laser. While soft lasers are low-level lasers that aid in tissue healing, hard lasers are high-energy output devices utilized for tissue cutting [Nagammai, 2022]. Studies on the biological effects of LLLT were conducted in 1967, and the development of the laser treatment paradigm started in 1971 [Hamblin, 2016]; since then, it has been utilized to treat a variety of disorders, including osteoarthritis, carpal tunnel syndrome, rheumatoid arthritis, and many other inflammatory conditions. When using a ruby laser to treat malignant cells, it was found that LLLT did not kill tumor cells; instead, it sped the healing process, which gave rise to the principle of photobiomodulation [Hamblin, 2016]. However, evidence suggests that the LLLT induces cellular biostimulation, speeds up tissue regeneration, enhances wound healing, and reduces pain and swelling through an anti-inflammatory effect. This is because the LLLT increases phagocytic activity and the number and diameter of lymphatic vessels, decreases the permeability of blood vessels and restores microcapillary function [He WL et al., 2015; Fabre et al., 2015]. The precise biological mechanism of the analgesic effect produced by the LLLT is still unknown [Ferrante et al., 2013]. To achieve its analgesic effects, LLLT stimulates the production of endogenous endorphins, lowers inflammatory cytokines and enzymes, modifies pain threshold, causes changes in the morphology of neurons, lowers mitochondrial membrane potential, and blocks fast axonal flow, which blocks neural conduction. [Domah et al., 2021; Ferrante et al., 2013; Oliveira Sierra et al., 2013]. Notably, LLLT has recently been used in research at wavelengths around 800 nm. In recent studies on LLLT, it has been shown that diode lasers with wavelengths of 940-980 nm are also effective in improving wound healing, reducing postoperative inflammation, and accelerating regeneration [Ferrante et al., 2013; Lobo and Pol, 2015; Kuboyama et al., 2014]. Accordingly, in this regard, the laser will stimulate the surrounding tissue regionally using a dual-wavelength (810,980nm) diode laser in addition to the areas primarily affected by the surgery, including the masseter muscle.

2. Hypothesis

H0: LLLT is not-significantly effective in reducing pain, trismus, and swelling after extraction of the impacted mandibular third molar. H1: LLLT is significantly effective in reducing pain, trismus, and swelling after extraction of the impacted mandibular third molar.

3. Aim

The current study aimed to examine the efficacy of LLLT using a dual-wavelength (810,980nm) diode laser on pain, swelling, and trismus that occurred after impacted third molar extraction.

4. Patients and method

This blind placebo-controlled randomized prospective clinical study involved 30 patients, 12 males and 18 females, aged between 18 and 34 years, with impacted mandibular third molars in similar positions (Class II-III and position B, according to Pell and Gregory's classification). They were randomly assigned to the

study and control groups using the coin toss method and divided into two equal groups, with 15 patients in each. The study was conducted between March 2022 and the end of November 2022. Study group: LLLT was administered right away following extraction of an impacted lower third molar. Control group: subjected to routine extraction of impacted lower third molar without application of LLLT. Patients who needed surgical extraction of their mandibular third molars (Class II-III and position B, according to Pell and Gregory's categorization) and whose condition was assessed clinically and radiologically met the inclusion criteria. Patients should have good oral hygiene and be free of any acute illnesses, as well as be between the ages of 18 and 40 years, be willing to comply with the study and be available for follow-up. Contraindications to laser therapy, systemic illness, local infection, tobacco usage, oral contraceptive use, pregnancy, and lactation were among the exclusion criteria. All patients signed a written informed consent after being given information regarding the study's purpose, the specifics of the surgical procedures, any anticipated complications, and potential adverse effects of the medications being used. Following surgery, the patients were givenAugmentin® tab. 625mg (amoxicillin 500mg and clavulanate 125mg) and Panadol® tab. 500mg (acetaminophen) as needed.

5. Operative procedure

Mandibular third molar extractions were performed under local anesthesia, which was obtained by inferior alveolar, lingual, and long buccal nerve block injection using the (lidocaine hydrochloride 2% local anesthetic cartridge 1.8ml with adrenaline 1:80,000 (Septodent®, France)). Next, a three-sided (trapezoidal)mucoperiosteal flap was made, and bone was removed using a round bur in a surgical straight handpiece (Castellini ®, Germany) with copious saline irrigation to expose the tooth. Tooth delivery was followed by meticulous irrigation of the surgical site with physiologic saline (0.9%). The flap was repositioned then wound closure. The length of time required for the tooth extraction using lasers (from the first incision to the final suture) was recorded.

6. Laser therapy

With an 8mm handpiece, laser therapy was administered using a gallium-aluminum-arsenide (Ga-Al-As) diode laser device (Quicklase®, UK). This laser has a continuous dual wavelength of 810 and 980 nm. Both the patient and the operator were shielding their eyes with safety goggles. Patients in the LLLT group received low-level laser light at six points immediately following surgery: three extraoral at the masseter muscle, including the origin and insertion, and three intraoral, placed at 0.5 cm from the operation site and administered on the occlusal, buccal, and lingual sides. In continuous mode, laser energy was delivered to the study group at a power of 400 mW (0.4 w) for 180s (30 s per point). The biostimulation handpiece was intraorally placed at the surgery site and touched extra orally to the masseter muscle for a total of 180 seconds in the control group, but the laser was not turned on.

7. Evaluation

Using a numeric rating scale (NRS), by which the intensity of the pain was estimated. Whose high ratings range from zero (no pain) to ten (the worst pain imaginable). By measuring the maximum distance between the cutting edges of the right maxillary and right mandibular central incisors, mouth openings were assessed before and after surgery. The mouth opening was measured three times using the same technique: before surgery, on the second and seventh postoperative days. Measurements were taken with a digital Vernier [Ra'ed Mohammed et al., 2013]. Using a measuring tape in centimeters, facial measurements were taken between the lateral corner of the eye and the angle of the mandible (Line A), the tragus and the outer corner of the mouth (Line B), and the tragus and soft tissue pogonion (Line C) [LATT et al., 2016]. As a baseline record, preoperative maximum mouth opening and facial measurements were taken. To calculate the rate of cheek swelling, the same measurement was repeated in the second and seventh days after surgery.

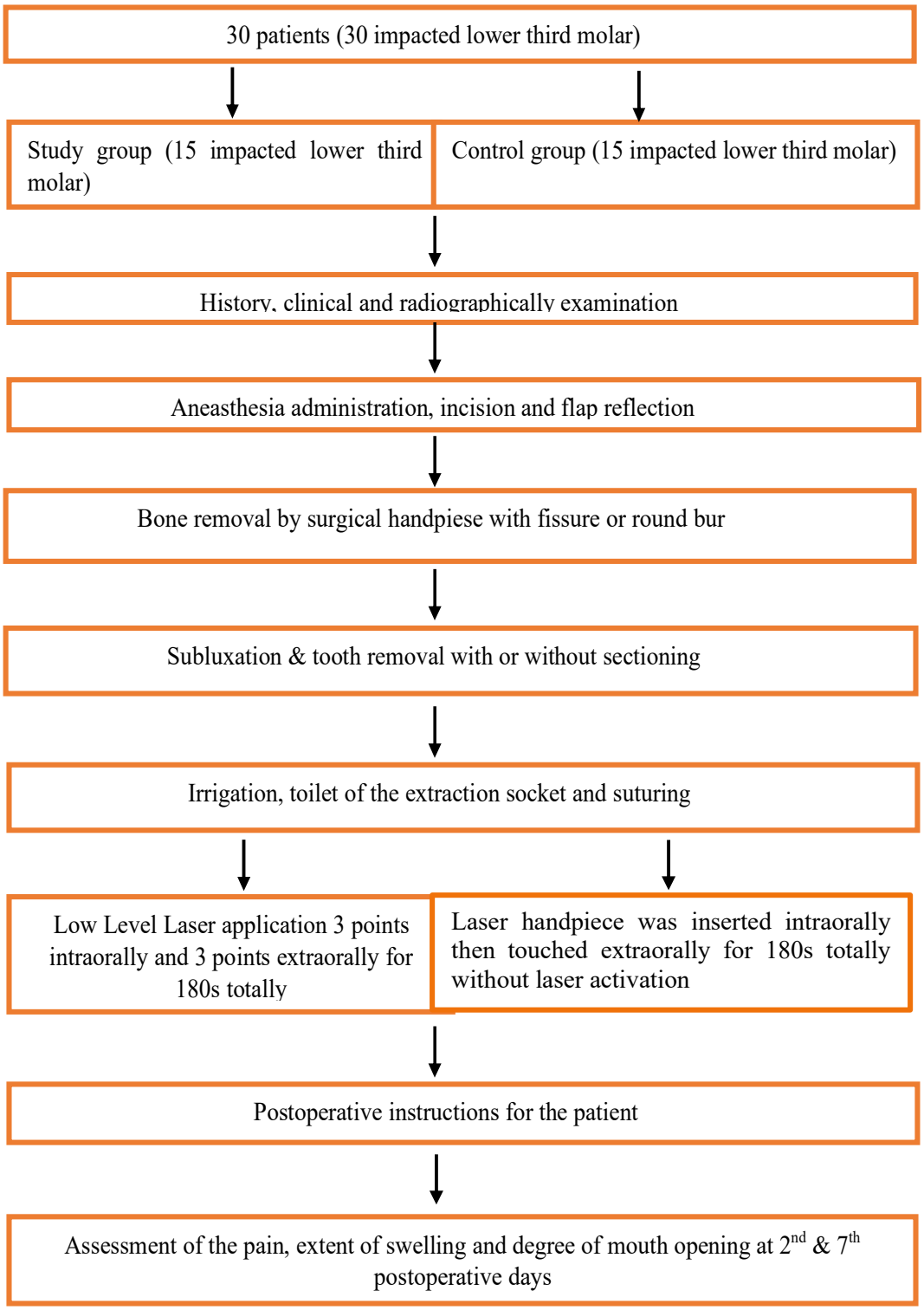

Fig.1: Study flow chart illustrating the basic steps of the study.

The average of the three different values of lines A, B, and C were calculated and reflected the swelling for that day [RAOUÂA et al., 2013, ZHANG et al, 2018]. The difference between measurements taken before surgery and each postoperative measurement done on the second and seventh days was recorded.

8. Statistical analysis

Data description, analysis, and presentation were performed using Statistical Package for Social Science (SPSS version 21, Chicago In press, Illionis, USA), Minimum, maximum, mean, standard deviation (SD), and standard error (SE) for quantitative variable while, median, mean rank frequency and percentage for qualitative variable, Fisher exact chi-square, Shapiro Wilk test of normality, Repeated Measure Analysis of variance, Wilcoxon Sign rank test and Mann- Whitney U test.

9. Result

Thirty patients with asymptomatic impacted mandibular third teeth were involved in the study. These had a mean age of 23.6 ± 4.75 years, with 12 males and 18 females (range, 18–34 years). Thirty molar extractions were carried out without complications. The time of surgery counting from the first incision to the last suture ($p>0.05$). 13 impacted molars were classified as cl II, and 17 impacted molars as cl III by Pell and Gregory ($p>0.05$). 17 mesioangulation, 7 vertical, 4 horizontal, and 2 distoangulation of impacted molars ($p>0.05$). All patients experienced primary healing and no abnormal bleeding throughout the procedures. There was no ecchymosis or hematoma-related alteration in skin color. None of the patients had any negative effects from the medication and laser therapy that were used.

Table 1. Descriptive and statistical test of Age among groups.

Groups	N	Mean	Std. Deviation	Std. Error	Minimum (year)	Maximum (year)	T-test	P value
Laser	15	23.867	4.868	1.257	18.000	34.000	0.230	0.820
Control	15	23.467	4.658	1.203	18.000	32.000		

Table 2. Demographic data among groups.

Vars.		groups					
		Laser		Control			
		N	%	N	%	test	P value
Gender[b]	M	5	26.67	7	46.67	2.778	0.427
	F	10	73.33	8	53.33		
Classification	M	8	53.33	5	33.33	1.667	0.644
	F	7	46.67	10	66.67		
Angulation	M	9	60.00	8	53.33	3.572	0.979
	V	3	20.00	4	26.67		
	H	2	13.33	2	13.33		
	D	1	6.67	1	6.67		
Side [b]	R	5	33.33	8	53.33	1.357	0.716
	L	10	66.67	7	46.67		

A=Fisher exact, b=chi square.

Table 3. Descriptive and statistical test of surgical Duration among groups.

Groups	Mean	Std. Deviation	Std. Error	Minimum (minutes)	Maximum (minutes)	T-test	P value
Laser	35.333	8.649	2.233	25.000	55.000	0.207	0.838
Control	35.933	7.176	1.853	27.000	56.000		

Recalled patients had their pain, edema, and trismus assessed. According to (Table 4), trismus was considerably lower in the study group than in the control group during the second postoperative day ($p=0.01$). However, on the seventh day, the values were comparable in both groups ($p>0.05$). In all evaluations, patients in the study group reported highly significantly less pain as compared to the control group (Table 5), as shown by NRS scores ($p = 0.002$ and $p = 0.001$ for the second and seventh postoperative days, respectively). in addition to three patients in the study group who did not require analgesics. For each group, postoperative edema developed. In comparison to the control group (Table 6), the study group exhibited highly significantly less postoperative edema on the second day ($p=0.029$); nevertheless, on the seventh day, the values were comparable between the two groups ($p>0.05$).

Table 4. Mean ± SD and P values of mouth opening (in mm) for all groups along the different observation periods.

Groups		Baseline	2-day	7th	F	P value	ES
Laser	Min.	26.600	22.400	26.500	3.843	**0.034**	0.222
	Max.	52.400	52.200	51.700			
	Mean	39.800	36.100	38.973			
	±SD	7.452	8.360	7.371			
Control	Min.	26.000	13.100	21.400	29.834	**0.000**	0.688
	Max.	50.600	40.900	43.800			
	Mean	41.040	29.400	36.200			
	±SD	6.733	8.033	6.052			
F		0.229	5.010	1.268			
P value		0.636	**0.033**	0.270			

Table 5. Descriptive and statistical test of Pain among groups and time.

Groups	Median	MR[1]	MR[2]	Median	MR[1]	MR[2]	Wilcoxon sign rank	P value
	2nd			7th				
Laser	2	7	10.60	0	0	10.57	3.275	**0.001**
Control	4	8	20.40	3	0	20.43	3.471	**0.001**
Mann-Whitney U		3.091			3.170			
P value		**0.002**			**0.001**			

MR1=Intragroup, MR2=Intergroup

10. Discussion

Growing interest has been shown in studying the physiological effects of LLLT and its various clinical uses in treating orofacial pain and acute and chronic inflammation, either as a single therapy or complementary therapy [Sigaroodi et al., 2023]. However, the absence of quality publications on the analgesic and anti-inflammatory effects of LLLT after surgically extracting third molars, along with the controversial results found, raises concerns about its effectiveness. Due to the wide range of factors, including the type of laser wavelength, power, pulse rate, time, and application mode, the ideal radiation parameters for this purpose have not yet been established. [Pergolini et al, 2022]. Some researchers found a substantial correlation between the length of the operation and trismus, pain, and overall analgesic consumption [Lago-Méndez et al., 2007]. In our study, we observed no difference in operation time between the control and study groups ($p>0.05$). The use of nonsteroidal anti-inflammatory medications (NSAIDs) and local or systemic corticosteroids may cause a variety of adverse effects. As a result, a novel, comfortable therapeutic approach without drugs is required.

LLLT was obtained in this study in a single visit, directly after the surgery; studies that used LLLT in repetitive sessions generally did not find a significant difference between LLLT and placebo for pain [Ferrante et al., 2013; Amarillas-Escobar et al., 2010; Kazancioglu et al., 2014]. Instead of focusing on the success obtained through repeated LLLT sessions, it would be more appropriate for the research to concentrate on achieving the highest level of therapeutic success in a single session. This is because repeated treatments waste time and require more work from both patients and physicians. This seems to be more of a trivial disadvantage of frequent LLLT sessions than a benefit. Because of this, researchers ought to concentrate on single-session applications, the efficacy of which might be statistically confirmed by conducting research using various laser parameters and various medical combinations. [Anand et al., 2013].

In the current study, LLLT was applied intraorally and extra orally because the intraoral application allows for maximum penetration and absorption at the surgical site. Some authors only applied LLLT extra orally [Kazancioglu et al., 2014] or only intraorally [López-Ramrez et al., 2012], while others conducted clinical trials applying LLLT both extra orally and intraorally [Aras et al.,2010; Sigaroodi et al., 2023; Carroll et al.,2014; Aoki et al.,2015]. However, extraoral treatment was adopted in addition to intraoral application because extraoral laser therapy may directly affect the masseter muscle, where the trauma of surgery might cause a spasm of the masseter muscle, whereas intraoral laser application does not directly affect that muscle [Aras et al.,2010]. A comparison of the efficiency of intraoral and extraoral laser administration supports this. They reported that extraoral laser therapy has better effects on improving pain intensity and trismus after impacted third molar surgery. Even though LLLT is effective in reducing pain, edema, and trismus following the extraction of impacted third molars, some studies have found a good effect of laser therapy while others have not [Ferrante et al., 2013]. Because of this, the ideal parameters of LLLT for biostimulation have not yet been determined [López-Ramírez et al., 2012]. According to studies, the pain reaches maximum intensity at 3 to 5 hours after surgery, lasts for 2 to 3 days, and then steadily subsides till day 7. Within 12 to 48 hours after surgery, postoperative swelling reaches its maximal strength and subsides between the fifth and seventh postoperative days. Trismus subsides when pain and edema decrease [López-Ramírez et al., 2012].

The current study's findings revealed that all groups experienced the most pain during the first two days following surgery. There was a significant difference between the days in each group after that, with the pain score tending to diminish over time until the seventh day. The study's findings also showed that the study group's pain scores were lower than those of the control group, with the difference being highly significant on the second and significant on the seventh day. The results of this study are in agreement with those of [Markovic and Todorovic2006; Aras et al.,2010; MarwahSafaa, 2019; Ferrante et al.,2013; Kazancioglu et al.,2014; Eshghpour et al.,2016], who observed that LLLT could minimize postoperative pain following surgical removal of the mandibular third molar. However, LLLT showed no beneficial effect on pain, according to [Amarillas-Escobar et al., 2010] and López-Ramrez et al., 2012] investigations findings. The results of this study showed that the difference in mouth opening between the study group

and the control group was significant on the second postoperative day (p=0.01) and non-significant on the seventh postoperative day (p>0.05), which was consistent with the findings of [Eroglu & Keskin, 2016; Aras et al., 2010] who found that LLLT has a positive effect on trismus. On the other hand, researchers [Momeni et al., 2022; Marwah Safaa et al., 2019; López-Ramrez et al., 2012] reported that LLLT had no positive impact on trismus.

In the present study, a difference in swelling was highly significant in the study group on the second postoperative day but not on the seventh. According to [Aras et al., 2010 ; Ferrante et al., 2013 ; Eshghpour et al., 2016], low-level laser therapy can reduce facial swelling, which is compatible with the findings of this study. Contrary to the findings of this study, [Momeni et al., 2022] and [Farhadi et al., 2017] found no statistically significant difference in swelling between the study and control groups.

11. Conclusion

As a result, LLLT using a dual-wavelength (810,980nm) diode laser with a 0.4W power provides a therapeutic option with clinically beneficial effects on pain, edema, and trismus, which are likely to arise after extraction of an impacted molar. Directly following the removal of an impacted molar, physicians might use a single session of LLLT using a diode laser to enhance healing and anti-inflammatory processes.

References

Ali S. Abdul-Kareem,Ali H. Al-Hussaini. (2019) Effect of platelet rich-fibrin on alveolar osteitis incidence following surgical removal of impacted mandibular third molars: A comparative study, journal of baghdad college dentistry, 34 63-70

Amarillas-Escobar, E. D., Toranzo-Fernández, J. M., Martínez-Rider, R., Noyola-Frías, M. A., Hidalgo-Hurtado, J. A., Serna, V. M., ... & Pozos-Guillén, A. J. (2010). Use of laser therapy after surgical removal of lower third molars impacted. J Oral Maxillofac Surg, 68, 319-324.

Anand, V., Gulati, M., Govila, V., & Anand, B. (2013). Low level laser therapy in the treatment of aphthous ulcer. Indian Journal of Dental Research, 24(2), 267.

Aoki, A., Mizutani, K., Schwarz, F., Sculean, A., Yukna, R. A., Takasaki, A. A., ... & Izumi, Y. (2015). Periodontal and peri-implant wound healing following laser therapy. Periodontology 2000, 68(1), 217-269.

Aras, M. H., & Güngörmüş, M. (2010). Placebo-controlled randomized clinical trial of the effect two different low-level laser therapies (LLLT)—intraoral and extraoral—on trismus and facial swelling following surgical extraction of the lower third molar. Lasers in medical science, 25, 641-645.

Barone, A., Marconcini, S., Giacomelli, L., Rispoli, L., Calvo, J. L., & Covani, U. (2010). A randomized clinical evaluation of ultrasound bone surgery versus traditional rotary instruments in lower third molar extraction. Journal of oral and maxillofacial surgery, 68(2), 330-336.

Bayar, G. R., Kuo, S., Marcelo, C. L., & Feinberg, S. E. (2016). In vitro development of a mucocutaneous junction for lip reconstruction. Journal of Oral and Maxillofacial Surgery, 74(11), 2317-2326.

Carroll, J. D., Milward, M. R., Cooper, P. R., Hadis, M., & Palin, W. M. (2014). Developments in low level light therapy (LLLT) for dentistry. Dental Materials, 30(5),
465-475.

Domah F, Shah R, Nurmatov UB, Tagiyeva N. (2021) The use of low-level laser therapy to reduce postoperative morbidity after third molar surgery: a systematic review and meta-analysis. Journal of Oral and Maxillofacial Surgery. 1;79(2):313-e1

Eroglu, C. N., & Keskin Tunc, S. (2016). Effectiveness of single session of low-level laser therapy with a 940 nm wavelength diode laser on pain, swelling, and trismus after impacted third molar surgery. Photomedicine and laser surgery, 34(9), 406-410

Fabre, H. S., Navarro, R. L., Oltramari-Navarro, P. V., Oliveira, R. F., Pires-Oliveira, D. A., Andraus, R. A., ... & Fernandes, K. B. (2015). Anti-inflammatory and analgesic effects of low-level laser therapy on the postoperative healing process. Journal of physical therapy science, 27(6), 1645-1648.

FARHADI, F., ESLAMI, H., MAJIDI, A., FAKHRZADEH, V., GHANIZADEH, M. & KHADEMNEGHAD, S. (2017). Evaluation of adjunctive effect of low-level laser Therapy on pain, swelling and trismus after surgical removal of impacted lower third molar: A double blind randomized clinical trial. Laser therapy, 26, 181-187.

Ferrante, M., Petrini, M., Trentini, P., Perfetti, G., & Spoto, G. (2013). Effect of low-level laser therapy after extraction of impacted lower third molars. Lasers in medical science, 28(3), 845-849.

Gelesko S, Long L, Faulk J, Phillps C, Dicus C, White RP Jr. (2011) Cryotherapy and topical minocycline as adjunctive measures to control pain after third molar surgery: an exploratory study. Journal of oral and maxillofacial surgery 2011;69:e324–e332.

Grossi, G. B., Maiorana, C., Garramone, R. A., Borgonovo, A., Creminelli, L., & Santoro, F. (2007). Assessing postoperative discomfort after third molar surgery: a prospective study. Journal of oral and maxillofacial surgery, 65(5), 901-917.

Hamblin, M. R. (2016). History of low-level laser (light) therapy. In Handbook of Low-Level Laser Therapy (pp. 53-70). Jenny Stanford Publishing.

He, W. L., Yu, F. Y., Li, C. J., Pan, J., Zhuang, R., & Duan, P. J. (2015). A systematic review and meta-analysis on the efficacy of low-level laser therapy in the management of complication after mandibular third molar surgery. Lasers in medical science, 30, 1779-1788.

Kazancioglu, H. O., Ezirganli, S., & Demirtas, N. (2014). Comparison of the influence of ozone and laser therapies on pain, swelling, and trismus following impacted third-molar surgery. Lasers in medical science, 29, 1313-1319.

Kuboyama, N., Ohta, M., Sato, Y., & Abiko, Y. (2014). Anti-inflammatory activities of light emitting diode irradiation on collagen-induced arthritis in mice (a secondary publication). Laser therapy, 23(3), 191-199.

Lago-Méndez, L., Diniz-Freitas, M., Senra-Rivera, C., Gude-Sampedro, F., Rey, J. M. G., & García-García, A. (2007). Relationships between surgical difficulty and postoperative pain in lower third molar extractions. Journal of oral and maxillofacial surgery, 65(5), 979-983.

Lobo, T. M., & Pol, D. G. (2015). Evaluation of the use of a 940 nm diode laser as an adjunct in flap surgery for treatment of chronic periodontitis. Journal of Indian Society of Periodontology, 19(1), 43.

López-Ramírez, M., Vílchez-Pérez, M. Á., Gargallo-Albiol, J., Arnabat-Domínguez, J., & Gay-Escoda, C. (2012). Efficacy of low-level laser therapy in the management of pain, facial swelling, and postoperative trismus after a lower third molar extraction. A preliminary study. Lasers in medical science, 27, 559-566.

Marković, A. B., & Todorović, L. (2006). Postoperative analgesia after lower third molar surgery: contribution of the use of long-acting local anesthetics, low-power laser, and diclofenac. Oral Surgery, Oral Medicine, Oral Pathology, Oral Radiology, and Endodontology, 102(5), e4-e8.

Marwah Safaa, Ali & Al-Adili SS.(2019). Low Level Laser Therapy on Postoperative Trismus and Swelling after Surgical Removal of Impacted Lower Third Molar. Indian Journal of Public Health Research & Development. 1;10(9).

Momeni E, Kazemi F, Sanaei-Rad P. (2022)Extraoral low-level laser therapy can decrease pain but not edema and trismus after surgical extraction of impacted mandibular third molars: a randomized, placebo-controlled clinical trial. BMC Oral Health. 20;22(1):417.

Nagammai, N. (2022). Laser biomodulation in dentistry. International Journal of Oral Health Sciences, 12(1), 15.
Nogales, C. G., Ferrari, P. H., Kantorovich, E. O., & Lage-Marques, J. L. (2008). Ozone therapy in medicine and dentistry. J Contemp Dent Pract, 9(4), 75-84.

Oliveira Sierra S, MeloDeanaA, Mesquita Ferrari RA, Maia Albarello P, Bussadori SK, SantosFernandes KP, et al.(2013) Effect of low-level laser therapy on the post surgical inflammatory process after third molar removal: Study protocol for a double-blind randomized controlled trial. Trials ;14:373

Pergolini, D., Del Vecchio, A., Palaia, G., Rocchetti, F., Cefalà, R., De Angelis, R., ... & Romeo, U. (2022). Photobiomodulation after Surgical Extraction of the Lower Third Molars: A Narrative Review. Oral, 2(1), 18-28.

Ra'ed Mohammed Ayoub Al-Delayme,Waleed Kh. Ismael,Mona AbdulhadeeAlsafi,(2013) Factors associated with facial swelling severity following impacted lower third molar surgery: A prospective study, journal of baghdad college dentistry, 25 122-128

Raouaa, B., Sameh, S., Nour, B. M., Abdellatif, C., & Jamil, S. (2013). Effects of low-level-laser therapy versus corticotherapy on pain, trismus and edema after surgical removal of third mandibular molars: A comparative study. Family Med Medical Sci Res, 2(111), 2.

Sigaroodi, A. K., Motevasseli, S., Maleki, D., Maleki, D., & Fard, R. S. (2023). Low-level laser and management of common complications after the mandibular third molar surgery: A double-blind randomized clinical trial. Dental Research Journal, 20.

Thaer Abdul Lateef, Salwan Y. H. Bede, Jamal A. Mohammed.(2010) The influence of prophylactic Dexamethasone on postoperative swelling and trismus following impacted mandibular third molar surgical extraction, journal of baghdad college dentistry 22 85-90

Zhang, W., Li, J., Li, Z. B., & Li, Z. (2018). Predicting postoperative facial swelling following impacted mandibular third molars extraction by using artificial neural networks evaluation. Scientific reports, 8(1), 1-9.
.

فعالية العلاج بالليزر منخفض المستوى لتقليل المضاعفات بعد خلع الضرس الثالث المطمور من الفك السفلي

أسامة عبدالكاظم علي[1]،* ، زينب فاضل مهدي[1]، بلسم سعدي عبدالواحد[2]

[1] معهد الليزر للدراسات العليا، جامعة بغداد، بغداد، العراق
[2]مستشفى مدينة الامامين الكاظمين التعليمي

*البريد الالكتروني للباحث: Usama.abdulkadim1202a@ilps.uobaghdad.edu.iq

الخلاصة

مقدمة : يعتبر خلع الضرس الثالث من الفك السفلي علاجًا روتينيًا. المضاعفات الأكثر شيوعًا بعد هذا الإجراء هي الألم وتشنج عضلات الفكين وانتفاخ الوجه. لمعالجة هذه المضاعفات ، تم استخدام الأدوية العلاجية ؛ ومع ذلك ، نظرًا لآثارها الجانبية ، فقد تطورت العلاجات غير الدوائية ، مثل العلاج بالتبريد ، وحزم الثلج ، والعلاج بالليزر منخفض المستوى (LLLT) ، والأوزون ، والتي تعالج هذه المضاعفات دون آثار جانبية. يحث الليزر منخفض المستوى على التحفيز الحيوي ، ويسرع تجديد الأنسجة ،

ويعزز التئام الجروح ، ويقلل من الألم والتورم من خلال تأثير مضاد للالتهابات. وذلك لأن الليزر منخفض المستوى يزيد من نشاط البلعمة ، وعدد وقطر الأوعية اللمفاوية ، ويقلل من نفاذية الأوعية الدموية ويعيد وظيفة الشعيرات الدموية الدقيقة.

الهدف : كان الغرض منه هو تقييم آثار العلاج بالليزر منخفض المستوى على المضاعفات الناتجة عن جراحة الضرس الثالث المطمور.

المواد والطرق : تم تسجيل 30 مريضاً في الدراسة الحالية وتم تقسيمهم بشكل عشوائي إلى مجموعتين متساويتين. تضمن الفحص السريري قبل الجراحة قياس الحد الأقصى لفتح الفم وقياسات الخد. تم تقييم موضع وتكوين الضرس الثالث السفلي المطمور ، والعظم المحيط ، والقناة السفلية ، والأسنان المجاورة باستخدام الأشعة السينية البانورامية. بعد الجراحة ، تم تطبيق العلاج بالليزر منخفض المستوى بشكل إضافي وداخل الفم. في اليومين 2 و 7 ، بعد الجراحة ، تم تقييم الحد الأقصى لفتح الفم وفحص الأبعاد مرة أخرى. تم استخدام الإحصائيات لتقييم كل قراءة.

الاستنتاجات : تشير النتائج إلى دلالة إحصائية للألم ، وتشنج عضلات الفك ، والتورم.

.

IJL, Issue 1, Vol. 23, 2024
https://doi.org/10.31900/ijl.v23i1.409

Research Article

IRAQI JOURNAL OF LASER

Refractive index biosensor based on offset technique of coreless fiber

Saraa J. Aldulimi*, Hanan J. Taher

Institute of Laser for Postgraduate Studies, University of Baghdad, Baghdad, Iraq
** Email address of the Corresponding Author: saraa.najm2101m@ilps.uobaghdad.edu.iq*

Article history: Received 27 Jul. 2023; Revised 5 Oct. 2023; Accepted 15 Oct. 2023; Published online15 Jun. 2024

Abstract: This paper suggested a biosensor structure using an offset technique between two similar coreless fiber (CF) segments spliced between two single-mode fibers (SMF) for refractive index (RI) measurement of the liquid pharmaceutical, where experimented with different lengths of CF sections for 10 mm, 15mm, 20 mm, and 25 mm with different offsets for 2.6 µm, 6.4 µm, and 18.3 µm of symmetric CF sections. This sensor tests different refractive indices (1, 1.333, 1.337, 1.369, 1.393) of liquid pharmaceuticals The wavelength shifting increases with decreasing length or displacement of offset. The highest sensitivity was achieved, 255.5 nm/RIU, with the smallest sensor size, corresponding to the highest refractive index of 1.393 for the Histadin syrup drug, obtained using the optimal length and offset. This sensor has the capability to detect various refractive indices of chemicals and biochemical liquids. Advantages of the proposed sensor include high sensitivity, adaptability, enabling faster real-time measurements, ease of manufacturing and operation, compact size, lightweight design, and low cost.

Keywords: Refractive index sensor, optical fiber biosensor, offset technique, coreless Fiber.

1. Introduction

Optical fiber biosensors (OFBS) are attracting an increasing number of researchers due to their advantages of high sensitivity and flexibility, enabling quicker and real-time measurements, ease of fabrication and operation, small size, lightweight, and low cost. This is because OFBS has a wide range of applications in the healthcare industry, including blood pressure monitoring, blood sugar monitoring, pharmaceutical dose control, drug identification, food control, and many other applications that require this type of sensor [1, 2].

Optical biosensors are technologies that track changes in light properties like refraction index, absorption, fluorescence, or light scattering brought on by the interaction that recognizes biological or chemical reaction processes by producing signals proportional to the concentration of an analytic in the reaction. Biological materials (such as enzymes, antibodies, antigens, receptors, nucleic acids, cells, and complete tissues) are analyzed using biosensors to assess the identity of illegal substances and to identify the formation of new pharmaceuticals [3-5]. Most optic fiber sensor structures achieve the principle work of Mach-Zehnder Interferometer MZI, which has been implemented using different fabrication techniques

such as optical fiber tapers [6, 7]. thin core fibers (TCF) [8], long-period grating cascade structures [9, 10] Photonic crystal fiber (PCF) [11], coreless fiber (CF)[12,13], and offset technique [14-16]. The offset structure of similar coreless fiber splits the light into two parts: one of them is the fundamental core mode propagating in the CF represented as core mode, and the other one is the drug sample represented as cladding modes; the different optical paths of the residual core mode and cladding modes could form an intermodal MZI [24]. The transmission spectrum of the interferometer is simply expressed as that of a two-mode interference:

$$I = I_{co} + I_{cl} + 2\sqrt{I_{co}\ I_{cl}\ \cos\emptyset} \quad (1)$$

Where I is the light intensity of the output light, Ico represents the intensities of the core, Icl defines as the cladding mode, and $\emptyset$ = is the phase difference of the two interference modes, which can be expressed as [25]:

$$\emptyset = \frac{2\pi(nco - ncl)L_{eff}}{\lambda} \quad (2)$$

Where nco represents the RIs of the optical fiber core, ncl is the effective cladding, L_{eff} represents the effective length of the two-mode interference paths, and λ is the wavelength in vacuum.

When $\emptyset = (2i + 1)\ \pi$, i is a positive integer, the interference dip appears, and the wavelength dip can be expressed as:

$$\lambda = \frac{2\pi(nco - ncl)Leff}{(2i + 1)\ \pi} \quad (3)$$

From Eq. 3, it can be seen that for the fixed interference path length, the position of the interference dip depends on the effective RI difference between the core and the cladding mode [26]. When the external environment RI changes, the effective RI of the cladding mode will change, while the effective RI of the fiber core mode will not change, which will lead to a change in the position of the wavelength dip [26], [25]. CF interacts with SMF to efficiently stimulate high-order cladding modes[17]. Meanwhile, CF can be used as a coupler in the sensor to split light and combine light. [18,19]. This work used the offset technique, compared to the other techniques, the offset technique has a simpler fabrication process with less complicated equipment.

In this study, was proposed a new structure has small size of the sensing region makes it easier to work with less susceptible to breakage, less consumption of coreless optical fiber when fabricating the structure, less waste of samples to be tested for their refractive index and lower cost compared to offset structure in previous studies. This structure achieved the highest sensitivity 255.5 nm/RIU, a smaller size due to using only 20 mm of sensing arm from CF segments. In the previous studies [20] proposed a single-mode fiber (SMF) sensor based on a core-offset inter-modal interferometer whose refractive index sensitivity was -64.889 nm/RIU in 2014 Jingli Fan et al [20]. In another study proposed a highly sensitive Mach-Zehnder interferometric refractive index sensor based on core-offset single-mode fiber the higher refractive index sensitivity of 78.7nm/RIU in 2015 Yong Zhao et al [21], while the proposed refractive index sensor based on the lateral offset of coreless silica interferometer achieved a higher refractive index sensitivity was 750 nm/RIU in 2018 Nur Faizzah et al. [22], and finally suggested S and U shape offset studying of the refractive index sensor based on coreless fiber higher sensitive was achieved in a novel S-shape equal 98.768 nm/RIU in 2022 Aya R. Mejble et al. [23].

This study showed the benefits of offset with similar sections of coreless fiber the sensitivity increasing when decreasing the length of coreless fiber sections. That achieved a smaller size of sensor device easy fabrication, easy to carry, low cost and it can link with accurate devices to be used in other applications. We used a structure for biosensor applications to detect the identity of liquid pharmaceutical droops and syrups, which, when increasing the refractive index, increases the wavelength shifting in a red direction.

2. Sensor Fabrication Process

The optical fiber sensing structure is shown in Figure 1, where d is the offset displacement, and L is the length of sensing regain. The single mode coreless-coreless single mode (SCCS) sensor structure comprises two segments of single-mode fiber (SMF) and two segments of coreless fiber CF in between. The four segments are spliced together. The schematic diagram of the (SCCS) sensor configuration is depicted in Figure 2 (a) the Left side for SMF input auto-splicing with CF, (b) the Right side for SMF input auto-splicing with CF, and (c) the offset splicing point of CF.

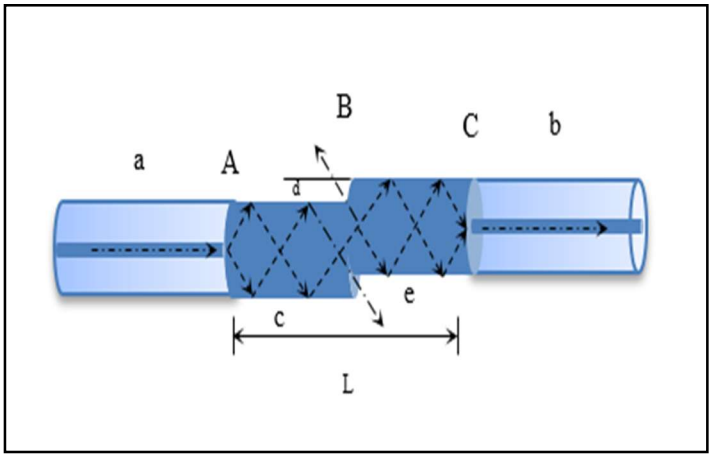

Fig.1. Schematic of sensing structure: A is the auto-splice point, B is the offset point, and C is the auto-splice point. c and e are similar sections of coreless fiber (CF). a, b are lead-in and lead-out of single-mode fibers (SMF).

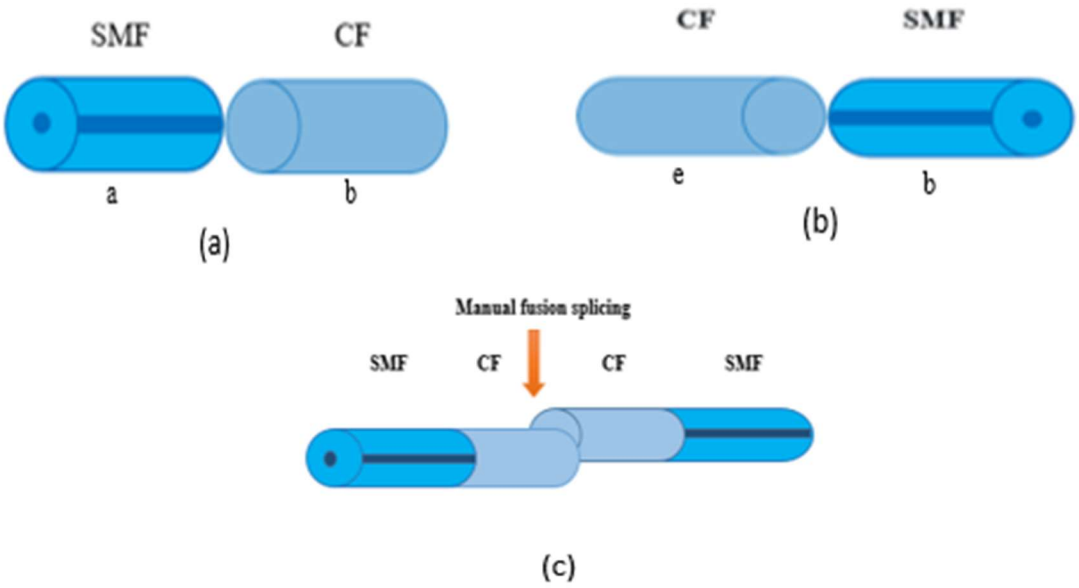

Fig.2: (a) Left side for SMF input auto splicing with CF, (b) Right side for SMF input auto splicing with CF and (c) Offset splicing point of CF.

The different offsets tested (2.6 µm, 6.4 µm, 12.1 µm, 18.3 µm), were tested by splicing each one of them with the different lengths of similar CF (10mm, 15 mm, 20mm, and 25mm). The offset point displacement was measured by microscope magnification 10X, and the length of CF was measured by a ruler. A microscope images for different offset distances (d) were shown in Figure 3 (a) d= 2.6 µm, (b) d= 6.4 µm, (c) d= 12.1 µm, and (d) d= 18.3.

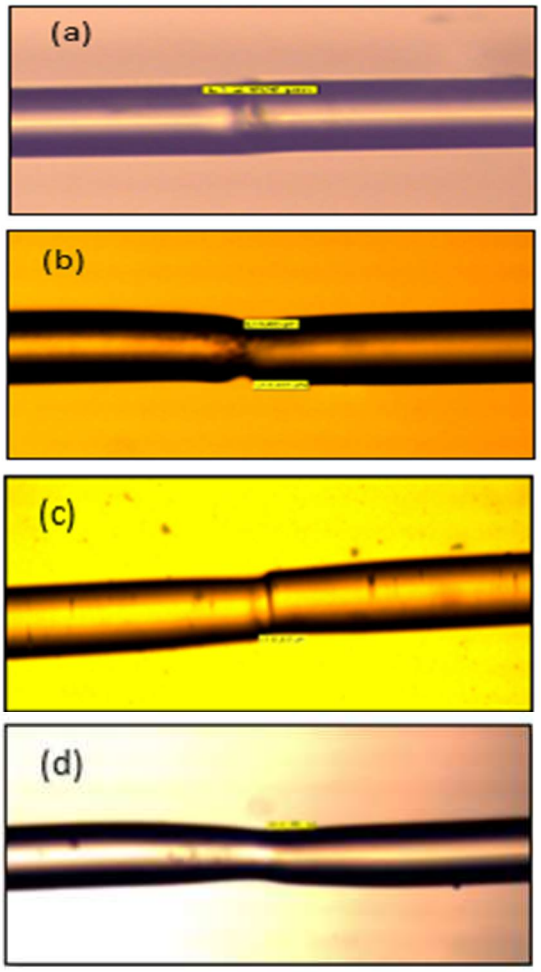

Fig.3: A microscope images for different offset distances, (a) offset for 2.6 µm, (b) offset for 6.4 µm, (c) offset for 12.1 µm, (d) offset for 18.3 µm.

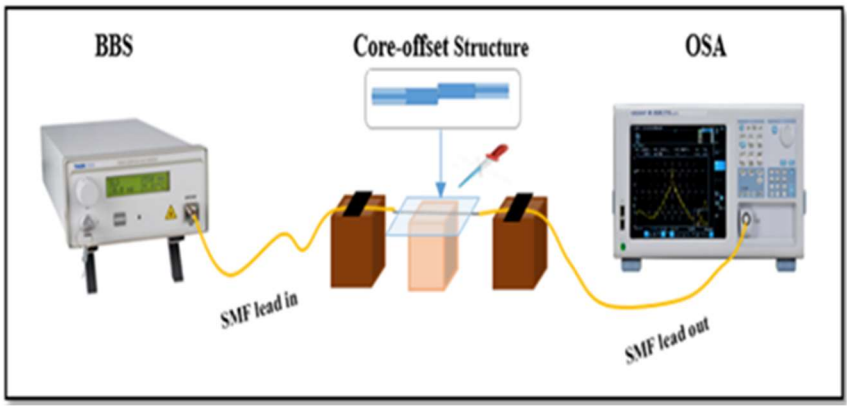

Fig.4: Sensor setup system.

The sensor setup system is shown in Figure 4. The structure configuration consisted of two SMFs lead in /lead out, and with SMFs lead in auto-spliced first section of CF (the coreless fiber is a special type of multimode fiber with uniform refractive index 1.444) (Thorlabs), a second symmetric section of CF that spliced with SMFs lead out and was spliced the two sections offset between them shows in figure 2 (a, b and c). The liquids pharmaceutical samples that were used for testing (Dististuled water, Nazordin droops, Allermine syrup, and Histadin syrup) have different RI (1.333, 1.335, 1.379, and 1.383) respectively. That is measured by (the ATAGO Refractometer). The sensor encompasses a broadband source (BBS) Thorlabs S5FC10055) with a wavelength range of (1400 nm to 1650 nm). To identify the response transmission spectra of the pharmaceuticals liquid sensor, BBS was joined to the SMF-CF-CF-SMF (SCCS) structure from the first section of SMF, and the second section of this structure was joined to an optical spectrum analyzer (OSA YOKOGAWA AQ6370C) display in Figure 4. A fusion splicer (Fujikura FSM-60S) with manual mode CF-CF offset splicing was used as shown in Figure 5.

Fig.5: CF-CF offset splicing.

3. Experiment results and dissection

In this work, the effect of length and offset distances on sensor sensitivity was investigated in this study were tested for each length (10mm, 15mm, 20mm, and 25mm) with different offsets (2.6 µm, 6.4 µm, 12.1 µm, 18.3 µm).

The sensitivity of the SCCS sensor for each offset was measured by wavelength shifting. The RI biosensor sensing performance was investigated as shown in Figure 6 (a, b, c, and d), Figure 7 (a, b, c and d), Figure 8 (a, b, c, and d), and Figure 9 (a, b, c and d) and Tables (1, 2, 3, and 4).

A. Experiment results and dissection for L=10 mm:

The first structure for L=10 mm with offset d=2.6 µm achieved higher sensitivity, which equaled 255.5 nm/RIU with wavelength shifts 23 nm, and the second structure with offset distance d=6.4 µm achieved sensitivity equaled 203.3 nm/RIU with wavelength shifts 18.3 nm while the third structure with offset distance 12.1 µm was achieved 218.8 nm/RIU with wavelength shifts 19.7 nm but it was unstable, finally the forth structure for 18.3 µm where the absence of dips this indicates that this offset with this length is not suitable.

Figure 6 displays how transmitted power varies with wavelength shifting for length L= 10 mm with each offset distance (a) d=2.6 µm (b) d= 6.4 µm, (c) d=12.1 µm, and (d) d=18.3 µm of similar sections of CF when the RI changes from 1 to 1.393.

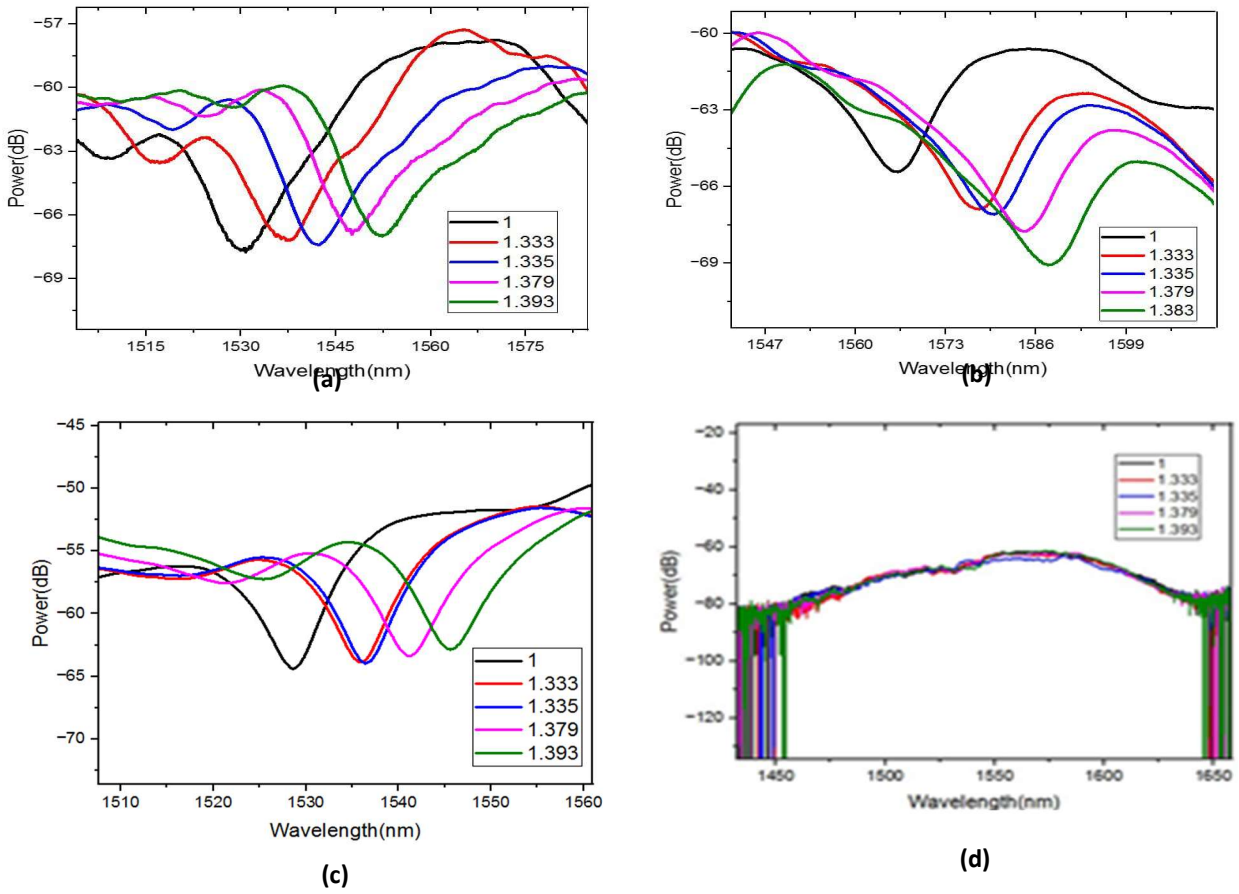

Fig.6: The Wavelength shifting at L=10 and variable d: (a) d=2.6 µm (b) d= 6.4 µm, (c) *d*=12.1 µm, and (d) *d*=18.3 µm.

Table 1. displays the wavelength shifts for L=10 mm at each offset distance.

Offset distance (µm)	2.6	6.4	12.1	18.3
Sensitivity (nm/RIU)	255.5	203.3	218.8	-
Wavelength shifts (nm)	23	18.29	19.7	-

B. Experiment results and dissection for L=15 mm

The first structure for this length with offset d=2.6 µm achieved a sensitivity equaled 222.7nm/RIU with wavelength shifts 20 nm, and the second structure for offset d=6.4 µm achieved a sensitivity equaled 227.7 nm/RIU with wavelength shifts 20.5 nm. In contrast, the third structure for offset 12.1 µm the absence of dips this indicates that this offset with this length is not suitable. Finally, the fourth structure for offset 18.3 µm achieved 231.1 nm/RIU with wavelength shifts 20.8 nm. Figure 7 displays the wavelength shifts for length L= 15 mm with each offset distance (a) d=2.6 µm (b) d= 6.4 µm, (c) *d*=12.1 µm, and (d) *d*=18.3 µm of similar sections of CF when the RI changes from 1 to 1.393.

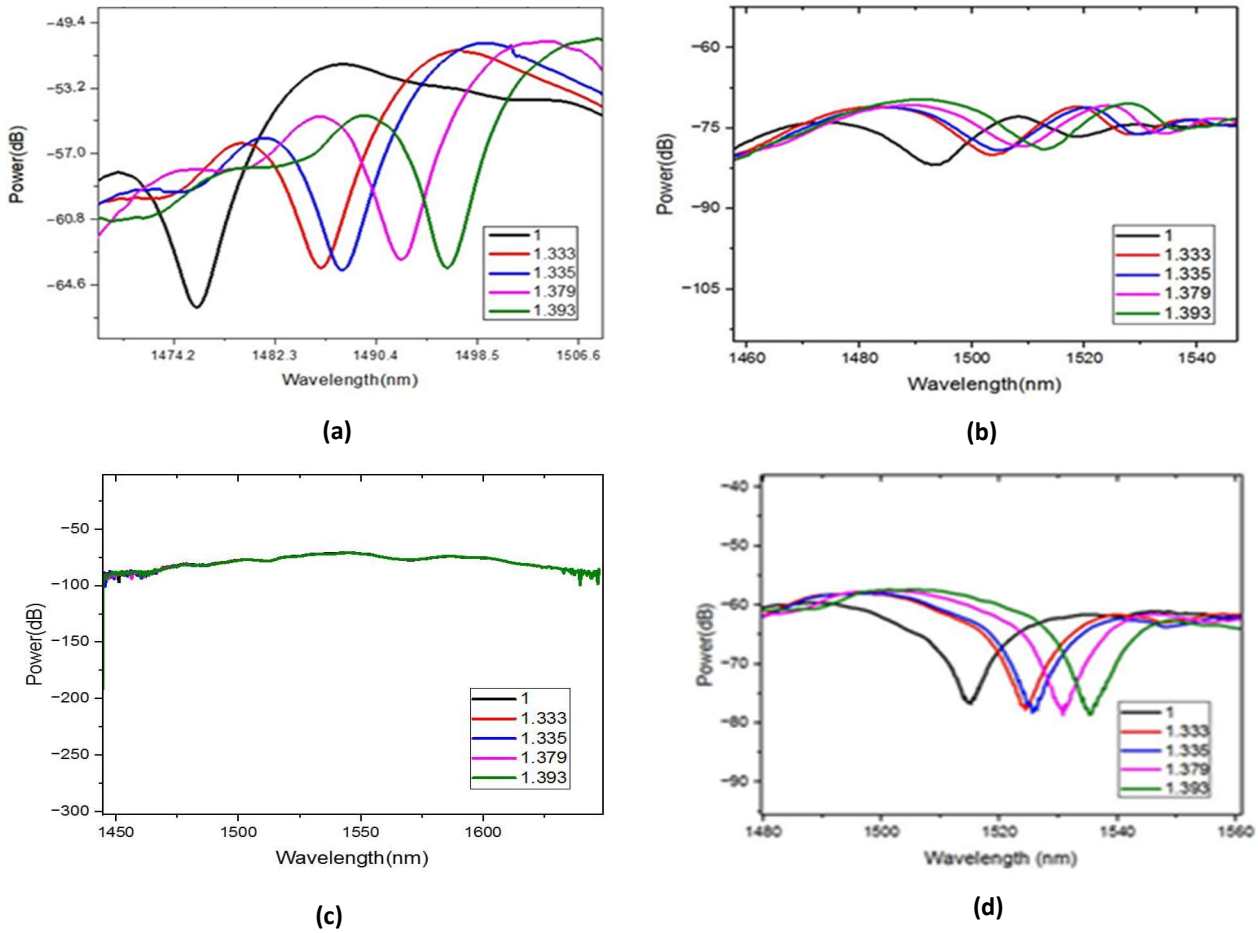

Fig.7: The Wavelength shifting at L=15 for offset distance d: (a) d=2.6 μm (b) d= 6.4 μm, (c) *d*=12.1 μm, and (d) *d*=18.3 μm.

Table 2. displays the wavelength shifts for L=15 mm at each offset distance.

Offset distance (μm)	2.6	6.4	12.1	18.3
Sensitivity (nm/RIU)	222.7	227.7	-	231.1
Wavelength shifts (nm)	20	20.5	-	20.8

C. Experiment results and dissection for L=20 mm

The first structure for this length with offset d=2.6 μm achieved a sensitivity equaled 212.7nm/RIU with wavelength shifts 19 nm, and the second structure for offset d=6.4 μm achieved a sensitivity equaled 214.4 nm/RIU with wavelength shifts 19.3 nm while the third structure for offset 12.1 μm the absence of dips this indicates that this offset with this length is not suitable, finally the forth structure for offset 18.3 μm achieved 231.1 nm/RIU with wavelength shifts 20.8 nm. Figure 8 displays the wavelength shifts for length L= 20 mm with each offset distance (a) d=2.6 μm (b) d= 6.4 μm, (c) *d*=12.1 μm, and (d) *d*=18.3 μm of similar sections of CF when the RI changes from 1 to 1.393.

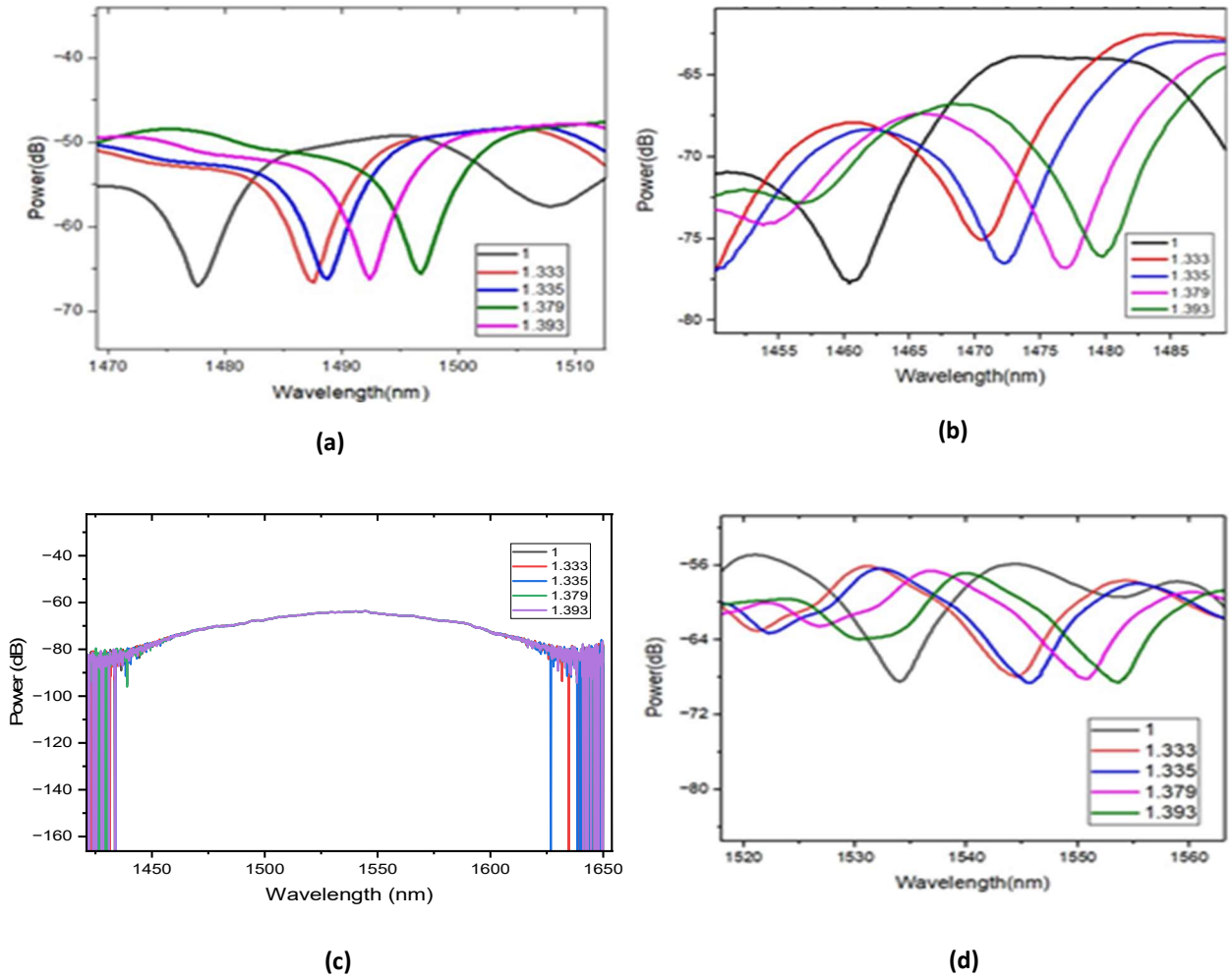

Fig. 8. The Wavelength shifting at L=20 for offset distance d: (a) d=2.6 μm (b) d= 6.4 μm, (c) *d*=12.1 μm, and (d) *d*=18.3 μm.

Table 3. displays the wavelength shifts for L=20 mm at each offset distance.

Offset distance (μm)	2.6	6.4	12.1	18.3
Sensitivity (nm/RIU)	212.7	214.4	-	227.3
Wavelength shifts (nm)	19	19.3	-	20.4

E. Experiment results and dissection for L=20 mm

The first structure for this length with offset d=2.6 μm achieved a sensitivity equaled 197.3 nm/RIU with wavelength shifts 17.8 nm, and the second structure for offset d=6.4 μm achieved a sensitivity equaled 190.4 nm/RIU with wavelength shifts 17.2 nm while the third structure for offset 12.1 μm achieved 220 nm/RIU with wavelength shifts 19.8 nm finally for offset18.3 μm the absence of dips this indicates that this offset with this length is not suitable, finally the forth structure for offset. Figure 9 displays the wavelength shifts for length L= 25 mm with each offset distance (a) d=2.6 μm (b) d= 6.4 μm, (c) *d*=12.1 μm, and (d) *d*=18.3 μm of similar sections of CF when the RI changes from 1 to 1.393.

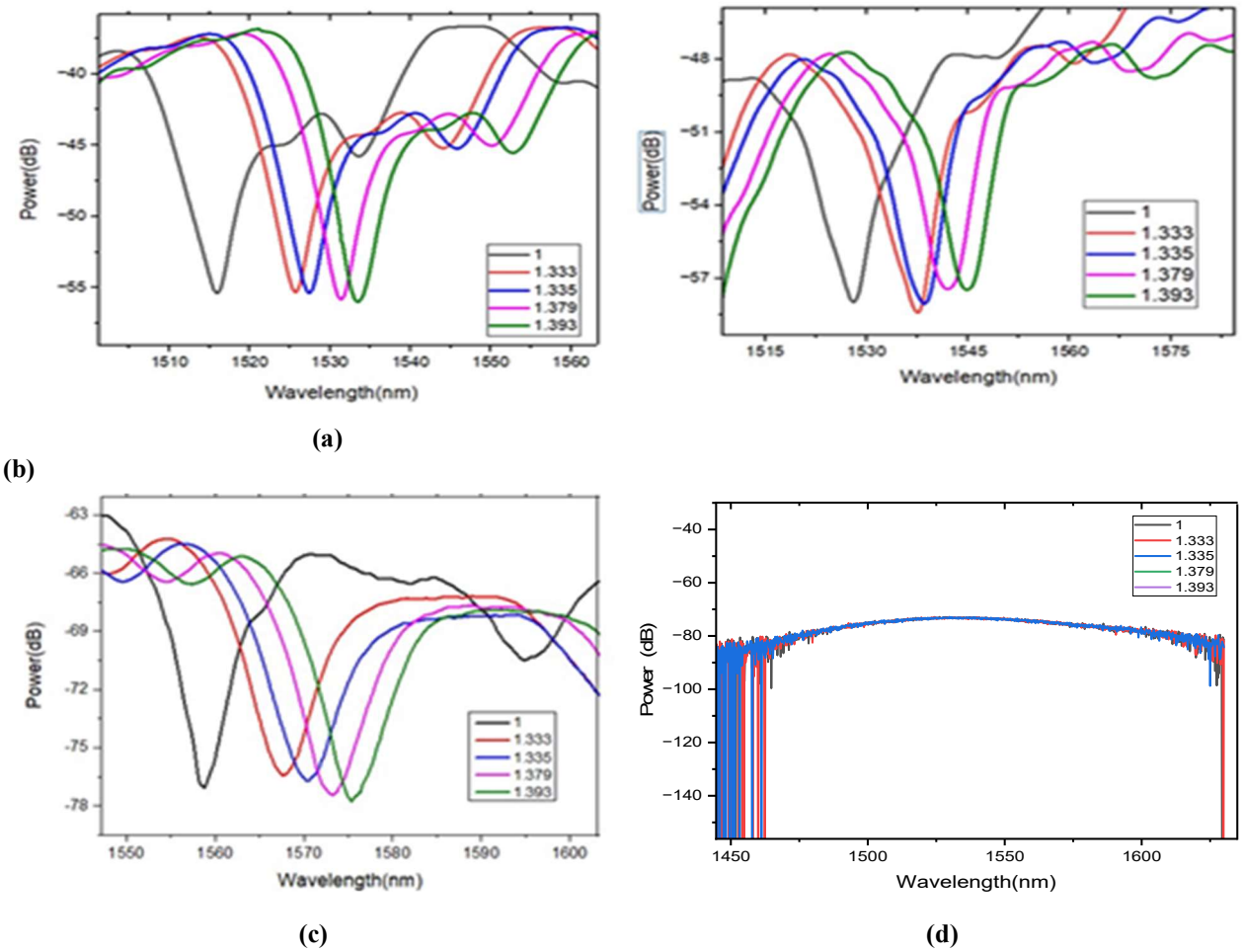

Fig.9: The Wavelength shifting at L=25 for offset distance d: (a) d=2.6 µm (b) d= 6.4 µm, (c) *d*=12.1 µm, and (d) *d*=18.3 µm.

Table 4. displays the wavelength shifts for L=25 mm at each offset distance.

Offset distance (µm)	2.6	6.4	12.1	18.3
Sensitivity (nm/RIU)	197.3	190.4	220	-
Wavelength shifts (nm)	17.8	17.2	19.8	-

We observed from this structure that sensitivity varied with length. The sensitivity increases as the length of the similar CF segments decreases. The wavelength shifts towards the long wavelength (red shift) when increasing the RI of samples. It is evident from the study of offset distance that the optimal offset at 2.6 µm with a length of CF-CF 10 mm. The reason for the high sensitivity of this new shape sensor is caused more evanescent waves could interact where there was more high order mode can be interference at three splicing areas when the refractive index was increased from 1 to 1.393. It has been proved that the offset and length of the CF - CF segments important parameters to increase the sensitivity of the sensor device. The refractive index biosensor synthesizes the merits of single mode coreless- coreless single mode (SMF-CF-CF-SMF) smart sensitive material with high flexibility in the design of accuracy in identifying and testing the construction of the drugs.

Table 5. Comparison between the sensitivities of this work and other RI sensors.

Sensor Structure	Offset Displacement	Refractive index range	Sensitivity (nm/ RIU)	Reference
Core offset FBG-SMF-SMF	8.1 µm	1.3232 to 1.3520	13.7592 nm/RI	[25]
SMF-peanut shape-SMF- core-off section-SMF	12 µm	1.333-1.373	-72.4	[26]
core offset SMF - SMF- SMF with tapered micrometers	7.5 µm	1.33 to 1.347.	16485 nm/RIU	[27]
SMF Taper-core-offset section AFMZI	6 µm	-	59.2	[28]
S and U-shapes study the effect of shape offset sensor	12.268 µm	1.33 to 1.38	98.786nm/RIU	[39]
SMF-CF-CF-SMF offset effect	2.6 µm	1 to 1.393	255.5 nm/RIU	In this study

4. Conclusions

In this work, a Refractive index biosensor based on the offset technique of coreless fiber was fabricated by the fusion splicer. The sensing part was composed of a similar section of CF that was spliced by the offset technique. The wavelength shifts of the sensor with different offset displacements and lengths were investigated. The experimental results showed that the sensitivity increased as the length of similar CF decreased, and when the offset displacement was 2.6 µm, and the length of a similar section of CF-CF was 10 mm, the RI sensitivity of 255.5 nm/RIU was obtained within the RI range from 1 to 1.393. The sensor exhibits the advantages of simple structure, high sensitivity, small size, low cost, and easy fabricating.

References

[1] A. Urrutia, K. Bojan, L. Marques, K. Mullaney, J. Goicoechea, S. James & S. Korposh. Novel highly sensitive protein sensors based on tapered optical fibers modified with Au-based nanocoatings. Journal of Sensors, 2016, 2016.
[2] Wang, B. T., & Wang, Q. (2018). An interferometric optical fiber biosensor with high sensitivity for IgG/anti-IgG immunosensing. Optics Communications, 426, 388-394.
[3] Damborsky, P.; Svitel, J.; Katrlik, J. Optical biosensors. Essays Biochem. 2016, 60, 91–100. [CrossRef] [PubMed
[4] Nikhil Bhalla, Pawan Jolly, Nello Formisano, and Pedro Estrela ‘’Introduction to biosensors‘’ Essays Biochem. 2016 Jun 30; 60(1): 1–8.
[5] Regatos, D. Biosensores ópticos de alta sensibilidad basados en técnicas de modulación plasmónica; Universidad de Santiago de Compostela: Barcelona, Spain, 2012.
[6] Lu, P.; Men, L.; Sooley, K.; Chen, Q. Tapered fiber Mach-Zehnder interferometer for simultaneous measurement of refractive index and temperature. Appl. Phys. Lett. 2009, 94, 131110.

[7] Li, B.; Jiang, L.; Wang, S.; Zhou, L.; Xiao, H.; Tsai, H.-L. Ultra-abrupt tapered Mach-Zehnder interferometer sensor. Sensors 2011, 11, 5729–5739.
[8] Li, L.; Li, X.; Xie, Z.; Liao, Z.; Tu, F.; Liu, D. Simultaneous measurement of refractive index and temperature using thinned fiber based Mach-Zehnder interferometer. Opt. Commun. 2012, 285, 3945–3949.
[9] Allsop, T.; Reeves, R.; Webb, D.J.; Bennion, I. A high-sensitivity refractometer based upon a long-period grating Mach-Zehnder interferometer. Rev. Sci. Instrum. 2002, 73, 1702–1705.
[10] Mata-Chavez, R.I.; Martines-Rios, A.; Torres-Gomez, I.; Selvas-Aguilar, R.; Estudillo-Ayala, J.M. Mach-Zehnder all Interferometer using two in-serie fattened gratings. Opt. Rev. 2008, 15, 230–235.
[11] Villatoro, J.; Finazzi, V.; Minkovich, V.P.; Pruneri, V.; Badenes, G.A. Temperature insensitive photonic crystal fiber interferometer for absolute strain sensing. Appl. Phys. Lett. 2007, 91, 091109.
[12] Wang, J.-N.; Tang, J.-L. Photonic crystal fiber Mach-Zehnder all Interferometer for refractive index sensing. Sensors 2012, 12, 2983–2995.
[13] Hu, L.M.; Chan, C.C.; Dong, X.Y.; Wang, Y.P.; Zu, P.; Wong, W.C.; Qian, W.W.; Li, T. Photonic crystal fiber strain sensor based on modified Mach-Zehnder interferometer. IEEE Photon. J. 2012, 4, 114–118.
[14] Sierra-Hernandez, J.M.; Castillo-Guzman, A.; Selvas-Aguilar, R.; Vargas-Rodriguez, E.; Gallegos-Arellano, E.; Guzman-Chavez, A.D.; Estudillo-Ayala, J.M.; Jauregui-Vazquez, D.; Rojas-Laguna, R. Torsion sensing setup based on three beam path Mach-Zehnder interferometer. Microw. Opt. Technol. Lett. 2015, 57, 1857–1860.
[15] Dong, X., Zeng, L., Chu, D., & Sun, X. (2022). Highly sensitive refractive index sensing based on a novel Mach-Zehnder interferometer with TCF-PCF composite structure. Infrared Physics & Technology, 123, 104134.
[16] Huerta-Mascotte, E., Sierra-Hernandez, J. M., Mata-Chavez, R. I., Jauregui-Vazquez, D., Castillo-Guzman, A., Estudillo-Ayala, J. M., ... & Rojas-Laguna, R. (2016). A core-offset Mach Zehnder interferometer based on a non-zero dispersion-shifted fiber and its torsion sensing application. Sensors, 16(6), 856.
[17] X. Yu, X. Chen, D. Bu, J. Zhang, S. Liu, In-fiber modal interferometer for simultaneous measurement of refractive index and temperature, IEEE Photon.Technol. Lett. 28 (2016) 189–192.
[18] Y. Zhao, X.-G. Li, L. Cai, A highly sensitive Mach-Zehnder interferometric refractive index sensor based on core-offset single mode fiber, Sens. Actuat. A: Phys. 223 (2015) 119–124.
[19] D.W. Duan, Y.J. Rao, L.C. Xu, T. Zhu, D. Wu, J. Yao, In-fiber Mach-Zehnder interferometer formed by large lateral offset fusion splicing for gases refractive index measurement with high sensitivity, Sens. Actuat. B: Chem. 160 (2011)1198–1202.
[20] D.W. Duan, Y.J. Rao, L.C. Xu, T. Zhu, D. Wu, J. Yao, In-fiber Mach-Zehnder interferometer formed by large lateral offset fusion splicing for gases refractive index measurement with high sensitivity, Sens. Actuat. B: Chem. 160 (2011) 1198–1202.
[21] Zhao, Y., Li, X. G., & Cai, L. (2015). A highly sensitive Mach–Zehnder interferometric refractive index sensor based on core-offset single-mode fiber. Sensors and Actuators A: Physical, 223, 119-124.
[22] Bahrain, N. F., Azmi, A. I., Abdullah, A. S., & Noor, M. Y. M. (2018).” Refractive index sensor based on lateral-offset of coreless silica interferometer”. Optics & Laser Technology, 99, 396-401.
[23] Aya R. Mejble, Hanan J. “S and U shape offset studying of the refractive index sensor based on coreless fiber”. Iraqi Journal of Laser, 2022, 21.2.
[24] Wahhab, A. A. A., Hammadi, Y. I., & Mansour, T. S. (2021). Design and Construct Nested Double Clad Multimode Fiber MZI (DC-MMF–NMZI) for Pregnancy Test. Journal of Mechanical Engineering Research and Developments, 44(10), 12-22.
[25] Zhang, Y. N., Sun, Y., Cai, L., Gao, Y., & Cai, Y. (2020). Optical fiber sensors for measurement of heavy metal ion concentration: A review. Measurement, 158, 107742.
[26] YAO, Qiqi, et al. Simultaneous measurement of refractive index and temperature based on a core-offset Mach–Zehnder interferometer combined with a fiber Bragg grating. Sensors and Actuators A: Physical, 2014, 209: 73-77.
[27] ZHOU, Yanfei; LIU, Yuan; ZHENG, Jie. An inline fiber Mach-Zehnder interferometer based on core offset and peanut shape for refractive index sensing. In: Optical Metrology and Inspection for Industrial Applications IX. SPIE, 2022. p. 396-403.
[28] LIAO, Yun-Cheng, et al. Ultrasensitive Microfiber Refractive Index Sensor Based on Mach-Zehnder Interference of Core Offset Structure. In: 2019 18th International Conference on Optical Communications and Networks (ICOCN). IEEE, 2019. p. 1-3.
[29] Aya R. Mejble* Hanan J. Taher. (2022). “ S and U shape offset studying of the refractive index sensor based on coreless fiber”. Iraqi Journal of Laser, 21(2), 33-40.

مستشعر معامل الانكسار الحيوي المعتمد على تقنية الأوفست للألياف عديمة النواة

سراء جمال إبراهيم* ، حنان جعفر طاهر

معهد الليزر للدراسات العليا، جامعة بغداد، بغداد، العراق

*البريد الالكتروني للباحث: saraa.najm2101m@ilps.uobaghdad.edu.iq

الخلاصة: اقترحت هذه الورقة بنية مستشعر حيوي باستخدام تقنية الإزاحة بين قطعتين متشابهتين من الألياف عديمة النواة (CF) مقسمة بين ليفين أحاديي الوضع لقياس حساسية معامل الانكسار للمستحضرات الصيدلانية السائلة. حيث تمت تجربة أطوال مختلفة لمقاطع CF لـ 10 ملم و15 ملم و20 ملم و25 ملم مع إزاحات مختلفة لـ 2.6 ميكرومتر و6.4 ميكرومتر و18.3 ميكرومتر لمقاطع CF المتناظرة. عند اختبار مؤشرات انكسار مختلفة (1، 1.333، 1.337، 1.369، 1.393) للمستحضرات الصيدلانية السائلة، يزداد الطول الموجي مع زيادة مؤشرات الانكسار، وتزداد الحساسية مع تقليل الطول أو الإزاحة. حيث تم تحقيق أعلى حساسية مع اصغر حجم للمتحسس هي 255.5 نانومتر/وحدة RIU، وهو ما يتوافق مع أعلى معامل انكسار قدره 1.393 لدواء شراب الهستادين، والذي تم الحصول عليه باستخدام الطول والإزاحة الأمثل. يتمتع هذا المستشعر الصغير بالقدرة على اكتشاف مؤشرات انكسار مختلفة للمواد الكيميائية والكيميائية الحيوية. يتمتع جهاز الاستشعار البيولوجي المقترح، ببنيته البسيطة وقدرات الاستشعار الخطية المحتملة، بالقدرة على التطور ليصبح أداة تنافسية وقابلة للتكيف لتحديد السوائل باستخدام معامل الانكسار. تشمل مزايا المستشعر المقترح الحساسية العالية والقدرة على التكيف، مما يتيح إجراء قياسات أسرع في الوقت الفعلي، وسهولة التصنيع والتشغيل، والحجم الصغير، والتصميم خفيف الوزن، والتكلفة المنخفضة.

IJL, Issue 1, Vol. 23, 2024
https://doi.org/10.31900/ijl.v23i1.416

Research Article

IRAQI JOURNAL OF LASER

Influence of scanning velocity on Co24.7Cr5Mo5.4W alloy built via selective laser melting on roughness properties

Raghad Ahmed Al-Aloos[1,2,*], Ziad A. Taha[1], Onur Çomakli[3]

[1]*Institute of Laser for Postgraduate Studies, University of Baghdad, Baghdad, Iraq*
[2]*Automated Manufacturing Dept., Al-Khwarizmi College of Engineering, University of Baghdad, 10071, Iraq*
[3]*Department of Mechanical Engineering, Faculty of Faculty of Engineering and Architecture, Erzurum Technical University, 25050, Erzurum*
* *Email address of the Corresponding Author: raghad@kecbu.uobaghdad.edu.iq*

Article history: Received 4 Sept. 2023; Revised 18 Oct. 2023; Accepted 19 Oct. 2023; Published online 15 Jun. 2024

Abstract: The utilization of Selective Laser Melting (SLM) in the production of intricate metal items has gained significant attention in the medical and dental sectors. Products created using SLM must possess surfaces that exhibit a high degree of smoothness. The objective of this research is to examine the impact of various laser process parameters, specifically the scan rate and hatch spacing, on the surface roughness of Co-Cr dental alloys fabricated in three dimensions (3D) by selective laser melting (SLM) technology. The results indicate that a scanning speed of 700 mm/s yields superior surface morphology and microstructure. The parameter investigation conducted in this paper resulted in the attainment of relative densities as high as 98.9% for the additively built workpieces. The present study focuses on investigating surface roughness in Co–Cr alloys fabricated using powder metallurgy techniques, namely selective laser melting.

Keywords: Selective Laser Melting technology, surface roughness, Co-Cr dental alloys.

1. Introduction

Selective Laser Melting (SLM) is a rapid prototyping technique that has been under development since the late 1980s and is applicable to a wide range of alloys [1-4]. The utilization of Selective Laser Melting (SLM) technology in the fabrication of metal powders is advised to achieve components with a high level of density, eliminating the necessity for additional thermo-mechanical procedures [5]. During the process of selective laser melting (SLM), the alloy's powder particles undergo complete melting with the application of a laser beam with varying energy or power levels [6]. Subsequently, the metal bath undergoes a transition from a liquid phase to a solid phase, leading to the development of physical-chemical and mechanical properties that are influenced by the specific processing technical parameters [7-10]. Selective Laser Melting (SLM) technology enables the production of metal components with intricate shapes [11-13] due to the technology's computer-aided design and computer-aided manufacturing (CAD/CAM) capabilities [14,15]. To facilitate the production of a component using Computer-Aided Design (CAD), it is important to engage in the creation of a three-dimensional design and subsequently generate a Standard Tessellation

Language (STL) file for the final part. Conversely, the Computer-Aided Manufacturing (CAM) component pertains to the physical processing of the part using specialized equipment [16-18]. Under these circumstances, it is advisable to utilize 3D printing or Rapid Prototyping (RP) technology to produce various industrial components, particularly metal elements used in medical prosthetics, including dental prostheses [19-22].

The technological parameters associated with selective laser melting (SLM) processing, namely scan speed and hatch spacing (H), have a significant impact on both the surface quality and mechanical qualities of metal parts [23-26]. The optimization procedure is necessary to determine the optimal values of these parameters, which are crucial for achieving the desired functional and durability qualities in the products obtained [27, 28]. As a result, it is imperative to exercise stringent control over laser processing parameters to achieve optimal roughness levels for the resulting surfaces. According to references [29, 30], certain post-processing activities conducted after selective laser melting (SLM) can be partially or completely omitted using this approach.

The objective of this experimental research is to investigate the effects of two technical parameters, namely scan speed (v scan) and hatching space (H), on the surface roughness of exterior surfaces in both non-mechanical grinding state and mechanical grinding state. In a recent study, Pupo et al. (2012) investigated the impact of different process parameters on the surface quality of Co-Cr alloys manufactured using selective laser melting (SLM). Hence, it is recommended to expand the scope of these assessments by incorporating comprehensive multi-layer formation studies. These experiments aim to investigate the impact of different processing parameters on the surface roughness of Co-Cr alloy products fabricated by Selective Laser Melting (SLM) technology. Hence, the primary objective of this laboratory investigation is to examine the impact of laser process parameters, specifically scan rate and scan hatching spacing, on the surface roughness of Co-Cr alloys made using selective laser melting (SLM) technology. These alloys are commonly employed in dental applications. The purpose was to examine the effects.

The surface has garnered significant attention in numerous research since it has been demonstrated that 90% of failures in engineering components are initiated by surface-related factors. These phenomena manifest themselves through mechanisms such as fatigue cracking, stress corrosion, wear, and erosion [31-38]. From the perspective of the medical and dental domains, the examination of the interaction between a surface and biological tissue raises the topic of attachment of microbiological organisms. Achieving complete surface smoothness is theoretically unattainable due to the inherent tiny texture left by the production components on any surface during the manufacturing process. The phenomenon being described is commonly known as surface texture or surface topography, which comprises a collection of elevated points and depressed areas, each characterized by distinct dimensions, intervals, and configurations (Blunt & Jiang, 2003).

A number of recent studies have been published, focusing on the application of selective laser melting (SLM) and its impact on the properties of products manufactured using CoCr powders. These studies investigate the influence of changing SLM process parameters on the features of the resulting products.
The study conducted by Hong et al. (2016) aimed to examine the impact of different laser process parameters, including laser power, scan rate, and scan-line spacing, on the surface roughness of a Co-Cr dental alloy. This alloy was fabricated using a three-dimensional (3D) printing technique known as selective laser melting (SLM). The experimental setup involved the utilization of a ytterbium fiber laser beam (specifically, the IPG YL-200 model) with a spot size measuring 0.08 mm and a maximum power output of 200 W. The laser beam was operated within an environment saturated with nitrogen gas, with a constant flow rate of 5 L/min. In the beginning, a test employing a single-line formation was conducted to ascertain the appropriate laser power (200 W) and scan rate (128.6 mm/s) that yielded beads with an optimal profile. The results of this work indicate that the surface quality of Co-Cr dental alloys manufactured by selective laser melting (SLM) is significantly influenced by laser process parameters. The prevention of balling during a single-line formation test was achieved by decreasing the laser intensity and increasing the scan rate. The surface quality of Co-Cr dental alloys produced by SLM is influenced by critical parameters such as laser power, scan rate, and scan-line spacing, as established by previous studies. The user did not provide any text to rewrite.

According to Tonellia et al. (2020), The samples under investigation were fabricated utilizing the selective laser melting (SLM) apparatus, namely the SISMA MYSINT100, which is equipped with a Yb-fiber laser operating at a wavelength of 1070 nm. The laser has a maximum power output of 200 W and can produce a focused spot with a nominal diameter of 50 µm. A diverse set of process parameters were considered to investigate a broad spectrum of energy densities (LED = 43.2–267.9 J mm−3). Therefore, the results have been categorized into three distinct groups based on the intensity of light-emitting diodes (LEDs): low (up to 100 J mm−3), medium (100−150 J mm−3), and high (150−270 J mm−3). A relationship was established between the value of LED (light-emitting diode) and various characteristics of parts produced using selective laser melting (SLM), including density, surface quality, microstructural features, and hardness.

Insufficient power output from the low LED results in incomplete melting of the feedstock particles, leading to a highly unstable liquid pool. Due to significant deficiencies in fusing, the SLM samples displayed a porosity level ranging from 1% to 7% in terms of area. Additionally, the top surface of these samples exhibited a high roughness with an average roughness (Ra) ranging from 13 µm to 7 µm. Furthermore, there was a notable variation in the microhardness of the samples, ranging from 18 HRC to 36 HRC. The utilization of medium and high light-emitting diodes (LEDs) has shown effective in achieving the complete fusion of all powder materials and the retrieval of intact sound components. Additionally, this process resulted in a significantly low level of porosity, ranging from 0.5% to 0.1%, and smoother upper surfaces with roughness average (Ra) values ranging from 5 to 2.5 micrometers. The primary flaws seen were gas porosities at the micro-scale. However, it should be noted that excessive energy density (LED > 200 J mm3) can lead to the occurrence of keyhole collapses. There appears to be no discernible correlation between the energy density and the quality of the lateral surfaces of the samples, as well as the size of the laser tracks, in both the transverse and longitudinal sections. The user did not provide any text to rewrite.
In their study, Marta Revilla et al. (2021) conducted a comparative analysis of the chemical composition, surface roughness, and ceramic shear bond strength between two distinct manufacturing procedures: subtractive (milled) and additive (SLM) groups. The specific manufacturing systems used in the additive group were EOS, 3D Systems Layer wise, Concept Laser 100W, and Concept Laser 200W. The focus of the investigation was on Co-Cr alloys. The chemical composition of milling and selective laser melting (SLM) Co-Cr alloys exhibited a notable disparity. The surface roughness of the Co-Cr specimens studied was found to be significantly influenced by both subtractive and additive manufacturing processes.

The study conducted tests on Co-Cr dental alloys produced by both the SML AM and milling techniques and determined similar values for ceramic bond strength. The user's text is not sufficient to rewrite in an academic manner.

2. Experiment

2.1 Characterization of Powders

In this investigation, the raw material utilized for the selective laser melting (SLM) technique was gas-atomized Co24.7Cr5Mo5.4W powder obtained from SENTESBIR, a research institution located in Turkey. The particles exhibit a mostly spherical morphology and are scattered throughout a variety of sizes, as evidenced by the Scanning Electron Microscope (SEM) images and histogram chart depicted in Figure 1. The mean diameter of particles within a certain size distribution is 30 µm, with a range spanning from 15 µm to 45 µm. Table 1 presents the chemical composition of the Co24.7Cr5Mo5.4W powder used in this study, as received from the manufacturer's datasheet.

2.2 Production of SLM samples

The experimental procedure involved the utilization of an industrial Selective Laser Melting (SLM) machine, namely the Mlab cusing R model manufactured in Germany. This machine was employed to fabricate the desired alloy in accordance with the predetermined shape specified by Computer-Aided Design (CAD) software.

Table 1. Chemical composition of Co24.7Cr5Mo5.4W powder.

Element	Co	Cr	W	Mo	Si
Percentage (wt%)	63.9	24.7	5.4	5	<1

Table 2. Physical mechanical properties of Co24.7Cr5Mo5.4W of powder.

Flowability (gr)	Density (gm/cm^3)	Thermal expansion coefficient (CTE) (1/K)	Melting range (°C)	Tensile strength (MPa)	Yield strength (MPa)	Youngs Modulus (GPa)
14s/50	8.50	12.9×10^{-6}	1380-1420	1150-1400	790-1000	210

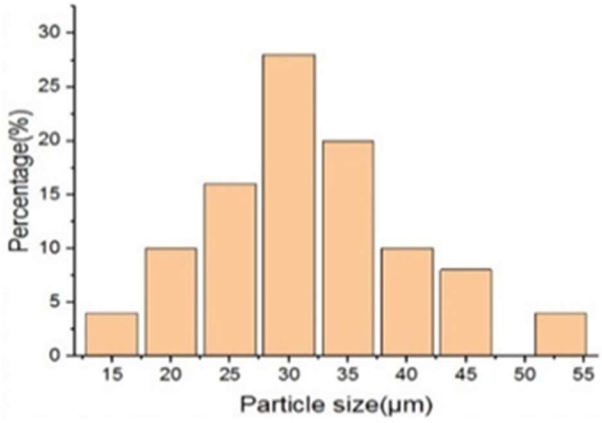

Fig. 1: SEM for the particle size and shape for the employed Co24.7Cr5Mo5.4W powder.

A total of eight sets of samples were generated, with each set consisting of three specimens measuring 15 (L) × 15 (W) × 4 (H) mm. The SLM system utilizes a continuous wave Ytterbium fiber laser to induce the melting of particles on the powder layer in a linear scanning pattern. The thickness of each layer is 25 μm, and these layers are printed using a zero-orientation building (0o). The initial coating of powder was evenly distributed onto a substrate composed of stainless steel. The procedure was iterated multiple times till achieving the ultimate thickness of the sample, which measured 4 mm. The process of selective laser melting (SLM) was conducted under controlled conditions, with a consistent laser output of 100 W, within an environment enriched with nitrogen. The individual effects of the scanning speed (v) and hatch space (h) process parameters on the product qualities were investigated using the one factor at a time method. The specific product attributes examined are presented in Table 3. The volumetric energy density (VED) is regarded as a significant measure for evaluating the outcomes of selective laser melting (SLM) results, as it encompasses the process parameters of the SLM process[42] .

$$VED = \frac{P}{v.h.t} \qquad (1)$$

Equation (1) represents the relationship between the volumetric energy density (VED) and the laser power (P), scanning speed (v), space (h), and thickness of a single powder layer (t). In this equation, P is measured in watts (W), and v is measured in millimeters per second (mm/s). hatch h is measured in millimeters (mm), and t is measured in millimeters (mm).

The samples underwent a mechanical grinding and polishing procedure, utilizing waterproof silicon carbide paper with varying grit sizes (80, 200, 400, 800, and 1200) sequentially under a continuous water stream. The specimens underwent a concluding polishing procedure utilizing a 0.5 μm diamond suspension on a polishing cloth affixed to a rotary grinding/polishing apparatus, followed by cleansing with ethanol to eliminate any impurities or debris.

The samples were subjected to surface morphology examinations using a scanning electron microscope (SEM) of the FEI-Quanta 250/USA model. This analysis focused on examining the cross-sections, worn areas, and corroded surfaces of the samples. The crystal phase structure and element distribution were examined using a GNR explorer X-ray diffractometer from Italy. The analysis utilized Cu Kα radiation with a wavelength of 1.5418 Å, and the measurements were taken on a 2θ scale ranging from 10◦ to 90◦. Additionally, an energy-dispersive spectroscope (EDS) is utilized. The Archimedes approach was employed to determine the relative density of the samples produced under various process conditions using the formula [43].

$$RelativeDensity\ \frac{\rho_{SLM}}{\rho_{Std}}\ \frac{\rho_{water}\times m_{air}}{(\rho_{Std}\times m_{air})-(\rho_{std}\times m_{water})} \qquad (2)$$

In equation (2), ρSLM represents the density of the Co24.7Cr5Mo5.4W alloy produced using selective laser melting (SLM). ρstandard denotes the standard density of the Co24.7Cr5Mo5.4W alloy. ρwater corresponds to the density of water at a temperature of 4 ◦C. mair represents the average mass of the SLM sample when measured in air, while m water represents the average mass of the SLM sample when measured in water. The relative densities of the selective laser melting (SLM) samples are presented in the table. The user's text is too short to be rewritten in an academic manner.

The measurement of surface roughness was conducted using a profilometer, namely the Mahr surface profilometer. The analysis of the specimens' surface roughness was conducted by measuring the parameters Ra and Rz. The software program utilized for this purpose was Marserve 20, developed by Mahr. The programme was configured with the following settings: The length of traversal is measured at 2.4 mm, whereas the standard critical wavelength is recorded at 0.25 mm. The velocity of the system is calculated to be 0.1 mm/s. The measurements were conducted utilizing a probe with a diameter of 2 mm, positioned perpendicular to the direction of polishing, and employing a cutoff length of 0.4 mm. The manufacturer has stated that the profilometer accuracy is 25 mm on the vertical scale and 1 mm on the horizontal scale. The experiment involved conducting three repetitions of each measurement and subsequently calculating the average value. The surface roughness was quantified through measurement

Table 3. SLM process parameters.

Process Parameter	value
P (W)	100
t (mm)	0.025
v (mm/s)	700 -1000
h (mm)	0.06 - 0.08

3. Results and Discussion

The selective laser melting (SLM) technique was utilized to fabricate samples of CoCrWMo alloy, employing various combinations of process parameters. The objective of this work was to investigate the features of these samples and determine the optimal combination of parameters. A study was conducted to

investigate the impact of different scanning speeds on the relative density at two distinct levels of hatch spacing, namely 0.06 mm and 0.08 mm. The relative density exhibited an increase with a decrease in scanning speed, as depicted in Figure 2, while maintaining a constant laser power of 100 W and layer thickness of 0.025 mm. The highest relative density, exceeding 98.0%, was achieved when the scanning speed was set to its lowest setting of 700 mm/s and the hatch spacing was increased to 0.08 mm. The influence of hatch space on relative density is observed mostly at elevated levels of laser power and scanning speed. The relative density experienced a decrease from 98.2% to 94.4% when the scanning speed increased to higher values, leading to a reduction in the energy input. In this scenario, the extent of overlap drops considerably, impeding the complete melting of the powder. Additionally, the absence of a bonding neck between successive phases leads to the creation of pores and a decline in relative density. The level of laser energy received by the powder during the Selective Laser Melting (SLM) process is rather low, resulting in incomplete melting of a significant number of powder particles present in the sample. The liquid phase of CoCrWMo is diminished during the printing process, leading to inadequate filling of cavities and holes in the CoCrWMo samples caused by incomplete powder bed melting. Consequently, the presence of defects is amplified. Furthermore, it can be observed that the microstructure of the specimen has a larger grain size. The form and size of the melt pool are unaffected by variations in scanning speed. The configuration of the molten pool is primarily influenced by the dimensions of the laser focal point, the spacing between successive laser passes, and the trajectory followed by the laser during scanning. The porosity is influenced by the scan speed. This finding is consistent with the study conducted by Shiwen Zou et al. (44), which examined the relationship between scan speed and defect size. The researchers observed that as the scan speed increased, the defect size also tended to increase. Additionally, they found that counterparts produced at higher scan speeds displayed fusion faults that were attributed to an inadequate fusing process. The microstructural analysis revealed that the cellular morphology of the selective laser melting (SLM) CoCrWMo alloy exhibits growth perpendicular to the molten pool border.

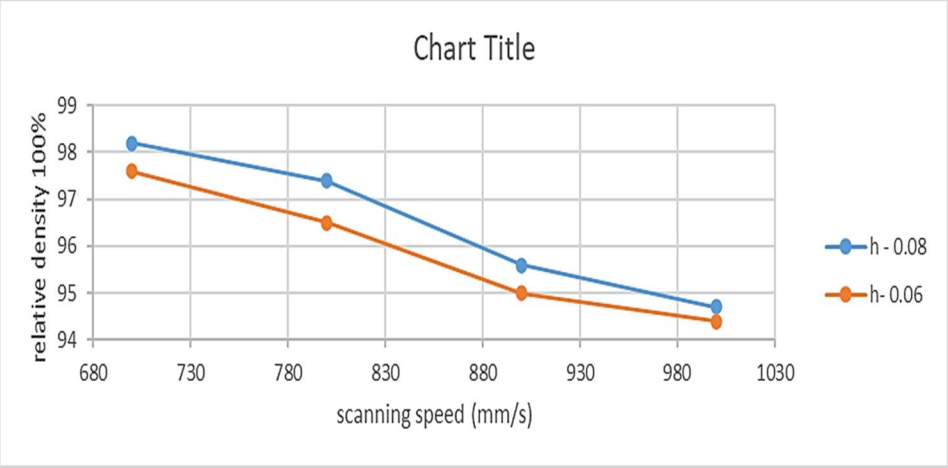

Fig.2: shows density curves for SLM-created Co24.7Cr5Mo5.4W alloys at a range of laser scanning speeds.

Metallographic analyses were conducted on the top surfaces of eight fabricated samples, as depicted in Figure 3, using scanning electron microscopy (SEM) imaging. The aim of this study is to examine the impact of scanning speed and hatch spacing on the surface quality of the produced puros, as indicated by the density and form. The results presented in Figure 5a indicate that the optimal surface can be achieved by employing a lower scanning speed of 700 mm/s and a higher hatch spacing of 0.08 mm. The Volumetric Energy Density (VED) values are 71.42 J/mm3 for a hatch space of 0.08 mm and 95.23 J/mm3 for a hatch space of 0.06 mm. These values suggest that the sample surface is smooth, as depicted in Figure 3a and Figure 3e. The relative density value ranges from 98.2% to 97.6%. The scanning speed and volumetric energy density yield the best results, along with a powder that is tightly bound and exhibits exceptional

fusion capability. When the scanning speed is increased to 800 mm/s, the pores on the surface become visible. Additionally, there is a noticeable increase in the number of balling particles, as depicted in Figure 3b and Figure 3f. The observed phenomena can be attributed to an excessive scanning speed, leading to insufficient energy input, which in turn causes incomplete melting of the powder and the subsequent creation of pores. Nevertheless, when the scanning velocity is heightened, and the energy density is diminished, the uppermost layer of powder fails to attain adequate heat for complete powder fusion. Consequently, this leads to a decrease in the formation of strong bonds between the powder particles and the emergence of voids inside the material. As a result, the relative density experienced a reduction ranging from 97.4% to 96.5%. When the scanning speed is increased to 900 mm/s, it is evident from the observations made in (Figure 3 g) that the presence of balling particles and pores becomes apparent on the surface. The energy density inside this particular region is measured to be within the range of 55.55-74.07 J/mm3. The acceleration in scanning velocity has resulted in a reduction of the duration of contact between the powder and laser, leading to a decrease in temperature for certain particles below their respective melting points. Consequently, the powder undergoes partial melting.

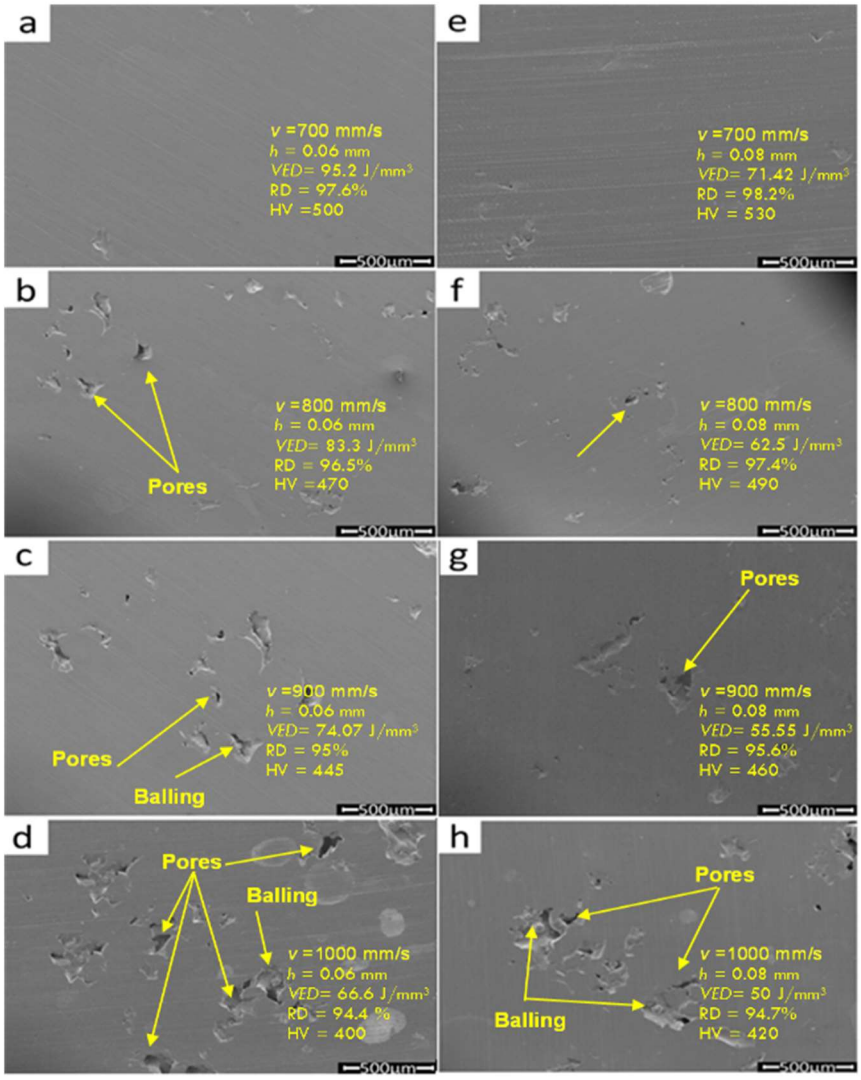

Fig.3: SEM images for Co24.7Cr5Mo5.4W alloy samples produced with different sets of process parameters after mechanical grinding.

In this particular scenario, the fusion of neighboring particles occurs as a result of the substantial generation of liquid material [28]. Nevertheless, it is important to note that the region where agglomeration takes place remains in a condition characterized by the coexistence of both liquid and solid phases.

The observed trend in the relative density of CoCrWMo alloy samples is a reduction as the scanning speeds, which correspond to the energy input, rise. Furthermore, the relative density ranges from 95.6 to 95 percent. When the scanning speed is increased to 1000 mm/s for hatch spaces of 0.08 and 0.06, the corresponding energy values (VED) are found to be 50 J/mm3 and 66.66 J/mm3, respectively. The presence of pores, unmelted powders, and agglomerated balling on the surface is of more concern, as larger-sized pores and balling particles are observed on the surface (Figure 3 d, h). The presence of spherical particles and pores on the surface of the preceding layer has an impact not only on the binding within the same layer but also on the binding across different layers, thereby influencing the overall density of the sample. As seen from the data presented in Figure 3 d and h, The relative density within this range is 94.7-94.4%

The X-ray diffraction (XRD) pattern of the CoCrWMo specimen is depicted in Figure 4. The X-ray diffraction (XRD) analysis reveals that the CoCrWMo alloy displays a combination of two distinct phases, namely the gamma (ɣ) phase with a crystallographic plane orientation of (111) in a face-centered cubic (FCC) structure and the zeta (ε) phase with a crystallographic plane orientation of (200) in a hexagonal close-packed (HCP) structure. In general, it is seen that CoCr-based alloys undergo a phase transition from the ɣ (111) phase to the martensite ε (200) phase as they are cooled. The creation of the ε (200) phase occurs as a result of a martensitic transformation triggered by thermal stress. The higher quantity of the FCC (Face-Centered Cubic) phase, denoted as ɣ (202), is likely retained due to the inhibitory conversion of the metastable ɣ (202) phase to the martensite ε (200) phase during rapid cooling of the molten pool.

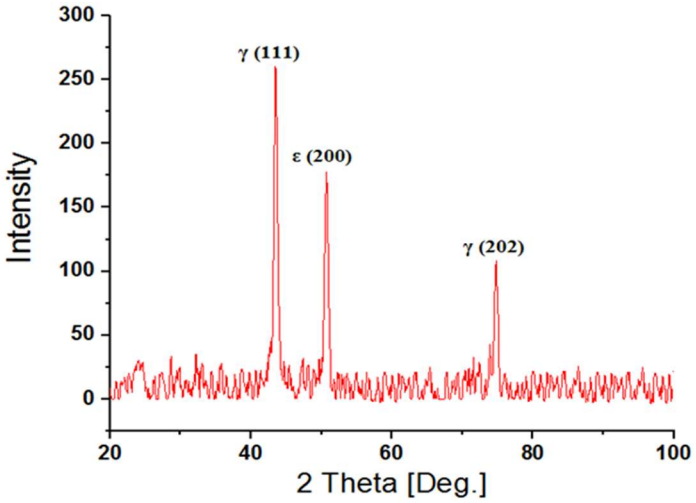

Fig.4: XRD pattern of the CoCrWMo specimen.

Figure 5 displays the microscope image of the CoCrWMo alloy, accompanied by demarcated regions indicating the local microanalysis of its chemical composition. Additionally, the spectrograms of the produced X-radiation are presented in the figure. A comprehensive examination of the notable regions is documented in the table. As depicted in the figure, the matrix of the tested material exhibits a greater concentration of Co and Cr as compared to the eutectic precipitates, wherein Mo, W, and Si are present in higher proportions. The state and texture of a surface, as well as the degree of surface roughness prior to undergoing mechanical grinding, resulted in varying surface profiles across the samples, depending on the specific processing method employed (see Figure 6). All of the samples displayed a comparable surface, characterized by heights ranging from 0.50 to -50 µm for the majority of the specimens. The Ra center line average (CLA), with an average roughness ranging from 20 to 31 µm, was found to have an impact on the friction coefficient, microhardness, and wear resistance of the materials (45).

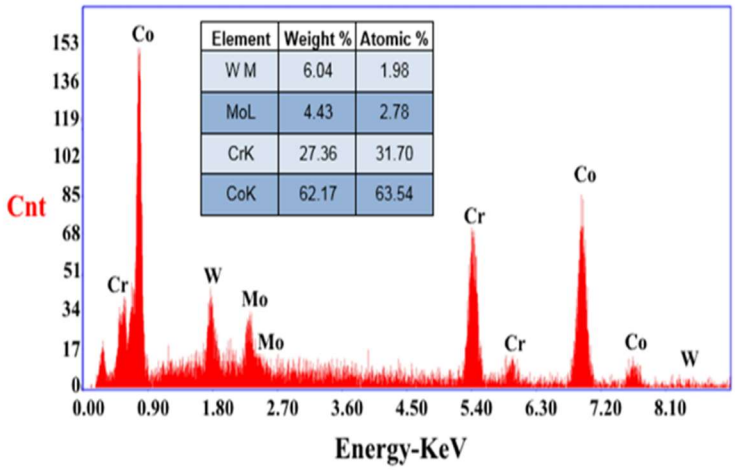

Fig. 5: EDS image spectrogram of Co24.7CrWMo.

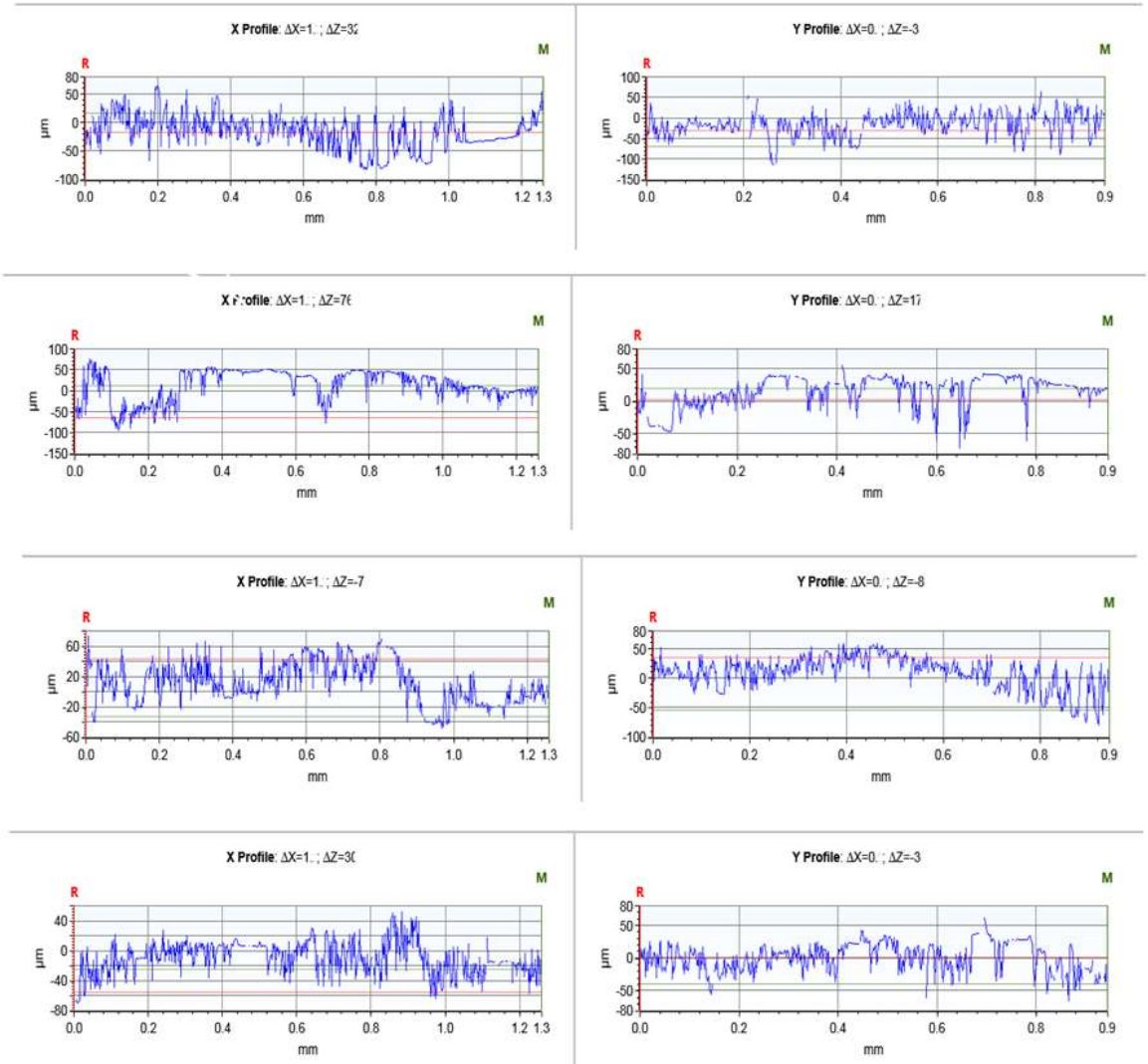

Fig.6: .Profilometry of the surfaces of the samples:(a)v=700mm/s h=0.06 µm ,(b) v=700mm/s h=0.08 µm,(c) v=800mm/s h=0.06 µm (d) v=800mm/s h=0.08 µm,(e) v=900mm/s h=0.06 µm,(f) v=900mm/s h=0.08 µm,(g) v=1000mm/s h=0.06 µm,and(h) v=1000mm/s h=0.08 µm.

The sample with a height of 30 µm had a relatively large average amplitude in the height direction (Rq), while the sample with the smoothest surface had the smallest Rq value (Table 2). In order to assess a surface state in the vertical direction, two parameters were employed: The Rp, Rv, and RT metrics validate that the samples subjected to Al_2O_3 and SiO_2 sandblasting exhibited the most polished surface, with the sample displaying the most pronounced profile variations and the sample showcasing the least pronounced profile differences (indicating the finest surface).

The CoCrWMo alloy produced via the process of selective laser melting is depicted in Figure 7. The plot illustrates the relationship between surface roughness and laser bulk energy density prior to the application of mechanical grinding, encompassing all relevant data points. Upon analysing the dispersed data points, it becomes evident that the process under consideration is selective laser melting (SLM) formation. The increase in energy density leads to a decrease in the top surface roughness (Ra) of the CoCrWMo alloy. Choose a representative specimen for surface analysis in the context of selective laser melting (SLM) additive manufacturing. In terms of morphological observation, Figure 7 displays the samples that have been generated using varying laser volume energy densities.

The observation reveals that when the laser bulk fluence is low (50 J·mm−3), a significant quantity of unmelted powder accumulates on the sample's surface. Additionally, the melting channel exhibits discontinuity, resulting in inadequate lapping effects. These outcomes can be attributed to the laser body's lower energy density. The high thermal energy poses challenges in achieving complete fusion of the powder, while the surface roughness is around 29 µm. The laser bulk energy density applied to the surface of the sample was measured to be 71 J·mm−3. The melting channel has a significant degree of overlap, demonstrating a continuous nature, with little instances of unmelted powder adhesion. Furthermore, the reduction in surface roughness is observed to be 25 µm. At elevated levels of laser bulk energy density (95 J mm−3), the melting channel observed on the surface of the lower sample exhibits enhanced smoothness and straightness, accompanied by a progressive reduction in surface roughness. The laser bulk fluence results in the generation of heat, which can cause the size to decrease to as low as 20 µm. Excessive elevation of temperature might result in the vaporisation of a portion of the powder, leading to the formation of circular voids.

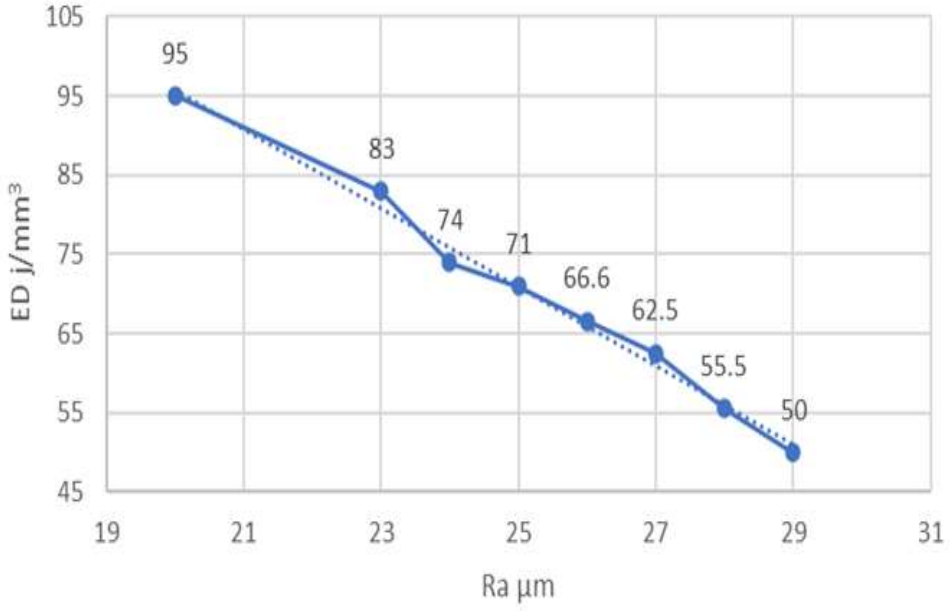

Fig. 7: Surface Roughness of Co24.7Cr5Mo5.4W alloys produced with SLM using different volumetric energy densities before mechanical grinding.

It is widely recognized that surfaces exhibiting elevated roughness levels, indicative of lower quality, tend to possess diminished fatigue resistance. Conversely, surfaces characterized by reduced roughness, signifying higher quality, exhibit enhanced fatigue resistance, as well as heightened resistance to corrosion. The excessive refinement of surfaces, resulting in a significant reduction in roughness, does not necessarily guarantee improved functionality of the components. In fact, it often leads to an unwarranted increase in production costs. Based on the data shown in Table 3 and Figure 8, an observation can be made regarding the relationship between surface roughness following mechanical grinding followed by a polishing procedure and volumetric energy density. The upper limit for roughness, as measured by the arithmetic average height (Ra), is 29 µm .The present study emphasizes the enhanced efficiency of mechanical grinding (MG) subsequent to selective laser melting (SLM) processing, as evidenced by a notable decrease in roughness values (Δ Ra) by 35%. One potential approach for analyzing the experimental results involves considering the energy density (VED). In this particular scenario, it is worth noting the following:

The specimens subjected to non-mechanical grinding (MG) exhibited the lowest roughness values when processed using selective laser melting (SLM) with an energy density (ED) of 95. The optimal settings of technological parameters for mechanical grinding (MG) specimens are often recommended to have a VED value of 95J.mm-3. The present study used a synthetic analysis to examine the findings, specifically focusing on the roughness (Ra) aspect. It is advisable to consider specific combinations of values for the two technological parameters, denoted as (H) and (vscan). The value of h is 60 µm, and the value of v is 700 mm/s. The present study employs a synthetic analysis to examine the findings, specifically focusing on the perspective of roughness (Ra).

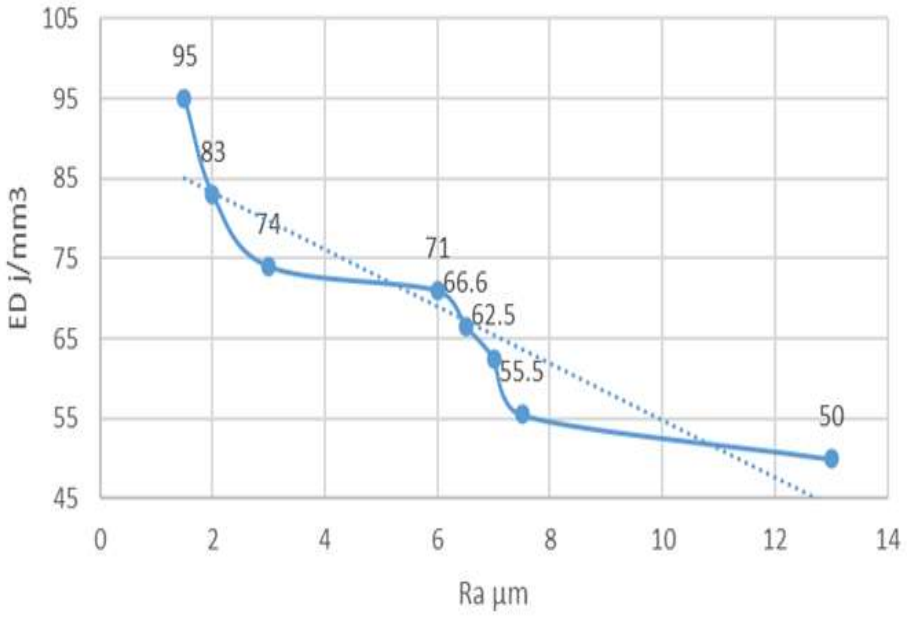

Fig. 8: Surface Roughness of Co24.7Cr5Mo5.4W alloys produced with SLM using various energy density after mechanical grinding.

Table 4. Surface Roughness of Co24.7Cr5Mo5.4W alloys produced with SLM using various energy density before and after mechanical grinding**.**

Ra(μm) before	Ra(μm) after	ED(j/mm^{-3})
29	13	50
28	7.5	55.5
27	7	62.5
26	6.5	66.6
25	6	71
24	3	74
23	2	83
20	1.5	95

The conducted experiments indicate that values of hatching space less than 60 μs and scanning speeds below 700 mm/s are not advisable for the selective laser melting (SLM) processing of the Co-Cr-W powder. This is due to the detrimental impact on the energy density (Ed), which in turn negatively affects the selective melting and solidification processes of the metal powder. One of the immediate outcomes of insufficient selective laser melting (SLM) processing is the production of exterior surfaces with elevated roughness.

4. Conclusions

The study discusses the utilisation of the Selective Laser Melting (SLM) technique employing a laser beam to treat Co-Cr-W metal powders. Eight sets of specimens were created using varied values of the variable technological parameters, namely hatching space (H), scanning speed (vscan), and energy density (VED). Measurements of roughness (Ra) were performed on surfaces subjected to mechanical grinding and non-mechanical grinding techniques. Based on the observed exterior surface roughness, the following conclusions have been derived.The optimal parameter combinations for non-mechanical grinding and mechanical grinding are determined to be H = 60 μm and vscan = 1000 mm/s. From a volumetric energy density (ED) perspective, it is not advisable to use scanning speeds (vscan) above 700 mm/s and pulse durations (H) exceeding 80 μs for selective laser melting (SLM) processing of Co-Cr-W powders, as these parameters will lead to elevated roughness values.

References

[1] Sapate K D and Tejashree Apte U 2017 IJCET 7(1)
[2] Yap C Y, Chua C K, Dong Z L, Liu Z H, Zhang D Q, Loh L E and Sing S L 2015 Appl. Phys. Rev. 2(4) 041101
[3] Puchades J R B 2012 Master thesis (Valencia: Universitad Politecnica de Valencia)
[4] Kruth J P, Badrossamay M, Yasa E, Deckers J, Thijs L and Van Humbeeck J 2010 International Symposium on Electromachining, Shanghai, China
[5] Koutiri I, Pessard E, Peyre P, Amlou O and De Terris Th 2018 J. Mater. Process. Tech. 255 536
[6] Prashanth K, Scudino G, Maity S, Das T and Eckert J 2017 Mater. Res. Lett. 5(6) 386
[7] Wen–Hou Wei and Shen J 2018 Int. J. Mater. Res. 109(5)
[8] Lin-Zhi W and Wen-Hou W 2018 Acta Metall. Sin. 31(8) 807
[9] Gu H, Gong H, Deepankar P, Khalid R, Starr TH and Stucker B 2013 24th, Annual international solid freeform fabrication symposium; an additive manufacturing conference, proceedings Austin TX 474
[10] Han J 2015 Rapid Prototyping J. 23(2) 217
[11] Goutianos S 2017 Adv. Mater. Res-Switz. 219
[12] Poprawe R, Hînke Ch, Meiners W, Schrage J, Bremen S and Merkt S 2014 Lect. N. Prod. 49
[13] Mager V, Bâlc N, Leordean D, Dudescu M C and Fockele M 2013 Appl. Mech. Mater. 371 280
[14] Kim H R, Jang S H, Kim Y K, Son J, Min B K, Kim K H and Kwon T Y 2016 Materials 9(7) 596

[15] Figliuzzi M, Mangano F and Mangano C 2012 J. Oral. Maxillofac. Surg. 41 858
[16] al-Aloosi, R. A., Çomakli, O., Yazici, M. & Taha, Z. A. (2022). Influence of Scanning Velocity on a CoCrMoW Alloy Built via Selective Laser Melting: Microstructure, Mechanical, and Tribological Properties. Journal of Materials Engineering and Performance, pp.1-8
[17] Raghad Ahmed Al-Aloosi, Zainab Abdul-Kareem Farhan, Ahmad H. Sabry," Remote laser welding simulation for aluminium alloy manufacturing using computational fluid dynamics model", Indonesian Journal of Electrical Engineering and Computer Science Vol. 27, No. 3, September 2022, pp. 1-1x
[18] Revilla-León, Marta, Al-Haj Husain, Nadin Methani, Mohammed Mujtaba, Ozcan Mutlu ," Chemical composition, surface roughness, and ceramic bond strength of additively manufactured cobalt-chromium dental alloys "THE JOURNAL OF PROSTHETIC DENTISTRY, VOLUME 125, ISSUE 5, P825-831, MAY 2021.
[19] Rajúková V, Polacek I, Toth T, Zivcak J, Izarikova G, Kovacevic M, Somos A and Hudak R 2016 Lekar a technika 46(4) 102
[20] Dikova T, Dzhendov Dz, Simov M and Katreva I 2015 Journal of IMAB 21(4)
[21] Dzhendov Dz and Dikova Ts 2016 Journal of IMAB 22(4) 1414
[22] Takaichi A, Suyalatu A, Nakamoto T, Joko N, Nomura N, Tsutsumi Y, Migita S, Doi H, Kurosu S, Chiba A, Wakabayashi N, Igarashi Y and Hanawa T 2013 J. Mech. Behav. Bionned. Mater. 21 67
[23] Baciu M A, Baciu E R, Bejinariu C, Toma S L, Dănilă A and Baciu C 2018 IOP Conference Series: Materials Science and Engineering 374 (1)
[24] Hong M H, Kim B K and Kwon T Y 2016 Applied Sciences 6(12) 401
[25] Fox J C, Moylan S P and Lane B M 2016 Proc. Cirp. 45 131
[26] Yadroitsev L and Smarov I 2011 Physcs. Proc. 12 264
[27] Perevoshchikova N 2016 Rapid Prototyping J. 23(5) 881
[28] Li Z, Kucukkoc I, Zhang D Z and LiU F 2016 Rapid Prototyping J. 24(1) 150
[29] Lober L, Flache Ch, Petters R, Uta Kuhn J 2013 Rapid Prototyping J. 19(3) 173
[30] Seifi M and Satko D 2018 Proceedings of the 9th International Symposion on Superalloy 718 515.
[31] Marwa K. Qate'a, Ali H. kadhum, Faiz F. Mustafa," The Influence of the Magnetic Abrasive Finishing System for Cylindrical Surfaces on the Surface Roughness and MRR ". Al-Khwarizmi Engineering Journal, Vol. 11, No. 3, P.P. 1- 10 (2015)
[32] Yahya M. Hamad "Improvement of Surface Roughness Quality for Stainless Steel 420 Plate Using Magnetic Abrasive Finishing Method ", Al-Khwarizmi Engineering Journal, Vol. 6, No. 4, pp. 10 – 20, 2010.
[33] Ali M. Khudhair, Furat I. Hussein," High Speed Shock Peening by Fiber Laser for Al Alloy 6061-T6 Thin Sheets", Journal of Materials Engineering and Performance volume 31, pages8585–8595 (2022)
[34] K. M. Aljanabi" Effect of High Energy Nd:Glass Laser on the Drilled in the 5052 AlMg Alloy" Iraqi J. Laser, Issue 2, Vol.18, pp.35-40 (2019).
[35] Ali M. Khudhair, Furat I. Hussein," Parametric Optimization for Fatigue Life of 6061-T6 Aluminum Thin Sheets Processed with High-Speed Laser Shock Peening", Iraqi J. Laser 20(2), 8-17 (2021)
[36] H.J.M. Alalkaw, Laser Peening on Aluminum Alloy 7049 Using Black Paint Surface, Al-Khwarizmi Eng. J., 2015, 11(3), p 54–60.
[37] Furat I. Hussein, Ziad A. Taha, Thaier A. Tawfiq, and Ahmed B. Jawad ," Laser Hole Drilling of Stainless Steel 321H and Steel 33 Using 3D CO2 Laser CNC Machine" Iraqi J. Laser, Part A, Vol. 10, pp. 15-21 (2011).
[38] Iman Shakir Tawfeeq, Zaid Aeyad Taha," Angular Laser Cleaning of Aluminum Al-4004 with Different Spot Sizes", Iraqi J. Laser 22(1), 9-17 (2023).
[39] Min-Ho Hong, Bong Ki Min, and Tae-Yub Kwon," The Influence of Process Parameters on the Surface Roughness of a 3D-Printed Co–Cr Dental Alloy Produced via Selective Laser Melting", Appl. Sci. 2016, 6, 401
[40] Lavinia Tonellia, Alessandro Fortunatoa, Lorella Ceschinib," CoCr alloy processed by Selective Laser Melting (SLM): effect of Laser Energy Density on microstructure, surface morphology, and hardness", Journal of Manufacturing Processes 52 (2020) 106–119.
[41] Marta Revilla-León, Nadin Al-Haj Husain, Mohammed Mujtaba Methani, Mutlu Özcan.
"Chemical composition, surface roughness, and ceramic bond strength of additively manufactured cobalt-chromium dental alloys", The Journal of Prosthetic Dentistry ,Volume 125, Issue 5, May 2021, Pages 825-831.
[42] Kumar, K.S. "Selective Laser Sintering/Melting. Comprehensive Materials Processing", vol 10. Elsevier, Amsterdam. 2014
[43] Slotwinski, J. A., Garboczi, E. J., and Hebenstreit, K. M., "Porosity Measurements and Analysis for Metal Additive Manufacturing Process Control," Journal of Research of the National Institute of Standards and Technology, vol. 119, pp. 494-528, 2014.

[44] Shiwen Zou, Zhenjiang Zhao, Wen Xu, Xiaoqing Ni, Liang Zhang, Wenheng Wu, Decheng Kong, Xing He, Li Wang, Chaofang Dong, “Effects of scanning speeds on the wear behavior of CoCrW alloy fabricated by selective laser melting”, Optics & Laser Technology 147 (2022) 107652.
[45] Hong, M.-H.; Min, B.K.; Kwon, T.-Y. “The Influence of Process Parameters on the Surface Roughness of a 3D-Printed Co–Cr Dental Alloy Produced via Selective Laser Melting”. Appl. Sci. 2016, 6, 401.

تأثير سرعة المسح عل سبيكة الكوبلت كروم ملبوديوم تنكستن المبنية عن طريق ذوبان الليزر الانتقائي على خصائص الخشونة

رغد أحمد الألوسي[2،1]*, زياد اياد طه[1] و أونور جوماكلي[3]

[1]معهد الليزر للدراسات العليا، جامعة بغداد، بغداد، العراق.
[2]قسم التصنيع الآلي، كلية الهندسة الخوارزمي، جامعة بغداد، 10071، العراق.
[3] قسم الهندسة الميكانيكية جامعة، كلية الهندسة والعمارة، أرزوروم التقنية ، 25050، أرضروم

*البريد الالكتروني للباحث:raghad@kecbu.uobaghdad.edu.iq

الخلاصة:اكتسب استخدام الصهر بالليزر الانتقائي (SLM) في إنتاج العناصر المعدنية المعقدة اهتمامًا كبيرًا في قطاعي الطب وطب الأسنان. يجب أن تمتلك المنتجات التي تم إنشاؤها باستخدام SLM أسطحًا تظهر درجة عالية من النعومة. الهدف من هذا البحث هو دراسة تأثير معلمات عملية الليزر المختلفة، وتحديداً معدل المسح وتباعد الفتحات على خشونة السطح لسبائك الأسنان Co-Crالمصنعة في ثلاثة أبعاد (3D) بواسطة تقنية الذوبان بالليزر الانتقائي .(SLM) تشير النتائج إلى أن سرعة المسح البالغة 700 مم/ثانية تنتج مورفولوجيا سطحية وبنية مجهرية فائقة. أسفرت دراسة المعلمات التي أجريت في هذه الورقة عن تحقيق كثافات نسبية تصل إلى 98.9٪ لقطع العمل المبنية بشكل إضافي. تركز الدراسة الحالية على دراسة خشونة السطح في سبائك Co-Crالمصنعة باستخدام تقنيات تعدين المساحيق، وهي الذوبان الانتقائي بالليزر.

IJL, Issue 1, Vol. 23, 2024
https://doi.org/10.31900/ijl.v23i1.403

Research Article

IRAQI JOURNAL OF LASER

In vitro study of the antibacterial property of 940 nm diode laser against Streptococcus mutans bacteria isolated from dental caries

Noha M. Jameel[1,*], Hanan J. Taher[1], Tahrir N. Aldelaimi[2]

[1]*Institute of Laser for Postgraduate Studies, University of Baghdad, Baghdad, Iraq*
[2]*College of Dentistry, University of Anbar, Iraq*
* *Email address of the Corresponding Author: Noha.Mohammed1202a@ilps.uobaghdad.edu.iq*

Article history: Received 13 Jul. 2023; Revised 27 Oct. 2023; Accepted 4 Nov. 2023; Published online 15 Jun. 2023

Abstract

Background: The main etiological element of dental caries is Streptococcus mutans (S. mutans) bacteria, so getting rid of this bacterium has a significant impact on how well restorative treatment goes. New approaches for eradicating bacteria in dentistry have been developed like lasers, metallic nanoparticles, and bioactive materials.
Aim of the study: This study's goal was to assess a diode laser's effectiveness as an antibacterial agent and then compare it with the antibacterial effect of chlorhexidine (CHX) against S. mutans bacteria.
Material and Method: The study was performed by using S. mutans microorganisms collected from patients with dental caries, then a bacterial suspension was prepared at a concentration of 106 CFU /ml and placed in an Eppendorf tube to be treated with various antibacterial modalities, the 30 samples were divided up into three experimental groups: Group I: Negative control group; Group II: Positive control group using 2% chlorhexidine; Group III: Irradiation with diode laser (1 watt output power for 30s exposure time). The number of colony-forming units (CFU) was counted for each group after 24 h of incubation on Mitis Salivarius Bacitracin agar (MSBA) plates.
Results: A significant reduction in the CFUs/ml of S. mutans bacteria was observed 24 hours following treatment by the two approaches (The diode laser and CHX). The findings of the study indicate a significant statistical difference (p-value < 0.01) between the two groups in comparison to the negative control group that did not receive any treatment. Furthermore, the group treated with the diode laser exhibited the greatest drop in bacterial count compared to the group treated with CHX.
Conclusion: Both diode laser and CHX have a good bactericidal effect, but the diode laser had an antibacterial effect superior to CHX. The diode laser was a successful and effective approach for eliminating bacteria and it can be employed as a step in the teeth restoration process.

Keywords: Chlorohexidine, Dental caries, Diode Laser, Disinfection, Laser irradiation.

1. Introduction

Dental caries is a complex, multifactorial, chronic, and dynamic disease that affects 95% of the population of all ages worldwide.(Sadony and Abozaid, 2020) It is mediated by biofilms and sugar in the presence of cariogenic bacteria (Qiu et al., 2020), in which dental hard tissues undergo phasic demineralization by acid produced through food fermentation by bacteria (Pitts et al., 2017). Gram-positive, facultative anaerobic streptococcus mutans is frequently found in the mouth is the main contributory factor to dental caries (Jassim, 2022). The main goal of dental restoration is to remove infected carious tissues and bacteria and replace them with a filling material in order to protect and preserve the remaining tooth structure. However, secondary caries is one of the main causes of restorative failure because it can develop if infected tissues, bacteria, and germs are not completely removed. (Selivany et al., 2020) There are many methods to reduce the occurrence of dental caries, including fluoride and chemical antibacterial agents (Liao et al., 2017; Shallal and Ahmed, 2022) but they are not usually very effective and may have unfavorable side effects, or the bacteria could become resistant to this antibiotic. (Toma and Aziz, 2023) As a result, various antibacterial techniques like lasers that have a strong bactericidal impact with no harmful side effects are needed. Using antibacterial treatments to help reduce the prevalence of infection-causing bacteria is a practice that dentists all around the world are starting to use. (Chalisha et al., 2021) Results from most research were related to the use of cavity disinfectants like chlorhexidine, laser technology, and sodium hypochlorite (NaOCl). Additional disinfection options were also evaluated in some studies. (Coelho et al., 2020)

Because of its antibacterial Efficiency, which includes those against S.mutans, and its antiplaque action, chlorhexidine has been widely utilized in dentistry. (Kandaswamy et al., 2018, Haydari et al., 2017) The majority of authors assessed chlorhexidine's effectiveness as a cavity disinfectant, and according to a number of findings, chlorhexidine is the most widely agreed-upon cavity disinfectant for use in clinical practice (Coelho et al., 2021). When chlorhexidine (CHX) was utilized prior to the application of adhesives, a reduction in residual microbiological contamination and enhancement of the seal of restoration were noted. (Ebrahimi et al., 2018) Many researchers have looked into the various capabilities and characteristics of CHX, including its capability to inhibit matrix metalloproteinases (MMPs) when used before the application of adhesive systems. (Mohammadi et al., 2020)

Rapid developments in laser technology (including wavelengths, techniques, and delivery systems) have made it possible to use it in a variety of disciplines, such as dentistry, physics, biology, biotechnology, and biochemistry. (Saleh et al., 2023) Numerous lasers, including diode lasers, Er-YAG, and Nd-YAG, have been shown to have bactericidal effects. (Wang et al., 2018) The diode laser has lately acquired popularity and is now prevalent in dental offices due to its low cost, portability, efficient bactericidal action through its thermal effect, and temperature rise that is within an acceptable range for permanent teeth (Bahrololoomi et al., 2017). Furthermore, whereas conventional disinfectants only penetrate a depth of 100 μm into the dentinal tubules, diode laser light can do so up to 1000 μm from the surface, making it an effective disinfectant. (Saafan et al., 2018). Also, there has also been a lot of interest in the efficacy of Er,Cr:YSGG lasers in eliminating bacteria since bacteria's water molecules make them a good target for Er,Cr:YSGG lasers, which destroy bacteria when energy is absorbed. (Tokuc et al., 2019)

This study's objective is to assess the antibacterial efficacy of a diode laser with a 940 nm wavelength on the survival of S. mutans bacteria and compare that antibacterial impact to that of chlorohexidine.

2. Material and Method

2.1. Samples Collection, Isolation, and Identification of S. mutans Bacteria

The plaque and saliva samples were obtained from patients with dental caries who visited the dental clinics at the College of Dentistry/University of Baghdad. The samples were obtained using sterile wet transport media, and they were later delivered by ice box to the laboratory. a total of 100 microliters of the obtained samples were grown for 24 h at 37o C on a plate of mitis salivarius bacitracin agar MSBA selective medium. To identify the isolated bacteria, The initial identification of S. mutans was done by conventional methods, which included microscopic examination and biochemical testing, while the final identification was carried

out using the more reliable polymerase chain reaction (PCR) method of detection in epidemiological studies.

2.2. Bacterial sample preparation

A single colony of S. mutans bacteria was taken and cultivated for 24 h at 37o C in BHI broth (HIMEDIA, India). The concentration was modified to 0.5 scale McFarland (1 ml of 0.5 McFarland containing nearly 108 bacteria). A 10-fold dilution to 0.5 McFarland suspension was done to achieve a concentration of 5×106 bacteria in 1 ml to reduce the number of bacterial colonies to be able to count them (Kasraei et al., 2014).

2.3. Laser irradiation

The bacterial solution was exposed to a 940 nm-wavelength diode laser (Epic, Biolase, USA). The output power was 1 W in continuous mode for 30 s of exposure time, delivered by a 200 µm fiber tip (E2-20, Biolase, USA). It was inserted into the sterile Eppendorf tubes containing 1 ml of bacterial suspension (5 × 10^6 cells/ml) with a spiral motion continuously in a clockwise direction from the bottom to the top of the tube, as shown in Figure 1. This ensures laser distribution evenly throughout the entire suspension volume. The laser tip was disinfected with 70% ethyl alcohol after each use. (Sadony and Montasser, 2019) The irradiated suspensions were cultured on MSBA overnight at 37°C.

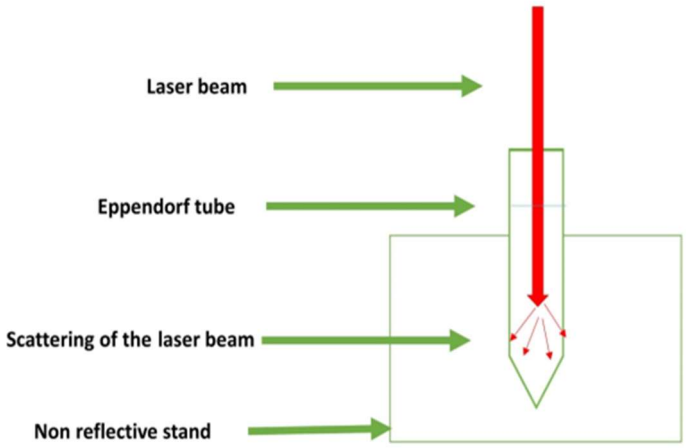

Fig.1: Laser arrangement of bacterial irradiation in the Eppendorf tube.

2.4. Experimental groups

Samples are divided into three experimental groups, each group having ten samples (n=10)
Group I: Negative control group bacterial suspension containing (106 CFU/ml) bacterial concentration without any treatment.
Group II: Positive control group into which 2% CHX
(CERKAMED, Poland) irrigation was used to treat the bacteria.
Group III: Irradiation of bacterial suspension by diode laser 940 nm 1 W output power, CW, 30 s exposure time.

2.5. Antibacterial activity determination

To assess the antibacterial activity, the reduction in bacterial number following exposure to different antibacterial treatments was the main focus of this study, as was checking how effective the treatment is. After treating all the samples of bacteria with different treatment modalities, bacterial counting using CFU/ml was done. This was achieved by taking a portion of the bacterial suspension (100 microlitres) and spreading it on bacterial growth selective media (MSBA) and cultured for 24 h after being serially diluted by 3-dilution folds 10l, 10-2, and 10-3. By using the following equation, the number of CFU was counted on the MSBA plates and determined per millilitre of the initial sample:
Number of CFU/ml = number of CFU x dilution factor (De Mandal and Passari, 2021, Buraihi and Alkurtas, 2020). Moreover, the following equation was used for calculating the killing percentage:
Percentage of killing = 100% – (CFU of the tested group/CFU of the control group) x 100% (Lee et al., 2006).

3. Results

The statistical analysis was completed by using SPSS (v 20). In order to process the data, a one-way analysis of variance (ANOVA) test was employed. Comparing several groups' means. Results were presented as mean and standard deviation (SD), with P values that are higher than 0.05 being statistically non-significant and P values that are less than 0.05, 0.01, and 0.001 being statistically significantly different. The level of significance between the tested means was ascertained using the LSD test represented by the letters from (A) to (C) in decreasing order. The results are summarized in Table 1.

Table 1. Descriptive statistics of three study groups after antibacterial treatment.

Group order	Group type	Mean (CFU/ml)	SD	LSD	P value
Group I	Negative control	500 x10^4	250	C	
Group II	Positive control (CHX)	34 x10^4	5.8	B	0.001
Group III	Diode laser	24 x10^4	3.6	A	0.001

SD = Standard Deviation, LSD = The significance level, P value = probability value.

The results are represented by the mean and standard deviation of CFU following the interventions; colony counts for both groups significantly decreased. Group III has the lowest mean value (24 x 10^4 CFU/ ml), followed by group II (34 x10^4 CFU/ ml). The bacteria untreated in the negative control group, which has the greatest mean value as represented graphically in Figure 2. A, B, and C letters indicate the different levels of significance. The LSD test was used to determine the differences between the tested means that were significantly different. Also, the percentage of killing of bacteria was presented in Table.2

Table 2. Percentage of killing of the study groups.

Tested group	Percentage of killing
Group I	0 %
Group II	99.32 %
Group III	99.52 %

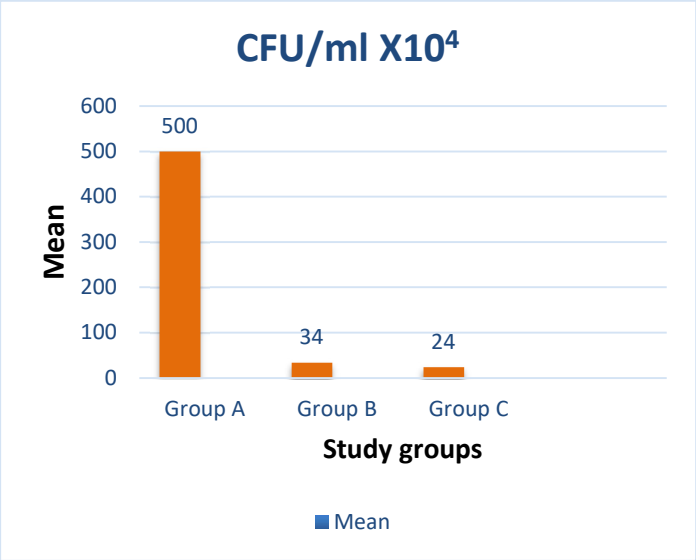

Fig. 2: Graphical representation of antibacterial activity among the tested groups.

Fig. 3: CFU of *S. mutans* bacteria on MSBA plates. Group A: Negative control (no treatment), Group B: Positive control (2% CHX irrigation), and Group C: Diode laser.

4. Discussion

The focus of the present study was to determine how the antibacterial properties of the 940 nm diode laser affected the survival of the S. mutans organisms. According to the results of the research, there were fewer bacterial colonies present, and there was a statistically significant difference between the CFU of the bacteria prior to and following irradiation (high significance P value 0.001). These results agree with a study performed by Robati et al. Streptococcus mutans and Lactobacillus bacteria at 108 CFU/ml concentrations were exposed to diode laser radiation at various doses and exposure durations to evaluate the laser's efficacy. The findings showed that the (980 nm) diode laser is especially effective at preventing the growth of the two types of bacteria at different times and doses 24 h after the irradiation (Robati et al., 2022), and this is strongly in line with the findings of the current study since the laser action was examined 24 h after exposure. This antibacterial action can be attributed to the photo-disruptive and thermal effects

of the diode laser's irradiation, which caused bacterial damage. (Nammour et al., 2021) When laser irradiation is done correctly, it is known to destroy bacterial cell walls, disrupt bacterial integrity, accumulate denatured proteins, cause cell lysis, and finally kill microorganisms. Additionally, protoporphyrin IX-containing and pigmented bacteria can be immediately destroyed by the diode laser's near-infrared light. (El Mobadder et al., 2022). A study by Hendi et al. used a laser with a 1 W output power and a 45-second exposure time for three subsequent exposures to test the antibacterial effects of 940 nm diode lasers on E. faecalis bacteria. The outcomes supported the findings of the current investigation, showing a decrease in bacterial colonies between the time they were exposed to 940 nm diode laser light and before exposure (P value 0.001). (Hendi et al., 2021) E. faecalis was destroyed by a 940-nm diode laser in a study by Castelo et al. They observed a 70% rate of bacterial killing by utilizing 3.5 watts of laser power in pulsed mode over a one-minute exposure length. More bacterial colonies were destroyed in the current study than in Castelo et al.'s examination because laser radiation of the bacterial suspension was applied continuously for 30 seconds, and this was consistent with the findings of the current study since 1 watt of power has the greatest ability to kill bacteria. (CASTELO et al., 2012)

One of the most popular disinfecting methods in dentistry for avoiding and inhibiting the growth of bacteria, particularly S. mutans, is chemical disinfection with chlorhexidine. (Mohan et al., 2016) Standard 2% CHX was employed in this investigation as a positive control because it is a disinfectant that is widely accessible on the market. The results of the investigation demonstrated that 2% CHX had high antibacterial properties and was effective against the S. mutans bacterium, as demonstrated by a decrease in CFUs/ml that provided a statistically significant difference (P value 0.001) when compared to the negative control group .

The results of this study agree with those of Vinothkumar, T. S. et al. They found that treating with 2% CHX greatly decreased the number of S. mutans and that diode laser was somewhat more effective at killing S. mutans than CHX. In comparison, CHX displays lesser antimicrobial properties than the diode laser, and this might be for various reasons, one of which is the photothermal effect of the laser. (Vinothkumar et al., 2020) The disinfectant's effectiveness is based on how well CHX sticks to microbe cell walls and lets intracellular components leak out. Small molecular weight components of the microorganism are released by CHX's bacteriostatic activity at low concentrations, but at higher concentrations, CHX causes cytoplasmic precipitation and/or coagulation, which is most likely brought on by protein cross-linkage and exhibits the bactericidal effect. (Mohan et al., 2016) According to the Hassaballah et al. investigation, the diode laser system is a more effective disinfectant for caries lesions than CHX and grape seed extract (Hasaballah et al., 2021). The study examined the efficacy of grape seed extract, CHX, and laser diode as primary disinfectants for dental cavities. There is agreement with the results of the present study, given that the outcomes of the diode laser group are better than those of the CHX group with a static difference (P value 0.001). When a laser beam contacts a tissue, a phenomenon known as photothermal interaction takes place in which the light energy is transformed into heat through a thermal interaction with the cellular molecules. It causes tissue to experience a number of effects, including heat, coagulation, vaporization, carbonization, and lastly, melting (Coluzzi, 2008). Theoretically, the intense absorption of laser light might cause the production of reactive oxygen species, which would kill bacteria directly by rupturing their cell membranes. (Yao et al., 2012)

5. Conclusion

According to the outcomes achieved from this study, the 940 nm diode laser has an antibacterial effect against bacteria that can cause tooth decay. So, it can be used as a potent disinfectant as a step in the tooth restoration process to help in bacterial elimination and cavity disinfection

References

BAHROLOLOOMI, Z., FEKRAZAD, R. & ZAMANINEJAD, S. 2017. Antibacterial effect of diode laser in pulpectomy of primary teeth. Journal of lasers in medical sciences, 8, 197.

BURAIHI, M. M. & ALKURTAS, S. A. 2020. The Photothermal Effect of 940nm Diode Laser on Enterococcus Faecalis Biofilm in Infected Root Canal. The Indian Journal of Pediatrics, 8, 480-486

CASTELO, B. P., MARTIN, B. B., RUIZ, P. M., RIVAS, M. B., BAHILLO, J., PEREZ, E. A., GUDE, F., MOOR, R. D. & VARELA, P. P. 2012. Combined sodium hypochlorite and 940 nm diode laser treatment against mature E. faecalis biofilms in-vitro.

CHALISHA, T. N., FEBRIANTI, N. N. & KUNARTI, S. 2021. Photodynamic Therapy 405 nm Diode Laser as Antibacterial for Cavity and Root Canal Sterilization. Conservative Dentistry Journal.

COELHO, A., AMARO, I., APOLÓNIO, A., PAULA, A., SARAIVA, J., FERREIRA, M. M., MARTO, C. M. & CARRILHO, E. 2021. Effect of cavity disinfectants on adhesion to primary teeth—a systematic review. International Journal of Molecular Sciences, 22, 4398.

COELHO, A., AMARO, I., RASCÃO, B., MARCELINO, I., PAULA, A., SARAIVA, J., SPAGNUOLO, G., MARQUES FERREIRA, M., MIGUEL MARTO, C. & CARRILHO, E. 2020. Effect of cavity disinfectants on dentin bond strength and clinical success of composite restorations—a systematic review of in vitro, in situ and clinical studies. International Journal of Molecular Sciences, 22, 353.

COLUZZI, D. J. 2008. Fundamentals of lasers in dentistry: basic science, tissue interaction, and instrumentation. J Laser Dent, 16, 4-10.

DE MANDAL, S. & PASSARI, A. K. 2021. Recent Advancement in Microbial Biotechnology: Agricultural and Industrial Approach, Elsevier.

EBRAHIMI, M., NASEH, A., ABDOLLAHI, M. & SHIRAZI, A. S. 2018. Can chlorhexidine enhance the bond strength of self-etch and etch-and-rinse systems to primary teeth dentin? Journal of Contemporary Dental Practice, 19, 404-408.

EL MOBADDER, M., NAMMOUR, S., NAMOUR, M., NAMOUR, A. & GRZECH-LEŚNIAK, K. 2022. Disinfection potential of 980 nm diode laser and hydrogen Peroxide (3%) in “critical probing depths” periodontal pockets: retrospective study. Life, 12, 370.

HASABALLAH, M., ABOU EL FADL, R., SHERIEF, D. & ABDELAZIZ, A. 2021. Comparison of efficacy of diode laser and grape seeds extract as cavity disinfectants in primary teeth-an in vitro study. Egyptian Dental Journal, 67, 1777-1785
.
HAYDARI, M., BARDAKCI, A. G., KOLDSLAND, O. C., AASS, A. M., SANDVIK, L. & PREUS, H. R. 2017. Comparing the effect of 0.06%-, 0.12% and 0.2% Chlorhexidine on plaque, bleeding and side effects in an experimental gingivitis model: a parallel group, double masked randomized clinical trial. BMC Oral Health, 17, 1-8.

HENDI, S. S., SHIRI, M., POORMORADI, B., ALIKHANI, M. Y., AFSHAR, S. & FARMANI, A. 2021. Antibacterial effects of a 940 nm diode laser with/without silver nanoparticles against Enterococcus faecalis. Journal of Lasers in Medical Sciences, 12.

JASSIM, R. K. 2022. Cavity Disinfection using Er,Cr:YSGG Laser by inducing Photo Acoustic streaming Master degree, University of baghdad.
KANDASWAMY, S. K., SHARATH, A. & PRIYA, P. G. 2018. Comparison of the effectiveness of probiotic, chlorhexidine-based mouthwashes, and oil pulling therapy on plaque accumulation and gingival inflammation in 10- to 12-year-old schoolchildren: A randomized controlled trial. International journal of clinical pediatric dentistry, 11, 66.

KASRAEI, S., SAMI, L., HENDI, S., ALIKHANI, M.-Y., REZAEI-SOUFI, L. & KHAMVERDI, Z. 2014. Antibacterial properties of composite resins incorporating silver and zinc oxide nanoparticles on Streptococcus mutans and Lactobacillus. Restorative dentistry & endodontics, 39, 109-114.

LEE, B. S., LIN, Y. W., CHIA, J. S., HSIEH, T. T., CHEN, M. H., LIN, C. P. & LAN, W. H. 2006. Bactericidal effects of diode laser on Streptococcus mutans after irradiation through different thickness of dentin. Lasers in Surgery and Medicine: The Official Journal of the American Society for Laser Medicine and Surgery, 38, 62-69.

LIAO, Y., BRANDT, B. W., LI, J., CRIELAARD, W., VAN LOVEREN, C. & DENG, D. M. 2017. Fluoride resistance in Streptococcus mutans: a mini review. Journal of oral microbiology, 9, 1344509.

MOHAMMADI, N., PARSAIE, Z., JAFARPOUR, D. & BIZOLM, F. 2020. Effect of different matrix metalloproteinase inhibitors on shear bond strength of composite attached to primary teeth dentin. European Journal of General Dentistry, 9, 147-151.

MOHAN, P. U., ULOOPI, K., VINAY, C. & RAO, R. C. 2016. In vivo comparison of cavity disinfection efficacy with APF gel, Propolis, Diode Laser, and 2% chlorhexidine in primary teeth. Contemporary clinical dentistry, 7, 45.

NAMMOUR, S., EL MOBADDER, M., MAALOUF, E., NAMOUR, M., NAMOUR, A., REY, G., MATAMBA, P., MATYS, J., ZEINOUN, T. & GRZECH-LEŚNIAK, K. 2021. Clinical evaluation of diode (980 nm) laser-assisted nonsurgical periodontal pocket therapy: a randomized comparative clinical trial and bacteriological study. Photobiomodulation, Photomedicine, and Laser Surgery, 39, 10-22.

PITTS, N., ZERO, D., MARSH, P., EKSTRAND, K., WEINTRAUB, J., RAMOS-GOMEZ, F., TAGAMI, J., TWETMAN, S., TSAKOS, G. & ISMAIL, A. 2017. Dental caries Nat Rev Dis Primers 3: 17030.

QIU, W., ZHOU, Y., LI, Z., HUANG, T., XIAO, Y., CHENG, L., PENG, X., ZHANG, L. & REN, B. 2020. Application of antibiotics/antimicrobial agents on dental caries. BioMed Research International, 2020.

ROBATI, M., YOUSEFIMANESH, H. & BAGHERI, S. 2022. Effect of low-level diode laser on streptococcus mutans and lactobacillus acidophilus growth: An invitro study. Journal of Oral Biology and Craniofacial Research, 12, 396-400.

SAAFAN, A., ZAAZOU, M. H., SALLAM, M. K., MOSALLAM, O. & EL DANAF, H. A. 2018. Assessment of photodynamic therapy and nanoparticles effects on caries models. Open Access Macedonian Journal of Medical Sciences, 6, 1289.

SADONY, D. M. & ABOZAID, H. E.-S. 2020. Antibacterial effect of metallic nanoparticles on Streptococcus mutans bacterial strain with or without diode laser (970 nm). Bulletin of the National Research Centre, 44, 1-6.

SADONY, D. M. & MONTASSER, K. 2019. Evaluation and comparison between the bactericidal effect of diode laser irradiation (970 nm) and silver nanoparticles on Enterococcus faecalis bacterial strain (an in vitro study). Bulletin of the National Research Centre, 43, 1-6.

SALEH, B. H., IBRAHIM, R. N. & AL-UGAILI, D. N. 2023. The Effect of Diode Laser on Viability and Antibiotic Sensitivity of Streptococcus mutans Isolated From Dental Caries. Iraqi Journal of Science, 583-593.
SELIVANY, B. J., KHADIM, M. A., SAEED, D. H. & SULIMAN, A. A. 2020. Effect of dispensing method and curing modes on the microleakage of composite resins. Journal of Baghdad College of Dentistry, 32, 9-15.

SHALLAL, L. F. & AHMED, M. A. 2022. Experimental In vitro Study to Assess the Antibacte-rial Activity of Thymus vulgaris Oil on Streptococ-cus Sanguinis. Journal of Baghdad College of Dentistry, 34, 17-27.

TOKUC, M., OZALP, S., TOPCUOGLU, N. & KULEKCI, G. 2019. Bactericidal effect of 2780 nm Er, Cr: YSGG laser combined with 940 nm diode laser in Enterococcus faecalis elimination: a comparative study. Photobiomodulation, Photomedicine, and Laser Surgery, 37, 489-494.

TOMA, J. J. & AZIZ, F. H. 2023. Antibacterial activity of three algal genera against some pathogenic bacteria. Baghdad Science Journal, 20, 0032-0032.

VINOTHKUMAR, T., RENUGALAKSHMI, A., EL-SHAMY, F., HOMEIDA, H., HOMMEDI, A. M., SAFHI, M. & ALSALHI, H. 2020. Antibacterial effect of diode laser on different cariogenic bacteria: An In-vitro study. Nigerian Journal of Clinical Practice, 23, 1578-1582.

WANG, X., CHENG, X., LIU, X., WANG, Z., WANG, J., GUO, C., ZHANG, Y. & HE, W. 2018. Bactericidal effect of various laser irradiation systems on Enterococcus faecalis biofilms in dentinal tubules: a confocal laser scanning microscopy study. Photomedicine and laser surgery, 36, 472-479.

YAO, N., ZHANG, C. & CHU, C. 2012. Effectiveness of photoactivated disinfection (PAD) to kill enterococcus faecalis in planktonic solution and in an infected tooth model. Photomedicine and laser surgery, 30, 699-704.

دراسة مختبرية للخاصية المضادة للبكتيريا لليزر الصمام الثنائي 940 نانومتر ضد بكتيريا المكورات العقدية الطافرة المعزولة من تسوس الأسنان

نها محمد جميل[1]*، حنان جعفر طاهر[1] ، تحرير نزال الدليمي[2]

[1]معهد الليزر للدراسات العليا، جامعة بغداد، بغداد، العراق
[2]كلية طب الاسنان، جامعة الانبار، العراق

*البريد الالكتروني للباحث: noha.mohammed1202a@ilps.uobaghdad.edu.iq

الخلاصة

الخلفية: العنصر المسبب الرئيسي لتسوس الأسنان هو بكتيريا المكورات العقدية الطافرة، لذا فإن التخلص من هذه البكتيريا له تأثير كبير على مدى جودة العلاج الترميمي. تم تطوير أساليب جديدة للقضاء على البكتيريا في طب الأسنان مثل الليزر والجسيمات النانوية المعدنية والمواد النشطة بيولوجيًا. الهدف من الدراسة: كان هدف هذه الدراسة هو تقييم فعالية ليزر الصمام الثنائي كعامل مضاد للبكتيريا ثم مقارنته بالتأثير المضاد للبكتيريا للكورهيكسيدين ضد البكتيريا.

المادة والطريقة: أجريت الدراسة على المكورات العقدية الطافرة بتركيز 10^6. تم الحصول على عينات من البكتريا من تسوس الأسنان ثم تم تحضير المعلق البكتيري ووضعه في أنبوب إيبندورف ليتم معالجته بمختلف الأشكال المضادة للبكتيريا، وقسمت العينات إلى ثلاث مجموعات تجريبية:المجموعة أ: مجموعة التحكم السلبية؛ المجموعة ب: مجموعة المراقبة الإيجابية باستخدام 2٪ كلورهيكسيدين ؛ المجموعة ج: التشعيع بليزرالصمام الثنائي (قدرة 1 واط لمدة 30 ثانية). تم حساب عدد الوحدات المكونة للمستعمرات لكل مجموعة بعد 24 ساعة من الحضانة على اطباق الوسيط المتخصص للبكتيريا.

النتائج: لوحظ انخفاض كبير في اعداد البكتيريا. أظهرت النتائج فرقًا إحصائيًا) قيمة ($p < 0.01$) لكلا المجموعتين مقارنة بمجموعة التحكم السالبة بدون علاج ، وأعطت مجموعة ليزر الصمام الثنائي أكبر انخفاض في اعداد البكتيريا من مجموعة الكلوروهكسيدين.

الاستنتاج: كان ليزر الصمام الثنائي وسيلة ناجحة وفعالة في القضاء على البكتيريا ، ويمكن استخدامه كخطوة في عملية ترميم الأسنان .

IJL, Issue 1, Vol. 23, 2024
https://doi.org/10.31900/ijl.v23i1.426

Research Article

Effect of laser cleaning parameters on aluminum 6061 surface properties

Zahraa M.saleh*, Ziad Aeyad Taha

Institute of Laser for Postgraduate Studies, University of Baghdad, Baghdad, Iraq
** Email address of the Corresponding Author: zahraa.mohammed1101a@ilps.uobaghdad.edu.iq*

Article history: Received 4 Oct.2023; Revised 14 Nov. 2023;Accepted 14 Nov. 2023; Published online 15 Jun. 2024

Abstract: This study investigates the crucial factors influencing laser cleaning processes, with a primary focus on aluminum 6061 surfaces. Laser power emerges as the central determinant, as higher power levels intensify the laser-matter interaction, leading to enhanced removal of oxide layers. A Microsecond fiber laser with a wavelength of 1064 nm was used in this study to identify optimal cleaning conditions, comprising parameters such as 3W power, a hatch value of 0.003, a speed of 150 mm/s, and a spot size of 200 µm. Furthermore, the research uncovers intriguing insights into the impact of cleaning speed on oxygen levels, revealing that higher speeds result in increased oxygen levels due to dual heat sources—laser beam and heat transfer from adjacent cleaned lines. The hatch parameter's role is highlighted in controlling the overlapping ratio, where closer line spacing leads to more effective cleaning and reduced surface oxygen content, while wider line spacing impedes cleaning between lines. Additionally, the study explores the potential enhancement of wear rates through laser cleaning, with material roughness playing a critical role, and notes that cleaned samples exhibit fewer defects in their microstructure compared to their uncleaned counterparts. These findings contribute valuable insights to the field of laser cleaning and its applications in surface treatment and material quality improvement.

Keywords: laser cleaning, aluminum 6061, oxide layer, roughness, wear.

1. Introduction

Nowadays, the aluminum alloy is a common material that widely used in industry due to its high strength, light weight , good weldability and corrosion resistance, it has good application in fields of shipbuilding, aerospace, and automobile [1-3]. However, aluminum has grate propensity to oxidize in the natural environment, with an oxide thin layer forming on the surface which is possibly contain impurities [4,5].
As is well-known, cleaning technology is particularly important for traditional industry like pre welding process in order to eradicate the contamination on the surface. Lately, there have been plenty of studies focusing on laser cleaning technology and its efficacy [6-8]. The main purpose of laser cleaning is to remove the oxide substrate on the metal surface. So, the cleaning of the oxide is generally identified by the oxygen content [2]. Latterly, some studies showed that laser cleaning has a significant effect on welding. Apparently, it could reduce welding defects with optimal laser cleaning parameters [9]. The laser cleaning

technique is an interaction between laser light and the substrate; therefore, the binding force between the substrate and the contaminant attached to the substrate surface is disrupted, and the contaminant on the substrate surface is detached from the substrate surface by evaporation, vibration, and impact [10,11]. Noteworthy, the energy density of the laser was the key factor affecting the cleaning process and surface quality In most cases, and the laser cleaning would cause an increase in surface roughness [12,13]. The proper laser cleaning process parameters can remove the rusting and grease from the workpiece surface[14]. Additionally, scanning speed has a significant effect on cleaning by changing heat accumulation on the surface of the rust layer [15,16]. When the roughness slightly increased with the laser power increasing also pulse frequency.

This study aims to remove the oxide layer from the aluminum 6061 surface through laser cleaning by using laser power, scanning speed, and line spacing (hatch) as variants of the cleaning process to examine their effects on the cleaning rate and identify the best parameters for removing oxide layer also explore the relationship between each variant and surface roughness.

2. Experimental procedures

In this study, aluminum alloy 6061 sheets (2 mm in thickness) were used as samples. The sample was cleaned with ethanol and air-dried at room temperature. The chemical composition of 6061 Al alloy is shown in Table 1.

Table 1. 6061 aluminum alloy chemical composition [17].

elements	Si	Fe	Cu	Mn	Mg	Zn	Cr	Al
experimental	0.6	0.36	0.2	0.05	0.95	0.04	0.13	Reminder
standard	0.4-0.8	≤ 0.7	0.15-0.4	≤ 0.15	0.8-1.2	≤ 0.25	0.04-0.35	Reminder

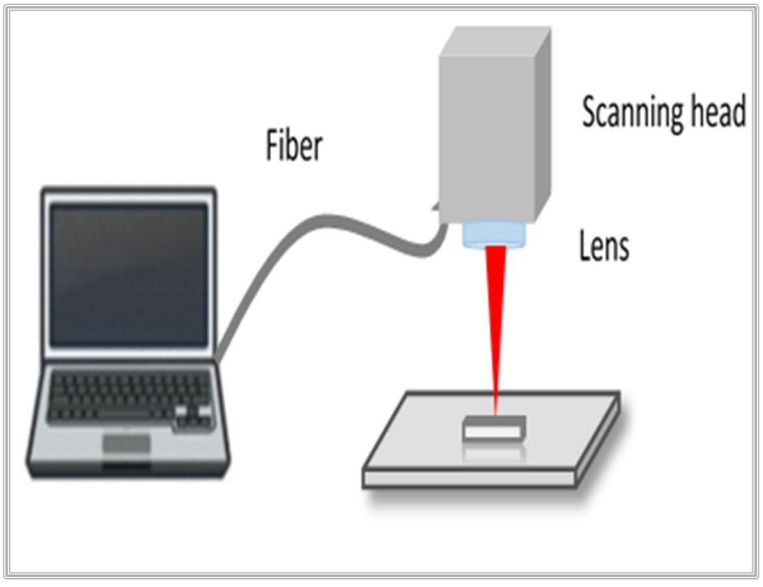

Fig. 1: Schematic of laser cleaning system.

Table 2. Main parameters of laser cleaning.

Parameter	Symbol	Value	Units
Wavelength	λ	1064	nm
Average power	P	10	W
Pulse width	T	10	μs
Pulse spot size	d	200	μm
Pulse repletion rate	p.r.r	20	kHz
scanning speed	V	50-250	mm/s

For laser cleaning, a fiber laser was used in this research. The system was equipped with a galvanometric scanning head, which controls the laser beam's motion in two directions, as shown in Figure 1. A special computer software was used to control the scanning head and to input laser parameters of the cleaning process, which are presented in Table 2.

For laser cleaning, different parameters were employed during the experiment, like speed, power, and hatch (line spacing). A number of trial experiments were carried out before determining the requested experiment range based on the criteria of avoiding the whiting (overheating) and ablation of base material with the oxide layer. A laser cleaning procedure has been carried out on aluminum alloy 6061 to remove a thin oxidation coating by manipulating different parameters with different values; laser power was varied in the range of (1-6)W, scanning speed (50,100,150,200,250)mm/s, and hatch (0.0005, 0.001,0.005,0.01) mm. The laser used in this work was (ytterbium fiber laser). In order to study the effect of laser cleaning aluminum alloy substrate, for surface characterization, scanning electron microscopy (SEM) was used. The chemical compositions and the oxygen contents were characterized using an energy-dispersive spectrometer (EDS). Also surface roughness of each sample was measured. Three positions of each sample were selected to calculate the mean value. In order to clean the entire surface area, the special strategy was based on the overlap in two dimensions depending on the scanning speed and frequency in the X axes and line spacing (Hatch) in the Y axes, as shown in Figure 2.

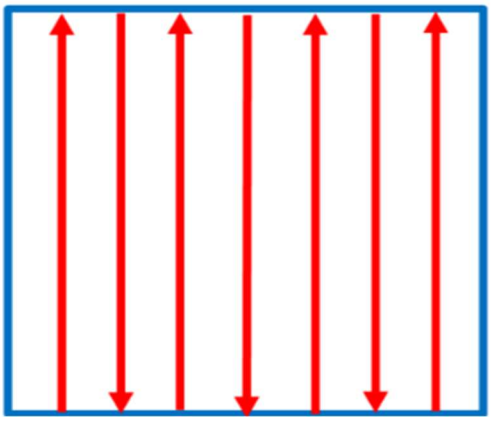

Fig.2: laser scanning strategy.

The overlapping rates of the X and Y axes can be calculated by using Eqs. (1) and (2) respectively[18].

$$Ox = \left(1 - \frac{v/f}{D+v\tau}\right) \times 100 \quad (1)$$

$$OY = \left(1 - \frac{P}{D}\right) \times 100 \quad (2)$$

Where ν is the beam scanning speed,f is the laser repetition rate, D is the laser spot diameter at the focal plane, τ is the pulse duration, and p is the step size (hatch).

For Wear rate investigation, sliding wear resistance has been conducted by a pin on steel disk method. The conditions through the tests were controlled to be: Normal force (N) = 5 N, speed of sliding (S) = 950 r.p.m, total sliding distance (D) = 65 mm, and time for the test were (5,10,15)min for each sample. Also, the roughness rate was measured by the SRT-6210 roughness device before and after the laser cleaning process.

3. Results and discussion

3.1. effect of laser power

Several power were employed from (1-10)W. Primary results showed that the power below 1 W was insufficient to influence the substance, with no reduction in oxygen content as well as no change in metal surface appearance (brightness), and the power above 6W, the oxygen content increased significantly, and an additional oxide layer formed with dark grey color and at maximum powers, the aluminum 6061 began to vaporize causing engraving of the metal surface. The effective laser cleaning parameter was from power 3 W to 6 W as the result of EDX clarified, as shown in Figure 3. The reduction in oxygen content exceeded 5W when compared to the uncleaned aluminum. The optimal outcome was observed at a 3W power level, a finding that agrees with the EDX mapping analysis in Figure 4; the mapping analysis of the aluminum 6061 surface shows oxygen content in green dots. Increasing the power above 5W led to a subsequent rise in the oxygen content, which was attributed to the formation of an additional oxide layer with a nanometer-scale on the metal surface, as shown in SEM images in figure (5) [19,20].Hence, the material exhibited a dark grey coloration at higher power levels.

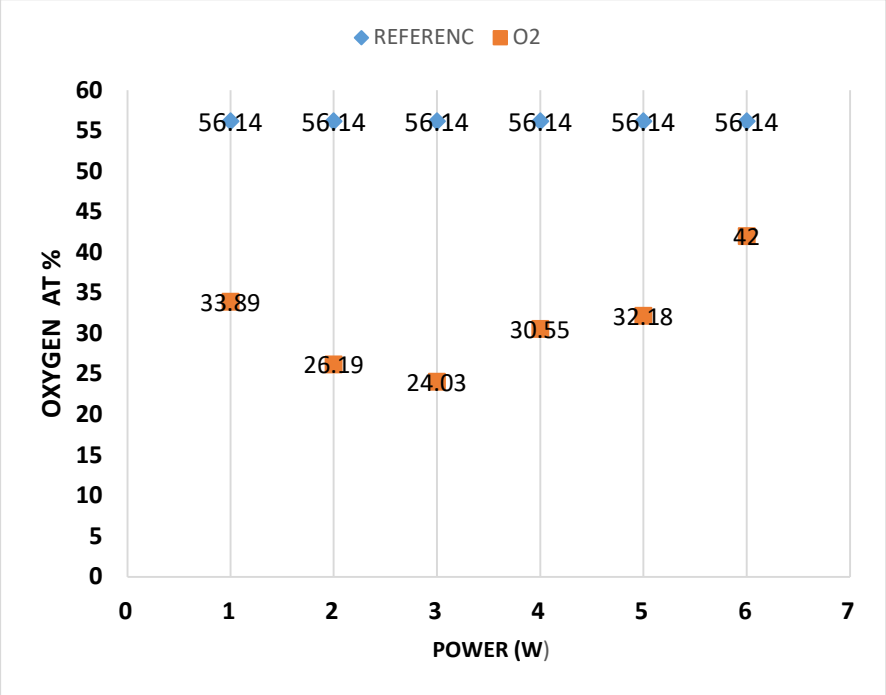

Fig. 3: surface oxygen content of the sample changes with cleaning power.

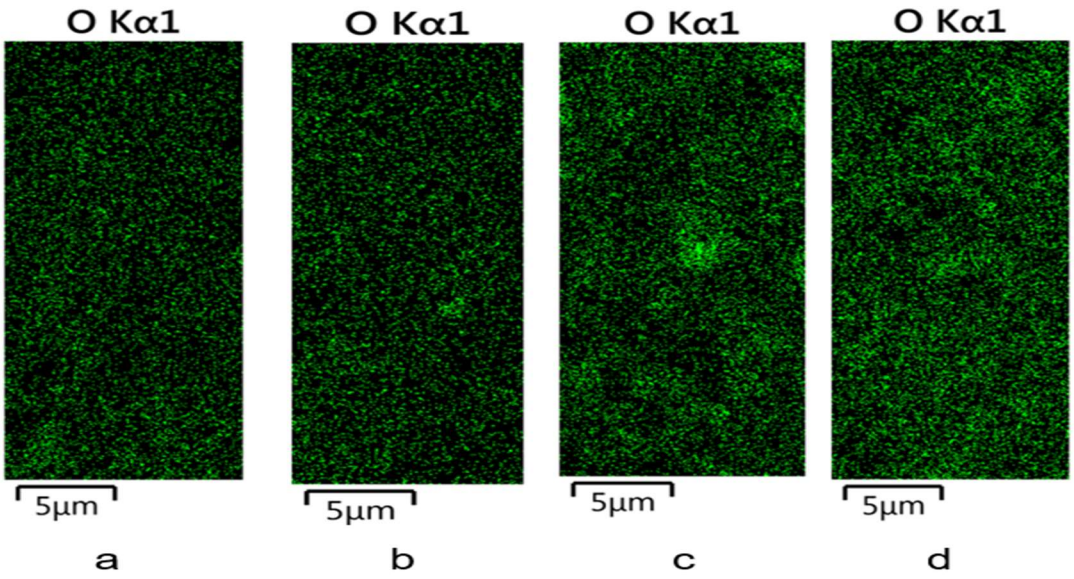

Fig. 4: EDS Mapping of oxygen content on the surface at (a) 2 W, (b)3 W ,(c) 4W, and (d) reference (no cleaning) the green dots are the oxygen particles.

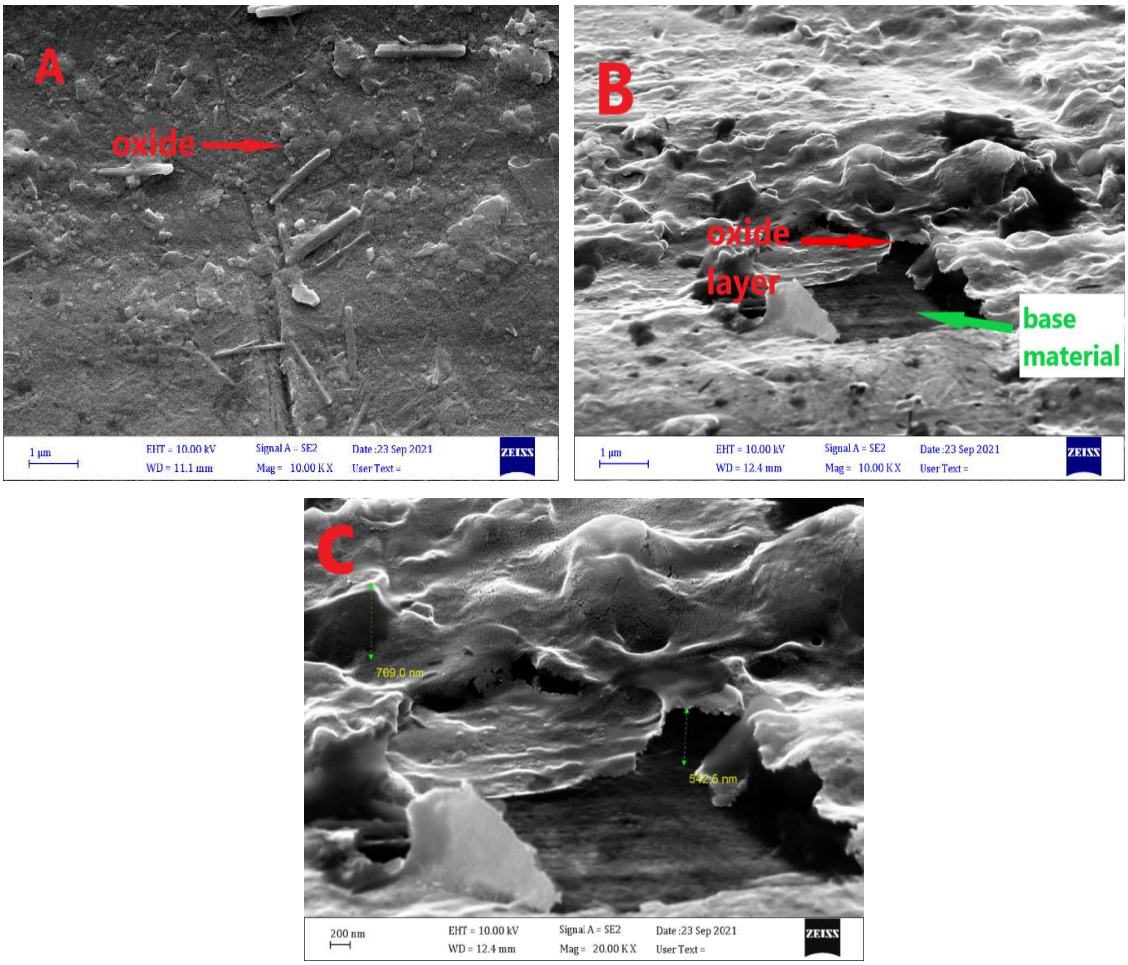

Fig. 5: SEM images for aluminum alloy 6061 A.as reserved B&C. different magnification for cleaned sample with power 5W speed ,150mm/s and hatch 0.004mm.

3.2. effect of laser cleaning speed

At low scanning speed (25mm/s) was not suitable for cleaning due to heat accumulation of aluminum, at (50mm/s) the oxygen content started to reduce, and the optimum result was from (100-150)mm/s the oxygen percentage was reduced by more than 40% from the uncleansed material, and then the oxygen content start to raise again as shown in Figure 6.

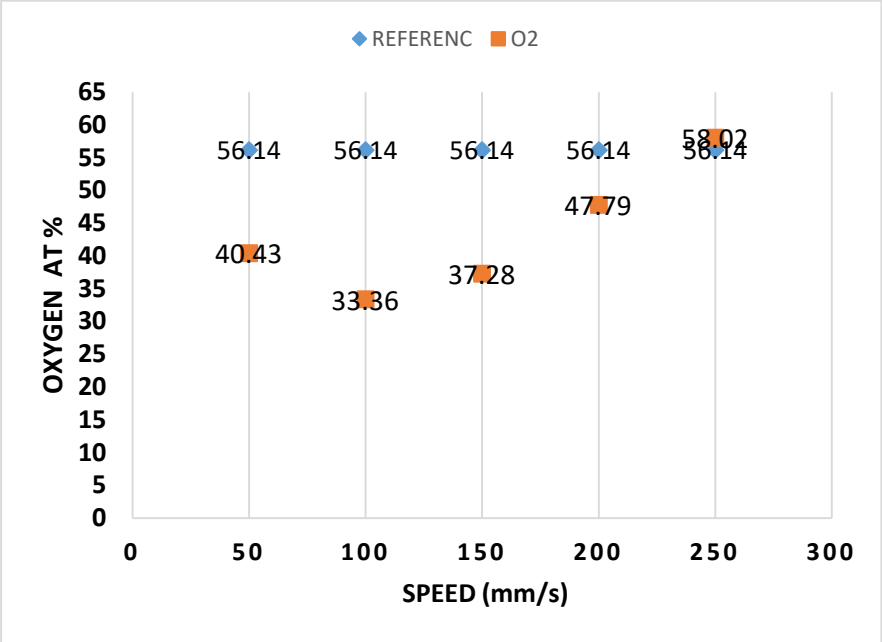

Fig 3 : Oxygen content change at different laser cleaning speeds.

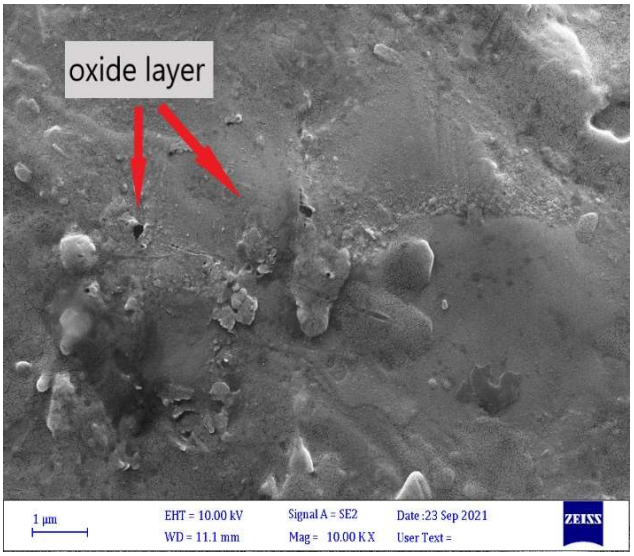

Fig.7: SEM images for aluminum alloy 6061 at high speed 400mm/s, power 3 W, and hatch 0.004 mm.

Beyond a speed of 400 mm/s, the cleaning process exhibited instability. Observations from the experiments revealed that the laser-material interaction initially proceeded normally but then transitioned into an aggressive interaction marked by sparks. This indicated the formation of an additional oxide layer, as shown in Figure 7; these findings contradicted previous research, which suggested that increasing speed would result in decreased energy absorption by the material because of the lower scanning speed of the laser; much more energy is given to the surface. This energy is absorbed and transformed in phonons that increase the material temperature [21]. We proposed that during laser scanning in a line pattern, high speeds introduce two sources of heat to the line: the first comes from the laser beam itself, while the second arises from the heat transferred from the previously cleaned adjacent line, effectively acting as a form of preheating for the material.

3.3. effect of line spacing (hatch)

Different hatch values were used from (0.0005 to 0.01) mm. At the smallest hatch, the oxygen content was high because of the high overlapping ratio, and it began to decrease by increasing the hatch value. At (0.005), the O2 percentage started to rise due to the diminished overlapping, so some places in the specimen will not be cleaned from the oxidation, as it is shown in Figure 8.

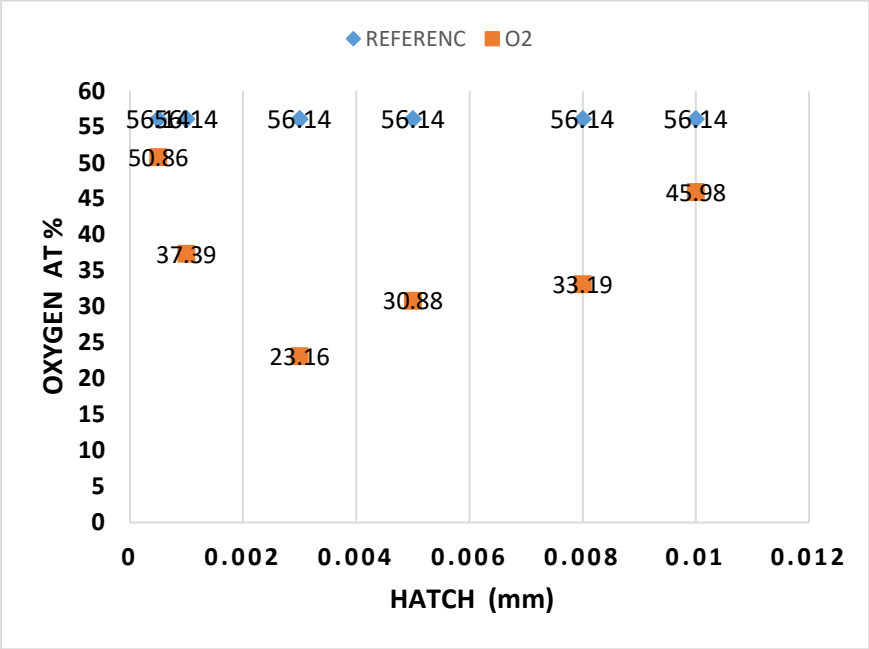

Fig. 4: surface oxygen content changes with Hatch.

4. Roughness test

Surface roughness plays a substantial role in the absorption of incident light by the laser-colored aluminum surface. This was due to the multiple reflections occurring within the hills and valleys of the surface, which lead to enhance the absorption rate hence improvement in the weld quality. Figures 9, 10 and 11 Shows the roughness test results for power, speed and hatch factor respectively .The roughness increases as the power increased less roughness rate was obtained at power 1W and the maximum roughness rate was at 6W power. Regarding the influence of speed, for speeds below 100 mm/s, the roughness of the base material was lower than that of the cleaned material. This behavior remained consistent for high speeds as well. The minimum

roughness value was observed at a speed of 150 mm/s. About the hatch factor the roughness value was high when the hatch was small because of high overlapping, and it became to decrease by increasing the hatch till it reached nearly the same value as base material.

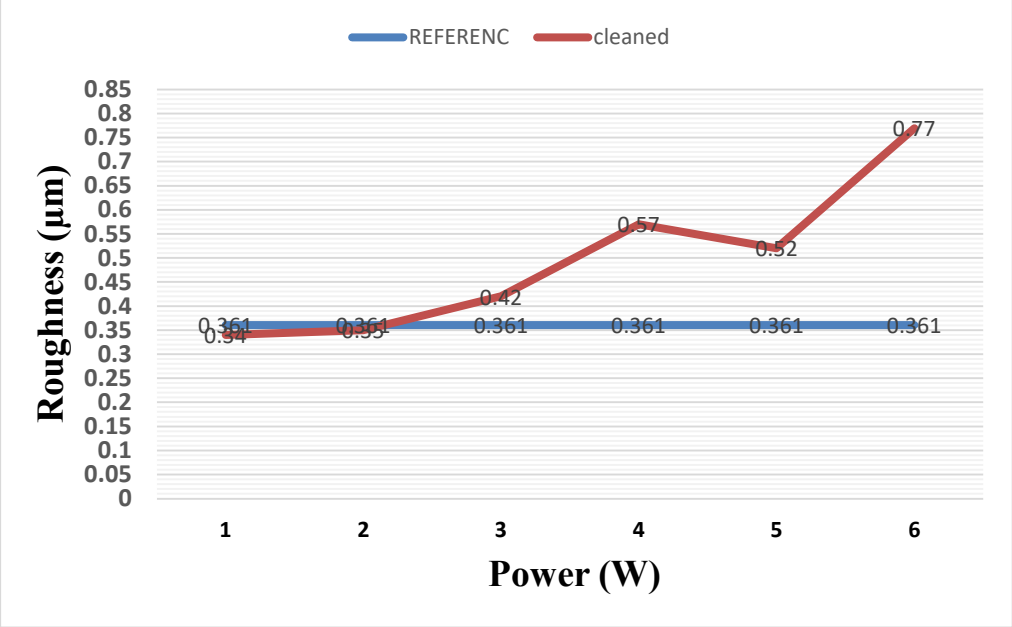

Fig. 9: The roughness for different power of cleaning.

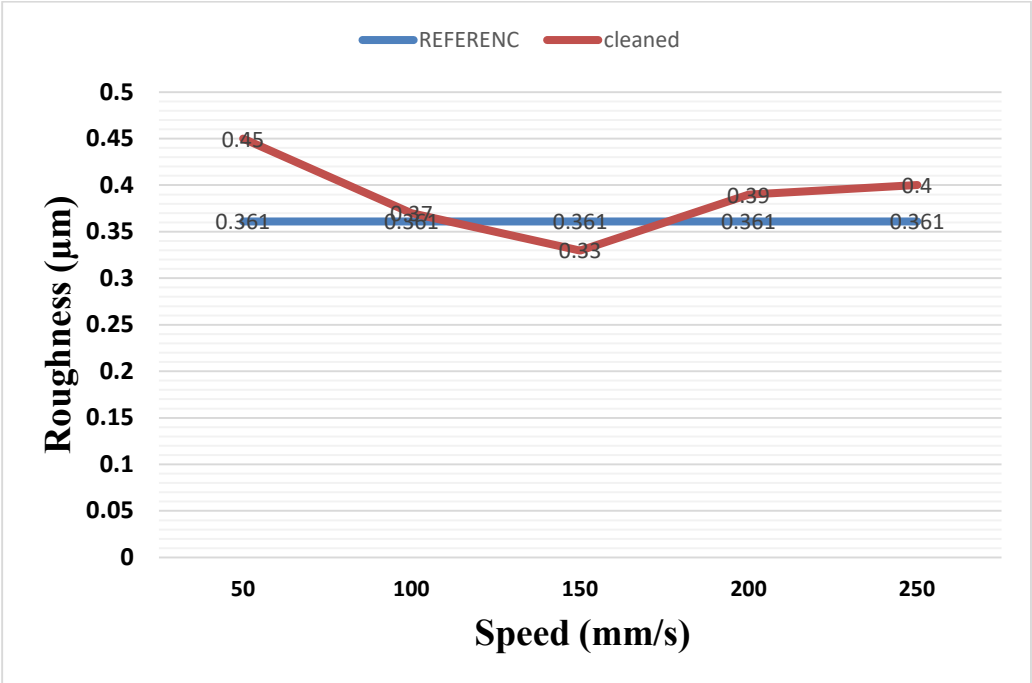

Fig. 10: The roughness for different speeds of cleaning.

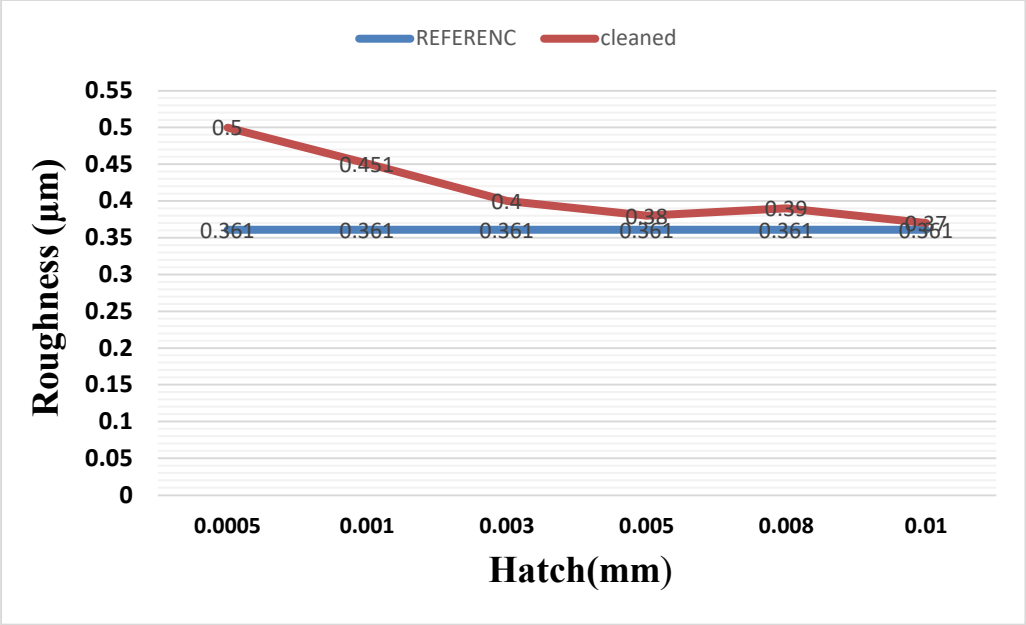

Fig. 11: The roughness for different line spacing (hatch).

5. Wear test

The wear resistance test was carried out for power (10% and 60 %) speed(50 and 150 mm/s) and hatch (0.0005 and 0.01mm). Also, the base material (without cleaning) was tested, and the samples were subjected to the same load for a similar period of time; Figure 12 illustrates the wear test results. The wear mainly increased with time increasing. The best result was at a power of 10 %, which is attributed to the low roughness value, which has a direct relation with the wear rate. Similarly, at 150mm/s speed, the wear rate was less than the base material due to the low roughness. The maximum wear rate was at 0.0005 mm hatch; this may be related to a new oxide layer of aluminum alloy that formed due to high accumulated heat; this oxide layer has low adhesion to the base material, which led to an increased depth of wear scar [22].

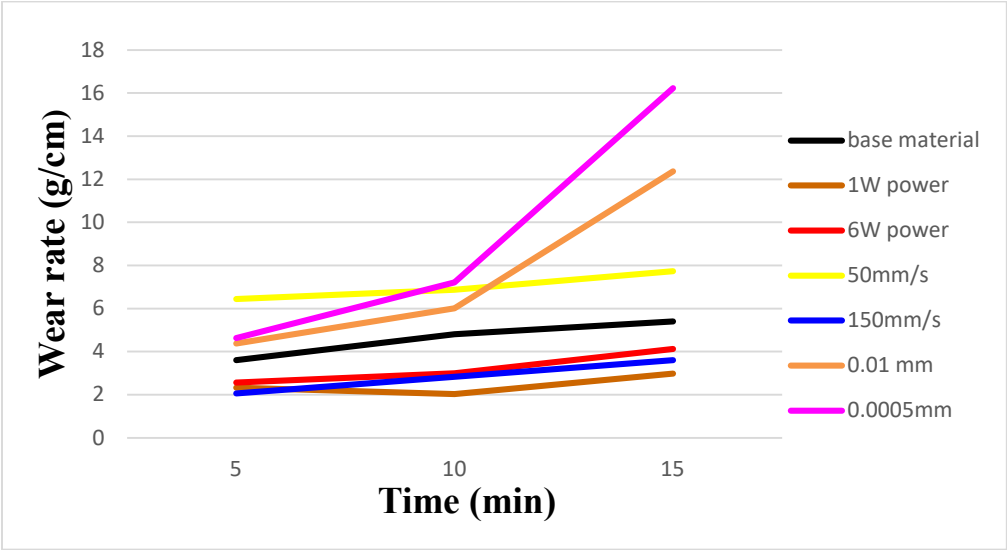

Fig. 12: Wear rate for aluminum 6061 cleaned with different parameters.

6. Conclusion

1. The key factor in the cleaning process is laser power, where higher power intensifies the laser-matter interaction, resulting in increased oxidation removal from the surfaces of aluminum 6061.
2. These effective cleaning results were achieved using parameters such as 3W power, a hatch of 0.003, a speed of 150 mm/s, and a spot size of 200 μm.
3. When cleaning at high speeds, oxygen (O_2) levels increase. The explanation is that during laser scanning in a line style, the high speed causes the line to receive heat from both the laser beam and the adjacent line that was cleaned previously, acting as preheating for the substances.
4. The hatch parameter plays a significant role in the cleaning process by controlling the overlapping ratio directly; closer line spacing leads to a higher overlapping ratio, resulting in more effective cleaning
5. Laser cleaning has the potential to enhance wear rate, with the extent of enhancement being directly related to material roughness. The microstructure of cleaned samples exhibits fewer defects compared to those left uncleaned.

References

[1] Hirsch, J. Recent development in aluminium for automotive applications. Trans. Nonferrous Met. Soc. China. 2014, 24, 1995–2002
[2] Zhu, Guodong, et al. "Investigation on the surface properties of 5A12 aluminum alloy after Nd: YAG laser cleaning." Coatings 9.9 (2019): 578.
[3] Khudhair AM, Hussein FI. High-Speed Shock Peening by Fiber Laser for Al Alloy 6061-T6 Thin Sheets. J Mater Eng Perform. 2022;31(10):8585-8595.
[4] Tawfeeq, I.S. and Taha, Z.A., 2022. Study the absorbance and band-gap of AL-4004 alloy via angular laser cleaning. Optik, 269, p.169842.
[5] AlShaer, A.W.; Li, L.; Mistry, A. The effects of short pulse laser surface cleaning on porosity formation and reduction in laser welding of aluminium alloy for automotive component manufacture. Opt. Laser Technol. 2014, 64, 162–171
[6] T. Shi, C. Wang, G. Mi, F. Yan, A study of microstructure and mechanical properties of aluminum alloy using laser cleaning, J. Manuf. Processes 42 (2019) 60-66
[7] M.K.A.A. Razab, A.M. Noor, M.S. Jaafar, N.H. Abdullah, F.M. Suhaimi, M. Mohamed, et al., A review of incorporating Nd: YAG laser cleaning principal in automotive industry, J. Radiat. Res. Appl. Sci. 11 (2018) 393-402
[8] Tawfeeq, I.S. and Taha, Z.A., 2022. The effect of laser parameters on the angular cleaning of aluminum 4004 alloy. Optik, 271, p.170078.
[9] Li R, Yue J, Shao X, Wang C, Yan F, Hu X (2015) A study of thick plate ultra-narrow-gap multi-pass multi-layer laser welding
[10] Bäuerle, D. Laser Processing and Chemistry; Springer Science & Business Media, Springer: Berlin, Germany, 2013.
[11] Shaker, E. and Taha, Z.A., 2023. Angular Laser Cleaning of Aluminum Al-4004 with Different Spot Sizes. Iraqi Journal of Laser, 22(1), pp.9-17.
[12] Zhang, Guangxing, et al. "Effect of laser cleaning process parameters on the surface roughness of 5754-grade aluminum alloy." The International Journal of Advanced Manufacturing Technology 105.5 (2019): 2481-2490
[13] Messaoudi H, Mehrafsun S, Tromenschläger W (2017) Picosecond laser cleaning of hot stamped 22MnB5 steel. J Mater Sci Surface Eng 5(1):504–508
[14] Zhu, L., Sun, B., Li, Z., Pan, X., Chen, Y. and Cao, Y., 2020. The weld quality improvement via laser cleaning pre-treatment for laser butt welding of the HSLA steel plates. *Welding in the World*, *64*, pp.1715-1723.
[15] Wang Z, Zeng X, Huang W (2003) Parameters and surface performance of laser removal of rust layer on A3 steel. Surf Coat Technol 166(1):10–16
[16] Ali, S.N., Taha, Z.A. and Mansour, T.S., 2014. Laser cleaning using Q-switched Nd: YAG laser of low carbon steel alloys. Advances in Condensed Matter Physics, 2014
[17] 6. Davis JR. Aluminum and aluminum alloys. ASM international; 2001
[18] J. Sabbaghzadeh et al., "Effect of process parameters on the melting ratio in overlap pulsed laser welding," Metall. Mater. Trans. B 39(2), 340–347 (2008).

[19] Andreeva, Y.M., Luong, V.C., Lutoshina, D.S., Medvedev, O.S., Mikhailovskii, V.Y., Moskvin, M.K., Odintsova, G.V., Romanov, V.V., Shchedrina, N.N. and Veiko, V.P., 2019. Laser coloration of metals in visual art and design. Optical Materials Express, 9(3), pp.1310-1319
[20] Khafaji, N.Y., Demir, A.G., Taha, Z.A. and Previtali, B., 2019. Influence of Processing Gas Composition on Laser Colouring of Commercially Pure Titanium. Lasers in Engineering (Old City Publishing), 42.
[21] Maltais, J., Brochu, V., Frayssinous, C., Vallée, R., Godmaire, X. and Fraser, A., 2016. Surface analysis study of laser marking of aluminum. Proceedings of ICSOBA
[22] Ren, Y., Wang, L., Li, J., Cheng, W. and Ma, X., 2022. The surface properties of an aviation aluminum alloy after laser cleaning. Coatings, 12(2), p.273.

تأثير عوامل التنظيف بالليزر على خصائص سطح الألومنيوم 6061

زهراء محمد صالح ، زياد اياد طه

معهد الليزر للدراسات العليا، جامعة بغداد، بغداد، العراق

*البريد الالكتروني للباحث: Zahraa.mohammed1101a@ilps.uobaghdad.edu.iq

الخلاصة: تتناول هذه الدراسة التحقيق في العوامل الحاسمة التي تؤثر على عمليات تنظيف الليزر، مع التركيز الأساسي على سطوح الألومنيوم 6061. يظهر القدرة الليزرية كعامل محوري، حيث تزيد مستويات القدرة العالية من تفاعل الليزر مع المادة، مما يؤدي إلى إزالة محسنة للطبقات الأكسيدية. تحدد الدراسة شروط التنظيف الأمثل، متضمنةً معلمات مثل 3,واط من القدرة، قيمة تقاطع بمقدار 0.003، سرعة 150 ملم/ث، وحجم بقعة الليزر بمقدار 200 ميكرومتر. علاوة على ذلك، تكشف البحث رؤى مثيرة حول تأثير سرعة التنظيف على مستويات الأكسجين، مُظهرًا أن السرعات العالية تؤدي إلى زيادة مستويات الأكسجين نتيجة وجود مصدري حرارة مزدوجين - الشعاع الليزري ونقل الحرارة من خطوط التنظيف المجاورة. يتم التأكيد على دور معلمة التقاطع في التحكم في نسبة التداخل، حيث يؤدي التقاطع الأقرب بين الخطوط إلى تنظيف أكثر فعالية وانخفاض محتوى الأكسجين على السطح، بينما يعيق التقاطع الأوسع تنظيف الفجوات بين الخطوط. بالإضافة إلى ذلك، تستكشف الدراسة إمكانية تحسين معدلات التآكل من خلال تنظيف الليزر، حيث يلعب تخطيط المواد دورًا حاسمًا، وتشير إلى أن العينات المنظفة تظهر عيوبًا أقل في هيكلها المجهري مقارنةً بأقرانها غير المنظفة. تقدم هذه النتائج رؤى قيمة في مجال تنظيف الليزر وتطبيقاته في معالجة الأسطح وتحسين جودة المواد.

IJL, Issue 1, Vol. 23, 2024
https://doi.org/10.31900/ijl.v23i1.418

Research Article

IRAQI JOURNAL OF LASER

In vitro study the effect of laser photon-induced photoacoustic streaming on the enterococcus faecalis biofilm in complicated root canal system

Ghufran I. Ibrahim*, Hussein A. Jawad

Institute of Laser for Postgraduate Studies, University of Baghdad, Baghdad, Iraq
** Email address of the Corresponding Author: whitetooth666@gmail.com*

Article history: Received 11 Sept.2023; Revised 26 Nov. 2023; Accepted 2 Dec. 2023; Published online 15 Jun 2024

Abstract

Objective: The purpose of this in vitro study was to assess the efficacy of an erbium, chromium: yttrium scandium gallium garnet (Er, Cr: YSGG) laser using photon-induced photoacoustic streaming (PIPS) in the agitation of irrigation fluids in the complicated root system that infected with Enterococcus faecalis (E. faecalis).

Methods: The mesial roots of 90 recently extracted first and second lower human molars were separated, injected with Enterococcus faecalis suspension (except for the negative control group samples), and cultivated for thirty days. The samples were divided into five groups (n=15), first group acted as a positive control (inoculated untreated) (G1), syringe irrigation groups were irrigated with 5.25% sodium hypochlorite (NaOCl) (G2) and 2% chlorohexidine gluconate (CHX) (G4), laser groups were irrigated by 5.25% NaOCl (G3) and 2% CHX (G5) with Er, Cr: YSGG laser activation at 700 µs, 5 Hz, (0.25, 0.5, 0.75, 1, and 1.25) W. AFM, or atomic force microscope, was employed as a novel technique to obtain data in the isthmus region. A scanning electron microscope (SEM) was also used in the study to confirm the results obtained from an atomic force microscope parameter. Statistical Package for Social Sciences (SPSS) software was used to collect and analyze data, and the study groups' means were compared using analysis of variance (ANOVA).

Results: After the results were statistically analyzed, the laser group with 2% chlorohexidine gluconate and 5.25% sodium hypochlorite showed a significant decrease in surface roughness than the syringe irrigation and the positive control groups ($p<0.05$).

Conclusions: Based on the investigation's findings, the agitation of 2% chlorohexidine gluconate solution by Er, Cr: YSGG laser in photon-induced photoacoustic streaming at 1 W offers a better mechanism for bacterial biofilm removal than the conventional treatment technique. Whereas activation of 5.25% sodium hypochlorite with low-power laser at 0.25 and 0.5 W increased its efficacy.

Keywords: Atomic force microscope, 2% chlorhexidine gluconate, Enterococcus faecalis biofilm, Er; Cr: YSGG laser, sodium hypochlorite.

1. Introduction

The most well-known cause of root canal therapy failure is the continuation of intra-radicular infection due to inadequate bacterial clearance (Dioguardi et al., 2019). Microorganisms may survive even in fully managed teeth in dentinal tubules, canal irregularities, deltas, and isthmus regions (Nair, 2004). The isthmus

is a communication between two or three root canals with pulp tissue within them. Its anatomic complexity results in challenging debridement. The prevalence of isthmus in the mesial roots of permanent lower molars ranges from 80.6% to 100% on complete root investigation (Natanasabapathy et al., 2021). The purpose of the irrigating solutions is to clean and disinfect the portions of the root canal system that have skipped instrumentation because more than half of the root canal walls have remained untouched after canal instrumentation (Peters et al., 2001).

The most commonly used antibacterial irrigation solutions are sodium hypochlorite (NaOCl), which is an efficient organic solvent as well as a powerful antibacterial agent (Cullen et al., 2015), and chlorhexidine gluconate (CHX), which is a broad-spectrum antibacterial fluid that works to combat both gram-positive and gram-negative bacteria as well as yeasts (Abdelgawad et al., 2020). However, the isthmus regions are not accessed by instruments and may not be reached by irrigation solutions due to restricted penetration and diffusion of the irrigation solution, so the microorganisms may persist in these regions (Berutti et al., 1997). As a result, it is critical to work on novel strategies to ensure irrigation fluid reaches inaccessible places, thereby improving endodontic outcomes. Recently, the laser photon-induced photoacoustic streaming (PIPS) technique was introduced to activate the irrigation solution for improving root canal disinfection and cleaning (Rasheed and Jawad, 2021). This technique is used by an Erbium laser family in sub-ablative settings. An erbium, chromium: yttrium scandium gallium garnet (Er, Cr: YSGG), is a type of water-absorbing laser widely used in endodontics (Al-Karadaghi et al., 2015). Many factors are known to influence PIPS effectiveness, including the irrigant used, the canal dimensions, the area to be disinfected, and laser settings (Zhu et al., 2013). In this investigation, atomic force microscopy (AFM) was used to evaluate biofilm removal, which is a computer-driven mechanical microscope that can report surface roughness values quantitatively and provide high-resolution three-dimensional topographical imaging of biological samples.

This method has been commonly used to examine the mechanism of antimicrobial activity on bacteria, and it is a helpful instrument for biologists (Gadegaard, 2006). López-Jiménez et al. used AFM to examine the changes on the surface of E. faecalis after treatment with Erbium laser and diode lasers and concluded that AFM is a useful tool for determining microbial survivability as a measure of antimicrobial efficacy (López-Jiménez et al., 2015). While Kumar et al. assessed the efficiency of laser activation of sodium hypochlorite in eliminating multispecies biofilms from the mesial root of permanent molars using confocal microscopic imaging and found that the laser agitation displayed effective isthmus cleaning (Kumar et al., 2022).

The goal of this investigation was to assess the efficacy of Er, Cr: YSGG laser in PIPS by agitation of irrigation fluids in the isthmus, which was infected with a mature bacterial biofilm.

2. Materials and Methods

The Helsinki Declaration was considered in this study. The procedures utilized in this investigation obtained ethical approval. (BU-2022-488).

2.1 Selection and preparation of samples

90 recently extracted first and second lower human molars with an isthmus in the mesial root were chosen from a group of 100 molars (patients aged 23 to 40 years old). The teeth were collected from November 2022 to June 2023 at Martyr Dr. Wassim Dental Specialist Center/ Department of Oral Surgery. The reason for extraction was pulp pathology. All collected molars were imaged using cone-beam computed tomography and samples that have a continuous isthmus between the mesiobuccal and mesiolingual canals were selected (Figure 1) (Bago et al., 2023). Then all samples were kept in plastic tubes containing saline water and 0.1% crystals of thymol (Lab Grade, Lab Alley, Texas, USA) until the experiment' day.

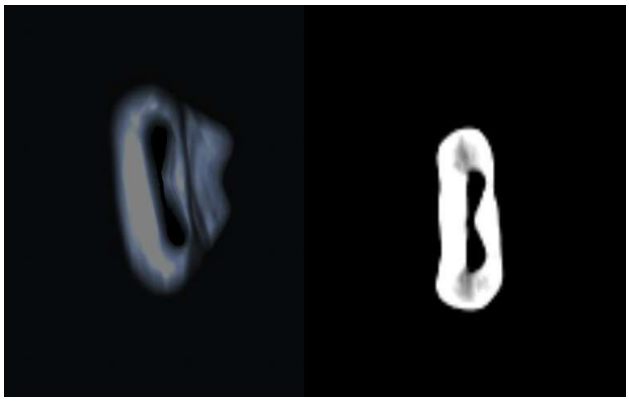

Fig.1. A CBCT image of a lower molar mesial root shows the isthmus between the mesiolingual and mesiobuccal canals.

The working length (WL) was determined by sighting the file tip through the apical foramen and subtracting 1 mm from the observed file length (Kumar et al., 2022). All canals were instrumented to this working length up to size 25/.04 NiTi engine files (X3 Never Break, Easy smile Co., USA) at speed (300 rpm) and torque (2 Ncm), as suggested by the manufacturer (Kimura et al., 2020). 5.25% NaOCl (Cerkamed, Poland) was delivered after each file size during the preparation process using an irrigation needle with side opening (Endo-Top, Hang Zhou Endo-Top Co., China). One ml of 17% EDTA (Cerkamed, Stalowa Wola, Poland) was utilized as the last irrigant, and it was kept inside for three minutes. During this time, the solution was stimulated for 30 seconds with an ultrasonic instrument (Guilin-Woodpecker Co., China).

The residual irrigation solutions were then removed by rinsing all of root samples with five milliliters of distilled water (Pioneer-Company, Iraq). cotton pads were used to clean the root's surface, and paper points were used to dry the canals (Sure endo, Sure-Dent Corporation, Korea) (Parente et al., 2010). All roots were separately inserted in Eppendorf tubes (Lab-Serv et al., India) and sterilized for 20 min at 121°C and 15 psi pressure.

2.2 Bacterial inoculation

E. faecalis colonies were obtained from an agar plate (Himedia, Mumbai, India), which was previously streaked by bacteria. Then activated by placing them in brain heart infusion (BHI) broth (Himedia, Mumbai, India) for 24 h. The obtained suspension was then subject to a series of dilutions to obtain suspension equal to the standard of McFarland (1.5×10^{8} CFU/ml) (Cheng et al., 2012).

The bacterial suspension was introduced into the root canals (except for 15 roots, which act as a negative control) using a 30 gauge irrigation needle until the canals were filled completely (Cheng et al., 2016). After that, each root specimen was placed in an Eppendorf tube and submerged in 1.5 ml of BHI broth. All sample containers were maintained under aerobic conditions at 37°C for 30 days. To ensure the availability of living bacterial cells during the incubation period, re-inoculation of the canals with the suspension was done every three days. The BHI was also replaced every day with a fresh one to provide good nutrition.

2.3 Treatment groups

At the end of the incubation time, an injection needle was used to remove the liquid medium from the tubes, and each root sample was subjected to multiple processes, including cleaning the samples' surfaces with sterile cotton pads dipped in 5.25% NaOCl. The samples were then placed in plain tubes filled with impression material (Kro-malgin, Vannini-dental, Italy) for easier handling. In pilot study, the laser pulse repetition rate was examined with different values (5, 10, and 15 Hz) and 5.25% NaOCl used as an irrigant. The results were obtained by the traditional colony formation unit (CFU). Finally divided randomly into five groups:

G1: The positive control group (n=15)
The samples of this group did not get any sort of therapy.

G2: 5.25% NaOCl+ syringe irrigation (SI) group (n=15)
The sample's canals were irrigated with 1 ml of 5.25% NaOCl delivered by 30-gauge irrigation needle and kept inside the canals for 2 min, then washed with 5 ml of distilled water.

G3: 5.25% NaOCl + Er, Cr: YSGG laser group (n=15)
The sample's canals were irrigated with 5.25% NaOCl and kept inside the canals for 2 min, throughout this time, the fluid was activated by a 2780 nm Er, Cr: YSGG laser (Biolase, Waterlase, CA, USA) at 700 µs, 5 Hz according to the pilot study, and (0.25, or 0.5, or 0.75, or 1, or 1.25) W for 60 seconds, three samples for each power. The laser was activated for 30 sec of (on) time, followed by 30 sec of (off) time, which was repeated twice (an overall duration of 60 sec). The canals were then rinsed with 5 ml of distilled water.

G4: 2% CHX +SI group (n=15)
An irrigation needle (30 gauge) was used to deliver 2% CHX irrigant in to the canals and kept inside the root canals for 2 min, then rinsed with 5 ml of distilled water.

G5: 2% CHX+ Er, Cr: YSGG laser group (n=15)
The sample's canals were irrigated with 2% CHX and kept inside the canals for 2 min, within this period, the irrigant was activated by a 2780 nm Er, Cr: YSGG laser for 60 sec at the same settings of the previous laser agitation group (G 3). The laser was activated for 30 sec of (on) time, followed by 30 sec of (off) time, which was repeated twice. The canals were then rinsed with 5 ml of distilled water. Prior to laser activation, infrared laser safety glasses (Innovative-Optics, Hemlock, USA) were worn. A new design water Lase iPlus /MD tip (MZ6 tip diameter = 600 m, length = 6 mm) was utilized.
The settings of water and air spray of the laser unit were both set to (off). The tip was placed just inside the canal opening, stayed fixed, and was not moved apically into the root canal during the procedure.

3. Preparation of the samples for AFM and SEM observation

In order to keep tooth-cutting debris out of the canals and isthmus, proper-sized paper points were put in the root canals. All roots were marked and cut longitudinally with a double-face diamond disk. A middle area of the isthmus area was marked for observation by the AFM (Nanosurf, Liestal, Switzerland) (Figure 2).

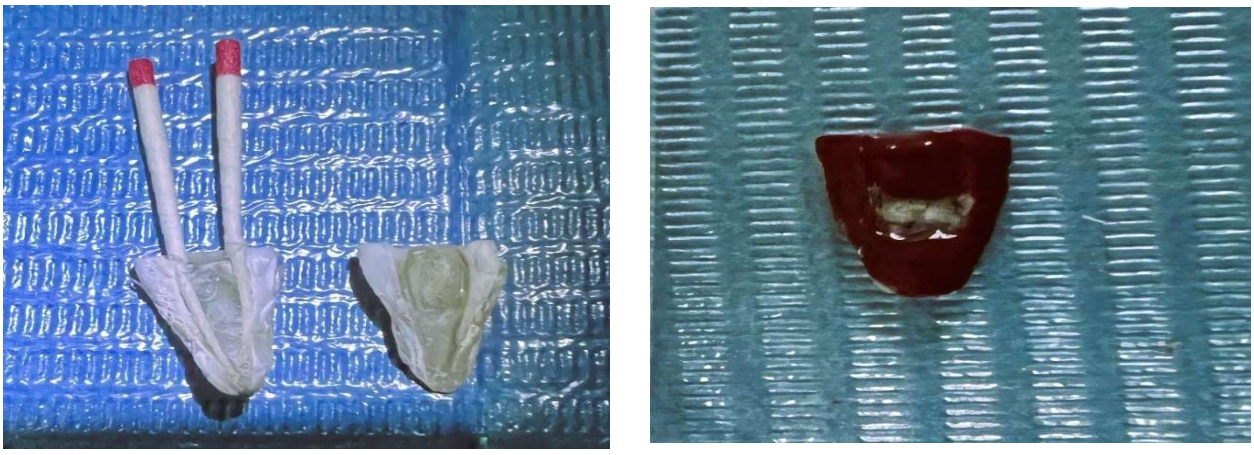

(a) **(b)**

Fig. 2. Root sectioning for AFM inspection: (a) a longitudinally divided root sample; (b) the center portion of the isthmus is marked on one root division prepared for the AFM observation.

The remaining halves of the roots were mounted on an aluminum base and metalized with a gold covering by vacuum evaporation, then a scanning electron microscope (SEM) (Inspect F-50, FEI Electron Optics International B.V., Netherlands) was used to examine the samples at 13 000 magnification power**.**

4. Statistical analysis

The Statistical Package for Social Sciences (SPSS) version 21 (IBM, Armonk, USA) was used to analyze the data. It was presented as a mean, and categorical data was represented by the standard deviation. The means of the tests were compared using analysis of variance (ANOVA). The least significant difference (LSD) test was used for calculating the significant differences among the tested means. Letters (A, B, C, D, E, and F) demonstrated the levels of significance, the letter (A) being the most significant and decreasing with the last one. Identical letters indicate that there are no significant variances in the measured means. $p>0.05$ results were regarded statistically not-significant, whilst $p\leq0.05$ was considered a significant value.

5. Results

Relatively low peaks and shallow valleys can be seen on the exterior of the uninoculated isthmus surface in figure 3 three-dimensional (3D) AFM image. The infected isthmus surface was depicted in figure 4 using an AFM image that had high peaks and low valleys. Also, a three-dimensional image of the isthmus surface after treatment with 2% CHX agitated by laser PIPS at 1 W showed a bumpy surface with round peaks and a few shallow valleys (Figure 5).

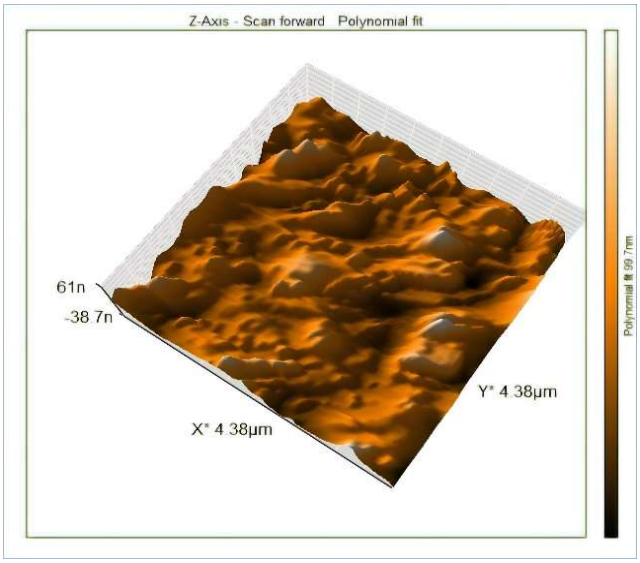

Fig.3. Three dimensions AFM image of uninoculated isthmus area about 6 mm away from the apex.

The root mean square roughness (Sq.) values that were measured for all groups samples were statistically analyzed and then compared to each other by ANOVA. The isthmus surface roughness was different among all groups under study ($p\leq0.05$). The lowest root mean square value was presented in the 2% CHX group that agitated by laser PIPS at 1 W (G 5), followed by 5.25% NaOCl group that agitated by laser PIPS at (0.25 or 0.5) W (G 3), 5.25% NaOCl+ SI group (G 2), and 2% CHX + SI group (G 4) respectively. The highest root mean square value was presented in the positive control group (G1).

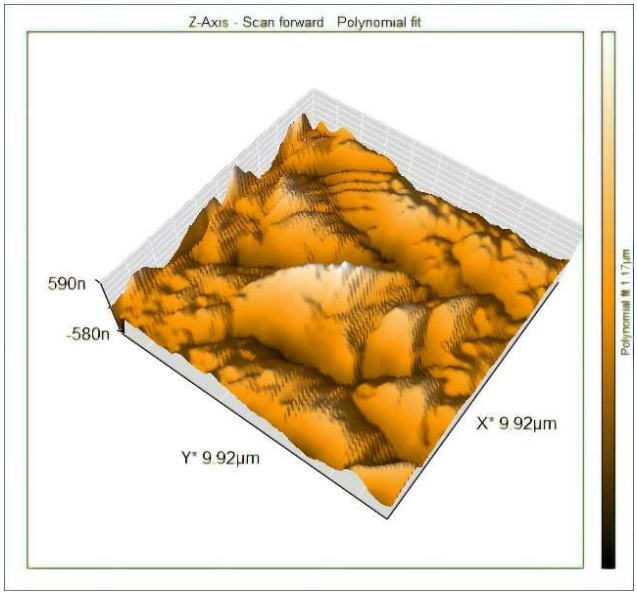

Fig. 4. Three dimensions image of the isthmus surface after inoculated with the bacteria suspension for 30 days.

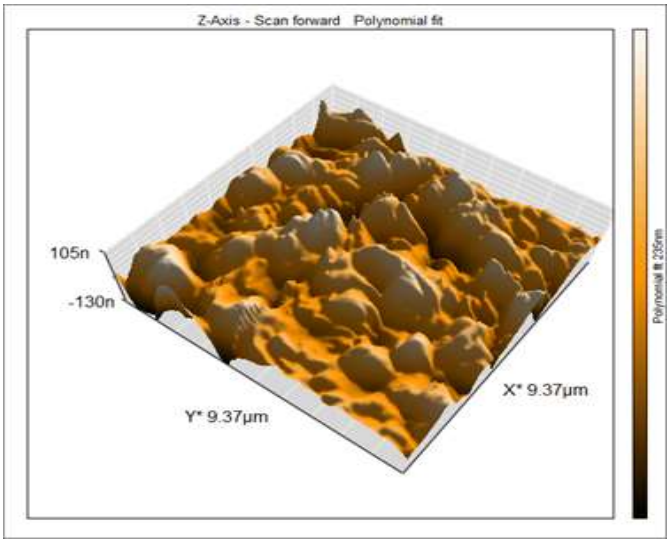

Fig.5. Three dimensions image of the isthmus surface after treatment with2% CHX agitated by laser PIPS at 1 W.

There was no significant difference found between the laser agitated at (0.25 or 0.5) W with NaOCl in this regard. The results of all test groups are shown in tables 1, 2, and 3 and in Figures 6 and 7.

Before the treatment, field emission scanning electron microscopy (FE-SEM) pictures were obtained at a distance of roughly 6 mm from the apex. These images showed that the isthmus surface was covered with debris and a thick layer of biofilm (Figure 8 a). On the other hand, after the CHX and laser treatment at 1 W SEM images showed a clean surface with open dentinal tubules (Figure 8b).

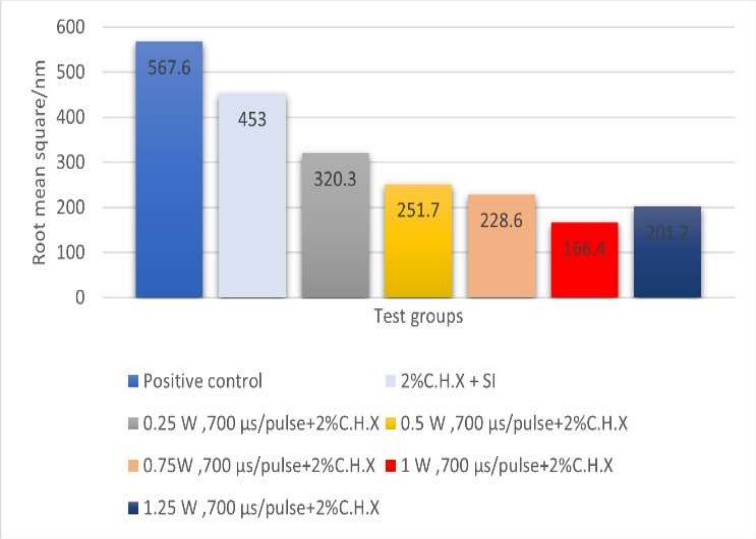

Fig. 6. Statistical columns chart showing the means of root mean square roughness values of positive control group (G 1), 2% CHX + needle irrigation group (G 4), and laser agitation 2% CHX group (G 5), the red column represents the best result.

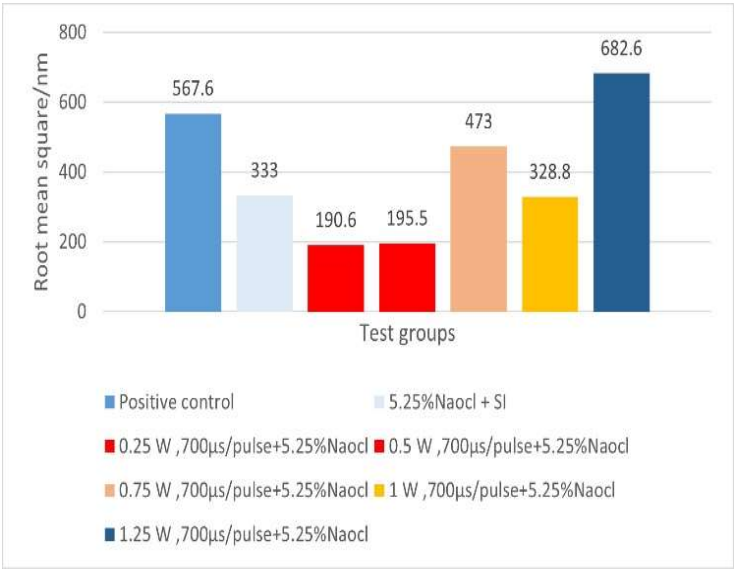

Fig.7. Statistical columns chart showing the means of root mean square values of positive control group (G 1), 5.25% NaOCl + needle irrigation group (G 2), and laser agitation of 5.25% NaOCl group (G 3), the red columns represent the best result.

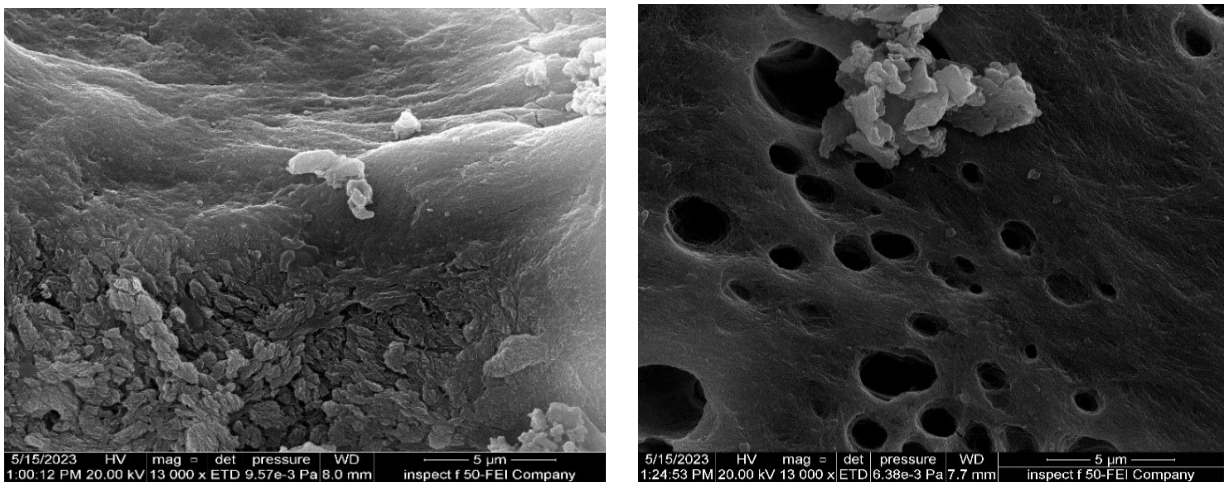

(a) **(b)**

Fig. 8. FE-SEM 13 000 magnification of the isthmus about 6 mm away from the apex (a) A positive control specimen (b) The same isthmus area after irrigated with 2% CHX + PIPS at 1 W.

Table 1. Means and standard deviations of root mean square values obtained from all samples treated with 5.25% NaOCl, means compared by one-way and two-way ANOVA.

Tested groups /5.25% NaOCl	Sq (root mean square) nm	P value
Negative control	17.73±3.9	
Positive control (G 1)	D 567.6±26.2	**0.001** **HSIG**
5.25% NaOCl + SI (G 2)	B 333.0±22.1	
	Laser group + 5.25% NaOCl (G 3)	
0.25 W, 700 µs	A 190.6±8.9	
0.5 W, 700 µs	A 195.5±14.2	
0.75 W, 700 µs	C 473±27.8	**0.001** **HSIG**
1 W, 700 µs	B 328.8±12	
1.25 W, 700 µs	E 682.6±16.2	
P value	**0.001**	

Abbreviations: Sq.: Root mean square roughness nm: Nanometer NaOCl: Sodium hypochlorite SI: Syringe irrigation W: Watt (unit of power), µs: Microsecond HSIG: Highly significant P value: Probability value

Table 2. Means and standard deviations of root mean square values obtained from all samples treated with 2% CHX, means compared by one-way and two-way ANOVA.

Tested groups /2% CHX	Sq (root mean square) Nm	P value
Negative control	17.73±3.9	
Positive control (G 1)	F 567.6±26.2	**0.001** **HSIG**
2% CHX + SI (G 4)	E 453.0±34.1	
	Laser group + 2% CHX (G 5)	
0.25 W, 700 µs	D 320.3±14.8	**0.001** **HSIG**
0.5 W, 700 µs	C 251.7±28.5	
0.75 W, 700 µs	B 228.6±26.3	
1 W, 700 µs	A 166.4±11.6	
1.25 W, 700 µs	B 201.2±12.9	
P value	**0.001**	

Abbreviations: Sq.: Root mean square nm: Nanometer CHX: Chlorohexidine gluconate SI: Syringe irrigation W: Watt (unit of power), µs: Microsecond HSIG: Highly significant P value: Probability value

Table 3. Means and standard deviations of root mean square values obtained from all samples treated with 2% CHX and 5.25% Naocl with laser agitation, means compared by one-way ANOVA.

Laser groups / 700 µs/pulse / Sq. (root mean square) nm			
Tested groups	**2% CHX 700 µs/pulse (G 5)**	**5.25% Naocl 700 µs/pulse (G 3)**	**P value**
0.25 W	320.3±14.8	**190.6±8.9	**0.001**
0.5 W	*251.7±28.5	**195.5±14.2	
0.75 W	*228.6±26.3	473±27.8	
1 W	***166.4±11.6	328.8±12	
1.25 W	*201.2±12.9	682.6±16.2	
	***, **, *** Significant groups**		

6. Discussion

Isthmuses act as a considerable challenge area for root canal cleaning and obturation; their ribbon shape, size, and extension laterally from the main canal make mechanical instrumentation impossible (Robberecht et al., 2023). So, irrigant solutions used during root canal preparation should be able to penetrate the entire root canal system for better endodontic outcomes and prognosis (Kumar et al., 2022). The current study showed how the efficiency of removing the biofilms from isthmuses was influenced by the laser agitation mechanism. In many past studies, molecular and culture methods have been used to determine the number of live bacteria in the root canals (Hoedke et al., 2021). Additionally, the viability of microorganisms in the lateral canals, isthmus, and root canal walls can be determined using a confocal laser microscope (CLSM) (Kumar et al., 2022). An atomic force microscopy (AFM) tool was used to examine the samples because it is easy to apply, precise, and available. The topography of the surface of the isthmus was studied by analyzing of surface roughness and particle size. Surface roughness analysis was characterized by calculating the height parameters including maximum height parameter (Sz.), root mean square roughness parameter (Sq.), and average roughness parameter (Sa.). In the present investigation, (sq.) was the dependent variable, which is regarded to be more sensitive to considerable deviations from the mean line than average roughness (Kumar and Rao, 2012).

According to the data, the isthmus surface that was not infected with bacteria had a computed root mean square value of extremely low (17.73±3.9 nm), whereas the surface after mature biofilm formation had a significantly higher sq. value of around (567.6±26.2 nm) ($p<0.05$). The surface's increased roughness indicates that the biofilm growth produced a rougher and more irregular surface. The measured sq. value of the samples that were treated with 2% CHX and Er, Cr: YSGG laser at (700 µs/pulse, 5 Hz, 1 W) of about (166.4±11.6 nm) is significantly less than the values measured after other methods ($p<0.05$). This indicates that laser PIPS agitation was a more successful method than other conventional techniques in minimizing the amount of E. faecalis biofilm on the isthmus surface.

PIPS is an advanced laser-agitation irrigation technology in which laser photons are generated at low energy levels and with short microsecond pulse durations. This enables lateral propagation of the shock wave in fluids at sub-ablative levels via photoacoustic and photomechanical phenomena. This eliminates the risk of thermal damage and enables effective three-dimensional streaming (Olivi and DiVito, 2016).

The laser PIPS technique is achieved by absorbing the laser energy by the irrigation fluid that fills the root canals, and without this absorption, no laser action is achieved. Therefore, the wavelength of the used laser must be near to the peak of the strong absorption of the material (Frayssinous et al., 2018). 2780 nm Er, Cr: YSGG laser are well-absorbed by water chromophore (Rand kareem Jassim, 2022). So high absorption of this laser energy is ensured by the irrigation solution used in this study, and a strong pressure and shockwaves propagate three-dimensionally within the root canal systems that are filled with fluids (Olivi and DiVito, 2016). Therefore, the irrigants can reach the difficult-to-access areas without needing to put the tip near the morphologically thinning apical third.

As it is known, the sodium hypochlorite irrigant is effective in the removal of bacterial biofilm, so a low-power laser was enough to improve its efficacy (Al Shahrani et al., 2014), which reflected in a decrease in the surface roughness at 0.25 and 0.5 W about of (190.6±8.9 and 195.5±14.2 nm). While, the CHX irrigation solution has low efficacy in removing biofilm (Clegg et al., 2006). So higher power is required not only to pump the liquid by generating a shock wave but also to create stronger cavitation, which makes the bacterial cell membrane weaker and easier for irrigants to enter (Gu et al., 2009). However, the resulting photomechanical phenomena worked to increase the effectiveness of irrigation solutions in disrupting the bacterial biofilm. The irrigation syringe becomes more efficient in conventional treatment when the needle end gets closer to the working length (Boutsioukis and van der Sluis, 2015). While, in laser PIPS agitation, the tip of laser device is not placed inside the canal and is restricted to coronal access in the canal orifice. Therefore, the PIPS technique allows minimum root canal preparation in order to retain healthy tooth structure, according to the minimally invasive endodontics (MIE) approach (Anjum et al., 2019) while ensuring that the irrigants can reach hard-to-reach areas. The SEM images revealed a large part of the isthmus surface and dentinal tubules as being free of bacterial biofilm after treatment with the laser agitation

method. This confirms the results obtained from AFM analysis and proves that the laser agitation is very effective in removing the biofilm from these areas.

The present study results are in a good agreement with many studies that tested the antimicrobial effect of Er family lasers and obtained similar results. Sahar-Helft et al. (Sahar-Helft et al., 2013), examined the actions of 2% CHX and Er: YAG using LAI on Enterococcus faecalis biofilm reported that the total number of microorganisms dramatically decreased after being treated with LAI and CHX. While, Aydin et al. (Aydin et al., 2020), compared the antimicrobial effects of sodium hypochlorite and 2% CHX irrigants agitated by Er, Cr: YSGG laser (LAI), and discovered that activating NaOCl and CHX irrigation fluids with Er, Cr: YSGG pulsed laser can be effective in the eradication of E. faecalis bacteria from the canals.
This experiment was limited by the possibility of tiny fragments forming during the cutting stage, which could raise the surface roughness rating. So, a paper point was inserted into the canal to keep debris out of the isthmus during the cutting process, however, this helped to lessen this disadvantage. Further limitation that could impact the results is the anatomical variance in the isthmus area of the chosen teeth.

7. Conclusions

In conclusion, the data given in this study indicate that Er, Cr: YSGG laser agitation improve the removal of microbial biofilm more than standard irrigation methods delivered by irrigation syringes. Furthermore, this laser had improved the effect of 2% CHX at a power value of 1 W, while agitation of 5.25% NaOCl by low-power laser at (0.25 and 0.5 W) was improved the sodium hypochlorite efficacy against the mature biofilm.

References

Abdelgawad LM, Asmail N, Latif SA, Safaan AM. Efficacy of diode laser and sonic agitation of Chlorhexidine and Silver-nanoparticles in infected root canals. Brazilian Dent Sci 2020;23:7-p.

Al-Karadaghi TS, Gutknecht N, Jawad HA, Vanweersch L, Franzen R. Evaluation of temperature elevation during root canal treatment with dual wavelength laser: 2780 nm Er, Cr: YSGG and 940 nm diode. Photomed Laser Surg 2015;33:460–6.

Anjum SA, Hegde S, Mathew S. Minimally invasive endodontics-A review. J Dent Orofac Res 2019;15:77–88.

Aydin SA, Taşdemir T, Buruk CK, Çelik D. Efficacy of erbium, chromium-doped yttrium, scandium, gallium and garnet laser-activated irrigation compared with passive ultrasonic Irrigation, conventional irrigation, and photodynamic therapy against Enterococcus faecalis. J Contemp Dent Pract 2020;21:12.

Bago I, Đurin A, Kanižaj D, Vuletić LB, Zdrilić IV, Anić I. The efficacy of a novel SWEEPS laser-activated irrigation compared to ultrasonic activation in the removal of pulp tissue from an isthmus area in the apical third of the root canal. Lasers Med Sci 2023;38:189.

Berutti E, Marini R, Angeretti A. Penetration ability of different irrigants into dentinal tubules. J Endod 1997;23:725–7.

Boutsioukis C, van der Sluis LWM. Syringe irrigation: blending endodontics and fluid dynamics. Endod Irrig Chem Disinfect Root Canal Syst 2015:45–64.

Cheng X, Chen B, Qiu J, He W, Lv H, Qu T, et al. Bactericidal effect of Er: YAG laser combined with sodium hypochlorite irrigation against Enterococcus faecalis deep inside dentinal tubules in experimentally infected root canals. J Med Microbiol 2016;65:176–87.

Cheng X, Guan S, Lu H, Zhao C, Chen X, Li N, et al. Evaluation of the bactericidal effect of Nd: YAG, Er: YAG, Er, Cr: YSGG laser radiation, and antimicrobial photodynamic therapy (aPDT) in experimentally infected root canals. Lasers Surg Med 2012;44:824–31.

Clegg MS, Vertucci FJ, Walker C, Belanger M, Britto LR. The effect of exposure to irrigant solutions on apical dentin biofilms in vitro. J Endod 2006;32:434–7.

Cullen JKT, Wealleans JA, Kirkpatrick TC, Yaccino JM. The effect of 8.25% sodium hypochlorite on dental pulp dissolution and dentin flexural strength and modulus. J Endod 2015;41:920–4.

Dioguardi M, Di Gioia G, Illuzzi G, Arena C, Caponio VCA, Caloro GA, et al. Inspection of the microbiota in endodontic lesions. Dent J 2019;7:47.

Frayssinous C, Fortin V, Bérubé J-P, Fraser A, Vallée R. Resonant polymer ablation using a compact 3.44 μm fiber laser. J Mater Process Technol 2018;252:813–20.

Gadegaard N. Atomic force microscopy in biology: technology and techniques. Biotech Histochem 2006;81:87–97.

Gu L, Kim JR, Ling J, Choi KK, Pashley DH, Tay FR. Review of contemporary irrigant agitation techniques and devices. J Endod 2009;35:791–804.

Hoedke D, Kaulika N, Dommisch H, Schlafer S, Shemesh H, Bitter K. Reduction of dual-species biofilm after sonic- or ultrasonic-activated irrigation protocols: a laboratory study. Int Endod J 2021;54:2219–28.

Kimura S, Ebihara A, Maki K, Nishijo M, Tokita D, Okiji T. Effect of optimum torque reverse motion on torque and force generation during root canal instrumentation with crown-down and single-length techniques. J Endod 2020;46:232–7.

Kumar BR, Rao TS. AFM studies on surface morphology, topography and texture of nanostructured zinc aluminum oxide thin films. Dig J Nanomater Biostructures 2012;7:1881–9.

Kumar K, Teoh Y, Walsh LJ. Root canal cleaning in roots with complex canals using agitated irrigation fluids. Aust Endod J 2022;00:1–10.

López-Jiménez L, Arnabat-Domínguez J, Viñas M, Vinuesa T. Atomic force microscopy visualization of injuries in Enterococcus faecalis surface caused by Er, Cr: YSGG and diode lasers. Med Oral Patol Oral Cir Bucal 2015;20:e45.

Nair PNR. Pathogenesis of apical periodontitis and the causes of endodontic failures. Crit Rev Oral Biol Med 2004;15:348–81.

Natanasabapathy V, Arul B, Santosh SS, Vasudevan A, Mahendran SS, Namasivayam A, et al. Prevalence and morphology of root canal isthmus in human permanent teeth using micro-computed tomography: A systematic review. Saudi Endod J 2021;11:142–53.

Olivi G, DiVito EE. Advanced Laser-Activated Irrigation: PIPS TM Technique and Clinical Protocols. Lasers Endod., Springer; 2016, p. 219–91.

Parente JM, Loushine RJ, Susin L, Gu L, Looney SW, Weller RN, et al. Root canal debridement using manual dynamic agitation or the EndoVac for final irrigation in a closed system and an open system. Int Endod J 2010;43:1001–12.

Peters OA, Schönenberger K, Laib A. Effects of four Ni–Ti preparation techniques on root canal geometry assessed by micro computed tomography. Int Endod J 2001;34:221–30.

Rand kareem Jassim HAJ. PDF Cavity Disinfection Using Er, Cr: YSGG Laser Induced Photoacoustic Streaming Technique: Iraqi J Laser 2022;21:41–7.

Rasheed SS, Jawad HA. Permeability of Radicular Dentine after Using Different Irrigant Activation Techniques Including Photo Induce Photoacoustic Streaming Technique. Iraqi J Laser 2021;20:43–50.

Robberecht L, Delattre J, Meire M. Isthmus morphology influences debridement efficacy of activated irrigation: A laboratory study involving biofilm mimicking hydrogel removal and high-speed imaging. Int Endod J 2023;56:118–127.

Sahar-Helft S, Stabholtz A, Moshonov J, Gutkin V, Redenski I, Steinberg D. Effect of Er: YAG laser-activated irrigation solution on Enterococcus faecalis biofilm in an ex-vivo root canal model. Photomed Laser Surg 2013;31:334–41.

Al Shahrani M, DiVito E, Hughes C V, Nathanson D, Huang GT-J. Enhanced removal of Enterococcus faecalis biofilms in the root canal using sodium hypochlorite plus photon-induced photoacoustic streaming: an in vitro study. Photomed Laser Surg 2014;32:260–6.

Zhu X, Yin X, Chang JWW, Wang Y, Cheung GSP, Zhang C. Comparison of the antibacterial effect and smear layer removal using photon-initiated photoacoustic streaming aided irrigation versus a conventional irrigation in single-rooted canals: an in vitro study. Photomed Laser Surg 2013;31:371–7.

دراسة مختبرية لتأثير التدفق الضوئي الصوتي المستحث بالفوتون بالليزر على الأغشية الحيوية للمكورات المعوية البرازية في نظام قناة الجذر المعقد

غفران اسماعيل ابراهيم* ، حسين علي جواد

معهد الليزر للدراسات العليا، جامعة بغداد، بغداد، العراق

*البريد الالكتروني للباحث: whitetooth666@gmail.com

الخلاصة

الهدف: الغرض من هذه الدراسة المختبرية هو تقييم فعالية ليزر الإربيوم والكروم: الإيتريوم سكانديوم الغاليوم باستخدام التدفق الصوتي الضوئي المستحث بالفوتون في تنشيط سوائل الري من خلال تقييم تأثيره في ابادة البكتريا في نظام الجذر المعقد الذي تم استعماره بالمكورات المعوية البرازية.

الطرق: تم فصل الجذور الاونسيه لـ 90 ضرساً سفلياً مقلوع حديثا، وحقنها بمعلق المكورات المعوية البرازية (ما عدا عينات المجموعة السيطرة السلبية)، وحضنت لمدة 30 يوماً. تم تقسيم العينات إلى خمس مجموعات (العدد = 15)، المجموعة الأولى كانت بمثابة السيطرة الإيجابية (الملقحة غير المعالجة) ,(G1) تم ري مجموعات الري بالمحاقن باستخدام هيبوكلوريت الصوديوم 5.25 (G2) %و2% جلوكونات الكلوروهيكسيدين(G4) ، وري مجموعات الليزر بهيبوكلوريت الصوديوم 5.25 (G3) %و2% جلوكونات الكلوروهيكسيدين (G5)التي تم تنشيطها بالليزر عند 700 ميكروثانية، 5 هرتز، (0.25، 0.5، 0.75، 1، و1.25) واط.. تم استخدام مجهر القوة الذرية كطريقة جديدة للحصول على النتائج في منطقة البرزخ؛ تم أيضًا استخدام المجهر الإلكتروني الماسح في الدراسة لتأكيد النتائج التي تم الحصول عليها من مجهر القوة الذرية.وايضا تم استخدام برنامج الحزمة الإحصائية للعلوم الاجتماعية لجمع وتحليل البيانات، واستخدم تحليل التباين لمقارنة مجموعات الاختبار.

النتائج: بعد تحليل النتائج إحصائيا، أظهرت مجموعة الليزر التي تحتوي على 2% جلوكونات الكلوروهيكسيدين و5.25% هيبوكلوريت الصوديوم انخفاضا ملحوظا في خشونة السطح مقارنة بالري بالمحاقن التقليدية ومجموعة السيطرة الإيجابية.

الاستنتاجات: استنادا إلى نتائج الدراسه، فإن تنشيط محلول 2٪ غلوكونات الكلوروهيكسيدين بواسطة الليزر باستخدام تقنية التدفق الصوتي الضوئي الناجم عن الفوتون عند 1 واط يوفر إزالة أفضل للأغشية الحيوية البكتيرية الناضجة من تقنية المعالجة التقليدية. بينما ادى تنشيط هيبوكلوريت الصوديوم باستخدام الليزر منخفض الطاقة عند 0.25 او 0.5 واط أدى إلى زيادة فعاليته.

IJL, Issue 1, Vol. 23, 2024
https://doi.org/10.31900/ijl.v23i1.412

Research Article

IRAQI JOURNAL OF LASER

A comparison between diode laser 976 nm and conventional technique in treatment of gingival fibromatosis

Esraa Ibrahim Marhab[1,*], Zainab.F Mahdi Al-Bawi[1], Afrah Adnan Khalil[2]

[1]*Institute of Laser for Postgraduate Studies, University of Baghdad, Baghdad, Iraq*
[2]*Department of Oral Diagnosis, College of Dentistry, University of Anbar, Iraq*
* *Email address of the Corresponding Author:* israa.ibrahim1202a@ilps.uobaghadad.edu.iq

Article history: Received 4 Aug.2023; Revised 1 Nov. 2023; Accepted 20 Nov.2023; Published online 15 Jun. 2024

Abstract

Background: Gingival fibromatosis (GF) is an expansion of the gingiva's connective tissue. Appeared during the onset of teeth eruption and postponed it. In order to remove this fibromatosis, a scalpel, electrocautery, or laser surgery is recommended.
The objective of the study: is to evaluate the efficacy of a diode laser (976 nm) and its comparative benefits in the management of gingival fibromatosis, as opposed to a scalpel.
Material and method: Forty patients who complained of functional and esthetical problems due to delayed eruption were divided into two groups, one for surgical treatment with conventional scalped and another one for surgical treatment with diode laser. Follow-up visits are scheduled on the third day of treatment, 1, 2, and 4th postoperatively. Clinical assessment is done by monitoring intra-operative bleeding, pain through the first week of treatment, functional interference, and clinical healing in follow-up visits. Overall satisfaction for patients and their parents was taken at the end of the treatment visits. The t-test and the Chi-square test were utilized as statistical methodologies for conducting data analysis.
Results: No or self-limiting bleeding in the laser group, lesser pain, and function interference in the laser compared with the conventional scalped group. Better clinical healing with the laser group through the first 2 weeks than with the scalpel group; all in each group cases achieve excellent healing at the 4th week postoperatively. All patients and their parents are very well satisfied with the outcomes.
Conclusion: Diode laser is preferable in surgical conducting of gingival fibromatosis to minimize postoperative pain and discomfort, enhance healing, and, ultimately, premium outcome.

Keywords: Delayed eruption, diode laser, gingiva, fibromatosis.

1. Introduction

Gingival fibromatosis (GF) is infrequent, benign, non-hemorrhagic fibrous growth of gingival tissue. Proliferative fibrous gingiva expansion throughout development causes cosmetic, functional, and masticatory oral cavity abnormalities and psychological pain (Ramakrishnan and Kaur, 2010). It frequently

begins around the time of permanent dental eruption and less frequently around the time of primary dentition eruption. If the expansion occurs prior to tooth eruption, thick fibrous tissue may impede or prevent tooth emergence (Dhadse et al., 2012). Typically, it aligns with the emergence of permanent incisors (Gonçalves et al., 2018). It may be broad or localized, and its intensity can vary (Gandhi et al., 2018) GF may manifest as "hereditary gingival fibromatosis (HGF)", which can manifest as a standalone entity or as part of a genetic illness or syndrome, or as "idiopathic gingival fibromatosis" (Gawron et al, 2016), Clinically, gingival tissues are often of normal hue, non-bleeding, firm, fibrotic consistency, and profuse stippling (Oubenyahya and Fiqhi, 2021).

Gingivectomy with an internal or exterior bevel incision is the recommended therapy for GF (Häkkinen and Csiszar, 2007). Selecting of surgical approach depends on the age of the patient and the stage of the eruption, external bevel excision is preferred in child patients and incomplete eruption, while the internal bevel is preferred when the eruption of teeth is complete at the optimal time of treatment variable, but the negative effect of fibromatosis on patients psychology and function suggesting to do treatment at earlier age. Radiography indicated two-thirds of the root developed, suggesting to parents that surgery may fix the issue (Almiñana-Pastor et al., 2017). Traditionally, the conventional scalpel and electrocautery have been the instruments of choice for surgical removal of gingival enlargement (Gontiya et al., 2011).

Laser surgery is novel because it allows the operator more control and provides a clean, hemostatic operating area, good cutting capacity, minimal tissue damage, minimal or no anesthesia, less oema, and less postoperative discomfort than previous methods (Beer et al., 2012). Few studies on the use of diode laser treatment have been reported in the literature. Camiloti et al. used a diode laser in the treatment of a seven-year-old girl suffering from generalized gingival fibromatosis on both arches. The patient received treatment well, reporting just minor pain throughout the first week (Camilotti et al., 2015). Aboujaoude and colleagues employed a diode laser and a scalpel to manage hereditary gingival fibromatosis in a pediatric patient aged six years. Generalized gingival fibromatosis was surgically removed from the patient's anterior area. The posterior portion employed an 810 nm diode laser. Reported that the diode laser method improves visibility, gingival contouring, and post-operative pain and discomfort. Diode lasers were expensive and time-consuming (Aboujaoude et al., 2016).

This study proceeds to compare a conventional scalpel and diode laser (976) in the treatment of gingival fibromatosis.

2. Material and method

The sample of the present study is forty patients (16 female and 24 male) ranging in age from 7 to 12 years old. They came to the pediatric departments of different specialized dental centers in different Iraqi health provinces with complaints of severe function interference. Clinical oral examinations determined gingival fibromatosis surgery for all patients. Some people undergo traditional surgery. The study involved the categorization of patients into two groups, namely Group A and Group B. Group A comprised 20 patients who underwent conventional surgical treatment using a scalpel (blade no. 15), while Group B consisted of 20 patients who received treatment using a diode laser at 976 nm (SOLASE). The research was conducted between December of 2021 and October of 2022. Patients with systemic diseases and mentally retarded patients were excluded from this study.

Complete medical and dental history, in addition to the assigned permission form, are taken from the patient's parents. Patients had pre-procedure X-rays. Chlorohexidine mouthwash was used as an intraoral antiseptic for approximately 30 seconds. Topical anesthesia was applied before injection of local anesthesia. Deep infiltration anesthesia with 1.2 mL cartilage containing (2% lidocaine and 1:80.000 of epinephrine) was given surrounding the fibromatosis. The borders of the lesion were demarcated with the diagnostic probe.

In group (A), the fibromatosis was resected completely with a scalpel, and the crowns of the involved teeth were discovered. Normal saline was utilized for irrigation at the operation site. The bleeding surgical margin was covered with gauze, and asked the patient to press until the bleeding was off. See Figure 1.

In group (B), firstly, the fiber tip was initiated to retain heat by fusing a thin layer of pigment, such as articulating paper on the end. The thermal energy will be concentrated in the thin absorbent material so there is less collateral damage, enhancing lesion excision and tissue thermal contact. To reduce beam reflections, all workers wore protective goggles, removed bright medical devices, jewelry, watches, etc., from the operation field, and controlled airborne pollution. The fibromatosis was resected in one piece by using a diode laser (976) in continuous wave mode and power 2.5W with a fiber tip perpendicular to the peripheral of the lesion until the lesion can be lifted easily from the crown of the tooth. The surgical site was left uncovered, as there was no bleeding, as illustrated in Figure 2.

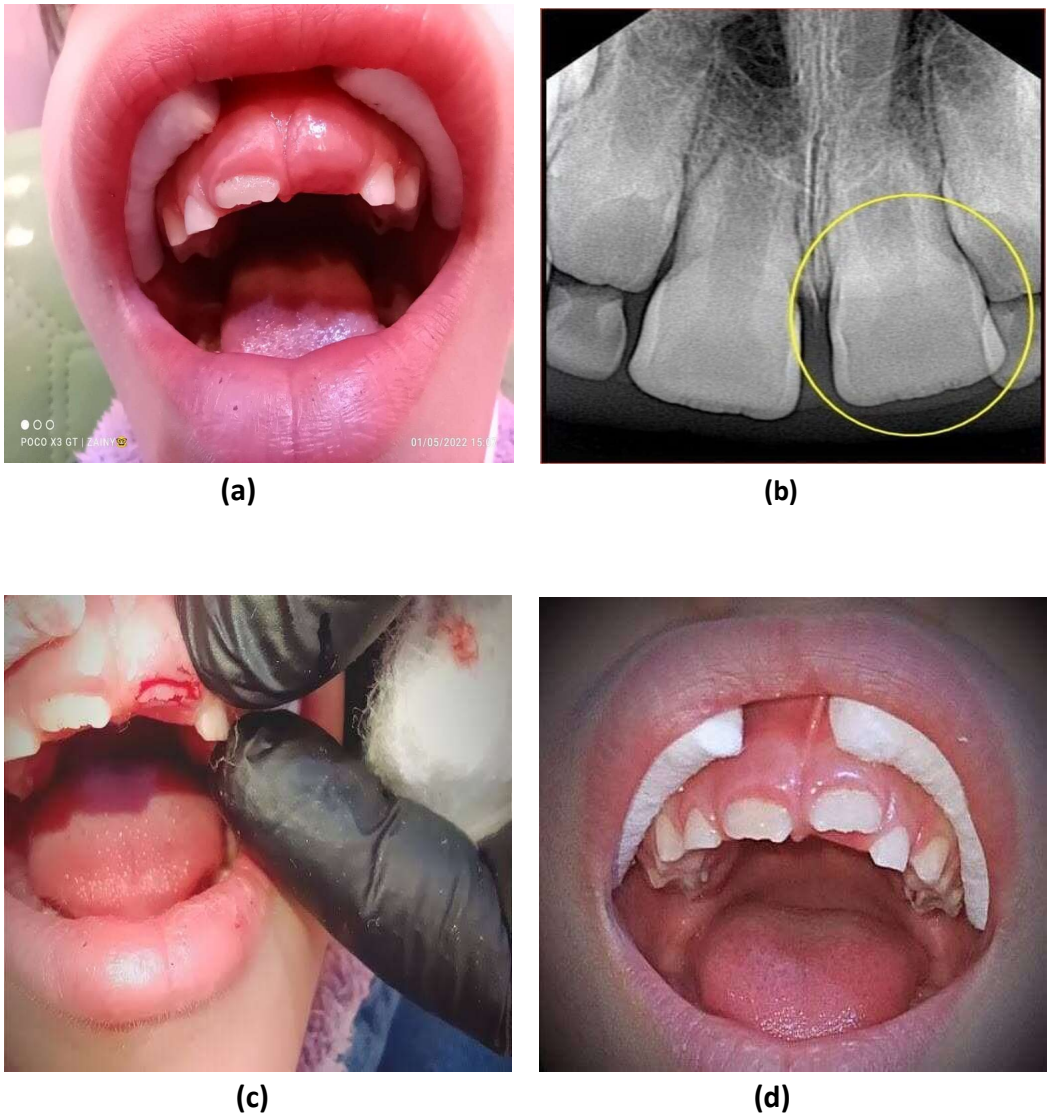

Fig.1: Surgical blade excision technique of gingival fibromatosis in left central incisor region for the 9-year-old female patient: (a) Pre-operative clinical feature, (b) Pre-operative per apical radiograph, (c) Immediately postoperative view and (d) Complete healing and eruption of the affected tooth after four weeks post-operatively.

For histological confirmation, all specimens were kept in 10% formaldehyde. To avoid subsequent infection, Patients are instructed to gargle twice a day with 0.12% chlorhexidine and given ibuprofen syrup as needed. All patients were monitored on the third day, then 1-2and4 weeks postoperatively for clinical evaluation. Clinical evaluations were done for the severity of bleeding noticed during and immediately after the procedure (1=no bleeding, 2= self-limiting, 3= required pressure, 4=required coagulation) (Musaa et al., 2017). The severity of pain by using a verbal rating scale (VRS) through the first week postoperatively (0 = no pain, 1= considerable discomfort). (2 = Moderate pain, 3= extreme pain) were written on a form for patients to fill out anytime they felt pain (Hjermstad et al., 2011). Clinical healing (healing index by Landry et al.: 1= very poor healing, 2= poor, 3= good, 4= very good, 5= excellent) & function interference (0=no interference, 1= mild interference, 2= moderate interference, 3= severe interference) evaluated in follow up visits (.Aldelaimi and Khalil, 2015). At the end of the follow-up, the overall satisfaction of patients and their parents about the outcome was evaluated (poor (%): 0–25, fair (%): 26–50, excellent (%): 51–75, excellent (%): 76–100) (.Aldelaimi and Khalil, 2015).

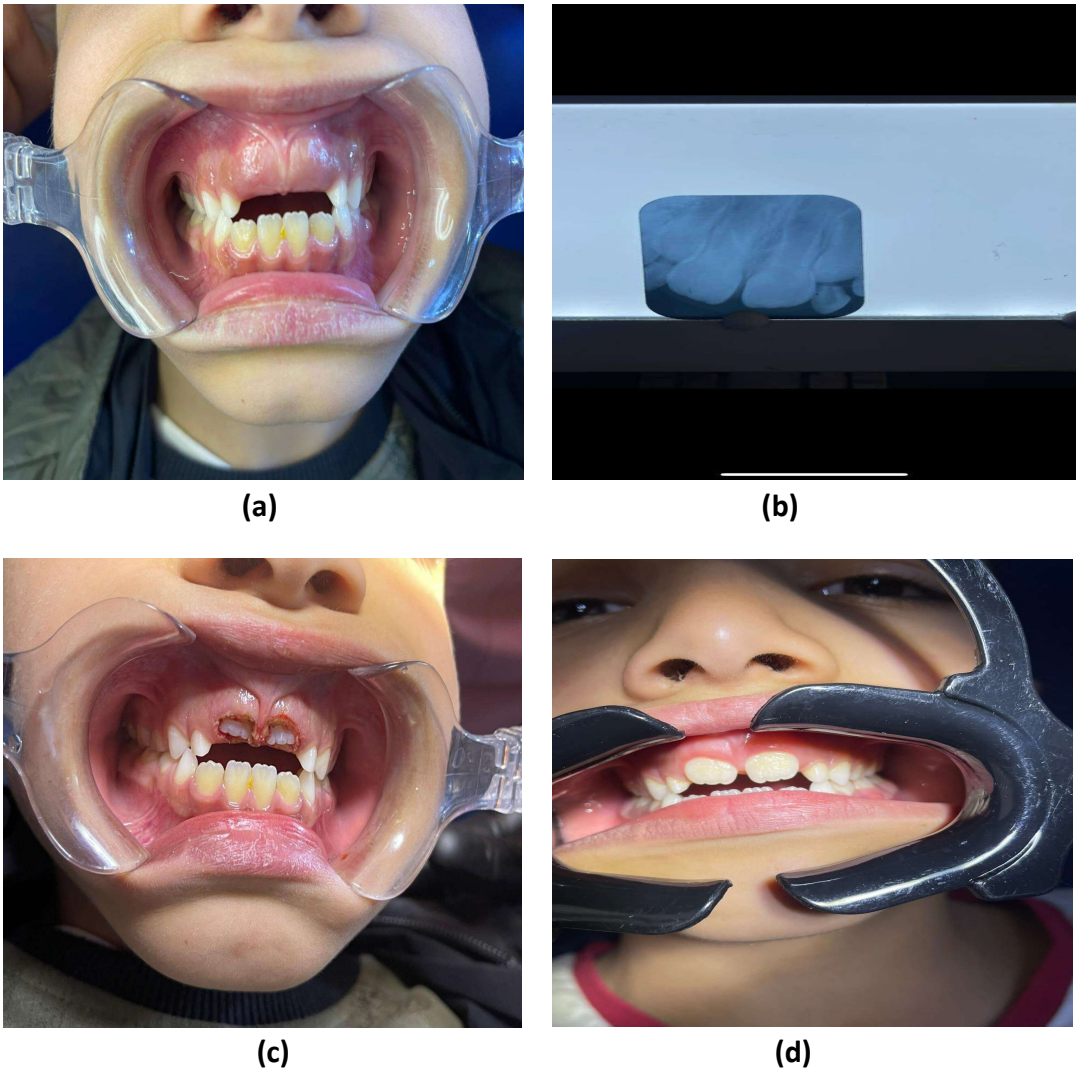

Fig. 2: Laser excision technique of gingival fibromatosis in central incisor region for 9-year-old male patient: (a) Pre-operative clinical feature, (b) Pre-operative per apical radiograph, (c) Immediately postoperative view and (d) Complete healing and eruption of affected teeth after four weeks.

3. Statistical analysis

Statistical P package for Social Sciences (SPSS) version 21 is used to interpret the data. Mean, standard deviation and ranges are provided. Frequencies and percentages show categorical data. Independent t-tests compared continuous variables. When the expected frequency was less than 5, the Fisher exact test replaced the Chi-square test to establish the link between provisional diagnosis and particular data. 0.05 Or less was significant.

4. Results

This study included 40 patients (16 female and 24 male). They ranged in age from 7 to 12 years. Table (1). They all had surgical resection of gingival fibromatosis either by a surgical blade or diode laser. They were allocated equally in two groups. In the laser group, 18 patients had no intraoperative bleeding, and only 2 patients had just self-limited bleeding, while in the surgical blade group, all 20 patients had intraoperative bleeding and required pressure. As in (Table 2). Postoperative pain scores differed significantly across approaches. The laser group had lower first-day discomfort than the surgical blade group (only 45% of patients scored mild pain in the laser group vs. 25% scored mild and 75% scored moderate in the surgical blade group).On the second day (15% mild pain in the laser group vs. 35% mild Pain in the surgical blade group). Both laser and surgical blade groups had no pain on other days. (Table 3). The clinical healing was significantly higher in the laser group compared to the surgical blade group on the third day (5% of patients scored Very poor healing in the laser group vs. 45% in surgical blade group), first week (15% of patients scored good healing vs. 0% in laser groups), in the second week (85% scored very good healing with laser vs. 15% in surgical blade group).

Table 1. Distribution of study patients by age and gender.

Demographic Data	Study groups Mean ± Sd	
	Surgical blade group	Laser Group
Age (Years)	**8.7±1.2**	**8.5±1.1**
Gender	N (%)	N (%)
Male	13(%56)	11(%55)
Female	7(%35)	9(%45)

Table 2. Percentage distribution of patients according to intraoperative bleeding score by study groups.

Study groups	Bleeding Score N (%)				
	None	Self-limiting	Required pressure	Required coagulation	Required Ligation
Laser Group Patient No.(20)	18 (90%)	2 (10%)	0(0)	0(0)	0(0)
Surgical blade group Patient No. (20)	0(0)	0(0)	20 (100%)	0(0)	0(0)

Table 3. Comparison between the study groups by means of postoperative pain score through seven days from operation time.

Study Groups	Postoperative Pain Mean ± Sd						
	1st day	2nd day	3rd	4th	5th	6th	7day
Group A	1.25±0.4	0.35±0.4	0 ± 0	0 ± 0	0 ± 0	0 ± 0	**0 ± 0**
Group B	0.45±0.5	0.15±0.3	0 ± 0	0 ± 0	0 ± 0	0 ± 0	**0 ± 0**
P value	0.001	0.05	--	--	--	--	--

There is no significant difference in the fourth week (Table 4). A statistical difference was found between the study groups in regard to postoperative function interference score. The function interference score was significantly higher in the surgical blade group as compared to the laser technique on the third day (in the laser group: 25% have no function interference, 45% and 30% moderate vs. 65% mild interference, 25% moderate and 10% severe in surgical groups), first week (in laser groups 40% scored no function interference and 60% mild function interference vs. 20% no interference, 70% mild and 10% moderate in surgical laser group). Both laser and surgical blade techniques had no function interference in the second and fourth weeks (Table 5). Regarding Patient satisfaction scores, there was no significant difference between study groups. 100% of the laser group and 95% of the surgical blade group reported excellent satisfaction. (Table 5).

Table 4. Comparison between the study groups by means of clinical healing score at three days, one week, two weeks, and four weeks.

Healing	Study groups		P value
	Group A Mean ± Sd	Group B Mean ± Sd	
3 days	1.55±0.5	1.85±0.4	0.01 SIG
1 week	2.15±0.4	2.85±0.4	0.01 SIG
2 week	3.1±0.5	3.85±0.4	0.01 SIG
4 week	5±0	5±0	NS

Table 5. Comparison of function score after three, one, two, and four weeks following surgery across study groups.

Function	Study groups		P value
	Surgical blade group Mean ± Sd	Laser Group Mean ± Sd	
3 days	1.45 ± 0.7	1.05 ± 0.8	0.03 SIG
1 week	0.9 ± 0.6	0.6 ± 0.5	0.05 SIG
2 week	0 ± 0	0 ± 0	--
4 week	0 ± 0	0 ± 0	--
P value	0.01 SIG	0.01 SIG	

Table 6. Overall satisfaction at the end of the follow-up visit.

Overall satisfaction	Study groups		P value
	Surgical blade group	Laser Group	
Poor $(0-25)\%$	0 (0)	0 (0)	---
Fair $(26-50)\%$	0 (0)	0 (0)	---
Good $(51-75)\%$	1(5)	0 (0)	Ns
Excellent $(76-100)\%$	19(95)	20(100)	Ns

5. Discussion

Laser technology and its applications in dentistry are evolving rapidly. Oral soft tissue surgery might employ diode lasers with wavelengths from 810 to 980 nm in Continuous or pulsed mode. Diode laser photothermal action removes oral mucosa lesions by excision or ablation/vaporization (Desiate et al., 2009). In photothermal, tissue absorbs radiant light and converts it to heat energy, hence altering tissue structure. When suitably administered, laser-tissue interaction may induce responses ranging from incision, vaporization, and coagulation (Kishen et al., 2007). Hemoglobin and melanin chromophores absorb the wavelengths of the diode laser more than dental hard tissue. Hence, it has selective action and can be used safely in cutting, blood coagulation, ablation, or vaporizing soft tissue near the dental structure with reduced damage and better recovery (Derikvand et al., 2016). The objective of the study is to characterize the efficiency of diode laser and assess its advantage over conventional surgical blade techniques for the treatment of gingival fibromatosis. The study depended on different clinical criteria that included intraoperative bleeding, postoperative pain and discomfort, clinical healing, function interference, and overall satisfaction. The result of this study suggests that diode laser surgery was effective in the treatment of gingival fibromatosis.

In this study, the definitive excision of fibromatosis was performed in a hemostatic field with good visibility in the laser group, whereas in the surgical blade group, visualization was hampered by bleeding, necessitating the application of pressure and dressing to the surgical site for coagulation. The temperature of soft tissue was raised by laser light. 60 C Causes coagulation. This is crucial to laser surgery. Photo-coagulation instantly denatures proteins, enzymes, and other bioactive compounds. Tissue collagen shrinks due to molecular changes. Irradiated tissue constricts against the proximal vasculature and shrinks blood vessel collagen, improving hemostasis. Laser damage to erythrocytes increased platelet aggregation and intraluminal thrombosis, reducing blood loss (Aoki et al., 2004). Laser hemostasis explains why the laser group had less blood loss. The study indicated that post-operative pain and discomfort disappeared on the third day of surgical treatment in both groups but showed significant differences in the first and second days post-operatively. These results are in line with results reported by Aboujaoude et al. (Aboujaoude et al., 2016). Thermal necrosis produced by tissue vaporization closes sensory nerve terminals and decreases their capacity to transmit stimuli, and denaturation proteins diminish discomfort in oral cavity diode laser surgery patients (Abdulhamed and Merry, 2012). Diode lasers may reduce pain by breaking down cell membrane sodium and potassium pumps, which impede impulse conduction (Chandna and Kedige, 2015). In this study, clinical healing with the laser group was less eventful, with faster recovery compared with the conventional technique on 3rd day and 1 week. At 2 weeks postoperatively, most cases healed with significant differences for faster healing in the laser group. On the last visit follow-up all patients achieved excellent healing. A diode laser application can accelerate wound healing by stimulating fibroblast proliferation, collagen synthesis, vascular proliferation, and increased epithelial cell division (Ghadimi et al., 2015). Regardless of bacterial contamination, laser tissue contact will reduce temperature and photon scatter to achieve tissue confinement at a distance from the wound. This lowers the temperature differential, stimulating tissue, energizing tissue molecules, and increasing local blood flow. A scatter gradient reduces energy to bio-modulating levels (Coluzzi and Parker, 2017). At the end of follow-up treatment, all patient and their parents were well satisfied with the outcome of both techniques, which is the ultimate goal of any

treatment. The gingival fibromatosis makes patients have aesthetic problems, severe function interference, and social well-being. Thus, they were very happy with the outcome, disregarding any treatment modality. The traditional surgical blade is still the gold standard tool because it is the most effective and cost-effective and does not necessitate as much extra skill or special precautions as a laser. In comparison to other laser types, the diode laser is a very effective alternative device in the excision of oral soft tissue when used properly with appropriate parameters. Diode lasers are very preferred by clinicians and patients due to their advantages, in spite of the special precautions and skills needed in comparison to conventional blades.

6. Conclusions

This study showed that diode laser 976nm was effective in the resection of gingival fibromatosis in continuous mode with a power of (2.5w). Better visibility during the surgery by diode laser due to the excellent hemostatic effect of the laser when compared to the traditional methodology. The use of a diode laser leads to minimal postoperative pain and discomfort with improved healing. The patients were well satisfied about the treatment of gingival fibromatosis.

Ethical consideration

The research was approved by the research ethics committee of the Institute of Laser for Postgraduate Studies, University of Baghdad. It has an ethical approval number (1385).

References

Abdulhamed, B.S. and Merry, B.T., 2012. Excision of soft tissue oral lesions by 810 nm diode laser. Iraqi Journal of Laser, 11(B), pp.21-27.

Aboujaoude, S., Cassia, A. and Moukarzel, C., (2016). Diode laser versus scalpel in the treatment of hereditary gingival fibromatosis in a 6-year old boy. Clinics and Practice, 6(4), p.895.

Aldelaimi, T.N. and Khalil, A.A., (2015). Clinical application of diode laser (980 nm) in maxillofacial surgical procedures. Journal of Craniofacial Surgery, 26(4), pp.1220-1223.

Almiñana-Pastor, P.J., Buitrago-Vera, P.J., Alpiste-Illueca, F.M. and Catalá-Pizarro, M., 2017. Hereditary gingival fibromatosis: Characteristics and treatment approach. Journal of clinical and experimental dentistry, 9(4), p.e599.

Aoki, A., Sasaki, K.M., Watanabe, H. and Ishikawa, I., (2004). Lasers in nonsurgical periodontal therapy. Periodontology 2000, 36(1), pp.59-97.

Beer, F., Körpert, W., Passow, H., Steidler, A., Meinl, A., Buchmair, A.G. and Moritz, A., (2012). Reduction of collateral thermal impact of diode laser irradiation on soft tissue due to modified application parameters. Lasers in medical science, 27, pp.917-921.

Camilotti, R.S., Jasper, J., Ferreira, T.B., Antonini, F., Poli, V.D. and Pagnoncelli, R.M., (2015). Resection of gingival fibromatosis with high-power laser. Journal of dentistry for children, 82(1), pp.47-52.

Chandna, S. and Kedige, S.D., 2015. Evaluation of pain on use of electrosurgery and diode lasers in the management of gingival hyperpigmentation: A comparative study. Journal of Indian Society of Periodontology, 19(1), p.49.
Coluzzi, S. Parker., 2017. Laser tissue interaction. Lasers in Dentistry—Current Concepts, pp.43 .

Derikvand, N., Chinipardaz, Z., Ghasemi, S. and Chiniforush, N., 2016. The versatility of 980 nm diode laser in dentistry: a case series. Journal of lasers in medical sciences, 7(3), p.205.

Desiate, A., Cantore, S., Tullo, D., Profeta, G., Grassi, F.R. and Ballini, A., 2009. 980 nm diode lasers in oral and facial practice: current state of the science and art. International journal of medical sciences, 6(6), p.358.

Dhadse, P.V., Yeltiwar, R.K., Pandilwar, P.K. and Gosavi, S.R., 2012. Hereditary gingival fibromatosis. Journal of Indian Society of Periodontology, 16(4), p.606

Gandhi, M., Tandon, S., Sharma, M. and Vijay, A., (2018). Nonsyndromic gingival fibromatosis: a rare case report. International Journal of C linical Pediatric Dentistry, 11(3), p.250.

Gawron, K., Łazarz-Bartyzel, K., Potempa, J. and Chomyszyn-Gajewska, M., 2016. Gingival fibromatosis: clinical, molecular and therapeutic issues. Orphanet journal of rare diseases, 11, pp.1-14.

Ghadimi, S., Chiniforush, N., Najafi, M. and Amiri, S., 2015. Excision of epulis granulomatosa with diode laser in 8 years old boy. Journal of lasers in medical sciences, 6(2), p.92.

Gonçalves, C.F., Mundim, A.P., Martins, R.F.S., Gagliardi, R.M., Santos, P.S.S. and de Toledo, O.A., 2018. Hereditary gingival fibromatosis: a case report with seven-year follow-up. Acta Stomatologica Croatica, 52(3), p.254.

Gontiya, G., Bhatnagar, S., Mohandas, U. and Galgali, S.R., 2011. Laser-assisted gingivectomy in pediatric patients: a novel alternative treatment. Journal of Indian Society of Pedodontics and Preventive Dentistry, 29(3), pp.264-269.

Häkkinen, L. and Csiszar, A., 2007. Hereditary gingival fibromatosis: characteristics and novel putative pathogenic mechanisms. Journal of dental research, 86(1), pp.25-34.

Hjermstad, M.J., Fayers, P.M., Haugen, D.F., Caraceni, A., Hanks, G.W., Loge, J.H., Fainsinger, R., Aass, N., Kaasa, S. and European Palliative Care Research Collaborative (EPCRC, 2011. Studies comparing numerical rating scales, verbal rating scales, and visual analogue scales for assessment of pain intensity in adults: a systematic literature review. Journal of pain and symptom management, 41(6), pp.1073-1093.

Musaa, F.E., Awazli, L.G. and Alhamdani, F., 2017. Gingival enlargement management using diode laser 940 nm and conventional scalpel technique (A comparative study). Iraqi Journal of Laser, 16(B), pp.1-9

مقارنة بين الدايود ليزر(976) والطريقة التقليدية لمعالجة الورم الليفي اللثوي

اسراء ابراهيم مرحب[1،*]، زينب فاضل مهدي الباوي[1] ، افراح عدنان خليل[2]

[1] معهد الليزر للدراسات العليا، جامعة بغداد، بغداد، العراق
[2]جامعة الانبار كلية طب الاسنان قسم الفحص والتشخيص الفمي

*البريد الالكتروني للباحث: israa.ibrahim1202a@ilps.uobaghadad.edu.iq

الخلاصة:

الخلفية والمعلومات : الورم الليفي اللثوي حالة من تمدد اللثة تحدث خلال بزوغ الاسنان وتاخر ضهورها . كل من تقنية استخدام الشفرة الجراحية والكي الكهربائي والليزر يمكن استخدامه لاستئصال الورم الليفي اللثوي.

الهدف من الدراسة: تقدير كفائة الدايود ليزر وفوائده فوق الشفرة الجراحية لمعالجة الورم الليفيي اللثويز.

المواد والطريقة: 40 مريض يشكون من المشاكل الوظيفية والجمالية بسبب تأخر ظهور الاسنان. قسموا الى مجموعتين ، احداهما للمعالجة بتقنية الشفرة الجراحية والاخرى للمعالجة باستخدام الليزر. جدولت لهم جلسات المتابعة لتقدير النتائج . تم استخدام اختباري واختبار مربع كي لتحليل البيانات.

النتائج والاستنتاجات: لايوجد نزف او نزف متوقف تلقائيا في مجموعة الليزر، الم اقل وممارسة للوظيفة افضل في مجموعة الليزر، شفاء اسرع في مجموعة الليزر مقارنة بمجموعة الشفرة الجراحية. كل المرضى او والديهم كانوا جدا راضين عن المعالجة. طبقا للنتائج ليزرالدايود جدا كفوء في معالجة الورم الليفي اللثوي.

IJL, Issue 1, Vol. 23, 2024 **Research Article**
https://doi.org/10.31900/ijl.v23i1.431

The clinical evaluation of oral fibroma lesion removal utilizing two types of diode lasers 980 nm and 450 nm

Saad Radhi Al Ghazali[1], Soudad Salman Ahmed[2] , Balsam.S.Abdulhameed[3]

[1]*Institute of laser for graduate students, University of Baghdad, Baghdad, Iraq*
[2]*Department of Physics, Faculty of Science, University of Baghdad, Baghdad, Iraq*
[3]*Consultant oral and maxillofacial surgeon BDS,FICMS,HD Laser*
** Email address of the Corresponding Author: saadtawi2020@gmail.com*

Article history: Received 24 Oct.2023; Revised 22 Dec. 2023; Accepted 27 Dec.2023; Published online 15 Jun. 2024

Abstract

There are a number of advantages to using diode lasers in oral surgery with varying wavelengths. Lasers offer several advantages, such as reduced recovery periods, the potential to combine tissue coagulation with surgical incisions, decreased discomfort, field disinfection, and a faster and more efficient healing process. These benefits result in a decreased reliance on medicine and enhanced patient comfort throughout the recovery phase. This includes a large AsxzwzA=increase in working efficiency at far lower power settings, among other things. As a result, unwanted effects can be greatly reduced. It also has a favorable effect on wound healing. The purpose of this study was to compare two diode lasers (450 and 980nm) to determine whether one is more effective at excision the oral fibroma lesion with less discomfort, no oedema, and faster healing. In this study, thirty-eight patients between the ages of 16 and 45 were included. The laser parameters setting for both wavelengths were a pulsed wave mode, tip diameter 400µm, and the initial wavelength applied at 1.3 W power. The current study demonstrated that the blue laser with a wavelength of 450 nm had more efficacy in excising the oral benign lesion. It exhibited reduced discomfort, decreased swelling, and rapid healing, as observed. The findings of this study indicate that the 450nm diode laser is superior in effectively eliminating the oral fibroma lesion in a clinical setting while causing minimal patient discomfort and almost no swelling. In contrast, the 980nm laser resulted in some discomfort and swelling that persisted for a longer duration. For such instances, the diode laser with a wavelength of 450 nm can be employed with greater effectiveness to eliminate the oral lesions.

Keywords: diode laser, wavelengths 450 and 980nm, clinical scores, oedema and pain.

1. Introduction

Oral benign lesions come in a variety of forms and might be the result of an isolated mouth discovery or a dermatological condition. The most frequent benign lesion of the oral mucosa is fibroma. Barker and Lucas devised criteria in 1967 to determine what constitutes a real fibroma. It is also referred to as an irritational fibroma, fibrous nodule or oral polyp, focal intraoral fibrous hyperplasia, and traumatic fibroma[1]. These oral lesions excised by several surgical techniques, including the use of electrosurgical scalpels,

conventional scalpels and lasers can be used to remove these lesions [2] Several different kinds of oral mucosal lesions can be diagnosed and treated using lasers, which are used by specialists in oral medicine. Frenectomies, epulis fissuratum, fibromas, gingival enlargements, gingivectomies, and specific crown lengthening procedures are just a few of the many procedures that can benefit from laser technology[3].

+-In oral surgery, lasers such as carbon dioxide (CO2), erbium-doped yttrium aluminum garnet (Er:YAG), neodymium-doped yttrium aluminum garnet (KTM, Nd:YAG), and diode are commonly employed and regarded as effective tools for specific procedures [4]. Among the use of a laser as a minimally invasive technique has many advantages, including its ability to be applied from a distance, increased visibility in the operating room, precision cutting, hemostasis, minimal cicatrization, superior infection control, excellent wound healing, decreased postoperative pain and swelling, and patient acceptance [5]. Diode lasers are gaining popularity in periodontal surgery because they are easily absorbed by pigments like melanin and hemoglobin, so low absorption by water and hydroxyapatite ensures their safety when employed near dental hard tissues [6].In dentistry, lasers have advanced to great heights, and as a supplementary method for soft tissue surgery, they have proven invaluable in oral surgery. The reason for this quick development is that lasers make it possible to perform soft tissue treatments quickly and effectively while maintaining good field visibility and hemostasis. In conjunction with scalpels, electrocautery, or high-frequency devices, lasers maximize patient comfort following surgery [7]. There are numerous uses for diode lasers in dentistry. It is a solid-state semiconductor laser that has potential applications in arsenic, gallium, and aluminum. It is possible to emit beams continuously or pulsed. When it comes to tissues that are pigmented with collagen, melanin, and hemoglobin, this laser absorbs lightest; in contrast, it absorbs less in dental hard tissues. Because of this, it can be used to surgically treat oral soft tissue lesions that are near dental structures without causing excessive bleeding [8]. Due to the characteristics of laser radiation, such as customizable energy and power densities and monochromatism, this technology also permits the use of particular therapeutic measures that have a variety of effects, such as quicker wound healing[9]. In this study, benign fibroma lesions of the mouth were excised using two different diode lasers. One was a blue laser operating at 450 nm, and the other was near-infrared, operating at 980 nm.

The current study aimed to evaluate the clinical scores (pain and oedema) in excision of oral fibroma lesions by two types of diode laser (blue laser 450 nm and near-infrared diode laser 980 nm).

2. Materials and methods

2.1. Age and sex

The mean age of examined sample was 27.93±14.44 year (16-45 year). The mean age of 450nm group was 40.6± 2.73-year-old (68.4%) of them female and (32.4%) male, while the mean age of 980nm group was 38.26±2.88 (57.8%) of them female and (42.1%) male, Figure (1 and 2).

2.2 Clinical Evaluation scores

1. Pain scale (Numeric rating scale)

Pain and discomfort were assessed using a rating scale. It is used to define pain intensity: no pain, mild pain, moderate pain and severe pain. The patients were given a questionnaire case sheet to fill out every day from the first day of surgery to the tenth day in order to document their level of pain and discomfort [10].

- 0= no pain
- 1-3= mild (nagging, annoying and interfering with activities of daily living ADLs).
- 4-6= moderate pain (interfering significantly with ADLs)
- 7-10= sever pain (disable unable to perform ADLs).

2. Oedema scale: determined as following [11]

- 0= No oedema.
- 1= very slight oedema (hardly visible).
- 2= slight oedema.
- 3= moderate oedema
- 4= sever oedema (extent swelling even beyond the application area).

2.2. Time of the irradiation and procedure of excision

The irradiation period for the 450nm operation was 2-3 minutes due to the non-contact mode and high absorption in hemoglobin. Tip cleaning was not necessary for the 450nm operation. However, the 980nm operation required 5-10 minutes. As a result of tip cleaning, the duration of the 980 nm may be prolonged to 15 to 20 minutes. However, the operational timeframe may vary depending on the size and location of lesion. The duration of follow-up varied depending on the clinical score. For instance, the follow-up period for the oedema score ranged from one to seven days, while for the pain score it ranged from one to ten days.

2.3. Statistical analysis

All data were tabulated and subjected to statistical analysis. Data analysis was performed using JMP 16 (Gary, USA). This analysis included descriptive and association tests for comparison between the two laser techniques. The student's t-test was used for measurable variables. The level of significance was set at $P \leq 0.05$.

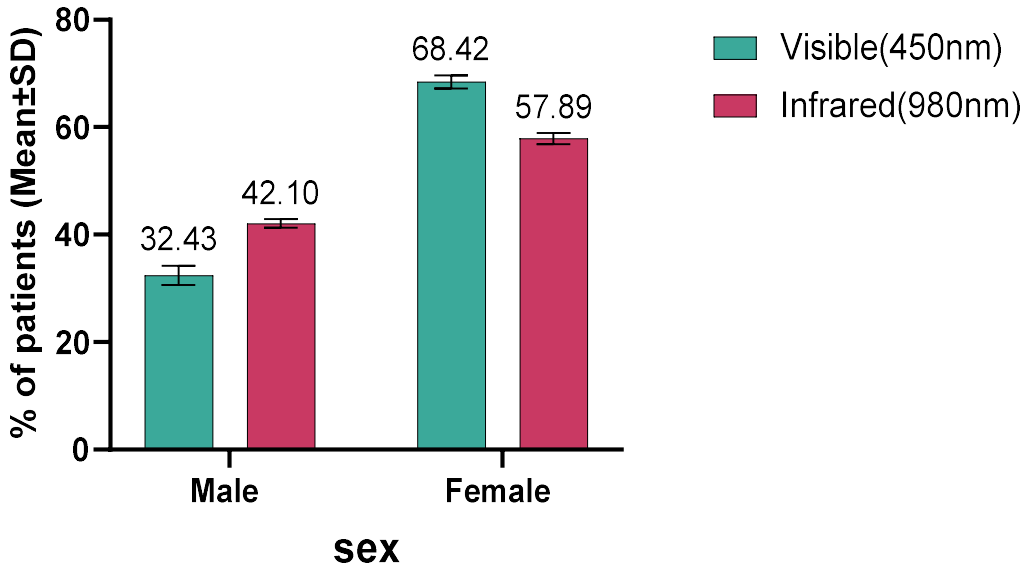

Fig. 1: Bar chart representation of mean value and standard deviation for Comparison between the study groups by gender, Blue-Laser and Infrared.

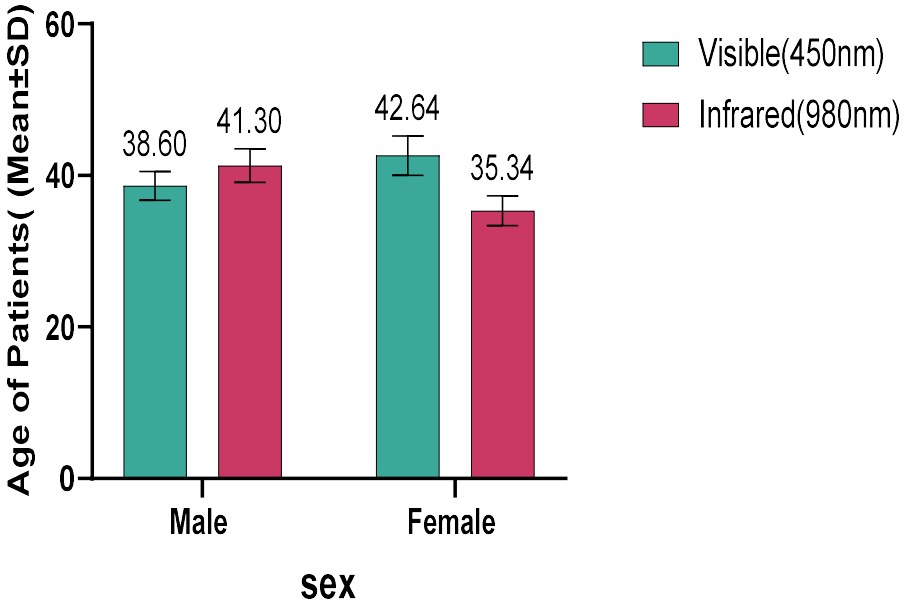

Fig. 2: Bar chart representation of mean value and standard deviation for the age of study groups.

3. Result

The findings of the research study, provides an analysis and interpretation of these findings, draws implications based on the results, and outlines potential avenues for further research. This study encompassed a cohort of 38 patients who underwent therapy for oral fibroma lesions.

3.1. Pain scores

The results of this study showed that there is a significant difference in pain levels between the two types of diode laser, where the pain scores differed significantly. 450nm treatments showed less pain (2.72±0.51) after one day of the laser surgery and 0 pain after one week compared to 980nm treatment where the pain score was (4.45±0.1) after one day of the laser surgery and (0.1±0.22) after one week, Table (1).

Table 1: Comparison between the study groups by means of pain score at three days, one week, two weeks, and four weeks after operation.

Post-operative pain	Study group		P value
	Visible(450nm) Mean±SD	Infrared(980nm) Mean±SD	
1st day	2.72±0.51	4.45±0.1	0.001
3rd day	0.92±0.51	2±0.3	0.003
One week	0	0.1±0.22	0.9918
Two weeks	0	0	-

3.2. Oedema

The findings of the study revealed a disparity in postoperative edema between the groups examined. As shown in Table (3), the comparison between 450nm and 980nm treatments reveals that the 450nm therapy significantly decreases swelling.

Table 3. Measurement of swelling at 2, 5, and 7 days postoperatively to draw comparisons between the study groups.

Swelling score								
Infrared (980nm)					**Blue laser 450nm**			
	None	**Slight**	**Moderate**	**Severe**	**None**	**Slight**	**Moderate**	**Severe**
2nd day	5(26.31)	5(47.73)	9(26.31)	0	17(89.4)	2(10.5)	0	0
5th day	14(73.6)	5(26.31)	0	0	19(100)	0	0	0
Seven days	19(100)	0	0	0	19(100)	0	0	0

Oedema scores: 0= none, 1= slight, 2= moderate and 3= server

3.4. Clinical cases

A. Case no: 1

The male patient, identified as KA and aged forty-five, presented at the clinic seeking assessment for a lesion located in the angle of the lower lip. The individual stated that the condition had persisted for a duration of one year. The fibroma lesion was confirmed through clinical diagnosis. A decision was made to do a session of laser-assisted surgery for the purpose of eliminating the lesion. The decision was made to utilize a blue diode laser with a wavelength of 450nm for this experimental procedure. The laser was operated at a power of 1.3W in pulsed wave mode, and an optical fiber with a diameter of 400µm was employed in a non-contact configuration, maintaining a distance of 1-2mm. The laser was moved at a speed of around 6mm/s, as depicted in Figure 2.

B. Case no: 2

The female patient, identified as AA and aged thirty-three, presented at the clinic seeking an examination of a lesion located in the mucosa of her cheek. The individual provided an account stating that the condition had persisted for a duration of two years. The fibroma lesion was confirmed through clinical diagnosis. The patient is experiencing pain and discomfort, necessitating the excision of the lesion. After careful consideration, it was determined that the most suitable approach would involve the utilization of an infrared diode laser (980nm) following a specific protocol. The laser will be operated at a power of 1.3W in pulse wave mode, utilizing an optical fiber with a diameter of 400µm. The laser will be applied in contact mode, as seen in Figure 3.

4. Discussion

Several fibroma oral lesions were collected for the current study. The diode laser (980 and 450nm) at 1.3W was used to successfully remove the analyzed lesions. Diode laser 980nm was applied in a contact mode, whereas 450nm was applied non-contactly (at a distance of 1-2 mm).

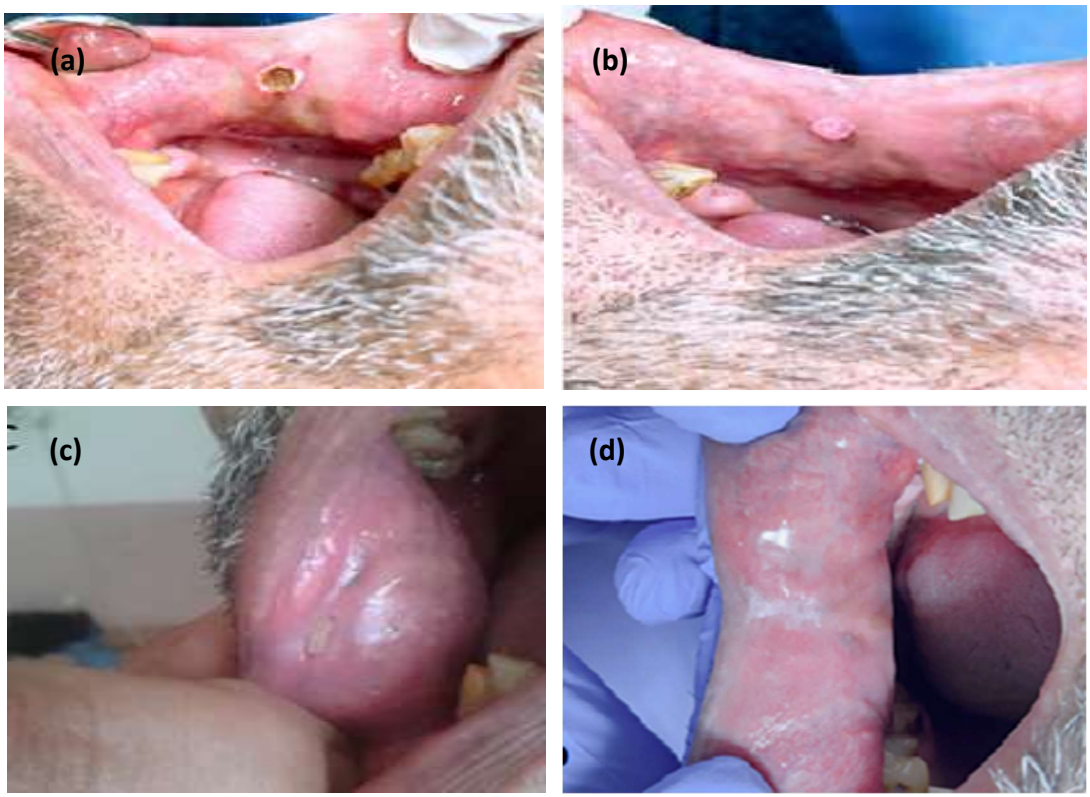

Fig. 4. Excision by diode laser 450nm. (A) Before treatment, (B) immediately after laser surgery, (C) One week after treatment and (D) Two weeks after treatment.

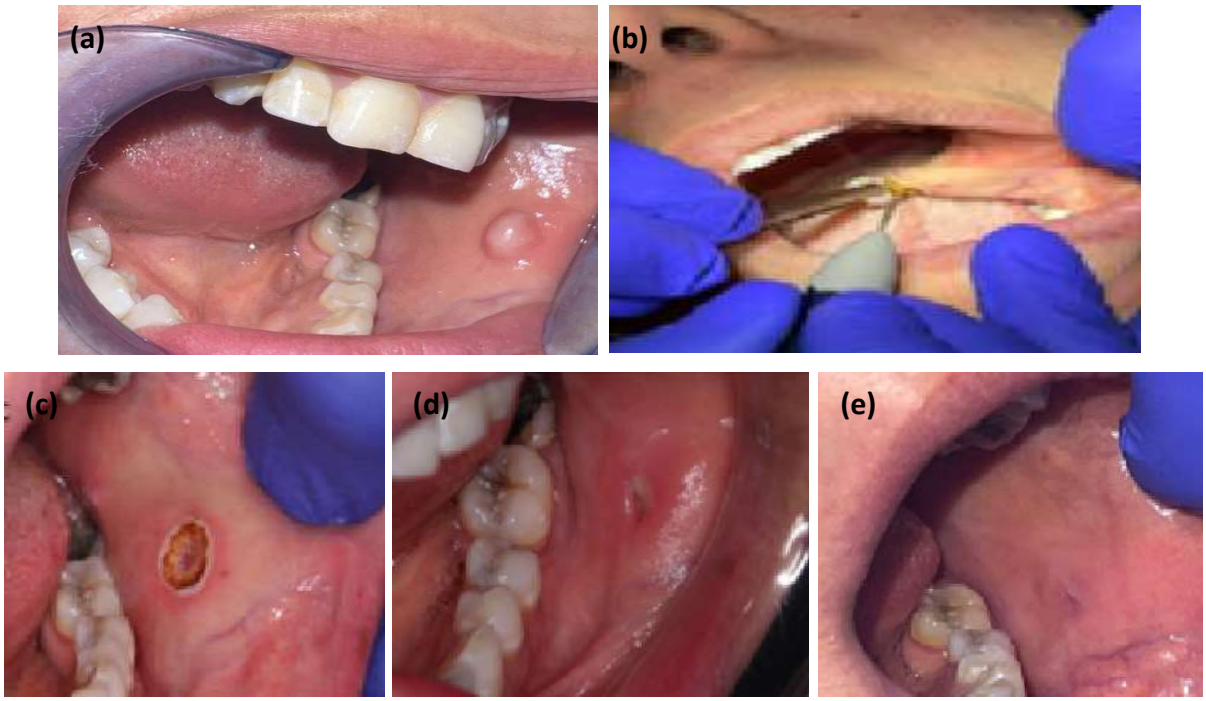

Fig.5: Excision by diode laser 980nm. (A)Before treatment, (B) During laser surgery, (C) Immediately after treatment, (D) One week after treatment, and (E) Three weeks after treatment.

Due to its portability, low cost, and high predilection for hemoglobin and dark pigments, the diode laser was employed to eliminate an oral benign lesion in the current experiment, reaping the many benefits of laser surgery. Patients favored laser surgery since it was a low-stress procedure for them during and after the procedure. Therefore, both patients and dental specialists can profit from diode laser because it is a minimally invasive treatment option.

Patients are administered local anesthetic, either in the form of topical application or injection, based on the specific nature of the lesion. This finding is similar with previous studies conducted by Azma et al and Gholizadeh et al which indicated that the necessity of local anesthesia injection is contingent upon the patient's pain threshold, as well as the size and location of the lesion [12, 13].

In the majority of cases, postoperative pain was alleviated as a result of the laser's capacity to inhibit nerve endings, hence mitigating postoperative discomfort. The observation indicated that the use of a 450nm treatment resulted in reduced post-operative discomfort, which subsequently resolved within a day following the surgical procedure. The pain experienced by patients undergoing diode laser surgery at a wavelength of 450nm was found to be lower compared to those undergoing surgery at a wavelength of 980nm. This difference in pain levels can be attributed to the fact that individuals undergoing the 450nm treatment had reduced instances of thermal necrosis[14]. The majority of patients necessitated modest postoperative analgesia. Previous research has indicated that variations in the diode laser's characteristics are contingent upon factors such as the wavelength and duration of its use. A separate investigation revealed that those who underwent laser treatment at a wavelength of 450nm experienced significantly reduced levels of pain and suffering following surgery, along with a higher level of overall satisfaction. The utilization of a diode laser operating at a wavelength of 450nm necessitates the implementation of a noncontact form of radiation delivery [14]. This particular mode of delivery has been seen to yield reduced levels of thermal necrosis. This observation is consistent with existing literature on the subject. The utilization of a diode laser with a wavelength of 450nm resulted in reduced intraoperative and postoperative hemorrhage and pain due to its robust cutting and coagulation capabilities.

It has been demonstrated that the laser can perform a hemostatic technique during surgery by occluding smaller diameter blood arteries and shutting lymphatic veins, hence minimizing postoperative complications including swelling and oedema. This study's findings corroborated those of Roy et al., who established that patients were contacted again after two weeks. In Addition, The blue laser has demonstrated additional benefits, such as a more pronounced bactericidal action through irradiation [15] result as Patients no longer reported any symptoms of pain associated with the lesion. The diode laser was found to have benefits in this investigation for both types of lasers. When it comes to benign lesion excision and reduced edema, however, laser diode 450nm triumphs over laser diode 980nm It has been reported that lasers can speed up the healing process and win over more patients. With laser surgery, there is less blood loss, faster sterilization, less bacteremia, and no need for sutures except for some lesions need suturing according to size of lesion and patients oral hyogen. He spoke of reduced pain and edema during and after the procedure, as well as lessened wound contraction and scarring [16]. This agrees with the study's findings that diode lasers, in general, speed wound healing, minimize bleeding, and alleviate pain. Although the 450-nanometer diode laser is displayed as the more practical option. When Gobbo et al. examined the efficacy of the blue group with the IR group, they discovered that the absence of any bleeding in the blue group was a major advantage compared to the IR group. Another study by Majeed and Aldelaimi when used 980nm to remove oral lesion showed that some of clinical score such as pain score and oedema took more than two weeks for the patient to heal completely [17] and this is with the consistence with our study where the diode laser 980nm almost showed the same result while blue laser need less than two weeks. The BLUE laser is widely regarded as the most comfortable medical device available; this is especially beneficial when dealing with sensitive patients like youngsters, the mentally ill, or those who are scared of needles [18]. One reason why the BLUE laser is associated with less discomfort after surgery is that it causes less heat damage to tissues. Because histological alterations are minimized, local inflammation can be reduced [19]. This is in line with the current study's findings, which indicated that the blue group experienced no bleeding, little discomfort, limited heat damage, less oedema, and a speedy recovery. Only lasers with an IR emission wavelength spectrum are considered for surgical use in the vast majority of published clinical works on oral surgery.

however, blue lasers have only lately been approved for medical usage. Since the blue laser's (450 nm) hemoglobin absorption is greater than that of the infrared laser's (980 nm), the 450 nm laser is recommended for larger lesions and deeper penetration. The blue laser works because its wavelength is absorbed not by water but by the chromophores in melanin and hemoglobin. This allows for the possibility of a number of improvements in the field of surgery, such as the elimination of blood loss and, in most circumstances, the necessity for sutures. Reduced number of procedures, no or minimal pain, high rates of functional and cosmetic success, minimal to no bleeding, and great visibility are all connected with this laser technology. Furthermore, a comparison between a 445nm semiconductor laser and a 970nm diode laser was performed by Braun et al when they determined that increased efficiency when cutting is to be expected. Clinically acceptable incision depths can be achieved with the non-contact use of a 445 nm laser without causing considerable denaturation of the soft tissues [20].

The benefits of using a 450 nm laser at very low power for oral surgery are confirmed by this investigation. It helps to control tissue bleeding, minimize the time of the intervention during surgery, and eliminate the need for anesthetic injections in most circumstances. From the patient's point of view, it allows us to lessen pain and avoid using sutures. During the follow-up, no signs of pain, discomfort, oedema, or infection arise, and no medication is required in more cases. There are no negative effects, and the recovery time is only one week. This corroborates the findings of Fornaini et al the 450-nm laser is safe and does not cause any tissue damage when used at an appropriate distance and for a brief duration. Lasers emitting at 450 nm had a far lower heating capability than those emitting at 980 nm [21]. In addition, 450 nm had a quieter working environment. The 450nm laser has the advantages of low noise during work, a thin coagulation layer, and efficient tissue vaporization. These characteristics suggest that the novel 450nm laser could be used as a therapeutic alternative in surgery. The cutting efficiency of a diode laser 445nm was found to be higher when compared to that of a diode laser 970nm and high-frequency surgery [20]. Furthermore, there are no signs of significant soft tissue injury when using the diode laser 445nm in non-contact mode, and incision depths are clinically acceptable. This observation agrees with the findings of this investigation. Blue laser light has a shorter wavelength and a higher absorption coefficient in the target chromophores hemoglobin and melanin, making it less scatter and penetrate tissue than near infrared laser systems. This shallow penetration allows for more accurate control of the laser's light and reduces the potential for accidents in deeper levels. Additionally, it is expected that the reduced thermal side effects will occur from the reduced absorption of laser energy in surrounding tissues due to dispersion. Soft tissues consist primarily of water, blood, color, lipids, and proteins. The red blood cells have a maximum absorption wavelength of approximately 450 nm. This leads to a high intake of energy, which can rapidly cause coagulation. Additionally, it results in efficient cutting of lesions with minimal lateral thermal effect, leading to reduced swelling and discomfort.

5. Conclusion

Diode laser removal of benign lesions has a low invasive approach and several therapeutic benefits, making it a viable therapy choice advantages include a shorter recovery time for the patient, less risk of infection, less postoperative pain, better management of bleeding, and higher patient satisfaction due to the absence of wound suturing in most circumstances. For surgical removal of an intraoral benign lesion, the diode laser (450-980 nm) can be utilized successfully with optimized parameters. The results of this study demonstrated that the 450-nanometer wavelength of the diode laser was superior to the 980nm wavelength in terms of performance.

References

[1] B. Diwan, U. Shirbhate, P. Bajaj, A. Reche, A. Pahade, Conventional Scalpel and Diode Laser Approach for the Management of Traumatic Fibroma, Cureus 15(10) (2023).

[2] L.S. Monteiro, R. Albuquerque, A. Paiva, J. de la Peña-Moral, J.B. Amaral, C.A. Lopes, A comparative analysis of oral and maxillofacial pathology over a 16-year period, in the north of Portugal, Int Dent J 67(1) (2017) 38-45.
[3] M.S. Ratre, P.A. Chaudhari, S. Khetarpal, P. Kumar, Effective management of focal reactive gingival overgrowths by diode laser: A review and report of two cases, Laser Therapy 28(4) (2019) 291-297.
[4] S.K. Verma, S. Maheshwari, R.K. Singh, P.K. Chaudhari, Laser in dentistry: An innovative tool in modern dental practice, National journal of maxillofacial surgery 3(2) (2012) 124.
[5] L. Perillo, A. Jamilian, A. Darnahal, Orthodontic Preparation for Orthognatic Surgery, A Textbook of Advanced Oral and Maxillofacial Surgery2014.
[6] F.E. Musaa, L.G. Awazli, F. Alhamdani, Gingival enlargement management using diode laser 940 nm and conventional scalpel technique (A comparative study), IJL 16(B) (2017) 1-9.
[7] D.J. Coluzzi, Fundamentals of dental lasers: science and instruments, Dental Clinics 48(4) (2004) 751-770.
[8] I. Gontijo, R.S. Navarro, P. Haypek, A.L. Ciamponi, A.E. Haddad, The applications of diode and Er: YAG lasers in labial frenectomy in infant patients, J Dent Child 72(1) (2005) 10-15.
[9] S. Kulkarni, M. Meer, R. George, Efficacy of photobiomodulation on accelerating bone healing after tooth extraction: a systematic review, LIMS 34 (2019) 685-692.
[10] S. Modarresi, M.J. Lukacs, M. Ghodrati, S. Salim, J.C. MacDermid, D.M. Walton, A systematic review and synthesis of psychometric properties of the numeric pain rating scale and the visual analog scale for use in people with neck pain, The Clinical Journal of Pain 38(2) (2022) 132-148.
[11] D.S.A. Rosa, A.C.C. Aranha, C. de Paula Eduardo, A. Aoki, Esthetic treatment of gingival melanin hyperpigmentation with Er: YAG laser: Short-term clinical observations and patient follow-up, J Periodontol 78(10) (2007) 2018-2025.
[12] E. Azma, N. Safavi, Diode laser application in soft tissue oral surgery, J Lasers Med Sci 4(4) (2013) 206.
[13] N. Gholizadeh, J.B. Taheri, Z. Namazi, F. Mashhadiabbas, S. Bakhtiari, A. Rahimzamani, M. Asnaashari, Excision of different oral benign exophytic lesions with a diode laser: A clinical case series, Lasers Med Sci 11(4) (2020) 502.
[14] M. Frentzen, D. Kraus, J. Reichelt, C. Engelbach, C. Dehn, J. Meister, A novel blue light diode laser (445 nm) for dental application, laser 8(3) (2016) 6-13.
[15] M.G. Mohammed, A.M. Maki, Effect of 410 nm Diode Laser Irradiation on the Growth of Burn Wounds-associated Bacteria, Pseudomonas Aeruginosa and Staphylococcus Aureus, IJL 16(B) (2017) 11-19.
[16] C. Fornaini, J.-P. Rocca, E. Merigo, 450 nm diode laser: a new help in oral surgery, WJCC 4(9) (2016) 253.
[17] A.A. Majeed, T.N. Aldelaimi, Treatment of intraoral pyogenic granuloma with diode laser 810-980 nm, JLI 21(1) (2022).
[18] I.S.E. Hashemi, D. Maleki, S.S. Monir, A. Ebrahimi, R. Tabari, E. Mousavi, Effects of Diode Low-Level Laser Therapy of 810 Nm on Pulpal Anesthesia of Maxillary Premolars: A Double-Blind Randomized Clinical Trial, Eur Endod J. 6(2) (2021) 155.
[19] G. Tenore, A. Mohsen, A. Nuvoli, G. Palaia, F. Rocchetti, C.R.T. Di Gioia, A. Cicconetti, U. Romeo, A. Del Vecchio, The Impact of Laser Thermal Effect on Histological Evaluation of Oral Soft Tissue Biopsy: Systematic Review, J Dent 11(2) (2023) 28.
[20] A. Braun, M. Kettner, M. Berthold, J.-S. Wenzler, P.G.B. Heymann, R. Frankenberger, Efficiency of soft tissue incision with a novel 445-nm semiconductor laser, Lasers in medical science 33 (2018) 27-33.
[21] C. Fornaini, E. Merigo, J.-P. Rocca, G. Lagori, H. Raybaud, S. Selleri, A. Cucinotta, 450 nm blue laser and oral surgery: preliminary ex vivo study, J Contemp Dent 17(10) (2017) 795-800.

التقييم السريري لاستئصال الآفة الحميدة في الفم باستخدام الليزر بالطولين الموجيين 450 و 980 نانومتر

سعد راضي طاوي الغزالي[1]، سؤدد سلمان احمد[2]، بلسم عبد الحميد[3]

[1]معهد الليزر للدراسات العليا، الكلية، جامعة بغداد، بغداد، العراق
[2]قسم الفيزياء، كلية العلوم ، جامعة بغداد، بغداد، العراق
[3]استشارية جراحة الوجة والفكين، مستشفى الكاظمية التعليمي، بغداد، العراق

*البريد الالكتروني للباحث: saadtawi2020@gmail.com

الخلاصة: يستخدم الليزرذو الصمام الثنائي بأطوال موجية مختلفة لما له من فوائد كثيرة في جراحة اسئصال الافات الفموية الحميدة بسبب امتصاصة الجيد من قبل اصباغ الميلانين والهميغلوبين مع امتصاص ضعيف من قبل المياه والهيدروكسبيتات مما يجعله امنا للاسخدام حول الانسجة الصلبة والاسنان حيث يساعد على تقليل فترات شفاء المرضى والقدرة على تخثر الأنسجة عند الشقوق الجراحية وألم أقل و تطهير موضع الجروح ، وكل ذلك يقلل من الحاجة إلى الدواء ويزيد من راحة المريض خلال فترة التعافي كما أن له تأثير إيجابي على التئام الجروح. هذا ويعمل الليزردايود بكفاءه عالية ضمن طاقة اقل ونتيجة لذلك يمكن تقليل التأثيرات الجانبية غير المرغوب فيها إلى حد كبير. ان الهدف من هذه الدراسة هو تقيم كفاءة الليزر ذو الصمام الثنائي بطوليين موجيين (450 و980 نانومتر) وتحديد فعاليتهما ضمن النتائج السريرية للمريض والنتائج التحليليه المختبرية للعينات بعد استئصال الآفات الفمويه الحميدة . شملت هذه الدراسة ثمانية وثلاثين مريضاً تتراوح أعمارهم بين 16 و40 عاماً. تم اعداد الليزر لكلا الطولين الموجيين موضع الدراسة على وضع الموجة النبضية، وقطر حافة اللياف القطع على قياس 400 ميكرومتر و بطاقة 1.3 واط. بينت نتائج الدراسة الحالية ان الليزرفي الطول الموجي 450 نانومتر كان أكثر فعالية في الحصول على نتائج سريريه تتضمن اقل الم للمريض بعد القطع واقل تورم ضمن موقع استئصال الافه وبالنتيجه شفاء اسرع في أقل من أسبوعين.

IJL, Issue 1, Vol. 23, 2024
https://doi.org/10.31900/ijl.v23i1.447

Research Article

IRAQI JOURNAL OF LASER

Evaluation of dentin topography after Er, Cr: YSGG laser irradiation and phosphoric acid etching using AFM, SEM and contact angle

Saja Qasim Salman*, Basima Mohammed Ali Hussein

Institute of Laser for Postgraduate Studies, University of Baghdad, Baghdad, Iraq
** Email address of the Corresponding Author: saja.qasem2102m@ilps.uobaghdad.edu.iq*

Article history: Received 7 Jan. 2024; Revised 7 Mar. 2024; Accepted 17 Mar.2024; Published online 15 Jun.2024

Abstract

Objective: The goal of this in vitro investigation is to assess laser irradiation and phosphoric acid etching effects on the dentinal surface topography.
Materials and Methods: A total of 48 sound human premolars extracted for orthodontic purposes were included in this study. Teeth were divided into four groups (n = 10), G1 without surface treatment, G2 etched with phosphoric acid 37% for 15 seconds, and G3 and G4 were treated with an Er, Cr:YSGG laser at the following settings: 1W, 1.5W, respectively with set other laser parameters at 20 HZ and 10% air/water ratio. The effects were evaluated using SEM, AFM, and contact angle.
Results: AFM and SEM images showed changes in the surface topography of the dentin with an increase in the surface roughness measurements and devoid from smear layer in the laser-treated groups compared to the control and phosphoric acid-treated groups. Also, highly significant differences ($p \leq 0.01$) were shown in the laser irradiation groups, specifically G3 with 1W, when compared with others considering contact angle measurement.
Conclusion: Er, Cr: YSGG laser can be used as an alternative to conventional phosphoric acid etching for etching and preparing dentin surfaces prior to restoration or bracket placement.

Keywords: Er, Cr: YSGG, phosphoric acid, dentin, SEM, and wettability test.

1. Introduction

Dentin adhesion is thought to be a more complex and difficult process than enamel adhesion because of its chemical composition, humidity, and morphological diversity. Furthermore, pathological and physiological processes might create morphological and biomechanical changes in the dentin is also unique [1]. In the conventional method, the smear layer is removed from the dentin surface by acid etching which also leads

to exposing collagen fibrils and dentinal tubules; this could help in resin monomer infiltration. Subsequently, hybrid layers form during the polymerization of the infiltrating resin monomers [2].

Acid etching of dentin has some shortages, such as increased dentin permeability and wetness, with an increased possibility of pulpal irritation and collagen denaturation, in addition to the time and risks or precautions [3]. In recent years, there has been a great interest in the use of lasers in dentistry for different purposes and applications, such as cavity preparation, caries prevention and detection, teeth bleaching, and dental implants [4, 5]. Because of its strong absorption by water and hydroxyapatite crystals, the Er, Cr:YSGG laser may effectively ablate enamel and dentin [6]. By providing uneven surfaces and open dentinal tubules without a smear layer, Er, Cr:YSGG laser irradiation with modified laser parameters or technique may generate energy suitable dentin surface adhesion [7]. When Er, Cr:YSGG laser energy is absorbed by tooth layers components, it causes evaporation of water, an increase in internal pressure, and microexplosion, resulting in the formation of a rough dentin surface [8-10]. Depending on the type and energy of laser applied to the surface, laser etching produces surface irregularities and roughening to a depth of 10 to 20 micrometers, which is comparable to that produced by the acid [11]. According to different laser applications in the dental field, laser etching might be suggested with advantages over traditional acid etching, including painlessness, the absence of vibration or heat generation, the creation of an uneven and fractured surface suited for adhesion, the absence of a smear layer, and increased tooth resistance to caries attack [12-14]. Er, Cr: YSGG Laser widely used in dentistry for different dental procedures, including cavity preparation [15], disinfection of prepared cavity and root canal [16, 17], and in bonding of esthetic restoration without thermal damage to dental pulp [18, 19].

The goal of this study is to estimate how much Er, Cr: YSGG laser is a suitable alternative source for phosphoric acid etching in dentin.

2. Material and Method

2.1 Sample Collection and Preparation

A total of (48) intact premolars were collected from different health centers and clinics in Baghdad. The volunteers were in the age range (18-35), and teeth were extracted for orthodontic treatment. Primarily, teeth were cleaned from blood, tissue remnants, and debris with dental scalar and prophylaxis dental paste; they were stored in 1% thymol solution until used. Preparations of samples were performed with the diamond disk, which is used to cut the occlusal surface of teeth to a level of central groove and expose the dentin surface.

The cutting procedure was done with the aid of a dental surveyor (Dentaurum para therm, German) and water irrigation to avoid any deterioration to the sample surface from hat generation during cutting; this also helped in the standardization of the procedures. The acrylic block was constructed with a cylindrical silicon mold of about 2.5 cm in length and 2 cm in diameter, as seen in Figure 1. Samples were assigned into four groups:-

G1: Samples without surface treatment

G2: Samples were treated with 37% orthophosphoric acid etchant

G3: Samples were treated with Er, Cr: YSGG laser (1W, 20 HZ, 10% air, and water ratio, 60µs (pulse duration), 66sec (irradiation time), 20mm^2 (irradiation area)

G4: Samples were treated with Er, Cr: YSGG laser (1.5 W, 20 HZ, 10% air, and water ratio, 60µs (pulse duration), 66sec (irradiation time), 20mm (irradiation area)

Laser parameters in G3 and G4 were selected according to the result of the pilot study.

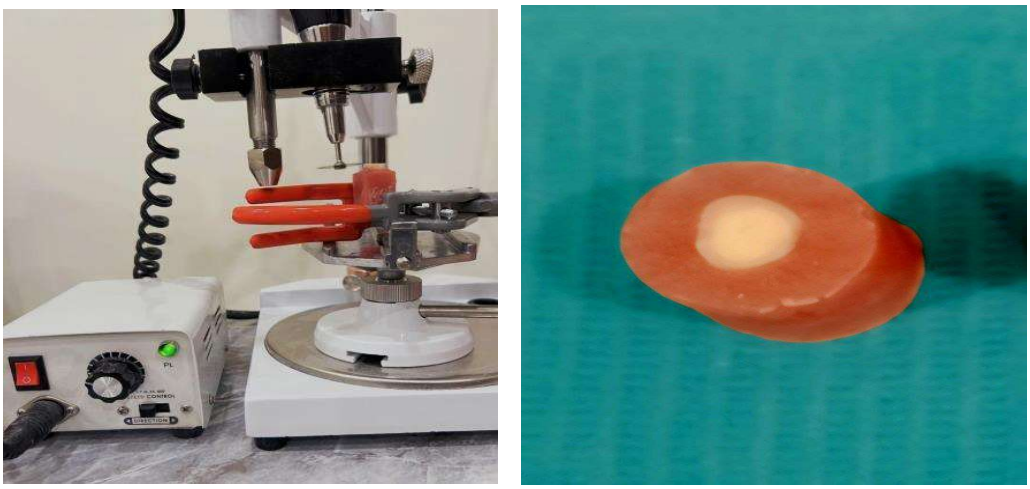

(a) **(b)**

Fig.1: Sample Preparation Procedure (a) de-cusped occlusal surface with diamond disk and dental surveyor (c) acrylic block construction.

2.2. Etching Application

A. Phosphoric Acid Application

Dentin samples of G2 were etched with 37% orthophosphoric acid gel (3M, ESPS, USA) for 15 seconds and rinsed vigorously with water for 20 seconds according to the manufacturer's instructions.

B. Laser Application

Er,Cr:YSGG laser with the MZ6 laser tip (WaterLase iPlus, USA) was used to irradiate specimens of G3 and G4. At a stand-off distance of about 2mm between the laser tip and the sample surface, the laser beam was directed perpendicularly to the dentin surface. For standardization of laser applications, laser irradiation was performed with the aid of a CNC machine (computerized numerical control unit) with a scanning speed of 0.3 mm/sec, as seen in Figure 2.

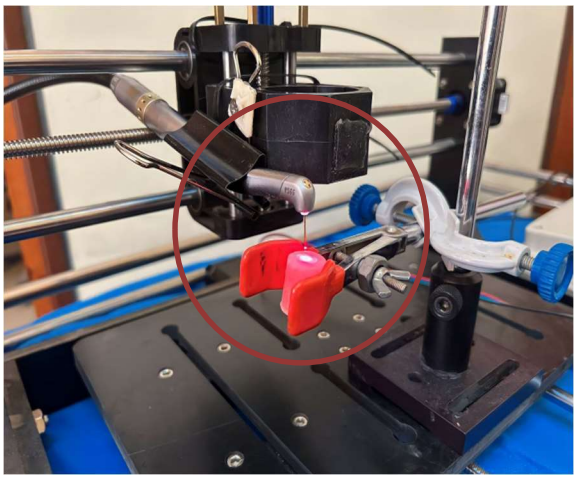

Fig.2: Laser irradiation of specimen surface with the aid of CNC machine.

2.3. Light Microscopic Evaluation

All samples were examined with a light microscope (Euromex microscope, Netherlands) before and after acid agent application and laser irradiation to evaluate their effects on the dentin surface.

2.4. SEM Examination

One sample representing each group was examined with SEM (Inspect F-50, FEI Electron Optics International B.V., Netherlands). Before being inspected with an SEM machine, the samples were sputtered with gold in a vacuum chamber. The morphological examination of the dentin surface was done.

2.5. AFM Evaluation

For more precise information about the surface changes and roughness of dentin, one sample from each group was examined with AFM (Nano surf, Liestal, Switzerland); the root mean square of surface roughness is displayed in contact mode by the atomic force microscope's scanning probe.

2.6. Assessment of Contact Angle

Ten samples from each group were examined with a contact angle instrument (CAM 110, Taiwan). The instrument was connected to a computerized digital camera to capture an image of the water drop on the sample surface within (30) seconds. The water drop was about 2µl, and the measurement was done at room temperature. Statistical analysis was performed using SPSS, version 24, at $p \leq 0.05$.

3. Result

3.1. Light Microscopic Evaluation

Light microscopic evaluation showed that there are scratching lines on the dentin surface for G1, which occurred during sample preparation, while for G2, the dentin surface was presented with a superficial effect of acid etching, and for laser groups, the G3 and G4 dentin surface had a uniform pattern of laser effect and surface irregularity as shown in Figure 3.

3.2. SEM Evaluation

SEM images for G1 showed high dental debris due to the sample preparation procedure, as shown in Figure 4a. For G2, the dentin surface was presented with partially occluded dentinal tubules and covered with a smear layer, as seen in Figure (4,b), while laser-irradiated groups (G3 and G4) were presented with clean, highly irregular surfaces devoid of a smear layer, as in Figures (4c, and d).

3.3. AFM Evaluation

Atomic force microscopy (AFM) evaluation showed that laser-irradiated groups (G3 and G4) have the highest value of surface roughness (Ra) compared to other groups (G1 and G2), as seen in Figures 5 and Table 1.

Table 1. Surface roughness using Atomic Force Microscopy for tested groups.

Groups	Ra (nm)
G1	60.82
G2	84.48
G3	404.5
G4	116.3

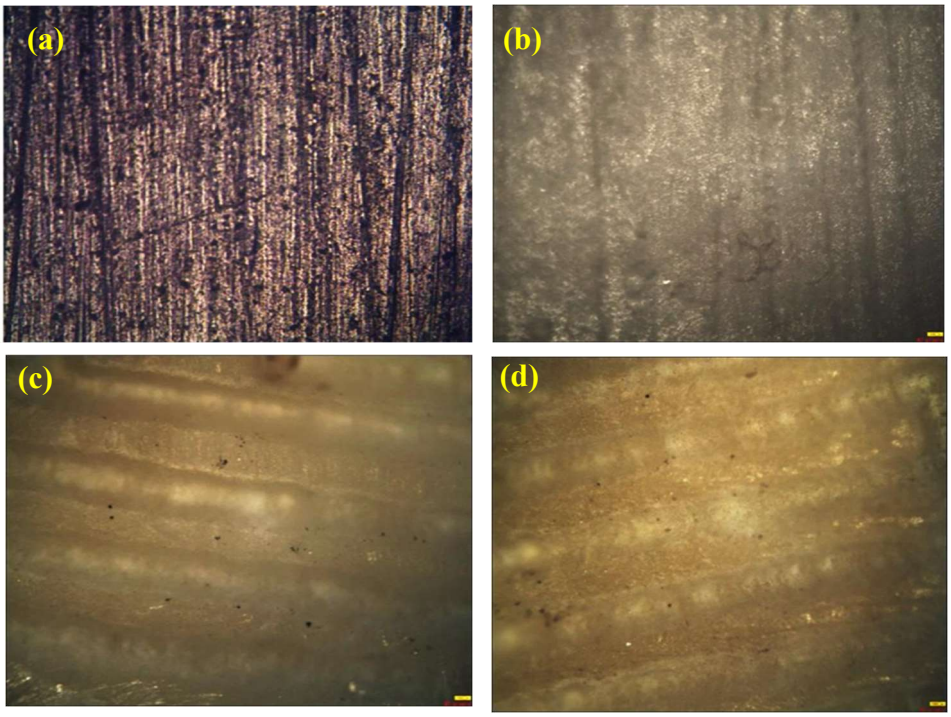

Fig .3: Light Microscopic Images of G1 (a) untreated dentin, G2 (b) acidic etched dentin, G3(c) laser irradiated dentin, and G4 (d) laser irradiated dentin at 4X magnification power.

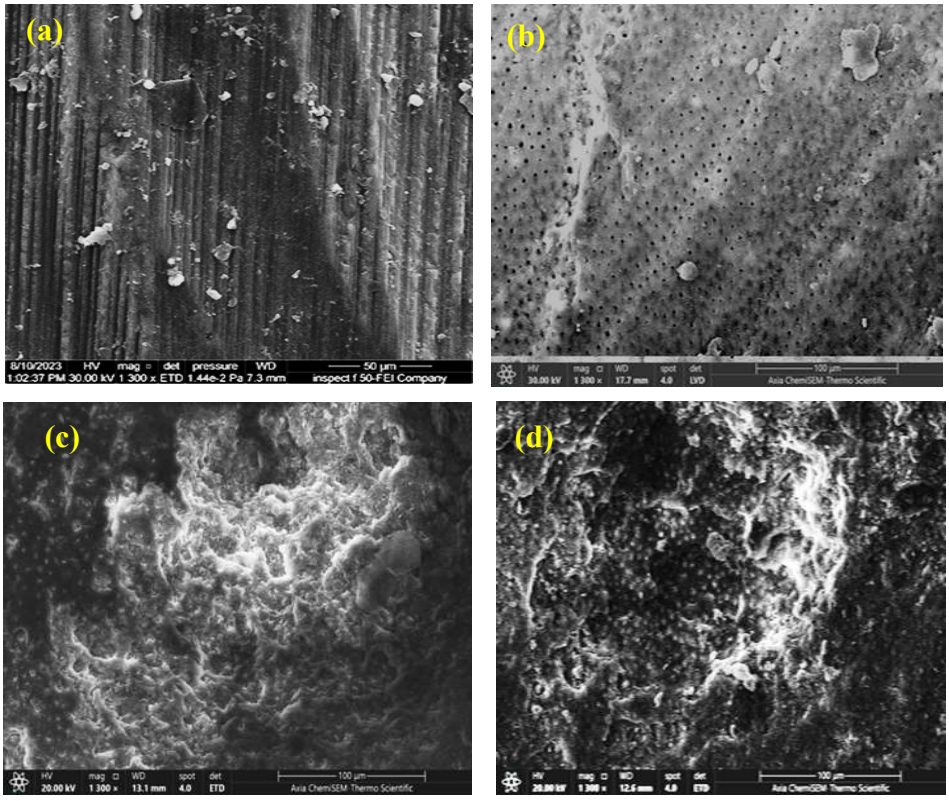

Fig.4: SEM Images of G1 (a) untreated dentin, G2 (b) acidic etched dentin, G3(c) laser irradiated dentin and G4 (d) laser irradiated dentin at 1300Xmagnification power

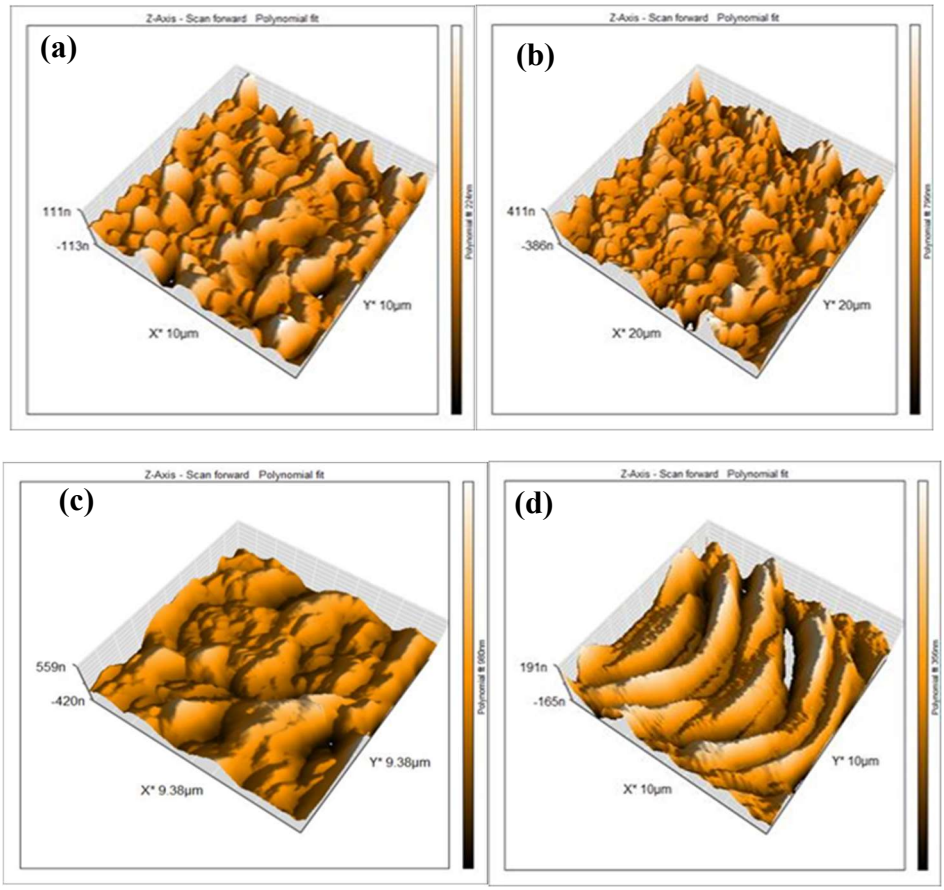

Fig .5: AFM Images of G1 (a) untreated dentin, G2 (b) acidic etched dentin, G3(c) laser irradiated dentin, and G4 (d) laser irradiated dentin.

3.4. Contact Angle Evaluation

Descriptive statistical analysis showed that the highest mean value of contact angle was in G1 (72.83) (without surface treatment), followed by G2 (48.18) (acid-treated samples), and the lowest mean of contact angle was in G3 (36.81) and G4 (37.13) Er,Cr:YSGG laser-irradiated groups. Statistical analysis using the ANOVA test showed a highly significant difference between the tested groups at ($p \leq 0.01$), as shown in Table 2. Tukey (HSD) test was performed for making a comparison between each two groups regarding contact angle. The result showed a highly significant difference between all groups, with no significant difference between the laser-irradiated group (G3-G4), as shown in Table 3.

Table2. Descriptive statistics and ANOVA test for contact angle in the tested groups.

Groups	Mean± SD	F-test				
		Sum of Squares	D.f	Mean Square	F-value	P-Value
G1	72.83±2.09	4491.476	3	1122.869	93.400	.000
G2	48.18±1.39	240.442	36	12.022		
G3	36.81±1.61	4731.918	39			
G4	37.13±1.18					

Table3. Tukey HSD test between each two groups.

Tukey HDS			
(I)	(J)	(I-J) Mean difference	Sig
G1	G2	24.65*	.000
	G3	36.02*	.000
	G4	35.70*	.000
G2	G3	11.37*	.001
	G4	11.05*	.000
G3	G4	1.68	1.000

5. Discussion

To reestablish function and aesthetics within the principles of optimum tooth structure preservation, bonding to hard dental tissues has been regarded as crucial in operative dentistry. Different dentin surface treatments can have an impact on the efficacy of dentin bonding techniques. [20]. The SEM, AFM, and light microscopic examination results of this in vitro study indicated an increase in surface roughness and irregularity of dentin samples in the laser-treated groups compared with the control and acid-treated groups. The increased surface roughness could be attributed to the different mechanisms of action of laser (thermal) and acid (chemical). The interaction of the Er:Cr:YSGG laser with the dentin's water and hydroxyapatite causes microexplosion and ejection of tooth particles that build on the dentin surface, resulting in a roughened surface [8]. Also, the increase in surface roughness in laser-treated dentine could be attributed to the absence of a smear layer, the presence of exposed dentinal tubules, and chimney-like formations. Furthermore, the laser may selectively remove the intertubular dentin by ablation rather than peritubular dentin since this site contains more water and a lower mineral concentration, which results in projecting dentinal tubules with a cuff-like appearance [21–23]. This research result was in line with Benderli et al., Mahdisiar et al., and Issar et al. [24–26], who found that exposure of dentin surfaces to the Er,Cr,YSGG laser produced a sponge-like appearance and a microscopically rough surface, which might be indicators of the melting and re-crystallization processes. While these findings disagree with those of Al Habdan et al. [27], which could be explained by higher power employed in their experiment (4.5W, 50Hz, and a tip-to-specimen distance of 0.5 mm). High power and frequency (4.5W, 30-50Hz) may result in high energy and temperature on the tooth surface, causing melting and resolidification and diminishing surface roughness. This is partially seen when G3 compared to G4 laser groups; higher energy delivered to the dentin surface may generate more heat, which leads to melting of the peritubular dentin. Acid etching destroys intertubular dentin, removing chimney-like structures and expanding the orifices of dentinal tubules. Furthermore, sequential acid etching reveals unknown depths of the demineralization zone [28]. The role of wettability in the stability of bonding between dentin and restoration is crucial. The depth of adhesive infiltration and dentin wettability influence the quality and durability of the resin-dentin hybrid layer [29]. A statistical analysis of the wettability test revealed that laser groups have a lower contact angle than the control and acid-etched groups. This result is related to the fact that when the surface roughness increases, the contact angle decreases, and the wettability is improved [30–32]. Surface irregularity and the existence or extent of the smear layer have a high impact on the surface's wettability [33]. The viscosities of a solution, surface roughness, and heterogeneity all have an effect on the contact angle [34]. The effect of laser in dental applications can be controlled by two groups of variables: the first is laser parameters such as power, wavelength, pulse duration, irradiation mode, and time, which are under the dentist's control, and the second is dentin optical properties, which differ between individuals [35]. Although trained dental personnel can still use the second set of criteria, they benefit from the freedom to choose laser parameters to achieve the purpose or goal of laser use.

6. Conclusions

Based on the findings of this study, Er, Cr: YSGG laser showed improvement in dentin surface topography and can be utilized as an alternate and safe method for surface etching. Laser parameters, specifically the power, are a major contributing factor in surface modification; 1W showed the best result considering surface roughness and wettability.

Reference

[1] Talal A, Nasim HM, Khan AS. Enamel etching and dental adhesives. InAdvanced Dental Biomaterials 2019 Jan 1 (pp. 229-253). Woodhead Publishing.
[2] Ayar MK, Erdemir F. Bonding strength of universal adhesives to Er, Cr: YSGG laser-irradiated dentin. Nigerian Journal of Clinical Practice. 2018;21(1):93-8.
[3] Hossain M, Nakamura Y, Yamada Y, Suzuki N, Murakami Y, Matsumoto K. Analysis of surface roughness of enamel and dentin after Er, Cr: YSGG laser irradiation. Journal of clinical laser medicine & surgery. 2001 Dec 1;19(6):297-303.
[4] Tzanakakis, E. G. C., Skoulas, E., Pepelassi, E., Koidis, P., & Tzoutzas, I. G. (2021). The use of lasers in dental materials: A review. Materials, 14(12), 3370.
[5] Haghighi HS, Skandarinejad M, Abdollahi AA. Laser application in prevention of demineralization in orthodontic treatment. Journal of lasers in medical sciences. 2013;4(3):107.
[6] Giray FE, Duzdar L, Oksuz M, Tanboga I. Evaluation of the bond strength of resin cements used to lute ceramics on laser-etched dentin. Photomedicine and Laser Surgery. 2014 Jul 1;32(7):413-21.
[7] Kurt A, Yilanci H, Yondem I, Usumez A. The effects of water flow rate on shear bond strength of self etch resin cement to dentin surface after Er, Cr: YSGG laser etching. Journal of adhesion science and Technology. 2017 Jun 18;31(12):1303-13.
[8] Mubaraq RM, Hussein BM. PDF Influence of Er: Cr; YSGG laser Desensitization on SBS of resin cement to dentin. Iraqi Journal of Laser. 2022 Jun 30;21(1):18-27.
[9] Al-Qaradaghi TS, Mahmood AS, Dayem RN. The Efficacy of Er: YAG Laser on Intrapulpal Temperature Rise of Class V Cavity Preparation. Iraqi Journal of Laser. 2011 Dec 13;10(B):9-14.
[10] Salman SQ, Hussein BM. Topographical Analysis of Human Enamel after Phosphoric Acid Etching and Er, Cr: YSGG Laser Irradiation: Laser etching of human enamel. Journal of Lasers in Medical Sciences.;14:e68-.
[11] Bhandari, D. P. K., Anbuselvan, G. J., & Karthi, M. (2019). Evaluation of resin penetration depth in enamel surface for orthodontic bonding exposed to five types of enamel conditioning methods: A scanning electron microscopic study. Journal of pharmacy & bioallied sciences, 11(Suppl 2), S221.
[12] Kumar G, Dhillon JK, Rehman F. A comparative evaluation of retention of pit and fissure sealants placed with conventional acid etching and Er, Cr: YSGG laser etching: A randomised controlled trial. Laser therapy. 2016;25(4):291-8.
[13] Al-Maliky MA, Frentzen M, Meister J. Laser-assisted prevention of enamel caries: a 10-year review of the literature. Lasers in Medical Science. 2020 Feb;35:13-30.
[14] Al-Qaradaghi TS, Mahmood AS, Dayem RN. The Efficacy of Er: YAG Laser on Intrapulpal Temperature Rise of Class V Cavity Preparation. Iraqi Journal of Laser. 2011 Dec 13;10(B):9-14.
[15] Kareem R. PDF Cavity Disinfection Using Er, Cr: YSGG Laser Induced Photoacoustic Streaming Technique: Rand kareem Jassim Hussein Ali Jawad. Iraqi Journal of Laser. 2022 Dec 17;21(2):41-7.
[16] Ibrahim GI, Jawad HA. Investigating the effect of Er, Cr: YSGG laser agitation of sodium hypochlorite on the removal of mature biofilm in the complex root canal systems using atomic force microscopy. Journal of Dental Research, Dental Clinics, Dental Prospects. 2023;17(3):154.
[17] Muhammed FS, Jawad HA. Pulsed Er, Cr: YSGG laser for surface modification of dental zerconia ceramic. Iraqi Journal of Laser. 2021 Aug 20;20(1):21-9.
[18] Al-Shammari AM, Salman AM, Al-janabi A. Safe and efficient dental cavity preparation by applying a gradient-in-power approach from Er, Cr: YSGG laser: an in-vitro study. Optics Continuum. 2023 Apr 15;2(4):917-32.
[19] Labunet A, Tonea A, Kui A, Sava S. The use of laser energy for etching enamel surfaces in dentistry—A scoping review. Materials. 2022 Mar 8;15(6):1988.
[20] Ramos TM, Ramos-Oliveira TM, Moretto SG, de Freitas PM, Esteves-Oliveira M, de Paula Eduardo C. Microtensile bond strength analysis of adhesive systems to Er: YAG and Er, Cr: YSGG laser-treated dentin. Lasers in medical science. 2014 Mar;29:565-73.

[21] Gurgan S, Kiremitci A, Cakir FY, Gorucu J, Alpaslan T, Yazici E, Gutknecht N. Shear bond strength of composite bonded to Er, Cr: YSGG laser-prepared dentin. Photomedicine and laser surgery. 2008 Oct 1;26(5):495-500.
[22] Beer F, Buchmair A, Körpert W, et al. Morphology of resin-dentin interfaces after Er, Cr:YSGG laser and acid etching preparation and application of different bonding systems. Lasers Med. Sci. 2012;27:835–841.
[23] Alkhudhairy F, Vohra F, Naseem M. Influence of Er, Cr: YSGG Laser dentin conditioning on the bond strength of bioactive and conventional bulk-fill dental restorative material. Photobiomodulation, photomedicine, and laser surgery. 2020 Jan 1;38(1):30-5.
[24] Benderli Y, Gökçe K, Kazak M, Gürsoy T. SEM comparison of acid-etching, ER, CR: YSGG laser and combined treatment on dentin surfaces. Balkan Journal of Stomatology. 2013 Jan;17(2):79-86.
[25] Mahdisiar F, Mirzaei A, Fallah A, Gutknecht N, Akhoundan S. Effect of duration of Er, Cr: YSGG laser etching on dentin morphology: an in vitro study. Lasers in Dental Science. 2018 Dec;2:213-9.
[26] Issar R, Mazumdar D, Ranjan S, Krishna NK, Kole R, Singh P, Lakiang D, Jayam C. Comparative evaluation of the etching pattern of Er, Cr: YSGG & acid etching on extracted human teeth-an ESEM analysis. Journal of Clinical and Diagnostic Research: JCDR. 2016 May;10(5):ZC01.
[27] Al Habdan AH, Al Rabiah R, Al Busayes R. Shear bond strength of acid and laser conditioned enamel and dentine to composite resin restorations: An in vitro study. Clinical and Experimental Dental Research. 2021 Jun;7(3):331-7.
[28] Yazici AR, Karaman E, Tuncer D, Berk G, Ertan A. Effect of an Er, Cr: YSGG laser preparation on dentin bond strength of a universal adhesive. Journal of Adhesion Science and Technology. 2016 Nov 16;30(22):2477-84.
[29] Ricci HA, Scheffel DLS, de Souza Costa CA, et al. Wettability of chlorhexidine treated noncarious and caries-affected dentine. Aust Dent J. 2014;59:37–42.
[30] Liu J, Lu P, Sun Y, et al. Wettability of dentin after Yb:KYW thin-disk femtosecond ablation. Lasers Med Sci. 2015;30:1689–1693.
[31]Farge P, Alderete L, Ramos SMM. Dentin wetting by three adhesive systems: Influence of etching time, temperature and relative humidity. J Dent. 2010;38:698–706.
[32] Ramos SMM, Alderete L, Farge P. Dentinal tubules driven wetting of dentin: Cassie-Baxter modelling. Eur Phys J. 2009;30:187–195.
[33] Katyal D, Subramanian AK, Venugopal A, Marya A. Assessment of wettability and contact angle of bonding agent with enamel surface etched by five commercially available etchants: An in vitro study. International Journal of Dentistry. 2021 Oct 8;2021.
[34] Marshall SJ, Bayne SC, Baier R, et al. A review of adhesion science. Dent Mater. 2010;26:e11–e16.
[35]Alkaisi A, Abdo SB. Modification of enamel surface morphology and strength using Nd: YAG laser with proper and safe parameters. European Journal of General Dentistry. 2021 Sep;10(03):123-8.

تقييم تضاريس العاج بعد التشعيع بالليزر والحفر بحمض الفوسفوريك عن طريق الفحوص المجهريه الدقيقه وزاوية التلامس

سجى قاسم سلمان* ، باسمه محمدعلي حسين

معهد الليزر للدراسات العليا، جامعة بغداد، بغداد، العراق

*البريد الالكتروني للباحث: saja.qasem2102m@ilps.uobaghdad.edu.iq

الخلاصة

الهدف: تم إجراء هذه الدراسة البحثية لتقييم تأثير إشعاع الليزر والحفر بحمض الفوسفوريك على تضاريس سطح العاج.

الطرق: تم استخدام (48) ضواحك بشرية سليمة تم قلعها لغرض تقويم الأسنان. ثم قسمت إلى أربع مجموعات (العدد = 10) G1 بدون معالجة سطحية، G2 محفور بحمض الفوسفوريك 37% لمدة 15 ثانية، G3 و G4 تمت معالجتها بالليزر Er,Cr:YSGG باستخدام المعلمات التالية (1 واط، 1.5 واط، 20 هرتز ونسبة هواء وماء 10٪).

النتائج: أظهرت صور الفحوصات المجهريه زيادة في خشونة سطح العاج بدون طبقة اللطاخة للمجموعات المعالجة بالليزر مقارنة بمجموعتي السيطرة والمعاملة بالفوسفور، كما أظهرت المجموعات المعالجة بالليزر فرق كبير للغاية مقارنة بالمجموعات الأخرى في زاوية التلامس.

الاستنتاجات: يمكن استخدام ليزر الاربيوم كروميوم كبديل للنقش التقليدي بحمض الفوسفوريك لحفر وتحضير سطح الأسنان قبل الحشوات الضوئيه وتقويم الاسنان.

IJL, Issue 1, Vol. 23, 2024
https://doi.org/10.31900/ijl.v23i1.455

Research Article

IRAQI JOURNAL OF LASER

Estimation of mean photon number based on single photon detection of weak coherent pulses

Hawraa A. Ghanem*, **Shelan K. Tawfeeq**

Institute of Laser for Postgraduate Studies, University of Baghdad, Baghdad, Iraq
** Email address of the Corresponding Author: hawraa.abd2201m@ilps.uobaghdad.edu.iq*

Article history: Received 28 Feb. 2024; Revised 24 Mar.2024; Accepted 27 Mar.2024; Published online 15 Jun.2024

Abstract: The demand for single photon sources in quantum key distribution (QKD) systems has necessitated the use of weak coherent pulses (WCPs) characterized by a Poissonian distribution. Ensuring security against eavesdropping attacks requires keeping the mean photon number (μ) small and known to legitimate partners. However, accurately determining μ poses challenges due to discrepancies between theoretical calculations and practical implementation. This paper introduces two experiments. The first experiment involves theoretical calculations of μ using several filters to generate the WCPs. The second experiment utilizes a variable attenuator to generate the WCPs, and the value of μ was estimated from the photons detected by the BB84 detection setup. The second experiment represents an accurate method for estimating the value of μ because of using single photon detectors with high timing resolution and low dark counts, in addition to using a Time-to-digital convertor with a bin size of 81 ps.

Keywords: single-photon detection, mean photon number, Poissonian statistics, time to digital conversion, weak coherent pulses.

1. Introduction

In classical cryptography, Alice and Bob, two distant parties, use a communication channel to communicate secretly in the presence of an unwanted third party Eve. The ultimate goal of secure communication is to guarantee that information is completely preserved from unauthorized access. Information security can be achieved theoretically by the one-time-pad (OTP) method if Alice and Bob communicate a long random string that is kept secret from Eve. It should be noted that avoiding using the same key again is crucial for the information security of the OTP method. This implies that the key may only be used once and must be the same length as the message [1].

The OTP is considered a very secure method, but it has major drawbacks that have prevented it from becoming widely used. The key distribution is the main problem. Since the security of the OTP depends only on the secrecy of the key, the key distribution method must be at least as secure as the OTP itself; there is no efficient classical method to fulfill this requirement [2].

Heisenberg's uncertainty and the quantum no-cloning principles have provided a completely new opportunity to facilitate the implementation of quantum cryptography. Using these physical properties in

quantum mechanics enables the secure exchange of a random key, which can be employed alongside the OTP scheme to be as close to unconditional security as possible [2,3]. This discovery led Bennett and Brassard to develop the BB84 protocol for secure key exchange [4].

The first and most widely used QKD protocol is called BB84, after its inventors, Bennett and Brassard. This is a prepare-and-measure protocol where Bob measures the quantum states after being prepared by Alice for encoding. The implementation setup of the polarization-encoded BB84 is shown in Figure 1. The photons are prepared by Alice with polarization selected at random from the following four states: horizontal (H), vertical (V), diagonal (D), and anti-diagonal (AD). Bob receives the photons one at a time via a quantum channel, which can be free space or optical fiber. Bob randomly selects Z or X basis (where Z basis is for V and H polarization, and X basis is for D and AD polarization) to measure each photon's polarization state [5]. The steps of implementing the protocol are shown in Table (1)[6].

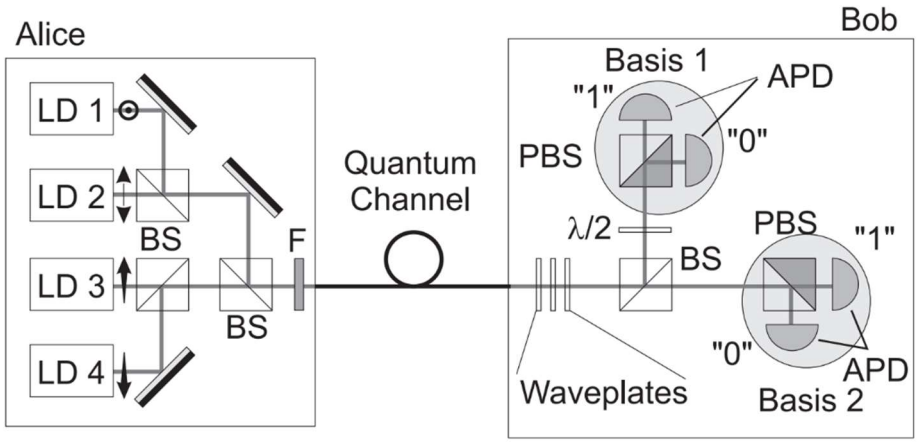

Fig. 1: Typical system for quantum cryptography using polarization coding (LD: laser diode, BS: beamsplitter, F: neutral density filter, PBS: polarizing beam splitter, λ/2: half waveplate, APD: avalanche photodiode) [5]

Table 1. BB84 protocol steps [6].

Alice's random bits	1	0	0	1	0	0	1	1	0
Alice's sending basis	R	D	R	D	D	D	D	D	R
Alice's photon polarization	↕	⤢	↔	⤡	⤢	⤢	⤡	⤡	↔
Bob's receiving basis	D	R	R	D	D	R	R	D	R
Bob's key bits	0		0		0	1	1	1	
Bob checks the bases with Alice			OK		OK			OK	
Bob and Alice check some keys OK bits randomly									
Sifted key			0					1	

To guarantee the security of QKD systems, they must be performed with single photon sources. These sources exhibit anti-bunching behavior and follow sub-Poissonian statistics. Thus, only a true single-photon source emits one photon at a time [7]. A perfect single-photon source generates single photons with 100% certainty, which means that there is a 0% probability of producing more than one photon or a vacuum state. Single atoms, ions, molecules, and solid-state emitters like quantum dots, color centers, carbon nanotubes, etc. These candidates have the potential to serve as sources for single photons. Despite the numerous efforts that have been made toward achieving a perfect single-photon source, it is still a difficult and challenging task [8]. These days, most QKD protocols utilize weak coherent pulses (WCPs) as an approximation to single photons. While these classical states are simple to produce, a fraction of them may contain two photons or more, which threatens the security of the key distribution process [9]. In brief, in the standard BB84 protocol, only signals that originate from single-photon pulses emitted by Alice are assured to be secure [10].

When attenuated laser pulses are employed as the source in the BB84 protocol. The vacuum components reduce the signal rate since there are no photons to be detected by Bob. The single photon components work perfectly, but the problem is in the presence of multiphoton components since each photon within the same pulse has the same polarization information. These multiphoton components make the protocol vulnerable to photon number splitting attacks, where Eve performs a photon number non-demolition measurement to determine Alice's multi-photon signals. Eve blocks part of Alice's single-photon signals so that Bob does not notice any change in the bit rate, steals one copy from multiphoton pulses, and sends the reminder to Bob over a lossless channel. After Alice and Bob reveal their basis during the sifting stage, Eve will have obtained complete knowledge about the key without being detected. However, decoy state protocols allow Alice and Bob to prevent the hypothetical PNS attacks [11,12].

In this paper, we present an acceptable estimation of the mean photon number achieved from the detected photons using the BB84 detection setup, which incorporates four single photon counting modules and a time-to-digital converter. Furthermore, we have successfully reduced the number of filters needed on the transmitter side to attain the necessary attenuation level for WCPs required in QKD systems.

2. Theory and concepts

Alice produces weak coherent pulses with a low mean photon number to approximate the single photon Fock-states. These pulses follow the Poisson statistics. The probability that one finds n photons in a coherent state is [13],

$$P(n,\mu) = \frac{\mu^n}{n!} e^{-\mu} \tag{1}$$

where μ is the mean photon number.

In second-order approximation, we obtain,

$$P(0) \approx 1 - \mu + \frac{\mu^2}{2} \tag{2}$$

$$P(1) \approx \mu - \mu^2 \tag{3}$$

$$P(2) \approx \frac{\mu^2}{2} \tag{4}$$

Accordingly, the probability that a non-empty pulse contains more than 1 photon becomes,

$$P(n \geq 2 \mid n > 0) = \frac{1 - P(0) - P(1)}{1 - P(0)} \approx \frac{\mu}{2} + \left(\frac{\mu^2}{2}\right) \tag{5}$$

The mean photon number can be practically calculated as follows,

$$\mu = \frac{P_{avg}}{P_{single}} \alpha \quad (6)$$

P_{avg} can be represented as [14],

$$P_{avg} = N\, h\, v\, f \quad (7)$$

$$P_{single} = h\, v\, f \quad (8)$$

where
P_{avg} is the average power of the laser source.
P_{single} is the average power of a single photon.
α is the level of attenuation.
N is the number of photons per pulse.
h is Planck's constant (6.634 x 10^{-34} J.s).
v is the frequency of the emitted photon in Hz.
f is the pulse repetition rate in Hz.

The number of photons per pulse is defined as,

$$N = \frac{P_{avg}}{P_{single}} \quad (9)$$

The attenuation level required to have single-photon generation is determined by,

$$\alpha = \frac{1}{N} = \frac{P_{single}}{P_{avg}} \quad (10)$$

Weak coherent pulses can be realized by utilizing calibrated attenuators to attenuate the laser pulses. These pulses are used in many implementations of QKD systems since they are extremely practical. One problem with WCPs with a low mean photon number, i.e., when $\mu = 0.1$, is that 5% of the non-empty pulses contain more than one photon[15]. Figure 2 shows the probability that a pulse of a coherent beam contains n photons for μ=0.1 [16].

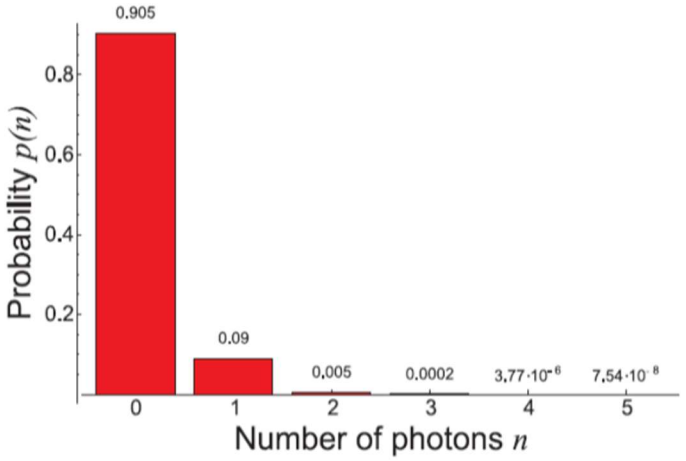

Fig. 2: Poisson distribution for $\mu = 0.1$ [16]

3. Experimental results and discussion

Two experiments were carried out to generate coherent pulses with a low value of μ. The first one is the traditional experiment that uses a laser source and optical filters. In the second experiment, a variable attenuator is implemented, and the time to digital converter (TDC) is used in determining the value of μ.

3.1. Generation of WCPs using optical filters and sheets of glass

Figure 3 illustrates the apparatus employed to produce WCPs using multiple filters and glass sheets. The laser source used in the setup is the nanosecond pulsed laser (NPL64B) from THORLABS. The operating wavelength is 640 nm, $P_{avg}\ of$ the laser source is 77 μW when it operated at f of 1 MHz with a pulse width(τ) of 5 ns. Neutral density filters (NDF) with a defined optical density (OD) were used. The OD determines the level of attenuation of the NDF applied to the laser pulses. The OD is defined as,

$$\text{OD} = log_{10}\left(\frac{1}{T}\right) \tag{11}$$

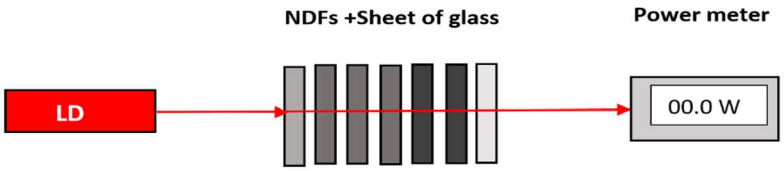

Fig. 3: setup for generating WCPs, LD: pulsed laser source, NDF: neutral density filter.

The specification of optical filters used in the experiment are listed in Table (2).

Table 2. Specifications of optical filters.

Filter type	OD	Transmittance (T)	No. of filters used
NE520B-A	2.0	0.01	2
NE13B-A	1.3	0.05	3
NE06B-A	0.6	0.25	1

The total transmittance (T) of these filters is determined as,

$$T = T_{NE520B-A} \times T_{NE520B-A} \times T_{NE13B-A} \times T_{NE13B-A} \times T_{NE13B-A} \times T_{NE06B-A}$$

In our experiment, two sheets of glass were used with a total transmittance of ≅ 0.155. The attenuation obtained by these combination becomes, α= 0.01× 0.01×0.05× 0.05 × 0.05 ×0.25× 0.155 =4.843 × 10^{-10}. Substituting the value of α in Eq. (6) will give a value of μ=0.12. To have 1 photon in every 10 optical pulses, i.e., μ =0.1, Eq. (10) is written as [17],

$$\alpha_{0.1} = \frac{0.1}{N}$$
$$P_{single} = h\,v\,f = 3.107 \times 10^{-13}\ \text{W}$$
$$N = \frac{77\times10^{-6}}{3.107\times10^{-13}} = 247827486$$
$$\alpha_{0.1} = \frac{0.1}{N} = 4.035 \times 10^{-10}$$

3.2 Estimating the value of the mean photon number from the WCPs detection

In this experiment, the QKD receiver based on the BB84 protocol, including the single photon counting modules and the TDC, is used to determine an acceptable estimation for the required value of μ. This method can be exploited in cases where the power meter is not capable of measuring the low-level attenuated light. Figure 4 illustrates the experimental setup for controlling the value of μ to generate WCPs. A combination of two NDFs (NE520B), a half-wave plate (AHWP05M-600), and a polarizing beam splitter (PBS121) was used as a setup functioning as a variable attenuator. This allows us to create WCPs with the desired mean photon number, denoted as μ_{des} .

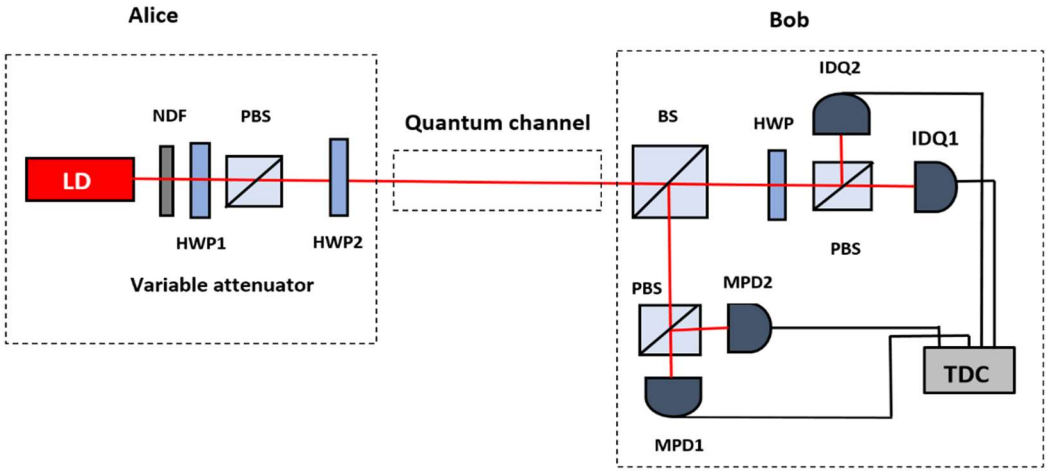

Fig. 4: setup for generating WCPs; LD: pulsed laser; NDF: neutral density filter; HWP: half-wave plate; PBS: polarizing beam splitter; BS: beam splitter; SPCM: single- photon counting module; TDC: time to digital converter

The rotation of the half-wave plate (HWP_1) provides a complete range of attenuation, i.e., allowing for the adjustment values of P_{avg} to be varied from maximum to minimum. Specifically, when the HWP_1 is set within the range of 0° to 45°, it is possible to achieve WCPs with lower values of the μ. These WCPs were then encoded with four different angles (0°, 22.5°, 45°, and 67.5°) for the BB84 protocol by using another half-wave plate (HWP_2) to represent bit values 1, 0, 0, and 1, respectively. The encoded photons were transmitted through the quantum channel to the BB84 detection setup. The BB84 detection setup, including four single-photon counting modules (SPCMs) series (ID100) with a dark count rate of less than 7 Hz and 40 ps timing resolution, and (MPD) with a dark count of one count per second and timing resolution of tenths of ps, were utilized to detect the WCPs. These SPCMs were connected to a four-channel (id800-

TDC, 8-Channel Time to Digital converter) with a bin size of 81ps for recording the number of detected photons for a detection time window of 5ns. Figure (5) illustrates the counts registered by the four SPCMs when HWP_1 was set at an angle of 33° which gives a low value of μ.

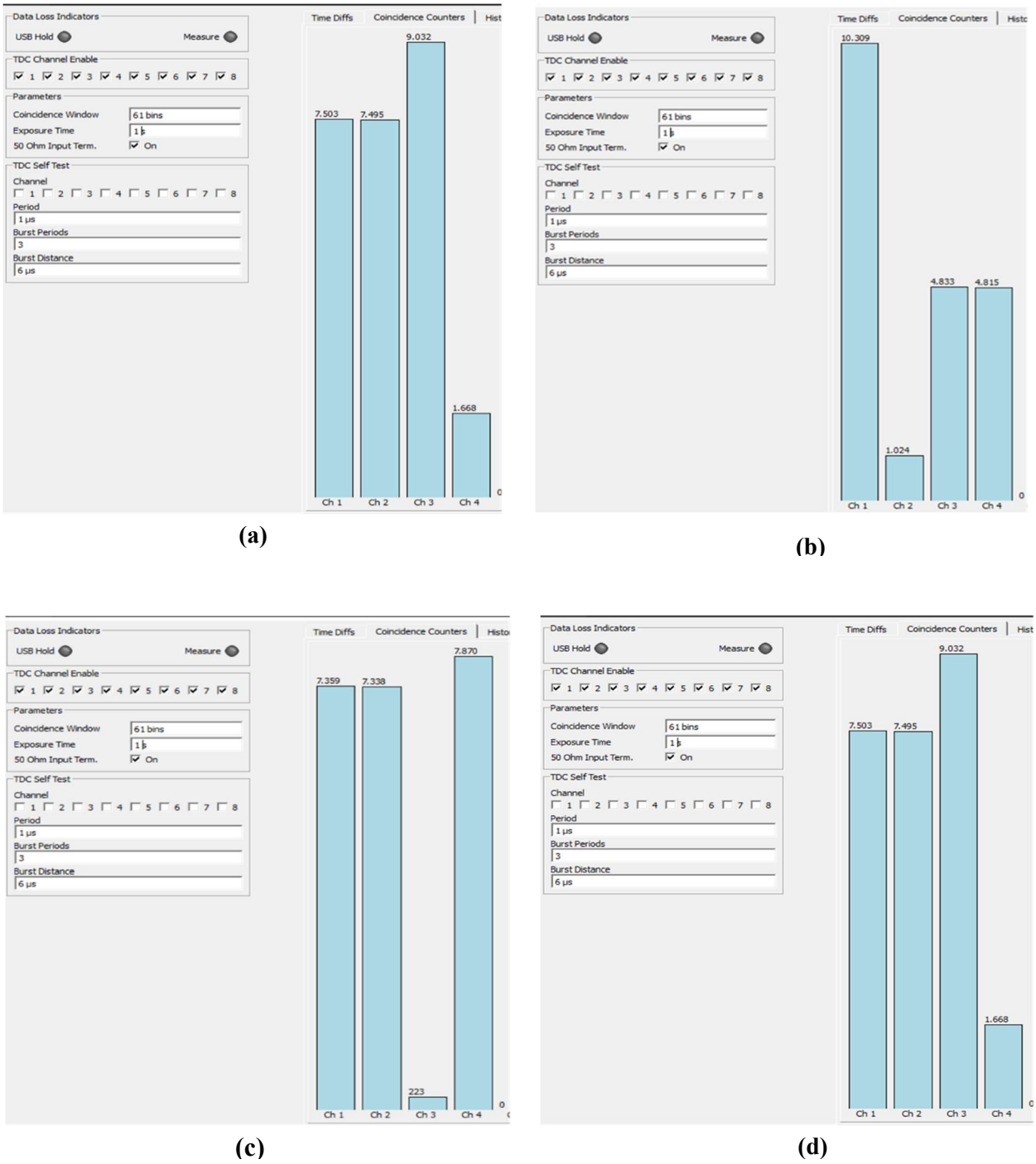

Fig. 5: The number of detected photons for HWP_2 angles of (a) 0, (b) 22.5, (c) 45 (d) 67.5, were: ch1 counts the photons detected by IDQ1, ch2 counts the photons detected by 1DQ2, ch3 counts the photons detected by MPD1, and ch4 counts the photons detected by MPD2.

μ_{des} can be estimated from the number of photons detected by four SPCMs [17]

$$N_{TDC} = \mu_{des} \cdot f \cdot \eta_d \quad (12)$$

Where
N_{TDC} is the number of detections per second measured by TDC.
η_d is detection efficiency for SPCM.

$$\mu_{des} = \frac{N_{TDC}}{f \times \eta_d} \quad (13)$$

The detection efficiency for each arm of the receiver setup can be calculated as,

$$\eta_{di} = \frac{\eta_c \times \eta_{b,i} \times \eta_{BOb}}{\eta_t} \quad (14)$$

Where
η_c is the quantum efficiency of the SPCM.
$\eta_{b,i}$ is the branching efficiencies, defined as the probability of a photon reaching a specific SPCM, where i= 1,2,3,4 for the four branches of the BB84 receiver.
η_{Bob} is the transmittance of Bob components.
η_t is channel transmissivity determined as, where $\eta_t = \frac{P_{received}}{P_{transmitted}}$

Table 3 shows the parameters used to calculate the detection efficiency.

Table 3 Experimental parameters used in the detection efficiency calculation.

Parameters		Value
Detector efficiency of (ID100)	η_{ID100}	36%
Detector efficiency of (MPD)	η_{MPD}	37%
Transmission of Polarizing beam splitter	T_{PBS121}	90%
Transmittance of Half Wave plate	$T_{\mathrm{AHWPO5M-600}}$	98%
Transmittance of Neutral density filter	$T_{\mathrm{NE13B-A}}$	5%
Branching efficiency	$\eta_{b,i,}$	50%
Channel transmissivity for a channel length of 1.5 m	η_t	96%

Where η_{di} is the detection efficiency for each arm of the BB84 receiver

$$\eta_{d1} = \frac{0.36 \times 0.5 \times 0.9 \times 0.98}{0.96} = 0.165$$

$$\eta_{d2} = \frac{0.36 \times 0.5 \times 0.9 \times 0.98}{0.96} = 0.165$$

$\eta_{d3} = \frac{0.37\times0.5\times0.9}{0.96}$ =0.173

$\eta_{d4} = \frac{0.37\times0.5\times0.9}{0.96}$ = 0.173

From the above relationship η_d can be defined as,[17]

$$\eta_d = \frac{1}{4}\sum \eta_{di} \quad (15)$$

$\eta_d = \frac{0.165+0.165+0.173+0.173}{4} \approx 0.17$

By substituting the value η_d in equation (13) the value of μ_{des} can be obtained as listed in Table (4)

Table 4. values of mean photon number estimated from Eq. (13).

HWP 2	N_{ch1}	N_{ch2}	N_{ch3}	N_{ch4}	N_{total}	μ_{des}
0°	7503	7495	9032	1668	25698	0.15
22.5°	10309	1024	4833	4815	20981	0.12
45°	7359	7338	233	7870	22790	0.13
67.5°	1259	21158	4633	4587	31637	0.19

The fluctuation in the mean photon number with the variation of the HWP angle is attributed to several factors, such as imperfect optical components specifications and detection efficiency mismatch.

4. Conclusion

Based on the experimental results, it can be concluded that the mean photon number can be estimated with enhanced accuracy by considering the detector efficiency, branching efficiency, and transmission efficiency within the BB84 detection setup. Additionally, by employing a simplified configuration consisting of only two neutral density filters (NDF), a half-wave plate (HWP), and a polarizing beam splitter (PBS), our suggested configuration reduces the need for additional filters to optimize the target mean photon number. This approach facilitates more efficient and precise measurements in QKD systems as it employs SPCMs with low dark counts and high timing resolution and TDC with a time resolution reaching 81ps .

References

[1] F. Xu, X. Ma, Q. Zhang, H. K. Lo, and J. W. Pan, “Secure quantum key distribution with realistic devices,” Rev. Mod. Phys., vol. 92, no. 2, pp. 1–68 (2020).
[2] H. Weinfurter and A. Laubeeau, "Experimental Quantum Key Distribution," Diploma Thesis, University of Munich, Germany, 1998.
[3] R. Etengu, F. M. Abbou, H. Y. Wong, A. Abid, N. Nortiza, and A. Setharaman, “Performance comparison of BB84 and B92 satellite-based free space quantum optical communication systems in the presence of channel effects,” J. Opt. Commun., vol. 32, no. 1, pp. 37–47 (2011)
[4] S. M. Salih and S. K. Tawfeeq, “Random signal generation and synchronization in lab-scale measurement device independent–quantum key distribution systems,” J. Opt. Technol., vol. 86, no. 3, p. 137, (2019).
[5] H. Zbinden, H. Bechmann-Pasquinucci, N. Gisin, and G. Ribordy, “Quantum cryptography,” Appl. Phys. B Lasers Opt., vol. 67, no. 6, pp. 743–748, (1998)
[6] S. M. Salih, S. K. Tawfeeq, and A. I. Khaleel, “Generation of True Random TTL Signals for Quantum Key-Distribution Systems Based on True Random Binary Sequences,” Iraqi J. Laser, vol. 18, no. 1, pp. 31–42 (2019).
[7] M. S. M. Leifgen, “Protocols and Components for Quantum Key Distribution Dissertation zur Erlangung des akademischen Grades doctor rerum naturalium im Fach Physik eingereicht an der Mathematisch-Naturwissenschaftlichen Fakult ¨ at der at zu Berlin von,” (2016).

[8] A. Jain, P. V. Sakhiya, and R. K. Bahl, “Design and Development of Weak Coherent Pulse Source for Quantum Key Distribution System,” Proc. CONECCT 2020 - 6th IEEE Int. Conf. Electron. Comput. Commun. Technol., no. 2, pp. 0–4 (2020).
[9] R. Alléaume et al., “Experimental open-air quantum key distribution with a single-photon source,” New J. Phys., vol. 6, pp. 1–14 (2004).
[10] H. K. Lo, X. Ma, and K. Chen, “Decoy state quantum key distribution,” Phys. Rev. Lett., vol. 94, no. 23, pp. 1–5 (2005).
[11] H.-K. Lo and N. Lütkenhaus, “Quantum Cryptography: from Theory to Practice,”(2007).
[12] J. W. Harrington, J. M. Ettinger, R. J. Hughes, and J. E. Nordholt, “Enhancing practical security of quantum key distribution with a few decoy states,” vol. 87545(2005).
[13] S. Félix, N. Gisin, A. Stefanov, and H. Zbinden, “Faint laser quantum key distribution: Eavesdropping exploiting multiphoton pulses,” J. Mod. Opt., vol. 48, no. 13, pp. 2009–2021, (2001).
[14] C. W. Park et al., “Single-photon counting in the 1550-nm wavelength region for quantum cryptography,” J. Korean Phys. Soc., vol. 49, no. 1, pp. 111–114 (2006).
[15] K. I. Hajim, S. K. Tawfiq, and A. M. Meki, “Quantum Cryptography and a Quantum Key Distribution Protocol,” vol. 3, pp. 1–10 (2004).
[16] F. A. Yassien, S. K. Tawfeeq, A. I. Khalil, and F. R. Aziz, “Generation of Weak Coherent Pulses for Quantum Cryptography Systems,” Iraqi J. Laser, Part A, vol. 9, no. 2, pp. 1–8 (2010).
[17] T. Sharma, A. Biswas, J. Ramakrishnan, P. Chandravanshi, and R. P. Singh, “Mitigating the source-side channel vulnerability by characterization of photon statistics,” pp. 1–8 (2023).

تحقيق تجريبي لتوليد نبضات ضعيفة متشاكهة بناء على كشف الفوتون المنفرد

حوراء عبد غانم ، شيلان خسرو توفيق

معهد الليزر للدراسات العليا، جامعة بغداد، بغداد،العراق

*البريد الالكتروني للباحث: hawraa.abd2201m@ilps.uobaghdad.edu.iq

الخلاصة: استلزم الطلب على مصادر الفوتون المنفرد في منظومات توزيع المفتاح الكمي (QKD)) استخدام النبضات الضعيفة المتشاكهة والتي تتميز بتوزيع بواسون. يتطلب ضمان الأمن ضد هجمات التنصت الحفاظ على معدل لعدد فوتونات قليل ومعروف للشركاء الموثوقين. مع ذلك، فإن تحديد معدل عدد الفوتونات بدقة يواجه تحديات بسبب الاختلافات بين الحسابات النظرية والتنفيذ العملي.تقدم هذه المقالة تجربتين.تتضمن التجربة الاولى حسابات نظرية لحساب معدل عدد الفوتونات بأستخدام عدة مرشحات لتوليد النبضات الضعيفة المتشاكهة. أما التجربة الثانية، فاستخدمت مخففًا متغيرًا لتوليد نبضات ضعيفة متشاكهة، وتم تقدير قيمة μ من الفوتونات التي تم اكتشافها بواسطة نظام الكشفBB84. وتمثل التجربة الثانية طريقة دقيقة لتقدير قيمة μبسبب استخدام كواشف الفوتون المنفرد ذات دقة توقيت عالية وقيم منخفضة للعد المظلم , بالاضافة الى استخدام محول الزمن الى اشارة رقمية بتقسيم 81 ps.

IJL, Issue 1, Vol. 23, 2024
https://doi.org/10.31900/ijl.v23i1.446

Research Article

IRAQI JOURNAL OF LASER

Comparative evaluative study of Erbium, chromium YSGG and wavelength-dual Diode lasers in oral soft tissue incision morphology: a histological ex vivo study

Alaa Jamal Al-Ani[1,*], Hanan J. Taher[1], And Ammar Saleh Alalawi[2]

[1] *Institute of Laser for Postgraduate Studies, University of Baghdad, Baghdad, Iraq*
[2] *Surgical Laser Unit, Maxillofacial Department, Al-Emamein Al-Kadhimein Medical City, Baghdad, Iraq.*
* *Email address of the Corresponding Author:* aalaa.jamal2102m@ilps.uobaghdad.edu.iq

Article history: Received 4 Jan. 2024; Revised 26 Mar. 2024; Accepted 1 Apr. 2024; Published online 15 Jun.2024

Abstract: Laser is an advantageous system that can be used in different medical applications, and one of them is soft tissue handling in periodontal and surgical dentistry. The recent research aimed to histologically compare the erbium, chromium YSGG laser, and wavelength-dual diode laser in oral surgical incisions according to cutting morphology.
Method: This was an ex vivo study using the pieces of tongue from the sheep as samples. 810(50%) + 980 (50%) nm diode laser was operated continuously (CW) with two average powers: 1.5 and 2.5 W. 2780 nm erbium, chromium YSGG laser was used in pulse mode with two average powers: 2.5 and 3.5 W. Incisions were made on the tongue parts, and after histopathological processing, the regularity and morphology of the incision and the cutting depth of each incision were measured under a light microscope.
Results: The regularity and morphology of erbium, chromium YSGG laser incisions were significantly higher in quality (especially those of the low output power of 2.5 W) than those of the diode laser (P value < 0.05). The cutting depth was significantly higher when the power increased, no matter the type of laser system (P value < 0.05).
Conclusions: Most regular incisions have been achieved with 2.5 W power of Erbium, Chromium YSGG laser.

Keywords: Laser; soft tissue; histology; incision; morphology.

1. Introduction

Soft tissue lesions within the oral cavity are very common and can have various clinical signs, including mucosal ulceration and nodular and colored lesions. These lesions may be painful or not, and they may be uncomfortable for the patient during food mastication, speech, or appearance. Clinicians must be able to distinguish between normal findings, anatomical variation, and abnormal tissue proliferation (pathological conditions) [1], [2]. Drugs, hot or spicy food, mechanical or chemical trauma, and immunological and systemic disease are different causes leading to these lesions, or they may be idiopathic. Some of the oral soft tissue lesions required surgical removal for histopathological diagnosis [3]. The laser is one of the most advanced surgical modalities and has an effective role in oral soft tissue treatment [4].

The semiconductor GA As powers the diode laser (DL) by producing wavelengths 400 to near IR spectrum. The majority of diode lasers use a flexible optical fiber to send laser beams in either a continuous or gated pulsed mode to the working field [5]. DLs operating with spectral ranges of 810 and 980 nm have been considered as a potential tool for oral soft tissue surgery [6]. Diode lasers are effective in cosmetic surgery such as gingivectomy and excision of oral lesions such as pyogenic granuloma and epulis fissuratum. Diode laser treatment offers advantages such as no bleeding, a clearer field, a shorter operation time, a disinfected site, faster healing, minimal postoperative pain, and a lower cost [7], [8].

Erbium, Chromium YSGG laser at 2780nm wavelength, free running pulsed laser, has proved to be useful for treating many hard tissue procedures and soft tissue operations since both water and hydroxyapatite crystals absorb a significant amount of this laser [9]. Er, Cr: YSGG laser was effective in oral soft tissue surgery such as gingivectomy and implants as it preserved the morphology of fibroblasts with no evidence of carbonization and less thermal damage extent in the tissue [10], [11].

The novelty of the research was using a dual-wavelength diode (810 nm most coagulated diode laser and a 980 nm laser, which is used more in fibrous tissue) in soft tissue incision and also using the pulsed laser (Er, Cr:YSGG), which is less used in soft tissue surgery.

Histologically, few studies compare both diode and Er, Cr: YSGG laser systems and no one talks about the most regular and deepest incision by the clinicians in both lasers. Current research aimed to histologically compare the morphology of cutting by both diode and Er, Cr: YSGG lasers to get the smoothest and the most regular incision in oral surgery.

2. Methods

2.1. Study design and samples collection

It was an experimental comparative study in animal specimens to evaluate both lasers with two different powers in every system for a more specific result between two wavelength laser systems. The variables were laser wavelength and average power.

The source of the samples was the tongue of the recently slaughtered Iraqi sheep (five tongues) aged 8– 17 months and irradiated within five hours after slaughter. The incision was made on the lateral surface of each tongue after cutting into small pieces; the dimensions of each piece were 1.5 cm length*2 cm width*1 cm thickness (Figure 1). For each laser type, there were two groups with two different average powers, each with seven pieces, so the whole number was 14 for each laser system.

2.2. Laser systems

The dual-wavelength diode laser (QUICKLASE 12W dual 4 (810+980), England, UK) was used with an optical fiber delivery system in continuous emission mode (CW), and a power meter (PINTUDY, Guangzhou, CN) was used for power adjustment. The second system was the Erbium, Chromium YSGG laser (WATERLASE I PLUS, California, USA) with a gold handpiece and MZ6 tip in pulse emission mode (PW). (The complete illustration of the laser group's parameters is shown in Table 1).

The laser radiation was made perpendicularly on the piece of tongue in contact mode, so the incision was made with a 1.5 cm length adjusted in 20 sec, and the horizontal speed of the operator was 0.75 mm/sec.

2.3. Histology

After finishing the laser surgery, each piece was placed in 10% formalin and sent for histological processing in the histopathological lab. The blocks were sectioned at five micrometers in microtone; the first section was neglected, and from each block, three sections were selected for Hematoxylin and Eosin (H&E) staining. The number of slides for each laser single group was 21, and 84 was the total number of slides. The microscope that was used for reading the results was the light microscope (GOWE Lab Instrument

Laboratory Binocular Head Biological Microscope, Japan) with an additional camera (5 MP USB CMOS Camera Microscope Digital Electronic Eyepiece with 0.5X C Mount Lens, mainland China) and software computer program (S-EYE 2.0, China).
The histological assessment criteria:
- Morphology and regularity of the incision: it has been scored from zero to four, where zero is the least incisional quality and four is the highest incisional quality (very ideal incision, which is similar to a cold blade incision, scored 4; the very rough and worst quality scored 0, with ≥2 smooth, linear borders mostly of the incisional margins and < 2 rough and uneven edges in most incisions).
- The depth of each incision: it has been measured in micrometers.

2.4. Statistical analysis

Data statistical analysis has been performed by SPSS. For data comparison between two systems and the four groups, the unpaired t-test, Mann-Whitney test, post hoc-tukey test, anova one-way test, and Kruskal-Wallis test were employed. The level of significance was 0.05.

3. Result and discussion

3.1. Result

A. Morphology and regularity of the incision

The Mann-Whitney test compared the medians of all samples of both laser systems and showed that the morphology and regularity of the incision quality of the erbium, chromiumYSGG laser was significantly higher than that of the diode laser, with a P value of 0.048 (<0.05), as shown in **Table 2** (**Figure 2 (a)**). When the Kruskal Wallis test compared the medians between the four groups of both laser systems, no significant difference was seen; the P value was 0.075 (>0.05), as shown in **Table 3**. Mann Whitney test compared the medians of each two groups of lasers: P value = 0.284 between first Group (G1) and G2, P value = 0.169 between G1 and G3, *P*= 0.875 between G1 and G4, *P*= 0.005 between G2 and G3, *P*= 0.201 between G2 and G4, *P* = 0.233 between G3 and G4. This means that the only significant difference can be found between G2 (2.5 W diode laser), where less quality of incision was seen, and G3 (2.5 W erbium, chromium YSGG laser), where higher quality of incision was seen (*P<0.05*), as shown in **Table 4**.

B. Cutting depth of the laser

The unpaired t-test compared the means and standard deviations (mean ± SD) of all samples of both laser systems. It showed that in the depth of the incision, between the Er, Cr: YSGG laser and diode laser, it was not significant difference, *P*= 0.212 (>0.05), as shown in Table 2. An ANOVA one-way test compared the means and standard deviations between four groups of both laser systems; they were significantly different, P value = <0.001 (Figure 2 (b), as shown in Table 3. A post hoc Tukey test compared the means and SDs of each of the two groups: P value = 0.424 between G1 and G3, P value =0.826 between G2 and G4, and P value = <0.001 between all other two groups. This means that there was a high significant difference between every double groups except between 1.5 W of DL (G1) and 2.5 W erbium, chromium YSGG laser (G3), and between 2.5 W of DL (G2) and 3.5 W erbium, chromium YSGG laser (G4), where nearly similar depths of the incisions were produced in these groups, as shown in Table 4, Figure3 illustrated some sections with regularity scores and depth measurement of the incision.

3.2 Discussion

The discussion of the first criterion, that every laser system works with a different delivery system since a small flexible fiber optic with bare glass fiber of diode is less controlled than that of the MZ6 of erbium,

chromium YSGG laser, which was rigid and not resisted by the tissue of the tongue according to the operator observation, second cause the higher power on any laser system can lead to less regularity due increase the power density which leads to more area being exposed to the photothermal effect; this leads to more histological artifacts through the tissue, then more irregular cutting, the significant difference between the highest power of diode and lowest power output of erbium, chromium YSGG laser is a clear example of this discussion, as in previous research, the diode laser of 980 nm and higher power 4W gives the poor quality of laser incision [12].

Additionally, depending on the laser category, other variables impact the results including the emission mode and the radiation frequency. As in the previous research, greater quality of incision was shown in the specimens with a high frequency and low power output of radiation [13]. Also, the specimens with lower tissue damage extent show better incisional quality, as in previous research the higher regularity score (mean) had been shown at Er family, especially with 20 Hz frequency and long pulse, and lower incisional quality had been seen at the diode laser [14]. Current result is controversial to the earlier study that said the creation of the micro-explosions of Er family laser on the tissue was the reason for the irregular shape (rough edge) of the incision [15]. The presence and absence of water or air spray also affect the regularity of this incision [14], [16]. This study shows that the wavelength and radiation per unit area affected the regular shape of the incision.

Regarding the second criterion, the choice of laser wavelength, laser parameters, and the implementation of control systems have an important part in determining the cutting depth of soft tissue incisions by laser [17]. In this current study, the laser parameters were chosen according to the surgeon's usage of these two laser systems in the oral soft tissue incision. According to the results, the low power of the diode laser had nearby cutting depth to the low power of the erbium, chromium YSGG laser, and the high output of the DL also had a comparable cutting depth to the high output of the erbium, chromium YSGG laser. This means the cutting efficiency of each of the two low or high parameters was comparable for the two laser systems, but the cutting depth was different in the power increase of each system. This means that the cutting depth did not show wavelength-dependent but nearly a linear response as laser power increases, and this agrees with previous studies [18], [19]. This was a controversy over a previous study that showed that when the wavelength increased from 810 to 1064 nm, the cutting depth decreased, and the cutting depth was not power dependent [5]. Fornaini et al. showed that the diode laser's incision depth ranges from 2 to 6 mm [18].

In oral tissues exposed to laser radiation, photon energy is converted to thermic energy through absorption. This results in a variety of thermal changes, which can include brief heating (between 42° and 50°), Denaturation of proteins and coagulation at 60°C, vaporization and ablation at 100° C, or even carbonization (over 200°C). This photothermal effect causes histological changes in the incisional and peri-incisional areas [21].

In the diode laser, the laser-tissue interaction mechanism depends on the radiation's absorption within the correlated chromophores. In the 800–1000 nm range of wavelengths, hemoglobin (μ A) = 4.1-1.1 cm-1 and melanin (μ A) = 134-61.7 cm-1 are the principal absorbers [5]. Thus, there is very little absorption in water (μ A) = 0.02-0.36 cm-1) [5]. This shows that the diode laser is not ideal for soft tissue cutting because the laser energy in the continuous mode spreads through a vast region of tissue, and there is a higher chance of larger thermal damage leading to less regular incision; nevertheless, excellent coagulation and hemostasis are produced by this energy's strong blood absorption [12].

In the erbium, chromium YSGG laser, the water is the main targeted chromophore, so it is an ideal system for soft tissue surgery with little heating in the surrounding tissue, thermal damage extent, and histological artifacts [22], [23].

Erbium lasers are a great option for surgical soft tissue operations since they feature water as their principal chromophore and also because they are pulsed lasers, which allows for thermal relaxation time, less thermal damage, and a more regular shape of the incision [11].

3.2.1 Figures, and Tables

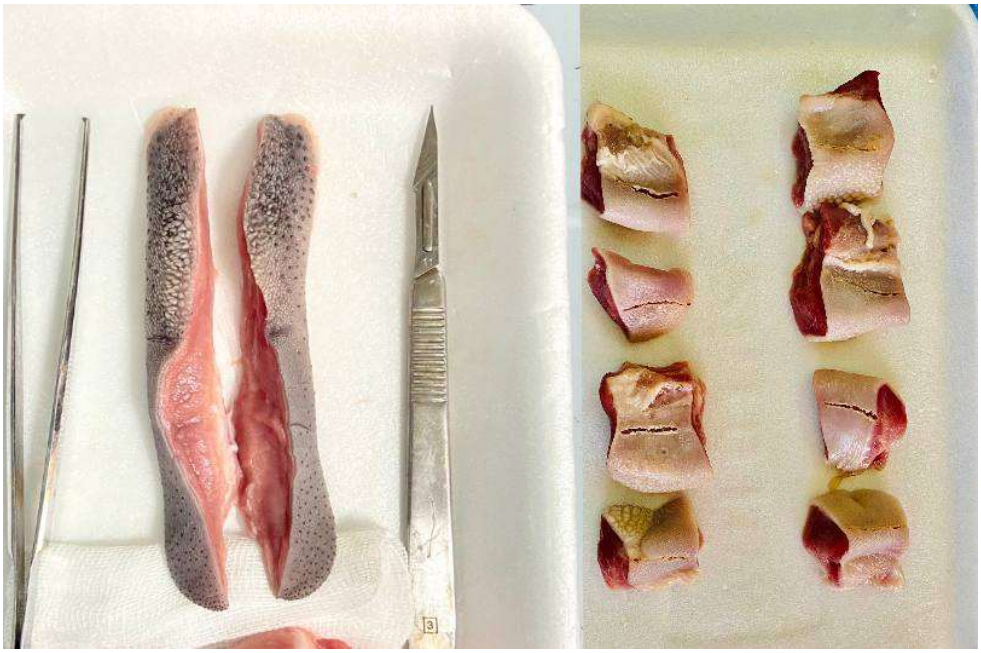

Fig. 1: Sample preparation and irradiation with Er, Cr: YSGG laser.

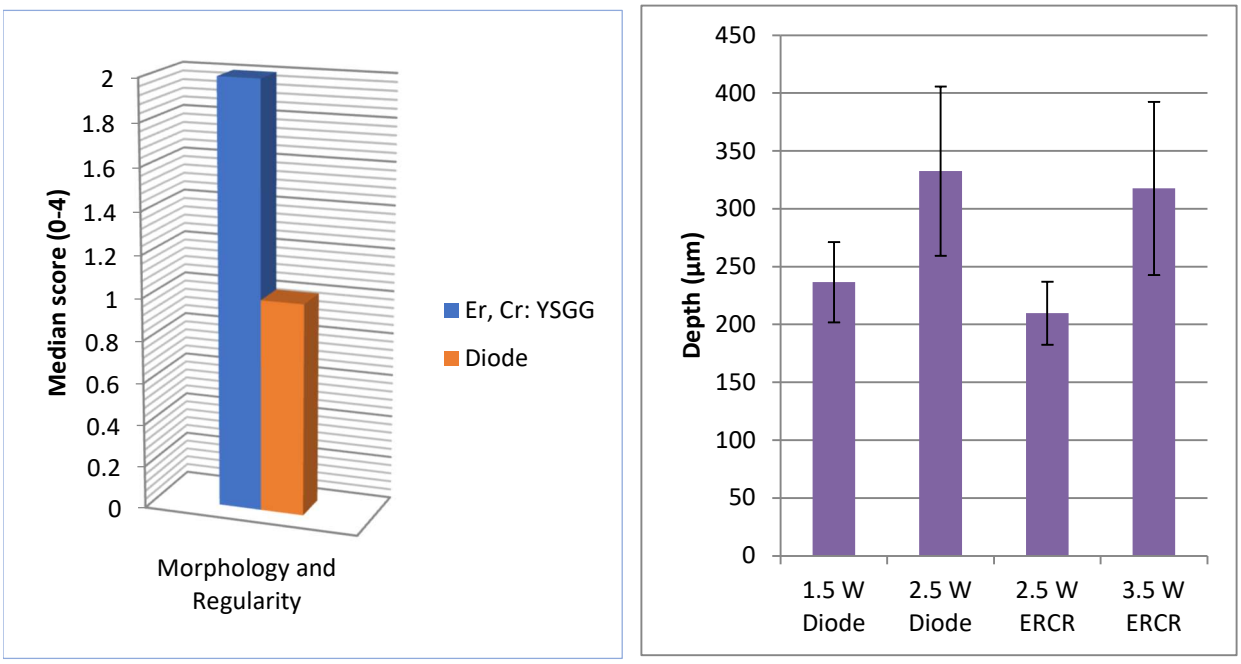

(a) **(b)**

Fig.2: (a) Morphology and regularity of incision, the result between the samples of two laser systems **(b)** Cutting depth in the samples of the four groups of two lasers.

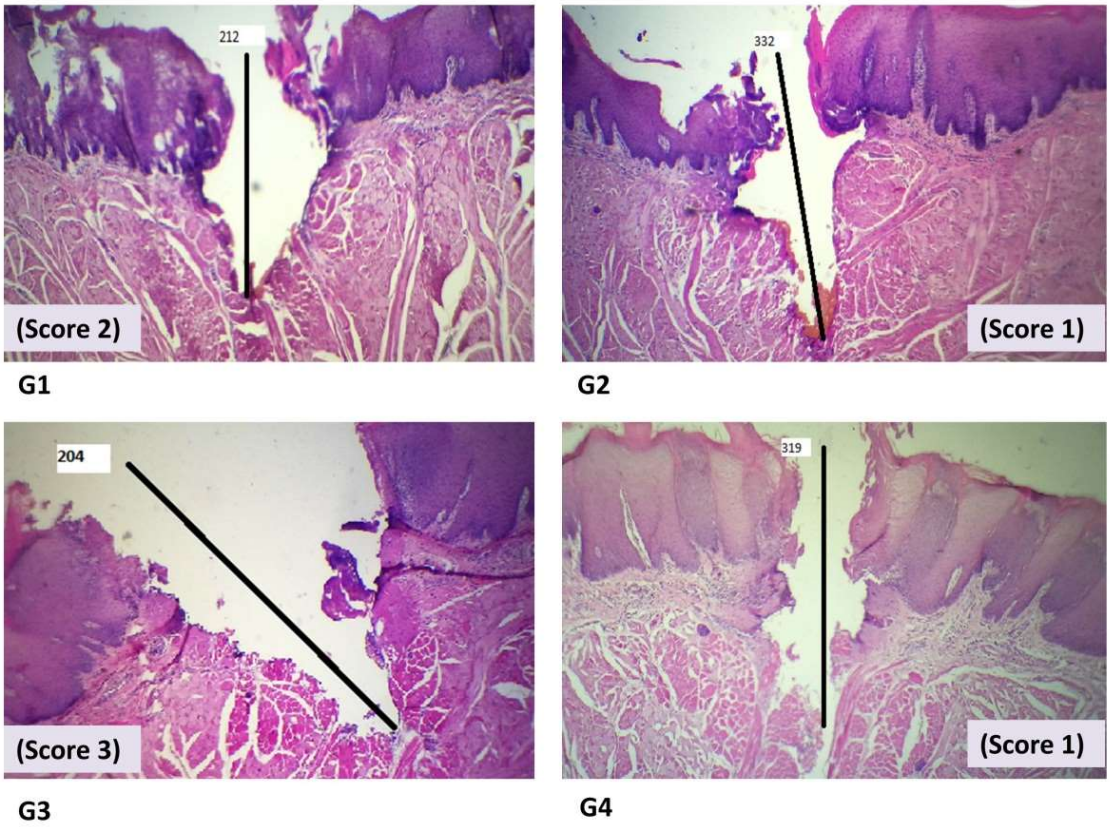

Fig. 3: Histological changes including regularity scores and incision depth in slides from four study group (4X magnification).

Table1. Detailed descriptions of laser parameters

Laser system group	Average Power(W) &Energy Per Pulse	Water/Air Spray %	Frequency (Hz)	Pulse Duration (µsec)	Peak Power	Power Density W/ cm²	Tip/ Fiber Optic Diameter (µm)
Group1: Diode dual ƛ(810+980nm)	1.5(CW)	___	___	___	___	1153.8	(400)
Group2: Diode dual ƛ (810+980nm)	2.5(CW)	___	___	___	___	1923	(400)
Group3: Er,Cr:YSGG ƛ 2,780 nm	2.5(PW) 50mJ/pulse	10/10	50	700	71.43	892.8	(600)
Group4: Er,Cr:YSGG ƛ 2,780 nm	3.5(PW) 70mJ/pulse	10/10	50	700	100	1250	(600)

Table 2. Data analysis between two laser systems samples.

Criteria	Test type	Diode laser N=42	Er, Cr: YSGG laser N=42	P value
Morphology regularity of the incision score (0-3)	Mann-Whitney test median (range)	1 (0-3)	2 (0-3)	**0.048**
Cutting depth of the incision (µm)	Unpaired t-test Mean± SD	284.6±74.46	263.67±77.87	**0.212**

Table 3. Data analysis between four groups of different powers and lasers.

criteria	Test Type	Group 1 N=21	Group 2 N=21	Group 3 N=21	Group 4 N=21	P value
Morphology and regularity of the incision	Kruskal Wallis test	1 (0-3)	1 (0-2)	2 (0-3)	1 (0-3)	0.075
Depth (µm)	ANOVA one-way test	236.62±34.6	332.57±73.05	209.81±27.24	317.52±74.82	<0.001

Table 4. Data analysis between every two groups of the different powers or lasers.

Criteria	Test type	1st group	2nd group	P value
Morphology and regularity of the incision	Mann Whitney test	1.5 W Diode	2.5 W Diode	0.284
			2.5 W ERCR	0.169
			3.5 W ERCR	0.875
		2.5 W Diode	2.5 W ERCR	0.005
			3.5 W ERCR	0.201
		2.5 W ERCR	3.5 W ERCR	0.233
Cutting depth of the incision (µm)	post hoc Tukey test	1.5 W Diode	2.5 W Diode	<0.001
			2.5 W ERCR	0.424
			3.5 W ERCR	<0.001
		2.5 W Diode	2.5 W ERCR	<0.001
			3.5 W ERCR	0.826
		2.5 W ERCR	3.5 W ERCR	<0.001

4. Conclusion

The microscopic investigations performed in this work have led to the finding that erbium, chromium YSGG laser samples, specifically the low-power (2.5 W) samples, produced the highest degree of incision regularity. The deepest incisions have been shown with the higher power outputs of the erbium, chromium YSGG and diode lasers (G2 and G4), while the shallowest cutting depths have been shown with the lower powers of the two systems (G1 and G3).

References:

[1] S. B. C. Tarquinio, M. A. Peres, L. J. C. De Oliveira, and K. D. Da Silva, "Oral Lesions in Soft Tissues," in Oral Epidemiology, M. A. Peres, J. L. F. Antunes, and R. G. Watt, Eds., in Textbooks in Contemporary Dentistry. , Cham: Springer International Publishing, 2021, pp. 251–263. doi: 10.1007/978-3-030-50123-5_15.
[2] E. Schmidt, Ed., Diseases of the Oral Mucosa: Study Guide and Review. Cham: Springer International Publishing, 2021. doi: 10.1007/978-3-030-82804-2.
[3] Prof. K. Kamburoglu, Dr. G. Sonmez, Esra EceÇakmak, Prof. E. Baris, and Prof. H. Altan, "Case presentation of oral soft tissue lesions by using ultrasound, terahertz and histopathology," Oral Surg. Oral Med. Oral Pathol. Oral Radiol., vol. 134, no. 3, p. e78, Sep. 2022, doi: 10.1016/j.oooo.2022.04.029.
[4] S. Srivastava, V. Ebenezer, and R. Balakrishnan, "Lasers in Oral and Maxillofacial Surgery- A Review," J. Pharm. Sci. & Res, vol. 15, no. 3, p. 1057, 2023.
[5] A. Hanke, R. Fimmers, M. Frentzen, and J. Meister, "Quantitative determination of cut efficiency during soft tissue surgery using diode lasers in the wavelength range between 400 and 1500 nm," Lasers Med. Sci., vol. 36, no. 8, pp. 1633–1647, Oct. 2021, doi: 10.1007/s10103-020-03243-4.
[6] E. Azma and N. Safavi, "Diode laser application in soft tissue oral surgery," J. Lasers Med. Sci., vol. 4, no. 4, pp. 206–211, 2013.
[7] Damanhour University (and PhD Student in Prosthodontic Department Alexandria University), Egypt and M. M. Sarhan, "Revolutionizing oral surgery: The benefits of diode laser for soft tissue lesion removal," J. Clin. Images Med. Case Rep., vol. 4, no. 4, Apr. 2023, doi: 10.52768/2766-7820/2390.
[8] H. Mazin Akram, O. Husham Ali, N. Kadhum Omran, and A. Omran Ali, "Diode Laser Versus Scalpel Gingivectomy," Biomed. Pharmacol. J., vol. 10, no. 4, pp. 1799–1804, Dec. 2017, doi: 10.13005/bpj/1295.
[9] prof. dr. Janez Diaci and prof. dr. Boris Gaspirc, "REVIEW Comparison of Er:YAG and Er,Cr:YSGG lasers used in dentistry," LA&HA J, vol. 2012, no. 1, [Online]. Available: https://www.laserandhealthacademy.com/media/objave/academy/priponke/1_13_laha_journal_2012_1a.pdf
[10] M. N. Alqutub, "Peri-implant parameters and cytokine profile among Peri-implant disease patients treated with Er Cr YSGG laser and PDT," Photodiagnosis Photodyn. Ther., vol. 37, p. 102641, Mar. 2022, doi: 10.1016/j.pdpdt.2021.102641.
[11] J. Orozco, D. Rico, L. Barrios, V. Hoyos, and P. Blanco, "Artefactos histológicos asociados a gingivectomía con láser y electrobisturí: serie de casos," Biomédica, vol. 43, no. 3, pp. 315–322, Sep. 2023, doi: 10.7705/biomedica.6930.
[12] C. Fornaini et al., "Four different diode lasers comparison on soft tissues surgery: a preliminary ex vivo study," LASER Ther., vol. 25, no. 2, pp. 105–114, 2016, doi: 10.5978/islsm.16-OR-08.
[13] P. Vescovi et al., "Nd:YAG laser versus traditional scalpel. A preliminary histological analysis of specimens from the human oral mucosa," Lasers Med. Sci., vol. 25, no. 5, pp. 685–691, Sep. 2010, doi: 10.1007/s10103-010-0770-4.
[14] L. Monteiro et al., "A histological evaluation of the surgical margins from human oral fibrous-epithelial lesions excised with CO2 laser, Diode laser, Er:YAG laser, Nd:YAG laser, electrosurgical scalpel and cold scalpel," Med. Oral Patol. Oral Cirugia Bucal, pp. 0–0, 2019, doi: 10.4317/medoral.22819.
[15] E. Merigo et al., "Laser-assisted surgery with different wavelengths: a preliminary ex vivo study on thermal increase and histological evaluation," Lasers Med. Sci., vol. 28, no. 2, pp. 497–504, Feb. 2013, doi: 10.1007/s10103-012-1081-8.
[16] F. F. Sperandio, D. T. Meneguzzo, L. S. Ferreira, P. A. Da Ana, L. H. Azevedo, and S. C. O. M. De Sousa, "Different air-water spray regulations affect the healing of Er,Cr:YSGG laser incisions," Lasers Med. Sci., vol. 26, no. 2, pp. 257–265, Mar. 2011, doi: 10.1007/s10103-010-0849-y.
[17] C. Fornaini et al., "450 nm Blue Laser and Oral Surgery: Preliminary ex vivo Study," J. Contemp. Dent. Pract., vol. 17, no. 10, pp. 795–800, Oct. 2016, doi: 10.5005/jp-journals-10024-1933.
[18] H. Wurm et al., "Comparative ex vivo Investigations on the Cutting Quality of the CO2 Laser and the Diode Pumped Er:YAG Laser," Front. Surg., vol. 8, p. 764450, Dec. 2021, doi: 10.3389/fsurg.2021.764450.
[19] S. Yammine, E. Jabbour, S. El Toum, and A. Cassia, "Histological Study of Induced Incisions on Rabbits' Tongues with Three Diode Lasers with Different Wavelengths in Continuous Mode," Scientifica, vol. 2018, pp. 1–8, 2018, doi: 10.1155/2018/2691942.
[20] C. Fornaini, J. P. Rocca, M. F. Bertrand, E. Merigo, S. Nammour, and P. Vescovi, "Nd:YAG and Diode Laser in the Surgical Management of Soft Tissues Related to Orthodontic Treatment," Photomed. Laser Surg., vol. 25, no. 5, pp. 381–392, Oct. 2007, doi: 10.1089/pho.2006.2068.
[21] SR Pohlhaus, "Lasers in dentistry: minimally invasive instruments for the modern practice," 2012, vol. 105, p. 211886.

[22] R. Kawamura et al., "Ex Vivo Evaluation of Gingival Ablation with Various Laser Systems and Electroscalpel," Photobiomodulation Photomed. Laser Surg., vol. 38, no. 6, pp. 364–373, Jun. 2020, doi: 10.1089/photob.2019.4713.
[23] G. Tenore et al., "The Impact of Laser Thermal Effect on Histological Evaluation of Oral Soft Tissue Biopsy: Systematic Review," Dent. J., vol. 11, no. 2, p. 28, Jan. 2023, doi: 10.3390/dj11020028.

عنوان البحث باللغة العربية(دراسة تقييمية مقارنة لليزر الاربيوم كروميوم YSGG وليزر دايود ثنائي الصمام مزدوج الطول الموجي في شكل شق الأنسجة الرخوة الفموية: دراسة نسيجية خارج الجسم الحي)

الاء جمال العاني[1]،*، حنان جعفر طاهر[1]، عمار صالح العلوي[2]

[1]معهد الليزر للدراسات العليا، جامعة بغداد، بغداد، العراق
[2]وحدة الليزر الجراحي، قسم جراحة الوجه والفكين، مدينة الامامين الكاظمين الطبية، بغداد، العراق.

*البريد الالكتروني للباحث: aalaa.jamal2102m@ilps.uobaghdad.edu.iq

الخلاصة: الليزر هو نظام مفيد يمكن استخدامه في تطبيقات طبية مختلفة، وأحدها هو التعامل مع الأنسجة الرخوة في جراحة الفم وماحول الاسنان. يهدف البحث الحالي إلى المقارنة النسيجية بين ليزر الإربيوم كروميوم YSGG وليزر الصمام الثنائي ثنائي الطول الموجي في الشقوق الجراحية الفموية وفقًا لشكل القطع. **الطريقة:** كانت هذه دراسة خارج الجسم الحي باستخدام قطع لسان من الأغنام كعينات. تم تشغيل ليزر ديود(50%)980 + (50%)810 نانومتر بشكل مستمر (CW) بمعلمتي قوى: 1.5و 2.5 واط. تم استخدام ليزر الإربيوم كروميوم YSGG 2780 نانومتر في وضع النبض بمعلمتي قوى: 2.5 و 3.5 واط. تم عمل شقوق في أجزاء اللسان، وبعد المعالجة النسيجية، تم قياس انتظام وشكل الشق وعمق القطع لكل شق تحت المجهر الضوئي. **النتائج:** كان انتظام وشكل شقوق ليزر الإربيوم كروميوم YSGG أعلى بكثير في الجودة (خاصة تلك ذات طاقة الخرج المنخفضة البالغة 2.5 واط) مقارنة بتلك الموجودة في ليزر الصمام الثنائي (قيمة $P < 0.05$). وكان عمق القطع أعلى بكثير عندما زادت الطاقة، بغض النظر عن نوع نظام الليزر (قيمة $P < 0.05$). **الاستنتاجات:** تم إجراء معظم الشقوق المنتظمة باستخدام قوة 2.5 واط من ليزر الاربيوم كروميوم YSGG.

IJL, Issue 1, Vol. 23, 2024
https://doi.org/10.31900/ijl.v23i1.444

Research Article

IRAQI JOURNAL OF LASER

Evaluation of 1470nm diode laser used in Haemorrhoidoplasty

Ali Fouad Rashid Al-Khazraji*[,1], Ahmed Waleed Ibrahim[1], Amgid Saeed Yaqub[2]

[1] *Department of Surgery, Al-Yarmouk Teaching Hospital, Baghdad, Iraq*
[2]*Department of Surgery, Baiji General Hospital, salah-Aldin, Iraq*
* *Email address of the Corresponding Author: aquarius77doc@gmail.com*

Article history: Received 30 Dec. 2023; Revised 5 Mar. 2024; Accepted 3 Apr. 2024; Published online 15 Jun. 2024

Abstract

Background: Hemorrhoids are a prevalent anorectal issue around the world, which can afflict a large number of people each year. Hemorrhoidal vein(s): When these veins become dilated and enlarged, they will turn into a morbid condition called hemorrhoidal disease. Lasers are mainly used to cut and or coagulate tissue. In this study, a 1470nm diode laser was used for the treatment of 10 cases with 2nd, 3rd, and 4th-degree hemorrhoids enrolled for hemorrhoido-plasty.

Aim of the study: Evaluation of the use of 1470nm-diode laser for treatment of second, third, and fourth-degree hemorrhoids by coagulative method and evaluate any possible complications.

Patients, Materials, and Methods: This is a prospective study with ten patients (all male). All patients were from the private clinic and were operated on using a 1470 nm diode laser for laser hemorrhoidoplasty between June 2022 and October 2022. All patients were surveyed and reported having one or more of the complications listed in the questionnaire paper (if any). Local anesthetic was used during the procedures.

Results: Patients experience mild pain during the administration of local anesthesia drugs. In the first postoperative week, mild pain in seven patients (70%) and moderate in three patients (30%). No patient experienced significant primary bleeding after the operation, and five patients (50%) had a seromucous discharge from the site of the operation that lasted for two to six days. No patient experienced infection. Urine retention was experienced in two patients (20%). With the exception of one patient who had minor skin prolapse, all patients saw improvements in their pre-operative symptoms and the disappearance of the hemorrhoid. During the follow-up period, none of them need to have a second laser treatment session. During the (four-week) follow-up period following the laser hemorrhoidoplasty, there was no recurrence observed or detected during the follow-up period, which was four weeks after the laser haemorrhoidoplasty. Every patient goes back to work within three to five days. All patients were satisfied with the outcome of the operation despite the minor complications that occurred post-operatively.

Conclusion: The clinical application of the 1470nm diode laser in surgical operations shows promise for routine use. It is a safe, acceptable, and remarkable substitute for traditional surgical treatment techniques and can be regarded as practical, effective, and easy to use

Keywords: 1470nm, diode laser, Hemorrhoids, haemorrhoidoplasty, treatment.

1. Introduction

Hemorrhoids may afflict over a million people annually; it is one of the most prevalent benign anorectal morbid disorders in the world [1]. The Hemorrhoids are defined as engorgement and distal displacement of typical anal cushions. One of the most important characteristics of hemorrhoids is the aberrant dilatation and distortion of the vascular channels, along with alterations in the breakdown of the connective tissue that supports the anal cushions. Hemorrhoidal venous cushions are normally found in structures of the ano-rectum and are always present unless an earlier intervention has been performed [2].

When the patient is in the lithotomy position, internal hemorrhoids, which are symptomatic anal cushions, typically lay at the 3, 7, and 11 o'clock positions. Furthermore, internal hemorrhoids at the secondary position are found in the space between the main site masses. External hemorrhoids are not actual hemorrhoids; instead, they are associated with venous channels of the inferior hemorrhoidal plexus, which are located deep in the skin around the anus. Typically, thrombosis, a painful acute condition, is the reason why external hemorrhoids are first identified [3].

Hemorrhoids are a type of disease that may cause patients symptoms and other complications. Bleeding, discharge, itching, pain, and symptomatic prolapse are the complaints [4].

Hemorrhoids incidence is as many as 36.4%. The human body normally has hemorrhoidal veins. Hemorrhoidal disease is a morbidly symptomatic disorder that develops as these veins enlarge and dilate. Straining will encourage vein congestion and hasten the development of hemorrhoids; it is common to see multiple cases in the same family and may have a significant genetic component. Vein dilatation is influenced by weightlifting, pregnancy, and any illness that raises intra-abdominal pressure. [5]

In general surgery, the primary uses of lasers are in tissue coagulation, vaporization, cutting, and excision. For most circumstances, "laser surgeries" essentially substitute the other devices used in conventional surgical (instruments) including electrocautery, cryosurgery, and scalpels. It was suggested that lasers will enable surgeons to perform more difficult procedures.[9](like fourth-degree hemorrhoids with no major wound, bleeding, or pain)

1.1 Study objectives

Assessment of the safety and effectiveness of the use of 1470nm-diode laser for treatment of second, third, and fourth-degree hemorrhoids by coagulative method and assessment of any possible complications and patients' satisfaction.

2.1 Patients

This is a prospective study with ten patients (all male). All patients were from the private clinic and were operated on using a 1470 nm diode laser for laser hemorrhoidoplasty between June 2022 and October 2022. Ten patients with symptomatic conditions of second, third, and fourth-degree hemorrhoids were included in this prospective study; all were male. The patients underwent laser hemorrhoidoplasty using a 1470nm diode laser at a private clinic under local anesthesia between June 20, 2022, and October 31, 2022. Patients' ages ranged from 32 to 65, with a mean age of 44.8 years, following a thorough description of the treatment and a discussion of its potential benefits and drawbacks as well as any anticipated complications. Preoperative evaluation: A case sheet was designed exclusively for the purpose of reviewing each patient's healthcare details and records. Age, symptoms (bleeding and discharge, nodule, itching, pain, and symptomatic prolapse), any prior surgeries, and past medical history are all considered a part of the patient's history.

A verbal agreement was obtained, a clinical evaluation of the patients and hematological investigations for virological infection, and complete blood count. Proctoscopy and digital rectal examination are part of the preoperative evaluation, which determines the degree of hemorrhoids, the number of piles, and any accompanying lesions or masses (if any).

A. Inclusion criteria

This study includes all patients who are older than 18 and have hemorrhoids of the second, third, or fourth degree.

B. Exclusion criteria

We excluded from our study patients with severe co-morbid illnesses, anal fissures, fistulas, and those who have first-degree hemorrhoids.

2.2 The Material

The medical laser system and accessories:

2.2.1. Laser system Specification

The laser system employed in this study was a class IV Medical laser system, a 1470nm diode laser that emits light at a wavelength in the near-infrared spectrum. The surgeon configured the laser aperture power output to vary between 0.5 and 15 Watts. Wuhan Dimed Laser Technology Co., Ltd. is the Chinese manufacturer of the diode laser (CHEYLAS-45JN) that is utilized, as shown in Figure 1.

Fig.1. laser device used.

2.2.2 Equipment

The following items are arranged on a tray with drapes, as shown in Figure 2. Allis tissue forceps, hypo-allergic surgical tape (4 inches), medical steel kidney dish, half-cut C-shaped proctoscopy, two syringes of 5 and 50 milliliters, Gauze swabs, Lidocaine solution 1% (50 milliliters), 100 milliliters of 0.9% isotonic normal saline, Lidocaine gel 5%, and a pair of gloves.
Also, doctor Google and completely shielded patient goggles are used during laser irradiation, as shown in Figures 3 and 4.

Fig.2. Equipment.

Fig.3. Doctor google.

Fig.4. Completely shielded patient google.

2.3 Procedure

With the patient in the lithotomy position and an antiseptic 10% povidone-iodine solution applied, No IV N.S.A.I.D. or sedation was used; instead, a 25 ml solution containing 1% lidocaine without epinephrine diluted by 25 ml normal saline (0.9%) (total 50 ml) was injected into the skin around the anus (4-5 ml) and deep in four quadrants around the anal canal (at 2-, 4-, 8-, and 10- o'clock) at a volume of roughly 10 ml each. Following the administration of local anesthesia, the c-shaped proctoscopy is inserted through the anus in order to identify the pile(s). Next, utilizing a laser handle with the bare optic fiber of 600µm diameter with an SMA905 connector, fixed 2-3mm beyond the edge of the terminal cannula, the laser energy is delivered at 8.0W power in pulsed mode, entering at the much-cutaneous junction at the base of the pile

and progressing to its pedicle. The pilot laser serves as a guide for the tip and depth of the laser optic fiber. Each pulse lasted 3 seconds (on) with a 0.6-second interval (off), (6.67Joules), using fan shape technique, the total amount of energy ranged from 150-200J per pile accordingly. A partial shrink of the pile volume serves as a sign to cease further radiation. To prevent overtreatment (overheating of the tissue), wet gauze with 0.9% normal saline was applied to a pile after each full set of pulses, with some pressure maintained for approximately thirty seconds. The skin opening kept open.

2.4 post-operative treatments

For each patient, postoperative follow-ups were recorded. Fix a date for the next follow-up visit, giving him a prescription for antibiotics and analgesia as follows:

1- Injectable antibiotic for 2 days followed by oral one for another 5 days.
2- Single injectable analgesic on the first day (if needed), followed by oral analgesia for 3-5 days.
3- Use of sitz bath twice daily for 15 minutes each time for the first 5 days.

3. Result and discussion

3.1 Results

The results of this study are based on the clinical evaluation of every patient through examination, complaints made by the patient during the procedure, and post-operative and clinical follow-up. Under local anesthetic, the surgery was tolerated by all of the patients. Ten patients are male. According to the grade of the pile(s), they were divided into three grades: grade two, consisting of six patients; grade three, consisting of three patients; and grade four, consisting of one patient. As shown in Table 1.

Table 1. Grades of hemorrhoids in 10 patients.

Grade	No. of Patients	Percentage (%)
2nd degree	6	60%
3rd degree	3	30%
4th degree	1	10%
Total	10	100%

In terms of the number of piles, there are four patients with three piles: two with second-degree piles and two more with third-degree piles; four patients with two piles, three of them with second-degree piles and the last one fourth-degree; and two patients with one pile, one of which is second-degree and the other third-degree, as shown in Table 2.

Table 2. Number of piles in each patient.

Number of Piles	No. of Patients	Percentage (%)
3	(**2**pat.)with 2nd degree (**2**pat.)with 3rd degree **Total 4**	40%
2	(3pat.)with 2nd degree (1pat.)with 4th degree **Total 4**	40%
1	(1pat.)with 2nd degree (1pat.)with 3rd degree **Total 2**	20%
Total	**10**	100%

After a 30-day follow-up, the hemorrhoid disappeared in all (100%) of the patients, with the exception of some redundant skin in the fourth-degree one. None of them required another laser therapy session. None of the patients experienced any serious intraoperative or postoperative complications; therefore, there was no need for hospitalization. During the four-week follow-up period following the laser hemorrhoidoplasty, no recurrence was found.

3.2 Post-operative complications/follow-up

Patients were followed on the 1st, 2nd, and 4th Post-operative weeks.

1. *Pain was classified as mild*, moderate, and severe, as the patients described it, to simplify the patients' pain assessments. Seven patients (70%) had mild pain, including two with three (second-degree) piles, three with two (second-degree) piles, one with one (second-degree) pile, and the final patient with one third-degree pile; three patients (30%) had moderate symptoms, including one with two (fourth-degree) hemorrhoids and two more with three(third-degree) piles, as indicated in table (3-3); the first postoperative day's pain necessitated the use of an injectable NSAID analgesic (olfen ampoule) to manage the pain, and then the pain decrease in the following days.

2. *Bleeding and discharge:*
As indicated by Table (3-3), no patient experienced significant primary bleeding (spontaneous bleeding after surgery) or reactionary bleeding (post-defecatory bleeding). Five patients 50% experienced a sero-mucus discharge; one patient had two (fourth-degree) piles (10%), two (third-degree) piles (20%), and two (second-degree) piles (20%). Postoperative seromucus discharge is identified by simple underwear soiling that lasts for two to six days until it ceases on its own without medical intervention.

3. *Retention of urine:*
This happens in two patients (20%), one of whom had three piles of third-degree hemorrhoids, and the last one had two piles of fourth-degree hemorrhoids and BPH. Both patients complained of burning during micturition and had minor difficulty urinating. The patients were treated conservatively with analgesics and encouragement to urinate; no additional intervention was required, as shown in Table 3.

4. *Infection According to Table 3*,
no patient (zero%) developed an infection during the postoperative period, and the postoperative period passed unnoticeably regarding the infection of the surgical site depending on the antibiotic regimen mentioned before.

5. *Return to work:*
Three patients (30%) return to work after five days, one with two (fourth-degree) hemorrhoids and two more with three (third-degree) hemorrhoids, because of pain, as mentioned before "three patients (30%) had moderate symptoms, including one with two (fourth-degree) hemorrhoids and two more with three(third-degree) piles". Whereas seven patients (70%) returned after three days, those with mild pain as mentioned before, "Seven patients (70%) had mild pain, including two with three (second-degree) piles, three with two (second-degree) piles, one with one (second-degree) pile, and the final patient with one third-degree pile" as shown in Table 3.

6. *Satisfaction:*
All patients (100%) are satisfied with the results of the operation and postoperative complaining, apart from the redundant skin of the one patient with 4th-degree piles who are reassured that this is not significant, as shown in Table 3. Yet they are completely satisfied with the result as no active bleeding, mass, itching, pain, symptomatic prolapse, or feeling of incomplete defecation.

7. *Recurrence:* As seen in Table 3, there was no recurrence during the follow-up period (0%) in this study.

Table 3. The results of the patients.

Post-operative complications / follow up	No. of Patients	Percentage (%)	Grade	No. of Piles
No pain	0	(0%)	/	/
Mild	7	(70%)	2nd and 3rd degree	Three, two, one piles
Moderate	3	(30%)	3rd and 4th degree	Three, two piles
Sever	0	0%	/	/
Bleeding & discharge Sero-mucous discharge	5	(50%)	2nd,3rd and 4th degree	-1 pat./2piles of 4th degree, -2 pat./3piles of 3rd degree, -2pat./3piles of 2nd degree
Retention of urine	2	(20%)	4th degree*1 and 3rd degree	two piles three piles
Need catheterization	0	0	0	0
Infection	0	0	0	0
Return to work	7 after three days 3 after five days	70% 30%	2nd and 3rd degree 4th and 3rd degree	Three, two, and one pile Three and two piles
Satisfaction	10	100%	2nd, 3rd and 4th*2 degree	Three, two, and one piles
Recurrence	0	0	0	0

*1 with BPH
*2 with redundant skin

3.3 Discussion

This study uses a diode laser operating at 1470 nm to treat hemorrhoids by minimally invasive laser-induced interstitial thermotherapy (coagulative effect, as mentioned before). The following characteristics were to be prospectively assessed in this study: pain, bleeding, retention of urine, surgical site infection, return to work, and overall patient satisfaction. Few cases in this study had post-procedural complications. Regarding postoperative pain, mild pain had occurred in (70%) of cases and moderate pain in (30%) of cases. This is in agreement with Brusciano et al. using Laser hemorrhoidoplasty (1470 nm); there were no major postoperative problems. Average level of pain after surgery: VAS (Visual Analog Scale) 2 (first 3 days)[6]. (Complication) Also in agreement with Paolo Giamundo Comparison: hemorrhoid laser operation (980 nm) versus band ligation Median post-operative pain VAS score 1.1 in laser hemorrhoid procedure [7]. Also, in agreement with Ferhatoglu et al. Hemorrhoidoplasty with laser (1470 nm) pain after 2 days of operation mean VAS score of 2.85 [8]. This is consistent with the hybrid digital guided HAL (hemorrhoidal artery ligation) with laser hemorrhoidoplasty scores of 2.82 and 1.28 on the third and seventh postoperative days, respectively, reported by De A et al. [9]

Regarding bleeding and discharge in this study, it is classified as:
1. Spontaneous bleeding post-operatively.
2. Post-defecation bleeding.
3. Sero-mucus discharge post-operatively.

There was no post-operative spontaneous bleeding or post-defecatory bleeding. In five cases (50%), there was a small amount of post-operative sero-mucus discharge, which lasted for two to six days after surgery before stopping on its own without the need for further treatment and bothered the patients because it was a hygienic concern.

In the study of Cantarella Francesco et al., in 15.4% of cases, seromucous discharge from the small incisions was observed in the first few weeks after therapy. There were no occurrences of postoperative bleeding. [10]. In a study of Hassan et al., Two cases (10%) out of 20 cases in the open hemorrhoidectomy group had bleeding, whereas one case (5% of the cases) in the laser hemorrhoidoplasty group had bleeding (the patient was taking aspirin) [11]. Regarding infection and abscess formation, no patient in this study suffers from infection. In the study of Cantarella Francesco et al., One out of 25 cases, or 4 percent, had an abscess [10]. In the study of Hassan et al., In the group that underwent laser hemorrhoidoplasty, one case—or roughly 5% of the total—had an abscess. [11]

Two individuals (20%) experience burning sensations during micturition with minor difficulty in urinating. These patients are treated conservatively with analgesics and encouraged urination; further intervention is not necessary. One patient had two fourth-degree piles and BPH; both conditions are attributed to his post-operative symptoms related to this problem; the second patient had three third-degree piles. In a study by Cantarella Francesco et al., Three out of 25 patients, or 12% of the total, experienced acute urine retention; this was most likely brought on by the spinal anesthetic rather than the surgery. [10] In studies by De A et al., Hassan et al., and Sabanci et al., Urine retention is not listed in their studies as a postoperative complication [9, 11, 12]. During the four-week follow-up phase, there is no recurrence rate in this study. In a study by Cantarella Francesco et al., Two out of twenty-five cases (8%) had the recurrence of recurrent post-operative bleeding, which happens three to six months after the treatment[10]. In the De A et al. study, Four patients experienced an occasional bleeding recurrence, and two out of 42 patients reported an incomplete prolapse cure after an average follow-up of sixteen months [9]. In a study by A.N.M. Jane Alam et al., The recurrence rate of hemorrhoids at a one-year follow-up was 5% [13]. In terms of satisfaction and return to work, all cases (100%) do so within three to five days after the procedure, and most patients are pleased with the way the pre-operative symptoms have resolved. This concurs with De A et al. In an average of 5.8 days following surgery, all patients resumed their regular activities [9].

3.4 Limitations of the Study

In this study, there are some limitations:
1. Small sample size.
2. Short follow-up period.
3. No comparative group.
4. All patients were male, no results and complications comparisons with female patients.

4. Conclusions

Diode 1470nm laser hemorrhoid-plastic is a safe and effective procedure associated with a low incidence of postoperative complications, despite the limitations of this study, which primarily focused on the feasibility, safety, and short-term outcome of the procedure. However, it does require the availability of instruments (Diode laser system) and a skilled, well-trained surgeon. For the treatment of hemorrhoids, these are superior tools to traditional surgical methods, as the hemorrhoidectomy is considered as the gold standard regardless of its surgical technique, as it resects the diseased tissue at once. Yet, it may cause pain, mucosal stenosis or anal stenosis, prolonged healing time, and bleeding postoperatively (early and delayed).

For all that many patients refuse operative management, laser hemorrhoidoplasty is a minimally invasive procedure that is considered an alternative that resolves all the above concerns, so it is superior from this point of view.

By employing laser interstitial thermotherapy, tissue coagulation can be accomplished with lower power densities than with tissue cutting. The benefits of using a laser include its ability to stop bleeding from severed vessels (haemostasis), its tolerance by patients under local anesthesia, and its decreased risk of complications during or even after the operation. So, 1470nm laser hemorrhoido-plasty is:

1. Safe.
2. Effective procedure.
3. Low incidence of post-operative complications.
4. Post-operative pain is more with increased no. of piles and their degree.
5. Sero-mucous discharge again is more with increased no. of piles and their degree.
6. Retention of urine is more with those who had BPH, 4th-degree hemorrhoid, and more no. of piles. (more pain).
7. Return to work lasts longer in those with more pain and thence larger piles or more no. of haemorrhoids, faster than respective procedures.
8. Redundant skin is seen in 4th degree pile(s), although it is not significant but bother the patient and may consider the operation is poor, under treatment or recurrence.

References

[1] Holzheimer RG. "Hemorrhoidectomy", (2004), indications and risks. Eur J Med Res; 9(1):18-26.

[2] Loder PB, Kamm MA, Nicholls RJ, Phillips RK. "Haemorrhoids: pathology, pathophysiology and aetiology". Br J Surg. 1994;81:946–954.

[3] Hamilton Bailey ML, Norman S. Williams, Christopher J.K. Bulstrode PRO (eds). SHORT PRACTICE OF SURGERY. 26th ed. CRC press Taylor &Francis Group; 2012. Ch73, p1236-1240, p1250-1256.

[4] Sneider EB, Maykel JA, (2010), "Diagnosis and management of symptomatic hemorrhoids". Surg Clin North Am; 90: 17-32, Table of Contents.

[5] Keighley, M., and Williams, N., eds. (1993), "Surgery of the Anus, Rectum and Colon", London: Saunders, WB, pp. 2576.

[6] Brusciano L, Gambardella C, Terracciano G, Gualtieri G, di Visconte MS, et al. "Postoperative discomfort and pain in the management of hemorrhoidal disease": laser hemorrhoidoplasty, a minimal invasive treatment of symptomatic hemorrhoids. Updates Surg. 2020;72(3):851-7.

[7] Giamundo P, Salfi R, Tibaldi MGL, Murru L, Valente M. "The hemorrhoid laser procedure technique vs rubber band ligation": a randomized trial comparing 2 mini-invasive treatments for second- and third-degree hemorrhoids. Dis Colon Rectum. 2011;54(6):693-8.

[8] Ferhatoglu MF, Kıvılcım T, Ekici U, Kebudi A. "Laser hemorrhoidoplasty procedure for grade two and three hemorrhoidal disease". A retrospectively prospective study, analysis of forty-seven patients. OSP J Surg. 2019;1:101.

[9] De Anushtup, Roy Prabal. "Hybrid digitally guided hemorroidal artery ligation with laser hemorrhoidoplasty": our experience with a new approach to hemorrhoidal disease. International Surgery Journal. 2021 Oct.;8(10):2968-2973.

[10] Cantarella Francesco, Aglietti Rebecca, Sturiale Alessandro. "Short Term Outcomes of Laser Pile Ablation (LPA) to Treat II-III Degree Symptomatic Hemorrhoidal Disease". Annals of Colorectal Research (Iranian Journal of Colorectal Research). 2021;9(2):69-72.

[11] Hassan Ahmed M., Shemy Gamal Galal. "Laser hemorrhoidoplasty versus open hemorrhoidectomy in Upper Egypt". AIMJ. 2021; Feb., DOI:10.21608/aimj.2021.57763.1397.

[12] Sabanci unal, Orug Taner,Uncu Erhan. "Laser hemorrhoidoplasty of a single surgical centre".Turk J Colorectal Dis.2021;31:31-34.

[13] A.N.M. Jane Alam, Akter Maksuda, Ahmed Nafiz Imtiaz Uddin, Afrin Khondaker Sajia, Barman Auditi, Rahman S.M.Mustafizur.Scholars Journal of Applied Medical Sciences.2021 May 9(5):663-669

تقييم تأثير الدايود ليزر 1470 نانومتر في علاج البواسير الشرجية بطريقة تخثير الدم

علي فؤاد رشيد الخزرجي[1]*، احمد وليد ابراهيم[1] ، امجد سعيد يعقوب[2]

[1] قسم الجراحة, مستشفى اليرموك التعليمي, بغداد, العراق
[2] قسم الجراحة, مستشفى بيجي العام, صلاح الدين, العراق

*البريد الالكتروني للباحث: aquarius77doc@gmail.com

الخلاصة

الخلفية: البواسير هي مشكلة شرجية منتشرة في جميع أنحاء العالم، والتي يمكن أن تصيب عددًا كبيرًا من الأشخاص كل عام .الأوردة في البواسير عندما تتوسع وتتضخم فإنها ستتحول إلى حالة مرضية تسمى مرض البواسير .يستخدم الليزر بشكل رئيسي لقطع و/أو تخثر الأنسجة .في هذه الدراسة تم استخدام ليزر ديود 1470 نانومتر في 10 حالات مصابة ببواسير من الدرجة الثانية والثالثة والرابعة عن طريق عملية رأب البواسير.

الهدف من الدراسة: استخدام الدايود ليزر ذو الطول الموجي 1470 نانومتر في علاج الدرجة الثانية والثالثة والرابعة من البواسير الشرجية وتقييم الأضرار الجانبية لهذا الأستخدام او اي مضاعفات محتملة.

المرضى, المواد, الطريقة: هذه دراسة مراقبة مستقبلية بوجود عشرة مرضى (جميعهم من الذكور)؛ كان جميع المرضى من العيادة الخاصة وخضعوا لعملية جراحية باستخدام ليزر ديود 1470 نانومتر لرأب البواسير بالليزر في الفترة ما بين يونيو 2022 وأكتوبر 2022، وقد تم استطلاع رأي جميع المرضى وأفادوا بوجود واحد أو أكثر من المضاعفات المدرجة في ورقة الاستبيان (إن وجدت). تم استخدام المخدر الموضعي أثناء العملية.

النتائج: معظم المرضى لم يعانوا من أي ألم أثناء العملية عدا الم بسيط اثناء حقن المادة المخدرة موضعيا ، كان هناك ألم خفيف في سبعة مرضى (70٪) ومتوسط في ثلاثة مرضى (30٪) في الأسبوع الأول بعد العملية. بالنسبة للأفرازات المخاطية المصلية خمس مرضى (50٪) كان هناك إفرازات مخاطية مصلية من مكان العملية استمرت 2-6 أيام ، ولم يصاب أي مريض بنزيف أولي مهم بعد العملية. لم يصاب أي مريض بالعدوى او الأخماج. كان لدى مريضين احتباس بسيط للبول تم متابعته بشكل تحفظي دون اي تداخل قسطاري للمثانة (20٪). كل المرضى كان لديهم تحسن في الأعراض ما قبل العملية واختفاء البواسير باستثناء مريض واحد كان لديه بعض التدلي الجلدي الذي كان يعاني من باسورين من الدرجة الرابعة. لم يحتج اي من المرضى إلى جلسة ثانية من العلاج بالليزر خلال فترة المتابعة. لم يتم الكشف عن أي رجوع للبواسير خلال فترة المتابعة التي كانت اربع أسابيع من رأب البواسير بالليزر.

عاد جميع المرضى إلى العمل في غضون 3-5 أيام. كان جميع المرضى راضين عن نتائج العملية على الرغم من المضاعفات البسيطة التي حدثت بعد العملية.

الأستنتاج: إن الاستخدام السريري لليزر 1470 نانومتر في العمليات الجراحية أثبت أنه مفيد للعمليات اليومية ، ويمكن اعتباره عمليًا وفعالًا وسهل الاستخدام ويوفر بديلاً آمنًا ومقبولًا ومثيرًا للإهتمام بدل تقنيات العلاج الجراحي التقليدية في البواسير.